



Tomas Bata University in Zlín
Faculty of Technology

Doctoral Thesis

Viscoelastic Modeling of Extrusion Film Casting for Polymer Melts: Investigation of Flow Stability

**Viskoelastické modelování extruzního lití
polymerních tavenin na válec: Výzkum stability toku**

Author: **Ing. Tomáš Barbořík**

Degree programme: P2808 Chemistry and Materials Technology

Degree course: 2808V006 Technology of Macromolecular Compounds

Supervisor: prof. Ing. Martin Zatloukal, Ph.D., DSc.

Reviewers: prof. Ing. Kamil Wichterle, DrSc., dr. h. c.
prof. Ing. Karel Kolomazník, DrSc.
doc. RNDr. Jiří Vlček, CSc.

Zlín, December 2018

© Tomáš Barbořík

The publication was issued in the year 2018.

Key words in Czech: Extruzní lití na válec, Neck-in defekt („krčkování“), Viskoelastické modelování, Numerická analýza, Polymer, Jednoosá, tahová viskozita, Planární tahová viskozita, Zatvrzování, Teplotou a tokem indukovaná krystalizace, Koeficient přestupu tepla, Konstituční rovnice, Modifikovaný Leonovův model

Key words: Extrusion film casting, Neck-in phenomenon, Viscoelastic modelling, Numerical analysis, Polymer, Extensional uniaxial viscosity, Extensional planar viscosity, Strain hardening, Temperature and stress induced crystallization, Heat transfer coefficient, Constitutive equations, Modified Leonov model

Full text of the scientific publication is available in the Library of TBU in Zlín.

ACKNOWLEDGEMENT

At this place, I would like to express my deepest thanks to my supervisor, Prof. Martin Zatloukal for his ideas, encouragement, guidance, patient, kind words and a great deal of time that he spent with me on getting over the small hurdles that occasionally appeared during a course of my study.

I would also like to thank Prof. Costas Tzoganakis for made it possible to spend my Canada research stay in such a vibrant environment as University of Waterloo without doubts is, for his kind advice and valuable comments on my research topic. This stay could not have been accomplished without the financial support provided by Tomas Bata University and Faculty of Technology and is also greatly appreciated.

I also wish to acknowledge Grant Agency of the Czech Republic (Grant registration No. 16-05886S) for the financial support.

Furthermore, I would especially like to thank my colleague and friend Jiri Drabek for being a companion over those great years spent at the university.

Last but not least, I wish to thank all my family for their persisting support and encouragement toward me at all times.

ABSTRACT

In the first part of this Ph.D. Thesis, the extrusion film casting process has been presented and negative phenomena that represent serious process limitation have been discussed. Following section is dedicated to the listing of both experimental and theoretical works and different mathematical models describing the extensional kinematic in film casting that have been published since 1970s. In the next section, novel viscoelastic extrusion film casting model utilizing 1.5D membrane approximation was derived considering single-mode modified Leonov model as the viscoelastic constitutive equation, energy equation, constant heat transfer coefficient, advanced crystallization kinetics taking into account the role of temperature, cooling rate and molecular stretch, crystalline phase dependent modulus and temperature dependent relaxation time. The model has been successfully validated for branched low-density polyethylenes and linear isotactic polypropylenes by using suitable experimental data taken from the open literature. The model has consequently been used for systematic parametric study in order to reveal the role of variety dimensionless variables (such as planar to uniaxial extensional viscosity ratio, extensional strain hardening, Deborah number, second to first normal stress difference ratio at the die exit, draw ratio, heat transfer coefficient and flow induced crystallization) on polymer melt/solid behavior during the extrusion film casting process with specific attention to unwanted neck-in phenomenon. Obtained knowledge together with the suggested model can be used for optimization of the extrusion die design (influencing flow history and thus die exit stress state), molecular architecture of polymer melts, processing conditions in order to minimize neck-in phenomenon as well as to optimize the production of flat polymeric films and porous membranes via extrusion film casting technology.

ABSTRAKT

Úvodní část této disertační práce je věnována popisu výroby tenkých polymerních filmů pomocí technologie lití na válec a souvisejících nestabilit toku, které mohou, pokud nastanou, redukovat procesní okno, a tak významným způsobem přispět k omezení produktivity a efektivity této technologie. V navazující části je podán přehled prací věnovaných této problematice jak z hlediska experimentálního, tak teoretického se zvláštním zřetelem na matematické modely popisující kinematiku daného procesu, které svým vznikem sahají až do 70. let minulého století. V další části práce je odvozen nový viskoelastický model pro technologii extruzního lití na válec, který je založen na 1.5D membránové aproximaci, konstituční rovnici modifikovaného Leonovova modelu, rovnici energie uvažující konstantní součinitel přestupu tepla, pokročilé kinetice krystalizace zohledňující vliv teploty, rychlosti chlazení a intenzity protažení makromolekulárních řetězců, dále na krystalinitě závislém modulu a teplotně závislém relaxačním čase. Model byl úspěšně validován pro rozvětvené nízkohustotní polyethyleny a lineární izotaktické polypropyleny za použití vhodných experimentálních dat převzatých z dostupné literatury. Následně byla provedena systematická parametrická analýza s cílem odhalit vliv materiálových a procesních parametrů vyjádřených pomocí řady, převážně bezrozměrných proměnných (jako např. poměru planární a jednoosé tahové viskozity, stupně zatvrzení při jednoosém protahování, Debořina čísla, poměru druhého a prvního rozdílu normálových napětí na konci vytlačovací hlavy, dlouhého poměru, koeficientu přestupu tepla nebo molekulárního protažení vedoucího k tokem indukované krystalizaci) na chování polymerní taveniny při procesu odlévání vytlačovaného filmu na válec se zvláštní pozorností k nežádoucímu jevu neck-in. Získané poznatky společně s nově navrženým modelem je možné využít k optimalizaci designu vytlačovacích hlav (ovlivňující tokovou historii a napětí na konci výstupní štěrby), molekulární architektury polymerních řetězců a zpracovatelských podmínek, a to jak za účelem minimalizace nestabilit typu neck-in, tak k optimalizaci výroby plochých polymerních fólií a polopropustných membrán pomocí technologie extruzního lití na válec.

LIST OF PAPERS

The following papers are encompassed in this doctoral thesis.

PAPER I

On the Role of Extensional Rheology and Deborah Number on the Neck-in Phenomenon During Flat Film Casting

Tomas Barborik, Martin Zatloukal and Costas Tzoganakis

International Journal of Heat and Mass Transfer. 2017. Vol. 111, p. 1296–1313.

AIS=0.767 and IF=3.891 by 2017.

PAPER II

Effect of die exit stress state, Deborah number, uniaxial and planar extensional rheology on the neck-in phenomenon in polymeric flat film production

Tomas Barborik and Martin Zatloukal

Journal of Non-Newtonian Fluid Mechanics. 2018. Vol. 255, p. 39–56.

AIS=0.769 and IF=2.293 by 2017.

PAPER III

Effect of heat transfer coefficient, draw ratio and die exit temperature on the production of flat iPP membranes

Tomas Barborik and Martin Zatloukal

Submitted for publication in International Journal of Heat and Mass Transfer.

PAPER IV

Viscoelastic simulation of extrusion film casting for linear iPP including stress induced crystallization

Tomas Barborik and Martin Zatloukal

Considered for publication in Journal of Rheology.

CONTENTS

ACKNOWLEDGEMENT.....	3
ABSTRACT	4
ABSTRAKT	5
LIST OF PAPERS	6
CONTENTS	8
STATE OF THE EXTRUSION FILM CASTING PROCESS.....	10
1. The Film Casting Process.....	10
1.1 Process Description.....	10
1.2 Flow Instabilities.....	12
1.2.1 Neck-in.....	13
1.2.2 Edge-beading.....	14
1.2.3 Draw Resonance	15
2. Mathematical Modeling of the Extrusion Film Casting Process	17
2.1 Literature Review	17
2.2 Mathematical models.....	22
2.2.1 One-dimensional Film Casting Model of Infinite Width.....	23
2.2.2 One-dimensional Film Casting Model of Varying Width	24
2.2.3 Two-dimensional Film Casting Model.....	24
THE AIMS OF THE DOCTORAL RESEARCH WORK	26
3. Viscoelastic Modeling of Non-isothermal Extrusion Film Casting Process Considering Temperature and Stress Induced Crystallization.....	27
3.1 Modified Leonov Model.....	27
3.2 Membrane Model of Film Casting	28
3.2.1 Velocity Field	29
3.2.2 Continuity Equation	30
3.2.3 Momentum Conservation Equation.....	31
3.2.4 The Stress-free Surface Boundary Condition.....	32
3.2.5 The Kinematic Free-surface Boundary Condition.....	32
3.2.6 Dimensionless Transformation	33

3.2.7	<i>Extrusion Film Casting Model for the Modified Leonov Model ...</i>	35
3.2.8	<i>Energy Equation</i>	37
3.2.9	<i>Boundary Conditions</i>	40
3.3	Numerical Scheme	41
	SUMARIZATION OF THE RESEARCH PAPERS	44
	THE THESIS CONTRIBUTION TO SCIENCE AND PRACTICE	51
	CONCLUSION	52
	REFERENCES	54
	LIST OF FIGURES	63
	LIST OF TABLES	64
	LIST OF SYMBOLS	65
	PAPER I	75
	PAPER II	95
	PAPER III	115
	PAPER IV	169
	LIST OF PUBLICATIONS	199
	CURRICULUM VITAE	203

STATE OF THE EXTRUSION FILM CASTING PROCESS

Extrusion film casting is an industrially significant process that has firm place among polymer processing technologies in practice. It can be categorized as a continuous, high-speed manufacturing process during that a thin, highly oriented films are produced. A great range of the plastic films and sheets produced by this technology can found their use in many different applications of daily and technical use: plastic bags, packing for consumer products, magnetic tapes for storage of audio video content, optical membranes for liquid crystal displays, air and vapor barriers, foils for capacitors, separator films for batteries in mobile devices and electric vehicles or as product for further processing by other technologies, such as thermoforming and biaxial orientation [1, 2].

Growing demands in an amount of production and quality of fabricated films together with introduction of new materials ask for new approaches in production line. Of particular interest and along the mechanical properties of the produced films is to keep film thickness uniform and width as close as possible to the designed extrusion die width. Besides, course of action based on a trial-and-error approach involved in design of film casting lines, the computer modeling can be utilized bringing the advantages of a reduced consumption of material during testing stage in commissioning of new casting line, a reduced time required for design and finally more efficient design. Thus, this strategy can provide better insight into the problem, extend the knowledge on relationships between process rheological quantities and suggest the possible approaches how to deal with them to optimize the process or give better understanding of underlying mechanics [2].

1. The Film Casting Process

1.1 Process Description

The production of film by the technology of extrusion film casting involves the several devices that take essential part in the entire process. The upstream part of the operation is processed by the extrusion machine where the polymer pellets are conveyed, homogenized and compressed by a screw, melted by means of dissipation and external heat sources, and thus the pressure require to push the polymer melt through the uniform slit die (center-fed T die or coat-hanger die) is generated. Once the polymer is emerged from the die that has typically small opening of about 1–2 mm, the second, downstream, stretching stage takes place where this thick sheet is intensively stretched in the machine direction by a constant rotating take-up drum, whose linear velocity is higher than the exit polymer velocity at the die, and simultaneously providing the sufficient cooling

rate to fix the final dimensions of so-called primary film, see Fig. 1. Moreover, by pulling the polymer melt at these conditions across the take-up length, the macromolecular orientation and thickness reduction to film is imposed. This solidified secondary film is subsequently handled by system of drums for winding-up by a winder to the rolls.

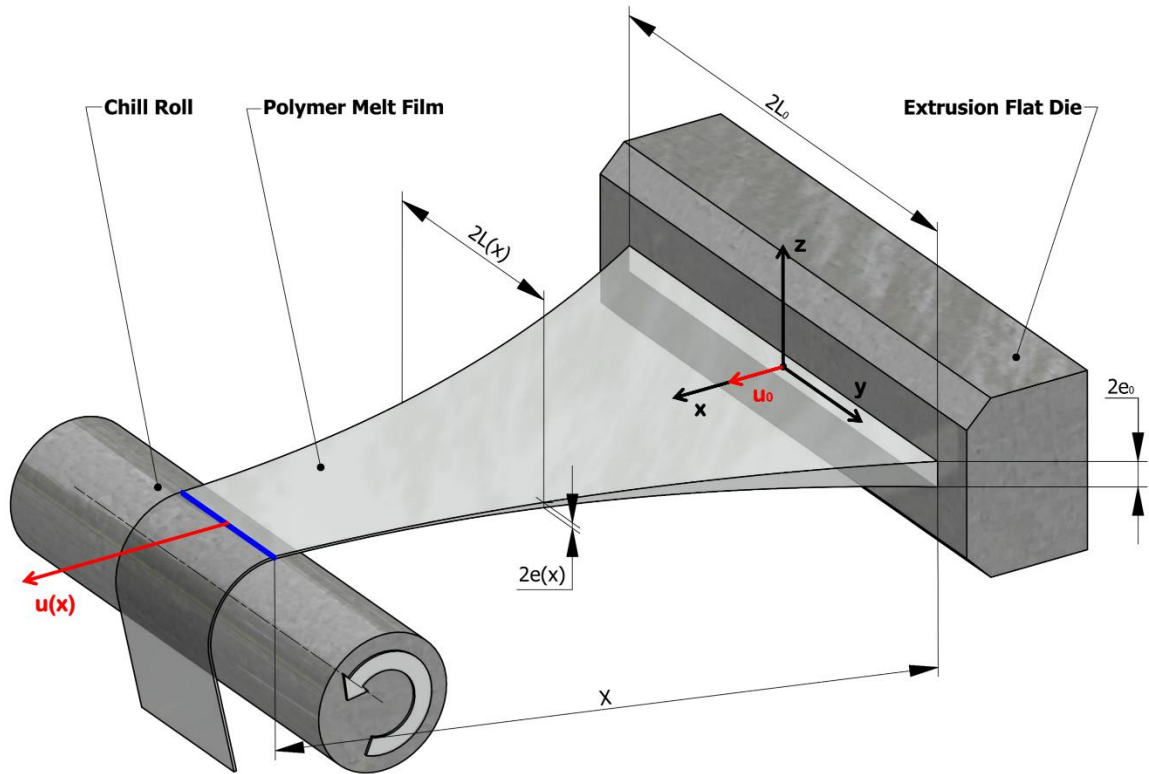


Fig. 1: Schematics of the extrusion film casting kinematics.

At the chill roll, several additional technological devices can be used to ensure a better contact line between film and a chill roll and to increase the rate of thermal transfer, such as air knife (a slit nozzle blows a jet of cooled air onto the film) or electrostatic pinning. In this composition, a high voltage wire is placed parallel to the grounded chill roll that creates an electrostatic discharged exerting the electrostatic force onto film to tight the contact film-chill roll. Another option with the similar result that can be used is vacuum box which function is based on suction of the air between the film and the chill roll and thus provide the negative pressure in this section for a better contact. Aside from cooling down on the chill roll, polymer film is naturally quenched, to a certain level depending also on the length of the drawing zone, by its travelling through the surrounding environment. This can be enhanced by introduction of convected air or an inert gas source to this section or by a film passage through a fluid bath [3]. Additionally, secondary film is about to undergo a treatment (plasma treating, heating and biaxial orientation) depending on the desired properties and purpose of the final product.

Specific attention should be paid to the polymer behavior in the drawing zone and to extensional conditions since this stage mainly determines the mechanical and optical properties that are accommodated by end-product [2, 4].

To produce highly functional films with tailored properties, multiple layers of different polymer melts can be coextruded and stretched, i.e. final properties of such film are constituted by traits of each layer. In this way, multilayer films with enhanced properties, such as impermeability to oxygen and moisture, strength, chemical resistance or color can be produced [5].

An alternative continuous manufacturing technology for the film production is called extrusion film blowing process. In this process, the extruded tube is inflated by an internal pressure into the shape of bubble having a thin wall thickness, quenched and hauled off. On par to this competing film production technology, films that are fabricated by extrusion film casting have a good transparency, thickness uniformity, smoother surface and are produced at higher production rate [2].

According to the current industrial practice where the wide variety of films is manufactured with requirement on its use in heterogeneous application, a broad range of materials is processed by producers for film casting technology. Frequently used polymeric materials include low density polyethylene, LDPE; high density polyethylene, HDPE; linear low density polyethylene, LLDPE; polypropylene, PP; polyethylene terephthalate, PET; and polystyrene, PS. Extrusion film casting is suitable for low viscosity polymers as well [6].

Owing to vast application variety of these films, there is request for production of wide range of sizes. Film width can range from 0.1 m to 10 m, thickness from 20 μm to 2000 μm [4] at production rate that varies from 70 to 200 m/min. The variation in thickness is reported ranging from 3 to 5 % [1].

1.2 Flow Instabilities

Several polymer processes involve the situation in which the polymer is stretched after initial extrusion. The presence of an air-polymer interface in the drawing zone allows to develop different kinds flow instabilities that place a serious limitation on required film quality and quantity. Their formation is influenced by the processing conditions, heat transfer and rheology of processed polymer. Some of them are observed in most cases, such as neck-in and edge-beading and others only under certain conditions that make the process unstable, such as draw resonance and film rupture. In the following subsections, their description is provided.

1.2.1 Neck-in

Upon exiting the die, the extruded polymer in form of thick sheet exhibits swelling due to viscoelastic nature of the most of the polymers. This molecular stress relaxation is consequently influenced by velocity field rearrangement that takes place during a transition from a confined shear flow in slit die to the extensional one in downstream. As a polymer sheet is hauled off further downstream and stable processing conditions are satisfied, its cross-sectional dimensions are monotonically reduced due to external drawing force exerted on sheet by a rotating take-up drum. Aside from desirable reduction in the film thickness, the reduction in film width is experienced. This defect is called neck-in and can be defined as the difference between film half-width at the die exit and final half-width of solidified film (Fig. 2).

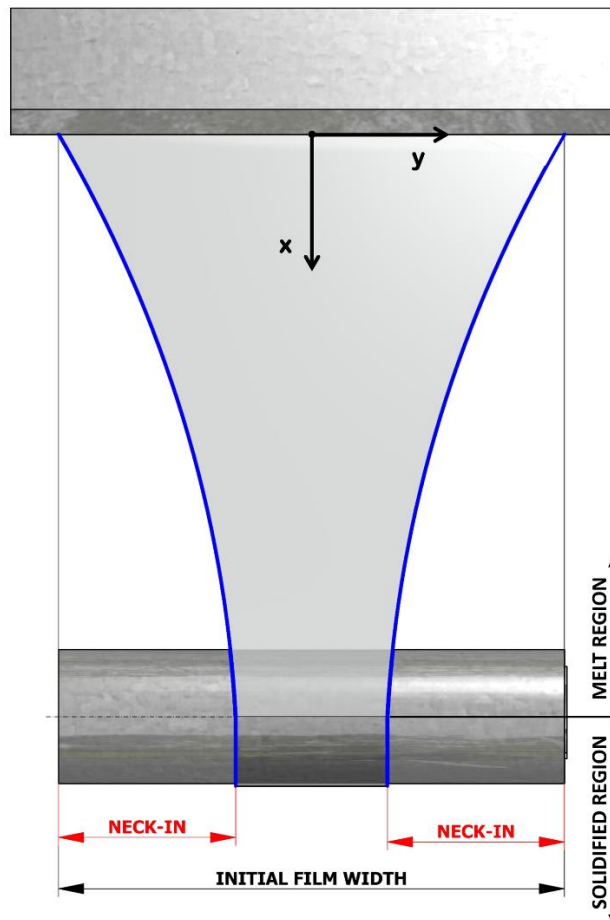


Fig. 2: Visualization of neck-in phenomenon during extrusion film casting.

To minimize the extent of neck-in phenomenon, a drawing length should be kept as short as possible (few centimeters in length) and wide flat die should be used. Neck-in magnitude is also severely impacted by viscoelastic properties of processed polymer melt. Theoretical predictions and numerical simulations

showed that the neck-in extent can be correlated with extensional viscosity hardening of the polymer melt [7–9].

1.2.2 Edge-beading

Beside the neck-in phenomenon, the interrelated defect termed as edge-beading or dog-bone defect is formed making the edge portions of the film substantially thicker than its central part (Fig. 3). The gauge of these elevated parts can be five times higher compared to the center and several centimeters wide. Predominant cause of edge-beads formation is edge-stress effect [10].

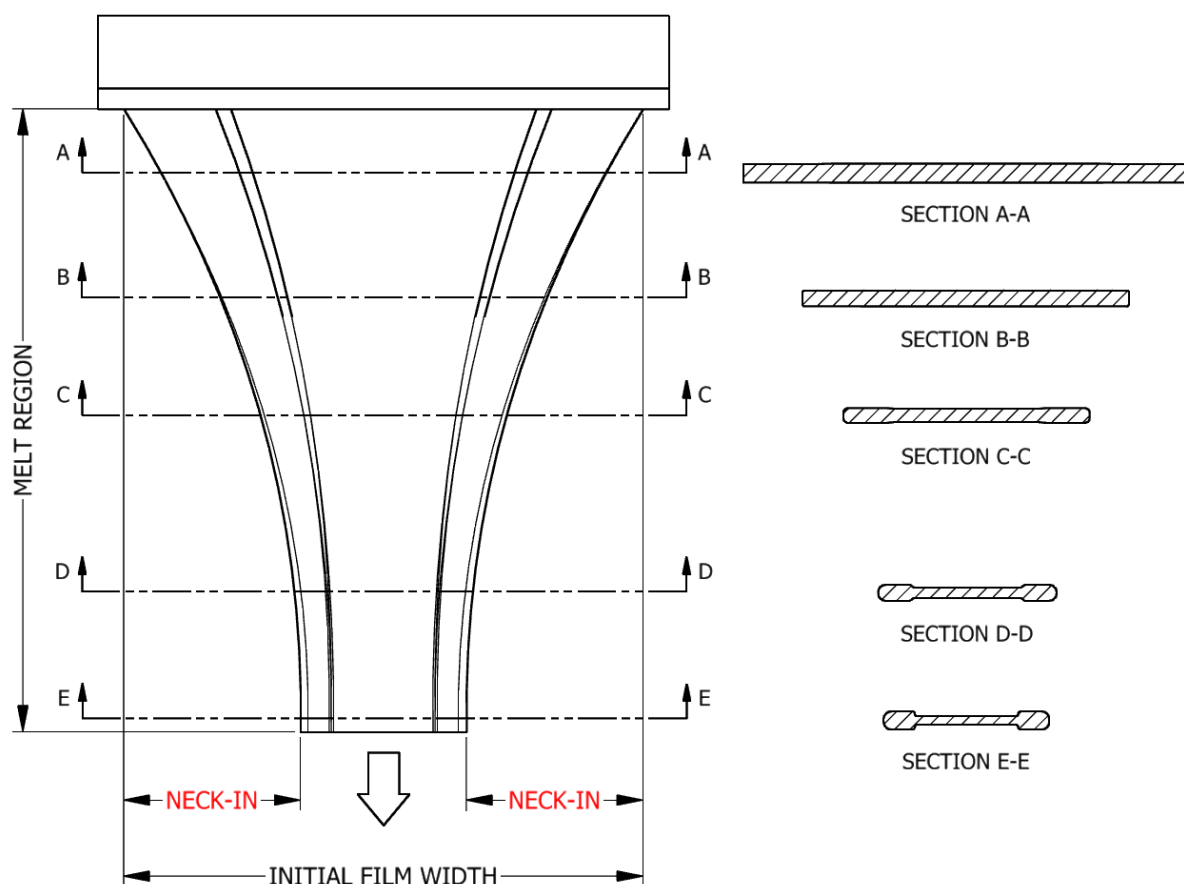


Fig. 3: Visualization of edge-beading phenomenon during extrusion film casting.

Consequently, those elevated edges are often trimmed by a slit razor, scrapped and potentially reprocessed in order to get even film surface. Disregard a large amount of waste material, there are another issue connected with edge-beads causing the air to be trapped between the film and chill roll resulting in turn to worse film quality. Even though formation of edge-beads represents a problem for reasons stated above and manufacturers make an effort to reduce them, their complete elimination might have a consequence in increased extent of neck-in phenomenon. Therefore, in the practice, the technological procedure can be found

when the formation of edge-beads is deliberately supported immediately after the polymer exits the die by the increased die lip opening at the ends of the slit die [4].

1.2.3 Draw Resonance

The stability of the process is considerably influenced by amount of stretching that is experienced by the film in the drawing zone. Thus, to evaluate the intensity of drawing in the take-up length, the draw ratio is introduced and since the take-up velocity is much greater than die exit velocity, its value is imposed higher than unity. The typical value of the draw ratio for the film casting operation is in range of 2 to 20 [4], albeit modern casting lines can operate in the much higher production rates. If the draw ratio achieves (for the given process conditions, die design and polymer used) some critical value, the transient hydrodynamic instability called draw resonance starts to occur, which may limit the processing window considerably.

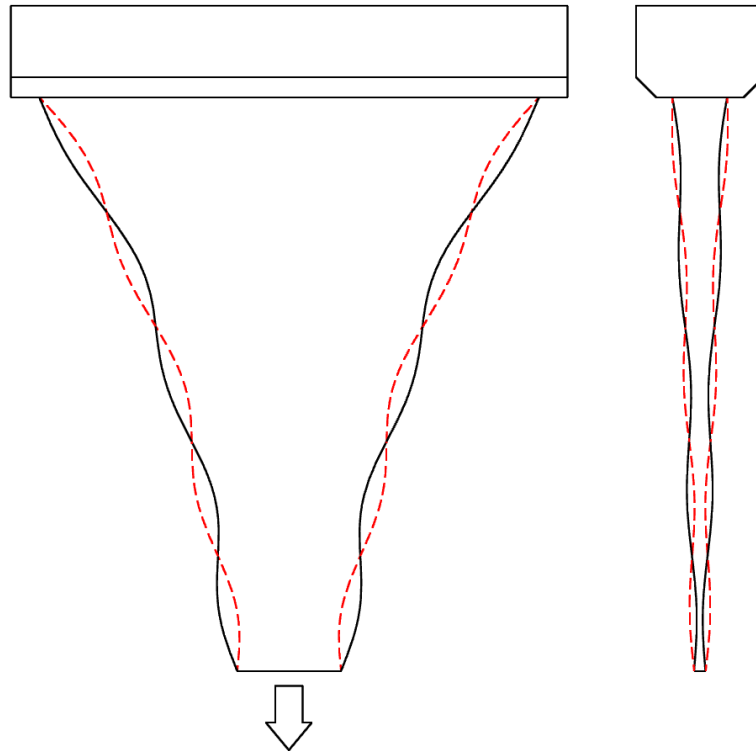


Fig. 4: Visualization of draw resonance experienced during extrusion film casting.

Among the signs of how this flow instability can be manifested belongs sustained oscillation in the film dimensions even though the volumetric flow supplied from the slit die and take-up speed is kept constant (Fig. 4). These sinusoidal oscillations of the same frequency in the film width and thickness (measured in the center of the film) are shifted to each other by the half-wave length (which is the maxima in width and corresponds to minima in thickness) and

vice versa [11]. However, it is worth to note that the results of numerical simulations suggests that the thickness disturbances in the central portion of the film are out-of-phase on par to those at edge part of the film and moreover, the oscillation amplitude is of higher value than that observed in thickness oscillation [12]. Lengthen drawing distance, increased cooling effects and utilization of polymers with strong extensional strain hardening behavior can stabilize process and shift the onset of draw resonance toward higher draw ratios.

Film breakage is another state that can be observed during the process of elevating draw ratio. In this case, the cohesive failure among the polymer chains causes the disintegration of the film if the critical in-film stress is exceeded due to the fact that chains cannot be longer reorganized in way to relieve local stresses in time frame imposed by the deformation. This can be seen in the polymers containing long chain branches or a high molecular weight portion that are processed in combination with high cooling rates in drawing zone, which results to good stability of the process but also in development of the high stretching stress [2].

2. Mathematical Modeling of the Extrusion Film Casting Process

2.1 Literature Review

Polymer sheet or filament drawing has received enormous amount of attention and been studied extensively over the past four decades both experimentally and theoretically (Tab. 1) due to its great importance in the polymer processing industry.

Table 1: Overview of steady-state analyses of film casting process (table adapted from [13–15] and updated for new studies).

Model Dimensionality	Viscous Fluids		Viscoelastic Fluids	
	Isothermal	Non-isothermal	Isothermal	Non-isothermal
1D	[16],[4],[17]	[6],[18],[19],[20],[21]	[22],[23],[24],[25],[26],[27]	[28],[29],[30],[31],[32],[33],[7],[8]
2D	[34]	[15],[35],[36]	[12],[37],[38],[39],[40],[30]	[41],[42],[43]
3D	[44]	[13]	[14]	

Initial efforts were made on a fiber spinning process for which the flow kinematics are similar from a mathematical point of view if considered as the one-dimensional flow case, for Newtonian and Maxwell fluids by Gelder [45] and Fisher [46, 47], respectively. Those studies were aimed on investigating the draw resonance phenomenon which was encountered for the first time by Christensen [48] and Miller [49], and who postulated that the nature of this phenomenon was not of viscoelastic nature because it could be observed in Newtonian fluids as well. Extending the process kinematics into two or three dimensions, the processes become different and one can observe phenomena in film casting that do not have a counterpart in fiber spinning, i.e. neck-in and edge-beading. The preliminary studies mentioned above provided the background for extended studies on EFC. Initial attempts to simulate EFC operations were dedicated to investigation of process stability and determination of draw resonance onset rather than to quantify the extent of neck-in phenomenon. The very first study on modeling of EFC process in this manner was carried out by Yeow [50] with utilization of numerical modeling. He used one-dimensional isothermal model for

Newtonian fluid (planar extensional free surface flow) for steady state solution and investigated the effect of introduced small two-dimensional perturbances on flow stability (namely transverse perturbations). The edge-effects, surface tension, aerodynamic drag and fluid inertia and gravity were neglected. A small curvature of the film together with uniform axial stress and axial velocity over film thickness were assumed. Due to the assumed kinematic in the free surface flow at the drawing section, the model could not capture an edge-bead defect and contraction in film width that was assumed to be infinitely wide. The Film thickness was allowed to vary in machine direction only.

Aird and Yeow [51] continued on this mathematical background for 1D model and extended analysis for power-law fluids. Consequently, Anturkar and Co [52] and Iyengar and Co [22, 53] utilized isothermal modified convected-Maxwell fluid and Giesekus constitutive equations for linear and non-linear analysis in simulations of viscoelastic fluids. First isothermal trials towards necking phenomena modeling were carried out by Sergent [54] and then by Cotto, Duffo and Barq [6, 18, 20] for non-isothermal conditions.

Another milestone work has been set by Dobroth and Erwin [10] who pointed out that the deformation flow in the drawing length comprises of two related regions and the extent of edge-beads and interrelated neck-in phenomenon is determined by the interplay between them through an edge stress effect. While the center of the film undergoes planar extensional deformation, the edge sections are subjected to uniaxial extensional one (see Fig. 5).

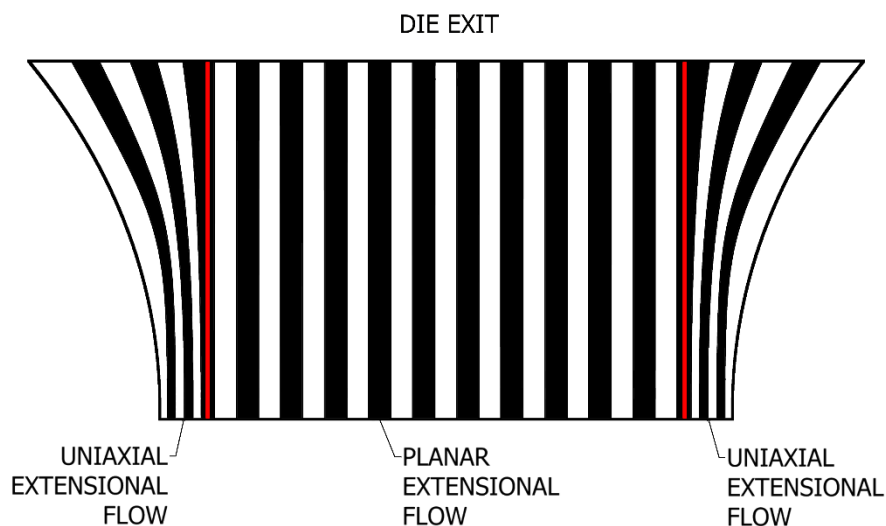


Fig. 5: Visualization of planar and uniaxial extensional flows during extrusion film casting.

In the case of fiber spinning, however, one can observe uniaxial extensional flow only. Some authors endeavored to relate and quantify the gauge of the

observed necking in terms of rheological parameters, such as shear, uniaxial and planar viscosity. Many authors reported that the strain hardening in uniaxial extensional viscosity may depress the extent of necking phenomena [37, 42, 55, 56]. This idea was continued by Ito [57], who related the neck-in extent to rheological parameters, such as the ratio of planar viscosities in axial and transverse directions, and derived an analytical equation for the edge line of a molten film of Newtonian and Maxwell fluid. Along the line of Dobroth and Erwin's article [10], who as the first recognized deformation type in the drawing area, Shiromoto [7, 8, 33], recently, presented the idea that the extent of the necking should not have been described by uniaxial extensional viscosity only in addition to take-up length but as the ratio of planar and uniaxial extensional viscosities reflecting the deformation type in the central and edge portion of the film in the drawing section. Aside from performing non-isothermal viscoelastic simulations, they also proposed a theoretical model based on force balance and deformation type of a film in order to predict necking behavior.

More recently, a 2D membrane model was presented by d'Halewyu [34] and Debbaut [37] for Newtonian and viscoelastic fluids, respectively. This frequently used model was capable of predicting the dog-bone defect, i.e. development of edge-beads, under the stationary conditions. Silagy et al. [58] proceeded forward and enriched the membrane model by a supplementary kinematic hypothesis that was originally brought by Narayanaswamy [59] in his paper on float glass stretching, and carried out an extended isothermal study on the influence of processing conditions on film geometry, and stability analysis of EFC for Newtonian and Maxwell fluid using the UCM constitutive equation. Because of the assumptions used in flow kinematics, this model was able to cover film width reduction and thus predict the neck-in phenomenon but was still not able to predict edge-beading. This limitation was removed in their succeeding work [12] where the 2D isothermal membrane model combined with PTT constitutive equation was developed and obtained steady and transient stability results compared with its 1D predecessor. In the following years, the 1D version of Silagy's membrane model was used in many studies and considerable amount of work has been done on EFC under non-isothermal conditions including crystallization effects by Lamberti et al. [21, 60–62], Lamberti and Titomanlio [62–65], and Lamberti [66]. A three dimensional model for EFC simulation was further developed by Sakaki et al. [44]. The resolution of model equations required a utilization of finite element method. Problem was considered as an isothermal and steady state Newtonian flow. A process parameter space was chosen to reflect the industrial processing conditions. Model captured the development of both neck-in and edge beading and the effect of DR , TUL and die width were investigated. They found out that the gauge of neck-in and edge beading was affected by DR and TUL but not by the die width. The extent of neck-in increased with increasing DR and TUL . Lately, this approach was extended by Zheng et al. [13] for non-isothermal steady Newtonian fluid. Kometani et al. [9] conducted both an experimental and

theoretical investigation of effects of rheological properties on neck-in in film casting. For two tested materials PP and LDPE with no remarkable difference in the viscoelastic properties except the extensional ones (LDPE showed the remarkable increase in extensional viscosity at high strain rates), the neck-in extent for PP under the condition of higher draw ratio was increased over LDPE where neck-in was constant and independent of the draw ratio. Based on these experiments, the authors concluded that neck-in phenomenon in film casting depends on the extensional rheological properties. Furthermore, they utilized simulation based on three different rheological models (the Newtonian, Bird-Carreau and Giesekus model) with aim to evaluate its applicability to the film casting modeling. Results obtained from simulation based on Giesekus model were in quantitative agreement with experimental observation for both polymers, however, the other two utilized models did not provide a data good describing prediction due to their inaccurate expression in extensional viscosity.

The influence of macromolecular architecture on the extent of necking phenomenon has been investigated by Ito et al. [57, 67] (effects of draw ratio and take-up length on necking for LDPE, HDPE and mLLDPE) and Baird et al. [68, 69] (effects of long chain branching and molecular weight distribution on necking for LDPE, mLLDPE and Ziegler-Natta catalyzed LLDPE). Research on multi-layer film casting considering Giesekus fluid has been performed in studies of Pis-Lopez and Co for steady state [70] and stability analysis [71].

Recently, Pol et al. [23, 28] and Chikhalikar et al. [29] have published a series of articles in which they have performed experimental and theoretical investigations of the effects of long chain branching and molecular weight distribution on the necking phenomenon extent. For this purpose, they have utilized the 1D membrane model, originally proposed by Silagy [58], the multi-mode eXtended Pom-Pom constitutive equation and the multi-mode Rolie-Poly stretch constitutive equation, respectively, for the long chain branched (LDPE, PP) and the linear (HDPE, PP) polymers. Fixing the DR and TUL , they found that the extent of necking is lesser for HDPE with a broader molecular weight distribution than that for LLDPE with a narrower molecular weight distribution and further that long chain branched LDPE necks-in to lower extent than linear HDPE or LLDPE. In the succeeding study, Pol and Thete [30] switched from the one-dimensional model that was used in their predecessor works on this theme to the two-dimensional model which was originally proposed by Ito et al. [57] incorporating UCM constitutive equations. Additionally, they derived analytical solution for low and high Deborah numbers. They found that while the film width of modelled LLDPE continuously decreased with increased draw ratio, the film width for LDPE decreased with increased draw ratio in case of long take-up lengths and remained constant for shorter ones. That is, there is existence of a locus of points in the attainable region that divides $DR-De$ plane into sections where the dependence of neck-in on draw ratio has opposite trends.

In their latest work [25], they addressed the effects of the individual viscoelastic relaxation modes of a polymer melt on its behavior in polymer melt extrusion film casting process using UCM and PTT constitutive equations and 1D isothermal membrane model. They found that experimental data for long-chain branched LDPE was described better by UCM model, whereas PTT model provided better simulation results for the linear LLDPE experimental data.

Even though, the real EFC manufacturing process involves complex kinematics and is considered as a 3D problem, whose numerical simulation can be very demanding, it has been proven by many authors that the EFC 1D membrane model (originally proposed by Silagy [58] and if used in combination with appropriate constitutive equations) is capable of providing results that are in good agreement with experiment data.

If viscoelastic constitutive equations are utilized, the additional boundary stress condition at the die exit must be specified. This boundary condition is given by both, flow in the die (upstream) and extensional flow in the drawing length (downstream). Thus, the accurate determination of this additional boundary stress value requires intensive numerical computation [72]. In the following paragraphs, a brief enumeration of approaches used in determination of these type of boundary conditions is provided.

Anturkar and Co [52] in their study, using modified convected Maxwell model, estimated axial component of stress tensor, τ_{xx} , as a mean stress value for fully-developed slit flow in a die of infinitely width. Silagy et al. [58] and [12] based on the works of Denn et al. [73] and Demay et al. [18, 74] assumed two different stress states at the end of the die. In the first case, an extra stress in machine direction, τ_{xx} , is equaled to zero and thus the extra stresses are entirely relaxed due to the die swell, or the second which assumed the mean value of extra stress after flow in an infinite die with a rectangular cross section while the transversal extra stress, τ_{yy} , is set to the value obtained from Newtonian solution. They found that initial stress conditions at the die have a little influence on the final film shape but the calculations were made only for low values of Deborah number. Iyengar and Co [22] have chosen different approach and instead of specifying axial stress component, they have set the ratio τ_{zz}/τ_{xx} at the value between two extreme cases for planar extensional flow and fully-developed slit flow in the die noting that the true stress ratio should have lied in their range. Iyengar [75] then reported that the both extreme cases with corresponding stress ratios provide very similar velocity and stress profiles. Debbaut et al. [37] in their viscoelastic study assumed initial stresses to be zero. Same as the approach in work of Smith [76].

For multilayer film casting analysis (based on the single-mode modified Giesekus model) Pis-Lopez and Co [70, 71] showed that if aspect ratio (defined

here as ratio of total film thickness at the die exit and drawing distance h_0/L is less than 0.05, the velocity and stress profiles converge to the same values does not matter whether the initial stress condition is based on the assumption of fully-developed slit flow or fully-developed planar extensional flow. In another study, utilizing multi-mode model approach, Denn [77] left the longest relaxation mode unspecified at the die exit and rest of the modes was set up with respect to this mode. In contrary, Christodoulou et al. [72] drawn that the shortest mode should be left unspecified with the reasoning that the longest mode $\tau_{xx(N)}^P$ is mainly determined by the flow inside the die, whereas the shorter modes $\tau_{xx(j)}^P$ are determined by the external flow in the air gap.

Beris and Liu [78, 79], in their study on fiber spinning for single mode UCM viscoelastic liquid, specified a die exit stress state via stress ratio of the normal to the axial stress, τ_{yy}/τ_{xx} , and not each component separately. This value has been approximated as the value under homogeneous steady extensional flow at an effective extensional strain rate. For viscoelastic multimode model, Denn [77] specified also $\tau_{xx(j)}^P/\tau_{xx(N)}^P$ for $j < N$ as extra condition to $\tau_{yy(j)}^P/\tau_{xx(j)}^P$ for all relaxation modes.

Devereux and Denn [80] suggested the same distribution among partial stresses as in the case of fully-developed capillary flow with neglected radial partial stresses. Remaining initial stresses were adjusted in order to meet the downstream boundary condition (see Eq. 2.1.1).

$$\frac{\tau_{xx(j)}^P}{\tau_{xx(N)}^P} = \frac{\lambda_j \mu_j}{\sum_{j=1}^N \lambda_j \mu_j} \quad (2.1.1)$$

Note that Gagon and Denn [81] simplified the aforementioned relation for wedge spectrum to form of

$$\frac{\tau_{xx(j)}^P}{\tau_{xx(N)}^P} = \frac{\lambda_j}{\lambda_N} \quad (2.1.2)$$

2.2 Mathematical models

Ideally, the proposed mathematical model should accommodate problem solution in three dimensions where all variables are dependent on all spatial coordinates and covers firstly, the development of the system over time, secondly, a non-isothermal conditions, thirdly, an influence of external forces (such as inertia and gravity) and finally, constitutive equations that can describe the

ultimate behavior of modelled polymer for given deformation and temperature history experienced by the polymer during the flow. The current problem is that consideration of all above mentioned factors in film casting modeling yields very complicated mathematical models, which cannot practically be solved by the existing mathematical tools. Therefore, different simplifying assumptions are applied to simplify the experimental reality leading to the film casting models that can be solved numerically in reasonable computational times. Those typical assumptions are provided bellow:

- Reduction in dimensionality: 1D, 1.5D and 2D;
- Isothermal conditions – constant temperature field
- Non-transient description
- Mechanically and thermally incompressible fluid
- Excluded effects of inertia
- Excluded effects of gravitational forces
- Constant boundary conditions
- Not realistic or simplified constitutive conditions
- Neglected aerodynamic drag
- Neglected surface tension
- Neglected die swell
- Neglected self-weight of the polymer
- Neglected edge-effects
- Excluded crystallization (temperature, flow-induced)
- Neglected the sag of film in non-vertical installations (film curvature)
- Effects from additional devices (air knife, vacuum box, electrostatic pinning)

2.2.1 One-dimensional Film Casting Model of Infinite Width

The first efforts to model extrusion film casting were dedicated to accommodate the basic behavior exhibited by a drawn polymer in the drawing zone [22, 50–52, 82]. This first approximation was based on an idea of the infinite film width. In this one-dimensional representation of flow kinematic, neck-in and edge-beading effects are not taken into account. Design of this model assumes that the velocity field can be described in the following way

$$\begin{aligned} v_x &= v_x(x, t) \\ v_y &= 0 \end{aligned} \tag{2.2.1.3}$$

that is, the flow deformation in the drawing region is mainly planar.

Despite to this limitation, the one-dimensional model of infinite width can present a convenient framework for parametric studies with good approximation

of real cast lines where the die width is superior over the take-up length [10]. Responses of the system to the input changes, such as processing conditions or material parameters, might be more readily correlated to changes in the output, such as effects on film thickness or onset of draw resonance. Moreover, it can be stated in a close-form, especially for simple Newtonian fluids, thus its solution does not require employment of numerical tools.

2.2.2 One-dimensional Film Casting Model of Varying Width

To overcome limitation stemming from the assumptions taken for the infinite width model, one-dimensional film casting model with variable film width was proposed [12, 58]. This simplified model that retain the capability to cover film width reduction in drawing length at reduced dimensionality of resolved problem, is based on assumption that all velocity components are exclusive function of a position in a drawing length, x , at certain time, t , and vary linearly with respect to its corresponding direction.

Thus, velocity field is assumed in form of

$$\begin{aligned} v_x &= v_x(x, t) \\ v_y &= yf(x, t) \end{aligned} \tag{2.2.2.4}$$

and continuity equation yields

$$v_z = -zg(x, t) \tag{2.2.2.5}$$

However, based on the numerical simulations of Debbaut et al. [37] for viscoelastic fluids and experimental observations of Dobroth and Erwin [10], the flow in downstream is divided into regions where the central part of the film exhibits planar extensional flow whereas lateral part shows uniaxial extensional deformation flow that is not fully in compliance with taken assumption of linearly varied velocity component in thickness direction with thickness.

2.2.3 Two-dimensional Film Casting Model

The lower dimensional variants of film casting model can provide a reasonable estimate of draw resonance onset or neck-in phenomenon extent, if used with advanced constitutive equations, but cannot account for edge-bead formation. Therefore, the two-dimensional models having the ability to better describe a complex flow situation experienced by the polymer in drawing length were developed [34, 37]. Essential idea comes from the statement that the one dimension of the film is small in comparison to others [34], which is so-called the membrane hypothesis. Film thickness is much smaller than the film width and the take-up length, hence the velocity component in machine and transversal direction

can be assumed independent of thickness direction, that is, uniform across the thickness.

Then, the velocity field in the casted molten film can be written in form of

$$v_x = v_x(x, y, t) \tag{2.2.3.6}$$

$$v_y = v_y(x, y, t)$$

and the continuity equation gives

$$v_z = -z \left(\frac{\partial v_x}{\partial x} + \frac{\partial v_y}{\partial y} \right) \tag{2.2.3.7}$$

THE AIMS OF THE DOCTORAL RESEARCH WORK

The major goal of the doctoral research work is to firstly, derive viscoelastic extrusion film casting model utilizing 1.5D membrane approximation, modified Leonov model as the constitutive equation and energy equation coupled with an advanced crystallization kinetic (considering thermally as well as stress induced crystallization) and secondly, to develop stable numerical scheme allowing to solve the proposed model in order to reveal the complicated relationship between polymer melt rheology, die design, process conditions and undesirable neck-in phenomenon. The key aims can be formulated as following:

- Validation of the proposed model predictions with literature experimental data for different polymer melts and processing conditions.
- Elucidate the role of planar to uniaxial extensional viscosity ratio, extensional strain hardening, Deborah number and die exit stress state (quantified via second to first normal stress difference ratio, $-N_2/N_1$) on the neck-in phenomenon.
- Quantification of the neck-in phenomenon via a simple dimensionless analytical equation.
- Investigation the role of heat transfer coefficient, draw ratio, die exit temperature and flow induced crystallization on the production of flat polymeric membranes with specific attention to neck-in phenomenon.

3. Viscoelastic Modeling of Non-isothermal Extrusion Film Casting Process Considering Temperature and Stress Induced Crystallization

3.1 Modified Leonov Model

The utilized constitutive equation is based on heuristic thermodynamic arguments resulting from the theory of rubber elasticity [83–88]. In this approach, a fading memory of the melt is determined through an irreversible dissipation process driven by the dissipation term, b . From mathematical viewpoint, it is relating the stress and elastic strain stored in the material as:

$$\underline{\underline{\tau}} = 2 \left(\underline{\underline{c}} \cdot \frac{\partial W}{\partial I_{1,c}} - \underline{\underline{c}}^{-1} \cdot \frac{\partial W}{\partial I_{2,c}} \right) \quad (3.1.8)$$

where $\underline{\underline{\tau}}$ is the stress, and W , the elastic potential, which depends on the invariants $I_{1,c}$ and $I_{2,c}$ of the recoverable Finger tensor, $\underline{\underline{c}}$,

$$W = \frac{3G}{2(n+1)} \left\{ [1-\beta] \cdot \left[\left(\frac{I_{1,c}}{3} \right)^{n+1} - 1 \right] + \beta \left[\left(\frac{I_{2,c}}{3} \right)^{n+1} - 1 \right] \right\} \quad (3.1.9)$$

where G denotes linear Hookean elastic modulus, β and n are numerical parameters. Leonov assumed that the dissipative process acts to produce an irreversible rate of strain, $\underline{\underline{e}}_p$

$$\underline{\underline{e}}_p = b \left[\underline{\underline{c}} - \frac{I_{1,c}}{3} \underline{\underline{\delta}} \right] - b \left[\underline{\underline{c}}^{-1} - \frac{I_{2,c}}{3} \underline{\underline{\delta}} \right] \quad (3.1.10)$$

which spontaneously reduces the rate of elastic strain accumulation. Here, $\underline{\underline{\delta}}$ is the unit tensor and b stands for dissipation function defined by Eq. 3.1.12. This elastic strain, $\underline{\underline{c}}$, is related to the deformation rate tensor, $\underline{\underline{D}}$, as follows

$$\overset{\circ}{\underline{\underline{c}}} - \underline{\underline{c}} \cdot \underline{\underline{D}} - \underline{\underline{D}} \cdot \underline{\underline{c}} + 2\underline{\underline{c}} \cdot \underline{\underline{e}}_p = 0 \quad (3.1.11)$$

where $\overset{\circ}{\underline{\underline{c}}}$ is the Jaumann (corotational) time derivative of the recoverable Finger strain tensor. In this work, the Mooney potential (i.e. $n=0$ in Eq. 3.1.9), and the dissipation function, b , proposed in [89] (see Eq. 3.1.12) have been employed.

$$b(\mathbf{I}_{1,c}) = \frac{1}{4\lambda} \left\{ \exp \left[-\xi \sqrt{\mathbf{I}_{1,c} - 3} \right] + \frac{\sinh \left[\nu (\mathbf{I}_{1,c} - 3) \right]}{\nu (\mathbf{I}_{1,c} - 3) + 1} \right\} \quad (3.1.12)$$

Here, ξ and ν are adjustable model parameters.

$$\mathbf{I}_{1,c} = \text{tr}(\underline{\underline{c}}) \quad (3.1.13)$$

$$\text{tr}(\underline{\underline{c}}) = c_{xx} + c_{yy} + c_{zz} \quad (3.1.14)$$

$$\mathbf{I}_{2,c} = \frac{1}{2} \left\{ \left[\text{tr}(\underline{\underline{c}}) \right]^2 - \text{tr}(\underline{\underline{c}}^2) \right\} \quad (3.1.15)$$

$$\mathbf{I}_{2,c} = c_{xx}^{-1} + c_{yy}^{-1} + c_{zz}^{-1} \quad (3.1.16)$$

Differentiating Eq. 3.1.9 with respect to the first and second invariant of the recoverable Finger tensor yields

$$\frac{\partial W}{\partial \mathbf{I}_{1,c}} = \frac{1}{2} G \left(\frac{\mathbf{I}_{1,c}}{3} \right)^n (1 - \beta) \quad (3.1.17)$$

$$\frac{\partial W}{\partial \mathbf{I}_{2,c}} = \frac{1}{2} G \beta \left(\frac{\mathbf{I}_{2,c}}{3} \right)^n \quad (3.1.18)$$

Combination of Eq. 3.1.8 with Eqs. 3.1.17–3.1.18 leads to the following expression for the extra stress tensor.

$$\underline{\underline{\tau}} = G \left\{ \underline{\underline{c}} \left[\left(\frac{\mathbf{I}_{1,c}}{3} \right)^n (1 - \beta) \right] - \underline{\underline{c}}^{-1} \left[\beta \left(\frac{\mathbf{I}_{2,c}}{3} \right)^n \right] \right\} \quad (3.1.19)$$

3.2 Membrane Model of Film Casting

In this Ph.D. thesis, the 1.5D membrane model developed by Silagy et al. [58] was used as the basic to model the extrusion film casting process. The model essentially features two hypotheses to facilitate the description of the stress and velocity field development in the film drawing. Firstly, the total stress in the film thickness direction is assumed to be equal to zero because this dimension is small compared to other dimensions and secondly, velocities in the width and thickness direction are allowed to vary linearly with y and z position, respectively, for the given x location, which represents a supplementary kinematic hypothesis

(formerly adopted in the work of Narayanaswamy [59] for the modeling of glass manufacturing by the float process) in order to reduce the dimensionality of the task. Even though, the dimensionality of the model can be considered as a unity (all model variables are x -direction dependent only), it possess the capability to predict both, the reduction in film thickness as well as film width shrinkage. From this point of view, the model might be considered as a pseudo 2D or 1.5D.

Furthermore, the inertia, gravity, surface tension and aerodynamic drag are neglected in this model because they are usually much smaller in comparison with the stresses generated in the viscoelastic polymer melt. Finally, the original membrane model for EFC is based on the assumption of process isothermality, which can be justifiable for small enough drawing lengths and/or very high draw-down speeds [19]. However, this assumption seems to be false under processing conditions, where the melt has enough time to cool down, i.e. fabrication of porous membranes [90–94]. Therefore, in this work, the process is treated as a non-isothermal considering a thermally induced crystallization as well as flow induced crystallization. The detailed description of the utilized model is provided below.

3.2.1 Velocity Field

The Cartesian system axes are directed as follows (Fig. 1): in-film-plane axes x and y , where x points in the streamwise direction and y is perpendicular onto it, and z axis is normal to the film xy plane with origin deployment in the cross-sectional center of gravity at the die exit. The dimensions of the film are denoted as follows: take up length is X , initial film half-width is L_0 , and initial half-thickness is e_0 . The intensity of film drawing is expressed in terms of draw ratio (DR) that relates the final tangential velocity of the film at the chill roll, $u(X)$, to the film velocity at the die exit, u_0 . The quantities without a zero subscript denotes non-initial corresponding dimensions at any given x position. The influence of extrudate swelling on the casting process is assumed to be negligible here. Using the symmetry of the problem and the kinematic hypothesis, the complexity of the velocity field involved in the film drawing is reduced, where each of the components is the function of all spatial and time variables. In the resulting form, the velocity field for steady solution is approximated as follows:

$$\begin{aligned} u &= u(x) \\ v &= v(x, y) = yf(x) \\ w &= w(x, z) = zg(x) \end{aligned} \tag{3.2.1.20}$$

where u , v and w are the velocity components in the machine, transverse, and thickness direction, respectively. The deformation rate tensor, which is based on Eq. 3.2.1.20, takes the following form:

$$\underline{\underline{D}} = \begin{bmatrix} \frac{du}{dx} & \frac{1}{2}y \frac{df}{dx} & \frac{1}{2}z \frac{dg}{dx} \\ \frac{1}{2}y \frac{df}{dx} & f(x) & 0 \\ \frac{1}{2}z \frac{dg}{dx} & 0 & g(x) \end{bmatrix} \quad (3.2.1.21)$$

Since the polymer flow in EFC is mainly extensional and in an effort to increase simplicity, the shear rate components can be neglected in favor of extensional ones in Eq. 3.2.1.21, which leads to the following final expression for the deformation rate tensor:

$$\underline{\underline{D}} = \begin{bmatrix} \frac{du}{dx} & 0 & 0 \\ 0 & f(x) & 0 \\ 0 & 0 & g(x) \end{bmatrix} \quad (3.2.1.22)$$

The film thickness is constant throughout the film width due to the assumed velocity field, where the v and w velocity components are dependent on x variable only and are allowed to vary linearly over the film width and thickness, respectively, due to the applied Narayanaswamy's supplementary kinematic hypothesis as mentioned above.

3.2.2 Continuity Equation

The continuity equation requires the conservation of mass at any given streamwise position and with the incompressibility hypothesis takes the following form.

$$\frac{d}{dt}(eL) + \frac{d}{dx}(eLu) = 0 \quad (3.2.2.23)$$

Since the transient solution of the equation is not an objective of this study, the derivative with respect to time can be neglected. For steady state solution, the derivative with respect to time is

$$\frac{d}{dt}(eL) = 0 \quad (3.2.2.24)$$

and thus, the volumetric flow rate at the die exit position and at any given streamwise position is given by Eq. 3.2.2.25 and Eq. 3.2.2.26, respectively.

$$e_0 L_0 u_0 = Q \quad (3.2.2.25)$$

$$e(x) L(x) u(x) = Q \quad (3.2.2.26)$$

It is important to mention that the volumetric flow rate Q here corresponds to $1/4^{\text{th}}$ of the cross-section only due to the process symmetry as show in [32].

3.2.3 Momentum Conservation Equation

Considering the membrane approximation for the thin film in the presence of a constant drawing force, the stresses are constant over the cross section of the film, which leads to the force balance having the following form

$$\frac{d}{dx} (\sigma_{xx} Le) = \frac{dF}{dx} = 0 \quad (3.2.3.27)$$

Neglecting gravity, inertia, aerodynamic friction and surface tension forces, the drawing force becomes x -direction independent, which is fully balanced by the stresses generated in the film.

$$F = \text{const} = \sigma_{xx} Le \quad (3.2.3.28)$$

In this equation, σ_{xx} stands for the first diagonal component of the total stress tensor, $\underline{\underline{\sigma}}$, which is defined via the extra stress tensor, $\underline{\underline{\tau}}$, as follows

$$\underline{\underline{\sigma}} = -p \underline{\underline{\delta}} + \underline{\underline{\tau}} = \begin{bmatrix} -p + \tau_{xx} & 0 & 0 \\ 0 & -p + \tau_{yy} & 0 \\ 0 & 0 & -p + \tau_{zz} \end{bmatrix} \quad (3.2.3.29)$$

where p stands for the isotropic pressure, $\underline{\underline{\delta}}$ is the unity tensor. As it can be seen from Eq. 3.2.3.29, the diagonal components of the total stress tensor are defined as

$$\begin{aligned} \sigma_{xx} &= -p + \tau_{xx} \\ \sigma_{yy} &= -p + \tau_{yy} \\ \sigma_{zz} &= -p + \tau_{zz} \end{aligned} \quad (3.2.3.30)$$

The membrane approximation requires zero value of the thickness-wise component of total stress tensor, $\sigma_{zz} = 0$, which leads to

$$0 = -p + \tau_{zz} \quad (3.2.3.31)$$

i.e.

$$\tau_{zz} = p \quad (3.2.3.32)$$

Substituting Eq. 3.2.3.32 back into expression for stress components Eq. 3.2.3.30, the hydrostatic pressure term is eliminated, which leads to the following final expression for the diagonal components of the total stress tensor

$$\begin{aligned} \sigma_{xx} &= \tau_{xx} - \tau_{zz} \\ \sigma_{yy} &= \tau_{yy} - \tau_{zz} \\ \sigma_{zz} &= 0 \end{aligned} \quad (3.2.3.33)$$

After substitution of σ_{xx} , which is given by Eq. 3.2.3.33, into Eq. 3.2.3.28, the final form of the force balance equation is obtained

$$(\tau_{xx} - \tau_{zz})Le = F \quad (3.2.3.34)$$

3.2.4 The Stress-free Surface Boundary Condition

Assuming the surface tension and air drag are negligible, the net force per unit surface at the film free surface is equal to zero:

$$\underline{\underline{\sigma}} \cdot \underline{\underline{n}} = 0 \quad (3.2.4.35)$$

where the $\underline{\underline{n}}$ is the unit vector normal to the free film surface. This yields the following expression relating the stress state of the film with the film half-width at given x position:

$$\left(\frac{dL}{dx} \right)^2 = \frac{\sigma_{yy}}{\sigma_{xx}} \quad (3.2.4.36)$$

3.2.5 The Kinematic Free-surface Boundary Condition

The fluid is enclosed in the boundaries of the free surface, which can be expressed as

$$\underline{\underline{u}} \cdot \underline{\underline{n}} = 0 \quad (3.2.5.37)$$

where $\underline{\underline{u}}$ is the tangential velocity at the film-air interface. Combination of Eq. 3.2.5.37 with the equation of continuity leads to

$$u(x) \frac{dL}{dx} - f(x)L = 0 \quad (3.2.5.38)$$

$$u(x) \frac{de}{dx} - g(x)e = 0 \quad (3.2.5.39)$$

where $f(x)$ and $g(x)$ are components of the deformation rate tensor (see Eq. 3.2.1.22) in the width and thickness direction, respectively, which can simply be expressed as

$$f(x) = \frac{u(x)}{L} \frac{dL}{dx} \quad (3.2.5.40)$$

$$g(x) = \frac{u(x)}{e} \frac{de}{dx} \quad (3.2.5.41)$$

3.2.6 Dimensionless Transformation

For the sake of simplicity and scaling purposes, the dimensionless transformation has been introduced into the previously derived equations (having similar form as in [58]). Corresponding dimensionless quantities are denoted here with the overline symbol. Dimensionless transformation for the extra stress tensor and total stress tensor is defined here as

$$\bar{\tau}_{ii} = \frac{\tau_{ii} e_0 L_0}{F} \quad (3.2.6.42)$$

$$\bar{\sigma}_{ii} = \frac{\sigma_{ii} e_0 L_0}{F} \quad (3.2.6.43)$$

whereas the dimensionless spatial dimensions and streamwise velocity component are

$$\bar{x} = \frac{x}{X} \quad (3.2.6.44)$$

$$\bar{e} = \frac{e}{e_0} \quad (3.2.6.45)$$

$$\bar{L} = \frac{L}{L_0} \quad (3.2.6.46)$$

$$\bar{u} = \frac{u}{u_0} \quad (3.2.6.47)$$

Dimensionless numbers, such as draw ratio, DR , Deborah number, De , aspect ratio, A , and dimensionless force, E , are defined as follows

$$DR = \frac{u(X)}{u_0} \quad (3.2.6.48)$$

$$De = \frac{\lambda u_0}{X} \quad (3.2.6.49)$$

$$A = \frac{X}{L_0} \quad (3.2.6.50)$$

$$\frac{1}{E} = \frac{FX}{G\lambda e_0 L_0 u_0} \quad (3.2.6.51)$$

Introducing the dimensionless transformation into the continuity equation (Eq. 3.2.2.26) and momentum conservation equation (Eq. 3.2.3.34) leads to the following dimensionless implicit forms

$$\bar{e}\bar{L}\bar{u} = 1 \quad (3.2.6.52)$$

$$\left(\bar{\tau}_{xx} - \bar{\tau}_{zz}\right)\bar{L}\bar{e} = 1 \quad (3.2.6.53)$$

Substitution of Eq. 3.2.6.52 into Eq. 3.2.6.53 gives

$$\left(\bar{\tau}_{xx} - \bar{\tau}_{zz}\right) - \bar{u} = 0 \quad (3.2.6.54)$$

and differentiating Eq. 3.2.6.52 and Eq. 3.2.6.54 with respect to x variable, one can obtain

$$\frac{1}{\bar{e}} \frac{d\bar{e}}{d\bar{x}} + \frac{1}{\bar{L}} \frac{d\bar{L}}{d\bar{x}} + \frac{1}{\bar{u}} \frac{d\bar{u}}{d\bar{x}} = 0 \quad (3.2.6.55)$$

$$\frac{d\bar{\tau}_{xx}}{d\bar{x}} - \frac{d\bar{\tau}_{zz}}{d\bar{x}} - \frac{d\bar{u}}{d\bar{x}} = 0 \quad (3.2.6.56)$$

After rearrangement, the derivative of the dimensionless film half-thickness and axial velocity with respect to x are finally defined as

$$\frac{d\bar{e}}{d\bar{x}} = -\left(\frac{1}{\bar{L}} \frac{d\bar{L}}{d\bar{x}} + \frac{1}{\bar{u}} \frac{d\bar{u}}{d\bar{x}}\right)\bar{e} \quad (3.2.6.57)$$

$$\frac{d\bar{u}}{d\bar{x}} = \frac{d\bar{\tau}_{xx}}{d\bar{x}} - \frac{d\bar{\tau}_{zz}}{d\bar{x}} \quad (3.2.6.58)$$

The dimensionless forms for $f(x)$ and $g(x)$ functions, which were derived from the kinematic free-surface boundary condition and appear in the deformation rate tensor, are the following

$$\bar{f} = \frac{L_0}{u_0} f(x) \quad (3.2.6.59)$$

$$\bar{g} = \frac{e_0}{u_0} g(x) \quad (3.2.6.60)$$

Finally, the dimensionless transformation for the x -direction derivative of the film half-width (arising from Eq. 3.2.3.33 and Eq. 3.2.4.36) yields

$$\frac{d\bar{L}}{d\bar{x}} = -A \sqrt{\frac{\bar{\tau}_{yy} - \bar{\tau}_{zz}}{\bar{\tau}_{xx} - \bar{\tau}_{zz}}} \quad (3.2.6.61)$$

3.2.7 Extrusion Film Casting Model for the Modified Leonov Model

To combine the modified Leonov constitutive equation and the extrusion film casting model equations, it is necessary to derive the equation for particular stress development along the x axis. The relationship between the dimensionless stress and the recoverable strain, imposed from the modified Leonov model (Eqs. 3.1.8 and 3.1.19), can be described by the following formula (for the case of the Mooney potential, i.e. when $n=0$ and $\beta \neq 0$):

$$\bar{\tau}_{ii} = \frac{E}{De} c_{ii} - \frac{E}{De} c_{ii} \cdot \beta - \frac{E}{De} c_{ii}^{-1} \cdot \beta \quad (3.2.7.62)$$

Differentiating this equation with respect to x leads to

$$\frac{d\bar{\tau}_{ii}}{d\bar{x}} = \frac{E}{De} \frac{dc_{ii}}{d\bar{x}} - \frac{E}{De} \beta \frac{dc_{ii}}{d\bar{x}} - \frac{E}{De} \beta \left(-\frac{1}{c_{ii}^2} \frac{dc_{ii}}{d\bar{x}} \right) \quad (3.2.7.63)$$

where $dc_{ii}/d\bar{x}$ stands for the x-direction derivative of the recoverable strain tensor. This term is defined by Eq. 3.1.11 and for each component of the recoverable strain tensor it takes the following form:

$$\frac{dc_{xx}}{d\bar{x}} = 2c_{xx} \frac{1}{\bar{u}} \frac{d\bar{u}}{d\bar{x}} - \frac{2\bar{b}}{\bar{u}} Z_x \quad (3.2.7.64)$$

$$\frac{dc_{yy}}{d\bar{x}} = 2c_{yy} \frac{1}{\bar{L}} \frac{d\bar{L}}{d\bar{x}} - \frac{2\bar{b}}{\bar{u}} Z_y \quad (3.2.7.65)$$

$$\frac{dc_{zz}}{d\bar{x}} = 2c_{zz} \frac{1}{\bar{e}} \frac{d\bar{e}}{d\bar{x}} - \frac{2\bar{b}}{\bar{u}} Z_z \quad (3.2.7.66)$$

where \bar{b} , Z_i and X_p are defined as

$$\bar{b}(I_{1,c}) = \frac{1}{4De} \left\{ \exp\left[-\xi\sqrt{I_{1,c}-3}\right] + \frac{\sinh\left[v(I_{1,c}-3)\right]}{v(I_{1,c}-3)+1} \right\} \quad (3.2.7.67)$$

$$Z_i = c_{ii} \left(c_{ii}^{-1} - c_{ii}^{-1} + X_p \right) \quad (3.2.7.68)$$

$$X_p = \frac{1}{3} \left(c_{xx}^{-1} + c_{yy}^{-1} + c_{zz}^{-1} - c_{xx} - c_{yy} - c_{zz} \right) \quad (3.2.7.69)$$

Combination of Eq. 3.2.6.58 and Eq. 3.2.7.63 leads to the dimensionless streamwise deformation rate, which takes the following form

$$\begin{aligned} & \bar{b} \left[\beta (Z_x - Z_z) - Z_x + Z_z \right] + \\ \frac{d\bar{u}}{d\bar{x}} = & \frac{\bar{b}\beta \left(\frac{1}{c_{zz}^2} Z_z - \frac{1}{c_{xx}^2} Z_x \right) + \frac{\bar{u}}{\bar{L}} \frac{d\bar{L}}{d\bar{x}} \left(c_{zz} (1-\beta) + \frac{\beta}{c_{zz}} \right)}{\beta (c_{xx} + c_{zz}) - c_{xx} - c_{zz} - \frac{\beta}{c_{xx}} \left(\frac{c_{zz} + c_{xx}}{c_{zz}} \right) + \frac{De\bar{u}}{2E}} \end{aligned} \quad (3.2.7.70)$$

Listed equations in sections 3.2.1–3.2.7 represent the basic isothermal viscoelastic 1.5D membrane model based on constitutive equation of the Leonov model. In order to enhance model into a non-isothermal variant with capability to predict crystallization, the energy equation with an appropriate crystallization kinetics has to be incorporated as described in the following paragraph.

3.2.8 Energy Equation

The energy balance equation [21] takes the following form and accounts for the temperature change, crystallinity and flow dependency of melt viscosity.

$$\frac{dT}{dx} = \frac{2HTC(T_a - T)L}{C_p \dot{m}} + \frac{\Delta H}{C_p} \frac{dX_c}{dx} \quad (3.2.8.71)$$

where, the $L(x)$ is film half-width, HTC is heat transfer coefficient, C_p is specific heat capacity, \dot{m} is mass flow rate in quarter-cross-section, ΔH is latent heat of crystallization, $T(x)$ and T_a is melt and ambient air temperature, respectively, and finally $X_c(x)$ stands for content of crystallinity in the polymer volume. Heat transfer coefficient was chosen to be a constant in this model as a simplification representing a total heat exchange with the surrounding environment. The temperature dependence of melt relaxation time, λ , is described by Arrhenius form with a constant activation energy E_a as follows

$$\lambda = \alpha_T \lambda_0 \quad (3.2.8.72)$$

$$\alpha_T = \exp \left[\frac{E_a}{R} \left(\frac{1}{T} - \frac{1}{T_r} \right) \right] \quad (3.2.8.73)$$

where λ_0 denotes melt relaxation time at the die exit, R is universal gas constant and T_r is reference melt temperature.

Crystallization kinetics

The crystallization kinetics model adopted in this doctoral thesis was originally drawn by Ziabicki [95, 96] and later modified by Lamberti [97]. The quiescent conditions are defined as

$$T_m = T_{mq}^0 \quad (3.2.8.74)$$

On condition that, the flow induced crystallization is not included, the polymer melting temperature and flow induced equilibrium melting temperature are equal.

The volume fraction of crystallized phase, χ_c , and function $P(t)$ expressing the non-linear description of crystallinity evolution, derived according time as

$$\chi_c(t) = \frac{X_c(t)}{X_{eq}} = 1 - \exp \left\{ -[P(t)]^{n_c} \right\} \quad (3.2.8.75)$$

where $K(t)$ is crystallization kinetics constant representing crystallization rate, X_{eq} is the equilibrium volume content of crystallinity (maximum in a crystal phase

that melt can possess) and constant n_c stands for a type of nucleation and crystal evolution. After differentiation with respect to time, the time-evolution formula is

$$\frac{dX_c(t)}{dt} = -X_{eq} \exp\left\{-[P(t)]^{n_c}\right\} \left\{-n[P(t)]^{n_c-1}\right\} \frac{dP(t)}{dt} \quad (3.2.8.76)$$

In the simplified form, the model kinetics proposed by Ziabicki [95, 96] and adopted in this work is as follows

$$K(t) = \frac{d}{dt} P(t) \quad (3.2.8.77)$$

$$K = K_{th} (1 + \dot{T}Z)^{1/n_c} \quad (3.2.8.78)$$

Here, K_{th} term is responsible for the low cooling rate crystallization, κ_1 , κ_2 and E_c are material parameters determined from isothermal test, R is gas constant and T_{mq}^0 denotes equilibrium crystallization temperature. B_{ath} and A_{ath} are material parameters included into the model by Lamberti considering the cooling history and promoting the model to be capable to describe a crystallinity evolution at high cooling rates.

$$K_{th} = \kappa_1 \frac{T(T_m - T)}{(T_m)^2} \exp\left[-\frac{E_c}{RT}\right] \exp\left[-\kappa_2 \frac{(T_m)^2}{T(T_m - T)}\right] \quad (3.2.8.79)$$

Effect of cooling rate on crystallization kinetics constant is covered by non-isothermal function, Z , taking form of

$$Z = -B_{ath} |\dot{T}|^{A_{ath}} \frac{(T_m)^5}{T(T_m - T)^5} \exp\left[\frac{E_c}{RT}\right] \quad (3.2.8.80)$$

where, cooling rate is marked as \dot{T} , the derivative of the film temperature with respect to time, t . The formula for the transition from time to spatial coordinates is following

$$\dot{T} = \frac{dT}{dt} = u \frac{dT}{dx} \quad (3.2.8.81)$$

After its application on Eq. 3.2.8.76 with dimensionless transformation introduced in section 3.2.6 and rearrangement, the final form of equation for the crystallinity evolution in dimensionless spatial coordinates demands

$$\frac{dX_c(\bar{x})}{d\bar{x}} = X_{eq} \exp\left\{-[P(\bar{x})]^{n_c}\right\} n_c [P(\bar{x})]^{n_c-1} \frac{dP(\bar{x})}{d\bar{x}} \frac{X}{\bar{u}u_0} \quad (3.2.8.82)$$

and semi-dimensionless form of energy equation, Eq. 3.2.8.71, is then given as

$$\frac{dT}{d\bar{x}} = \frac{2HTC(T_a - T)\bar{L}X}{C_p \dot{m}} + \frac{\Delta H}{C_p} \frac{dX_c}{d\bar{x}} \quad (3.2.8.83)$$

Effect of crystallinity on viscosity

Beside the effect of temperature on the melt relaxation time, the effect of crystallinity on viscosity is included into the model through the function μ_{X_c} that acts directly on the initial elastic modulus G_0 ; this approach was presented by Titomanlio in [98].

$$G = \mu_{X_c}(X_c)G_0 \quad (3.2.8.84)$$

This S-shaped function remains unity as the amount of crystallinity in volume is low and at the certain point starts to deviate and sharply raise simulating the phase transition from melt to the solid state:

$$\mu_{X_c}(X_c) = 1 + f \exp\left(-\frac{h}{X_c^m}\right) \quad (3.2.8.85)$$

It is worth to note that Eq. 3.2.6.54 is no more globally satisfied as in the original model proposal [58] where modulus G was taken as a constant and from now on must be treated as follows

$$\int_0^{\bar{\tau}_{xx}(X)} d\bar{\tau}_{xx} - \int_0^{\bar{\tau}_{zz}(X)} d\bar{\tau}_{zz} - \int_0^{\bar{u}(X)} d\bar{u} = 0 \quad (3.2.8.86)$$

Flow-induced crystallization

Effect of flow on crystallization is described via molecular strain that increases both growth and nucleation rates. In the used formulation [99], melting temperature is continuously modified according to the current molecular strain as follows

$$T_m(S_F) - T_{mq}^0 = \frac{1}{2} \left[\tanh\left(\frac{S_F - A_1}{A_2}\right) + 1 \right] (A_3 S_F + A_4) \quad (3.2.8.87)$$

where T_{mq}^0 and $T_m(S_F)$ is equilibrium and quiescent melting temperature, and A_{1-4} are experimentally determined parameters, S_F is stretch function expressed here in the following form

$$S_F = I_{1,c} - 3 \quad (3.2.8.88)$$

In the proposed formula, the molecular stretch is measured over the first invariant of recoverable Finger tensor $I_{1,c}$.

3.2.9 Boundary Conditions

The complex and essential explicit model equations constituted in the previous section, namely Eqs. 3.2.6.57, 3.2.6.61, 3.2.7.70, 3.2.7.64, 3.2.7.65, 3.2.7.66 has to be solved with the appropriate set of the boundary conditions. Detailed description of the utilized boundary conditions is provided below.

Upstream boundary conditions:

Taking advantage of the dimensionless transformation, the initial half-width, half-thickness, and streamwise velocity are equal to one.

$$\bar{u}(0) = 1 \quad (3.2.9.89)$$

$$\bar{e}(0) = 1 \quad (3.2.9.90)$$

$$\bar{L}(0) = 1 \quad (3.2.9.91)$$

Due to the employment of the energy equation together with crystallization kinetics equation, two additional conditions for initial melt temperature and crystallinity content (assumed to be a zero) are invoked.

$$T(0) = T_{DIE} \quad (3.2.9.92)$$

$$X_c(0) = 0 \quad (3.2.9.93)$$

Since a viscoelastic constitutive equation is involved in this study, it is necessary to define initial boundary conditions for all three diagonal components of the extra stress tensor $\bar{\tau}_{xx}(0)$, $\bar{\tau}_{yy}(0)$ and $\bar{\tau}_{zz}(0)$ by using Eq. 3.2.7.62. To do that, diagonal components of the recoverable strain tensor at the die exit must be determined as the first by solving the following set of equations

$$\frac{E}{De} \left[(c_{xx} - c_{zz})(1 - \beta) + \beta(c_{zz}^{-1} - c_{xx}^{-1}) \right] - 1 = 0 \quad (3.2.8.94)$$

$$c_{xx}c_{yy}c_{zz} = 1 \quad (3.2.8.95)$$

$$\frac{N_2}{N_1} = - \frac{E \left[c_{zz} - c_{yy} + \beta(c_{yy} + c_{yy}^{-1} - c_{zz} - c_{zz}^{-1}) \right]}{De\bar{u}} \quad (3.2.8.96)$$

Eq. 3.2.8.94 arises from the momentum conservation equation 3.2.3.34 by combination of Eqs. 3.2.6.54, 3.2.7.62 and 3.2.9.89 whereas Eq. 3.2.8.95 represents the incompressibility condition for the given flow situation. Eq. 3.2.8.96 represents normal stress difference ratio at the die exit, which is defined as the ratio of the secondary normal stress difference and primary normal stress difference

$$-\frac{N_2}{N_1} = -\frac{\bar{\tau}_{zz}(0) - \bar{\tau}_{yy}(0)}{\bar{\tau}_{xx}(0) - \bar{\tau}_{zz}(0)} \quad (3.2.9.97)$$

note that, in this equation $\bar{\tau}_{xx}(0) - \bar{\tau}_{zz}(0) = 1$ as the result of Eq. 3.2.6.54 and Eq. 3.2.9.89. As it can clearly be seen from Eq. 3.2.8.96, the $-N_2/N_1$ ratio, which characterizes the polymer melt stress state at the die exit region, has to be provided in order to calculate the initial boundary conditions for the extra stress tensor.

Downstream boundary conditions:

Downstream boundary condition, draw ratio, is prescribed as the desired value that is satisfied by a priori unknown magnitude of the drawing force.

$$\bar{u}(X) = DR \quad (3.2.9.98)$$

3.3 Numerical Scheme

To solve the full set of first-order ordinary differential equations, the numerical scheme based on the 4th order Runge-Kutta method implementing adaptive step-size control was adopted. Process of calculation is commenced by guessing a value of drawing force followed by iterative determination of the stress boundary condition at the die through the components of the recoverable elastic strain tensor to satisfy Eqs. 3.2.8.94, 3.2.8.95 and 3.2.8.96 along with the other boundary conditions for the die exit region, that are constant with the force, and thus do not require evaluation in every iteration (Eqs. 3.2.9.89, 3.2.9.90, 3.2.9.91 and $-N_2/N_1$ ratio). Then the main set of eight differential equation is solved in the following order: crystallization kinetics including flow induced crystallization equations (Eq. 3.2.8.82), energy of equation (Eq. 3.2.8.83), film half-width (Eq. 3.2.6.61), axial velocity (Eq. 3.2.7.70), film half-thickness (Eq. 3.2.6.57) and components of the recoverable elastic strain tensor (Eqs. 3.2.7.64–3.2.7.66). Depending on wheatear the desired draw ratio is achieved, the initially estimated drawing force was iteratively updated (increased/decreased) for every following calculation until convergence using the bisection method. Oscillations in the temperature profile development, that were occasionally present in the calculations inflicting the instability of computation, were fixed by applied

stabilizing method of weighting the result of Eq. 3.2.8.83 for actual and previous position x . Due to a geometrical symmetry of the film, only $1/4^{\text{th}}$ of the film cross-section was used in the calculation as showed in [32]. This basic computational scheme for the determination of unknown process variables was looped according demands of currently conducted parametric studies and eventually complemented by module for a grid linear interpolation to create parametric maps. It was preferred to develop the solver itself in the C++ programming language, to avoid a black box effect, which could have appeared in the case of using a built-in solver in any other commercial mathematical-modeling software. To visualize the obtained data for particular solutions, the solver was coupled with GNUPLOT plotting software for automatic graph generation. Typical computational time for one calculation of prescribed DR was about 1 minute on the PC with the following hardware specifications: CPU: Intel Core i7-7700 at 3.60 GHz, RAM: 32 GB DDR4, GPU: AMD Radeon Pro WX 4100 with 4 GB of video memory, SSD: HP Z TurboDrive G2 512 GB. A schematic representation of the utilized numerical scheme is provided in Fig. 6.

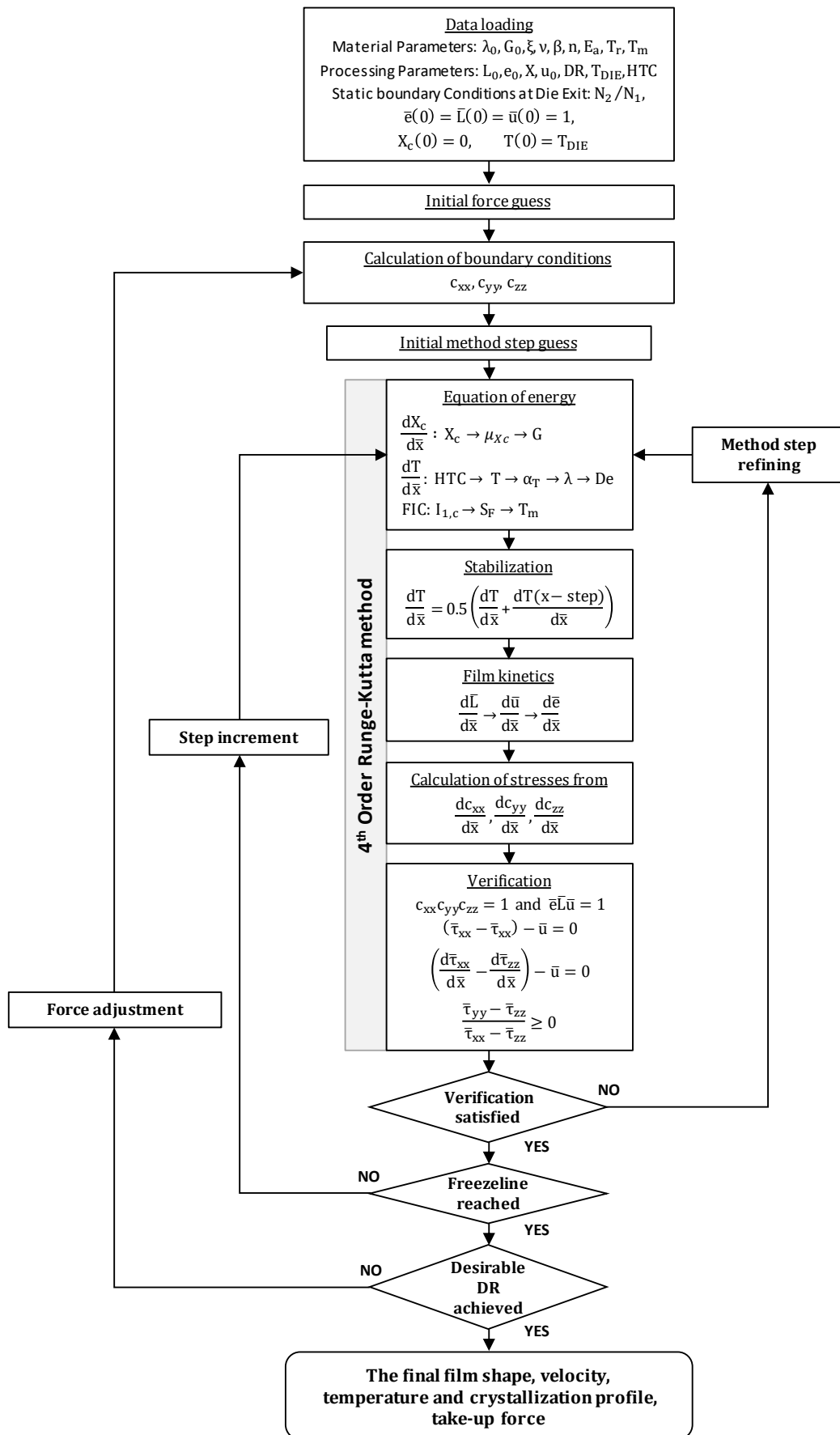


Fig. 6: Flow chart of iteration scheme used to solve of non-isothermal viscoelastic film casting model.

SUMARIZATION OF THE RESEARCH PAPERS

PAPER I–IV

Development of viscoelastic non-isothermal film casting model including temperature and stress induced crystallization

The entire derivation of viscoelastic non-isothermal extrusion film casting model considering temperature and stress induced crystallization is provided in the section 3 of this doctoral thesis.

PAPER I–II

Effect of die exit stress state, Deborah number, uniaxial and planar extensional rheology on the neck-in phenomenon in polymeric flat film production

The effect of second to first normal stress difference ratio at the die exit, $-N_2/N_1$, uniaxial extensional strain hardening, $\eta_{E,U,max}/3\eta_0$, planar-to-uniaxial extensional viscosity ratio, $\eta_{E,P}/\eta_{E,U}$, and Deborah number (via changing the drawing distance, X), De , on the neck-in, NI , has been investigated via viscoelastic non-isothermal modeling utilizing 1.5D membrane model [58] and a single-mode modified Leonov model as the constitutive equation [84, 89]. Based on the performed parametric study, it was found that an increase in $-N_2/N_1$ ratio and De increases both, the maximum attainable normalized neck-in, $NI^*=NI/X$, as well as its sensitivity to $\sqrt{\eta_{E,P}/\eta_{E,U}}$. There exists a threshold value for Deborah number and $\eta_{E,U,max}/3\eta_0$, above which, the NI^* starts to be strongly dependent on the die exit stress state, $-N_2/N_1$. It was found that such critical De decreases if $-N_2/N_1$, $\eta_{E,U,max}/3\eta_0$ increases and/or $\frac{\eta_{E,P,max}}{4\eta_0} / \frac{\eta_{E,U,max}}{3\eta_0}$ decreases. Numerical solutions of the 1.5D membrane viscoelastic model, utilizing modified single-mode Leonov model as the constitutive equation, were successfully approximated by a dimensionless analytical equation (Eq. 99) expressing the NI^* with $\eta_{E,U,max}/3\eta_0$, $\eta_{E,P}/\eta_{E,U}$, $-N_2/N_1$ and De as follows

$$NI^* = \frac{1}{\sqrt[\theta]{\frac{\eta_{E,U,\max}}{3\eta_0}}} \left\{ A_1 \left[1 - \exp(-\alpha_1 De^{\phi_1}) \right] \left(\sqrt{\frac{\eta_{E,P}}{\eta_{E,U}}} - 1 \right) + \delta A_2 \left[1 - \exp(-\alpha_2 De^{\phi_2}) \right] \right\} \quad (99)$$

with δ defined as

$$\delta = 1 + \psi_1 \arctan \left(\psi_2 \frac{N_2}{N_1} \right) \arctan \left(\psi_3 \frac{\eta_{E,U,\max}}{3\eta_0} \tanh(\psi_4 De) \right) \quad (100)$$

where $A_1=0.593$, $\alpha_1=1073.742$, $\phi_1=2.113$, $A_2=0.471$, $\alpha_2=99.757$, $\phi_2=1.162$, $\theta=7.43$, $\psi_1=1.027$, $\psi_2=-0.849$, $\psi_3=0.514$, $\psi_4=3.953$.

Suggested equation was tested by using the experimental data taken from [42], [23, 25, 28] and [7] for five different polyethylenes where $0.011 \leq De \leq 0.253$, $0.825 \leq \frac{\eta_{E,P}}{\eta_{E,U}} \leq 1.910$, $2.047 \leq \frac{\eta_{E,U,\max}}{3\eta_0} \leq 10.096$ and $0.017 \leq -\frac{N_2}{N_1} \leq 0.680$. As it

can be seen in Fig. 7a, the proposed equation can describe for the given polymer melts and processing conditions the experimental data very well within the whole range of investigated Deborah numbers.

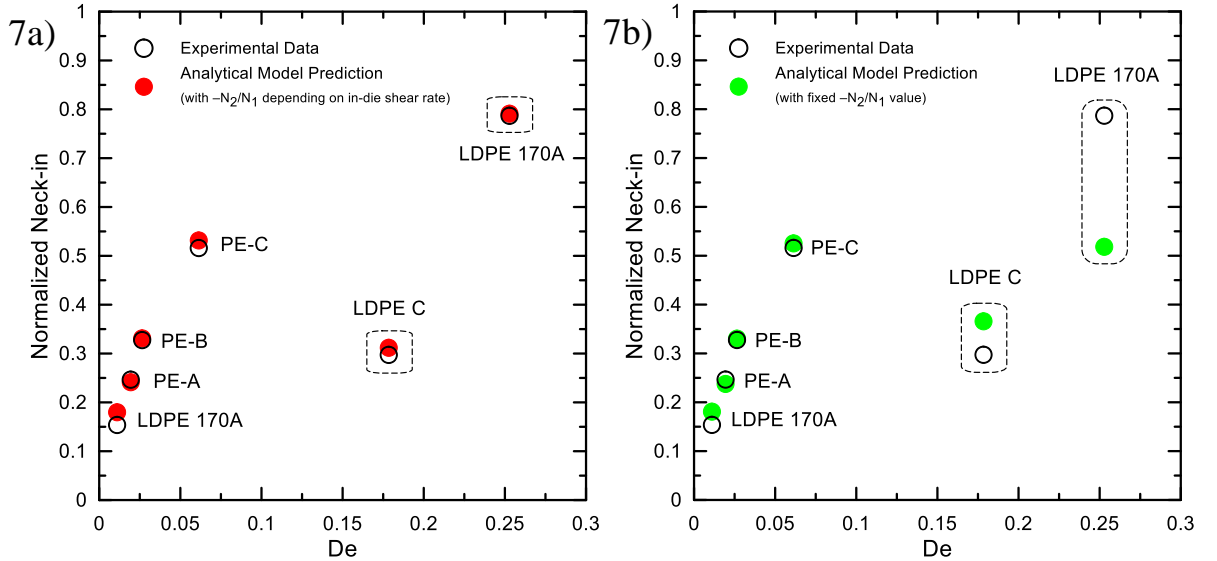


Fig. 7: Normalized maximum attainable neck-in value, NI^* , as the function of Deborah number for LDPE 170A, PE-A, PE-B, PE-C, and LDPE C polymers for the processing conditions summarized in Table 6 in [27]. Experimental data (taken from [23, 25, 28], [7] and [42]) and proposed analytical model predictions (Eq. 99) are given here by the open and filled symbols, respectively. (7a) $-N_2/N_1$ is given by the modified Leonov model predictions for particular die exit shear rates, which are provided in Table 7 in [27] for each individual case, (7b) $-N_2/N_1$ is considered to be constant, equal to 0.2.

Interestingly, the neck-in predictions for Deborah numbers larger than 0.1 became unrealistic, if the $-N_2/N_1$ at the die exit region is not taken into account, which confirms the existence of critical Deborah number, above which, the neck-in phenomenon starts to be strongly dependent on the die exit stress state (see Fig. 7b). It is believed that the obtained knowledge together with the suggested simple analytical model can be used for optimization of the extrusion die design (influencing flow history and thus die exit stress state), molecular architecture of polymer melts and processing conditions to suppress neck-in phenomenon in a production of very thin flat films.

PAPER III

Effect of heat transfer coefficient, draw ratio and die exit temperature on the production of flat iPP membranes

In this part, stable numerical scheme has been developed for 1.5D film casting model utilizing viscoelastic modified Leonov model as the constitutive equation [58, 84, 89] and energy equation coupled with crystallization kinetics of semicrystalline polymers taking into account actual film temperature as well as cooling rate [95–97]. Model has been successfully validated on the experimental data for linear isotactic polypropylene taken from the open literature [100].

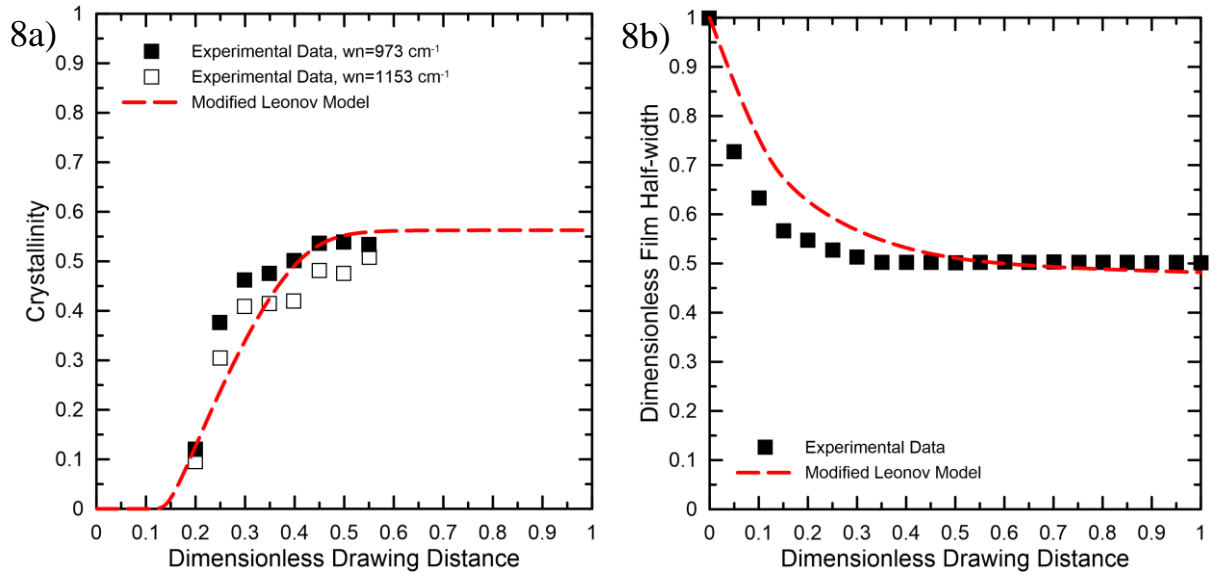


Fig. 8: Comparison between experimental data for iPP T30G ($T_{DIE}=200^{\circ}\text{C}$) and given processing conditions ($De=6\cdot 10^{-4}$, $DR=34.7$, $X=0.4\text{ m}$) taken from [100] and model predictions for dimensionless drawing distance variables considering constant heat transfer coefficient, $HTC=16\text{ J}\cdot\text{s}^{-1}\cdot\text{K}^{-1}\cdot\text{m}^{-2}$. (8a) Dimensionless Final Half-width, (8a) Film crystallinity.

Aspect ratio, A , (0.25–4), draw ratio, DR , (3–140), heat transfer coefficient, HTC , ($1.5\text{--}28\text{ J}\cdot\text{s}^{-1}\cdot\text{K}^{-1}\cdot\text{m}^{-2}$) and die exit melt temperature, T_{DIE} , (200, 225 and 250°C) were systematically varied in the utilized model in order to understand the role of process conditions on the onset of crystalline phase development in production of iPP flat porous membranes via cast film process. It was found that numerically predicted crystallization onset border in A vs. DR dependence for given HTC and T_{DIE} (see example in Fig. 9a) can be successfully approximated by the following simple analytical equation:

$$A = \exp[q_{Xc}(HTC, T_{DIE})] DR^{k_{Xc}(HTC, T_{DIE})} \quad (101)$$

where $q_{Xc}(HTC, T_{DIE})$ and $k_{Xc}(HTC, T_{DIE})$ are given as

$$k_{Xc}(\text{HTC}, T_{\text{DIE}}) = (\gamma_k T_{\text{DIE}} + \delta_k) \text{HTC}^{(\alpha_k T_{\text{DIE}} + \beta_k)} \quad (102)$$

$$q_{Xc}(\text{HTC}, T_{\text{DIE}}) = (\alpha_q T_{\text{DIE}} + \beta_q) \ln(\text{HTC}) + (\gamma_q T_{\text{DIE}} + \delta_q) \quad (103)$$

These equations utilize 3 independent variables (DR , HTC and T_{DIE}) and 8 parameters ($\alpha_k = -0.0056$, $\beta_k = 0.3421$, $\gamma_k = 0.0077$, $\delta_k = -1.2102$, $\alpha_q = 10^{-4}$, $\beta_q = -1.0453$, $\gamma_q = 0.0089$, $\delta_q = -0.3079$).

Utilizing isothermal as well as non-isothermal numerical calculations, it was possible to determine processing conditions (in terms of DR , A and HTC at $T_{\text{DIE}} = 200^\circ\text{C}$) for linear iPP, for which isothermal simulations are too simplistic and therefore the neck-in phenomenon cannot be predicted realistically (see Fig 9b).

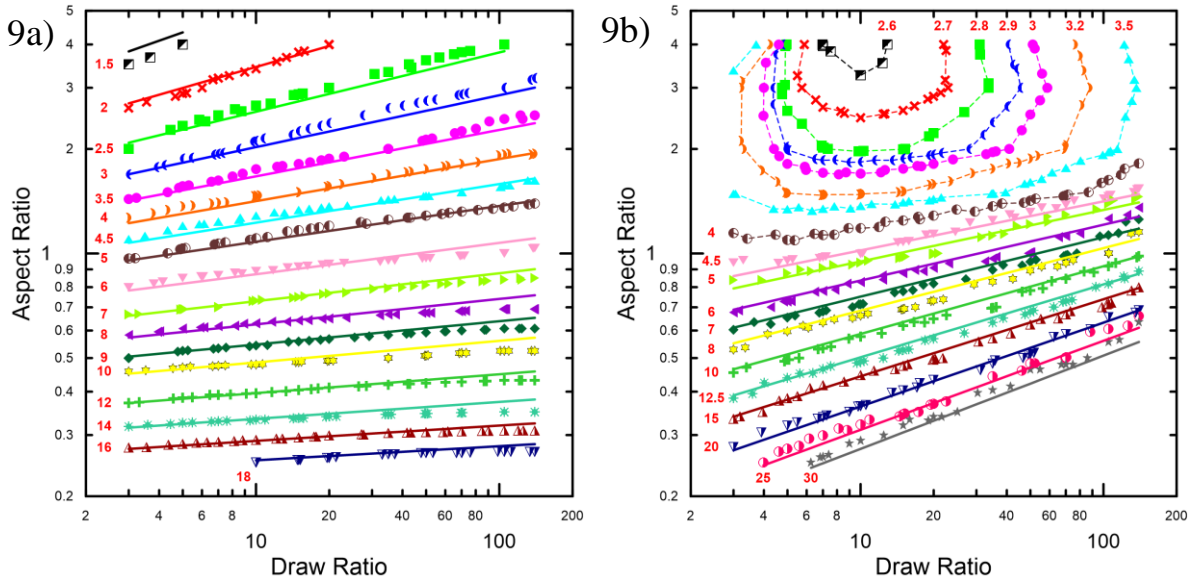


Fig. 9: Effect of draw ratio and heat transfer coefficient (see numbers in $\text{J}\cdot\text{s}^{-1}\cdot\text{K}^{-1}\cdot\text{m}^{-2}$ provided at each data set) on the critical aspect ratio for linear iPP at die exit temperature equal to 200°C . (9a) Crystallization onset borders defining conditions for film production with (area above the border symbols) and without (area below the border symbols) the crystallized phase, (9b) Isothermality boundaries below which the non-isothermal and isothermal calculations gives practically the same neck-in values.

It was possible to find out the following analytical approximation for the “isothermality boundary” in A vs. DR dependence for different $HTCs$, which is applicable within the following range of processing variables: $DR \in \langle 3 - 140 \rangle$, $A \in \langle 0.25 - 4 \rangle$ and $HTC \in \langle 4 - 30 \rangle \text{ J}\cdot\text{s}^{-1}\cdot\text{K}^{-1}\cdot\text{m}^{-2}$.

$$A = \exp[q_{\text{iso}}(\text{HTC})] \text{DR}^{k_{\text{iso}}(\text{HTC})} \quad (104)$$

where $k_{\text{iso}}(\text{HTC})$ and $q_{\text{iso}}(\text{HTC})$ are defined as

$$k_{iso}(HTC) = \alpha_{iso} \ln(HTC) + \beta_{iso} \quad (105)$$

$$q_{iso}(HTC) = \gamma_{iso} \ln(HTC) + \delta_{iso} \quad (106)$$

These equations utilize 2 independent variables (DR , HTC) and 4 parameters obtained by numerical data fitting ($\alpha_{iso}=0.067$, $\beta_{iso}=0.0406$, $\gamma_{iso}=-0.8479$, $\delta_{iso}=-0.9701$).

Finally, the effect of A , DR , HTC and T_{DIE} on the dimensionless film half-width and axial velocity, temperature and crystallinity (all as the function of dimensionless drawing distance) was systematically investigated via non-isothermal simulations for linear iPP. It was found that neck-in can be reduced if A or DR decreases or if HTC or T_{DIE} increases. It has also been showed that produced film crystallinity increases if A increases or if DR or T_{DIE} decreases. The most interestingly, it has been revealed that if the HTC increases above some critical value, film crystallinity increases, reaching the maximum and then decreasing. This suggests that there exists optimum HTC for given material and processing conditions, at which the amount of crystalline phase is maximal. It is believed that the utilized numerical model together with suggested stable numerical scheme as well as obtained research results can help to understand processing window for production of flat porous membranes from linear iPP considerably.

PAPER IV

Viscoelastic simulation of extrusion film casting for linear iPP including stress induced crystallization

Here, 1.5D film casting membrane model proposed by Silagy [58] was generalized considering single-mode modified Leonov model as the viscoelastic constitutive equation [84, 89], energy equation, constant heat transfer coefficient, advanced crystallization kinetics taking into account the role of temperature, cooling rate [95–97] and molecular stretch [98], crystalline phase dependent modulus [65] and temperature dependent relaxation time [8]. The model has been successfully validated for the linear isotactic polypropylene by using suitable experimental data taken from the open literature as it can be seen in Fig. 10.

It has been found that for the given processing conditions, utilization of flow induced crystallization significantly improves predictions for the film temperature and crystallinity whereas its effect on the neck-in phenomenon and axial velocity profile is predicted to be small. Consequent parametric study has revealed that inclusion of FIC in the model allows to predict realistic plateau in the temperature profile as well as monotonic increase in the film crystallinity for the increased

HTC (see Figure Fig. 10b). It was also shown that there is some threshold HTC value (about $12 \text{ J}\cdot\text{s}^{-1}\cdot\text{K}^{-1}\cdot\text{m}^{-2}$ for the studied iPP and given processing conditions), above which melting temperature is changed considerably, abruptly and more closely to the extrusion die due to FIC (see Fig. 11a).

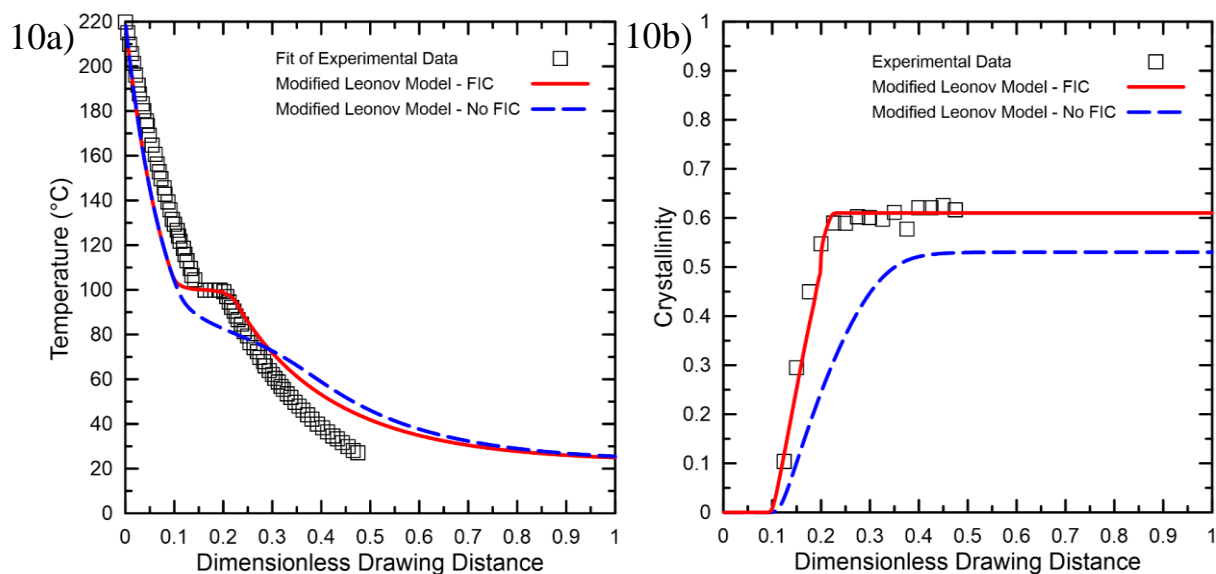


Fig. 10: Comparison between film casting model predictions with and without consideration of Flow Induced Crystallization, FIC, and experimental data taken from [66], $HTC=31 \text{ J}\cdot\text{s}^{-1}\cdot\text{K}^{-1}\cdot\text{m}^{-2}$. (10a) Temperature profile, (10b) Crystallinity profile.

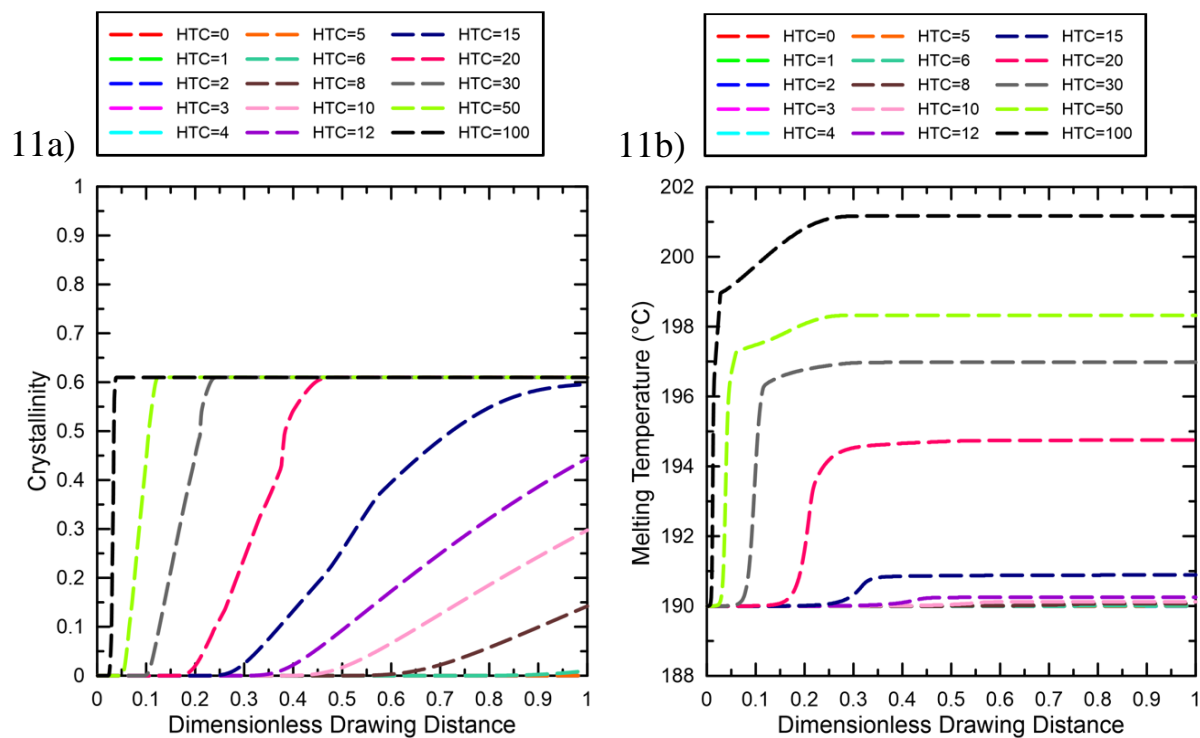


Fig. 11: Predicted effect of HTC on the film crystallinity (left) and melting temperature (right) for iPP at the reference processing conditions.

THE THESIS CONTRIBUTION TO SCIENCE AND PRACTICE

The proposed model and numerical scheme for the viscoelastic, non-isothermal extrusion film casting modeling utilizing a 1.5D membrane model, a modified Leonov model and an advanced crystallization kinetics together with the findings clarifying the fundamental role of variety dimensionless variables (such as planar to uniaxial extensional viscosity ratio, extensional strain hardening, Deborah number, second to first normal stress difference ratio at the die exit, draw ratio, heat transfer coefficient and flow induced crystallization) can be used for material, die design and process conditions optimization in order to minimize unwanted neck-in phenomenon as well as to optimize the extrusion film casting process for different applications of daily and technical use (such as for example separator films for batteries in mobile devices and electric vehicles, foils for capacitors, optical membranes for liquid crystal displays, air and vapor barriers, magnetic tapes for storage of audio video content, packing for consumer products, plastic bags or as product for further processing by other technologies).

The suggested numerical scheme together with the proposed stabilization can be used as the good basic for the viscoelastic non-isothermal modeling of advanced and industrially important polymer processing technologies, in which flow induced crystallization plays the key role.

CONCLUSION

First part of this work summarizes the current state of knowledge in area of polymeric film production via extrusion film casting process and different types of flow instabilities occurring in this technology, such as neck-in, edge beading and draw resonance. Specific attention has been paid to introduction of different approaches for the film casting modeling based on the open research literature.

In the second part of this work, generalized 1.5D film casting membrane model utilizing single-mode modified Leonov model as the viscoelastic constitutive equation and energy equation coupled with advanced crystallization kinetics (taking into account the role of temperature, cooling rate and molecular stretch) has been proposed and successfully tested against relevant experimental data taken from the open literature. By using of the proposed model, it was possible to clarify the role of variety dimensionless variables such as planar to uniaxial extensional viscosity ratio, extensional strain hardening, Deborah number, second to first normal stress difference ratio at the die exit, draw ratio, heat transfer coefficient and flow induced crystallization on the production of polymeric flat films. The key research findings are summarized below:

- It was found that the film casting modeling by using multi-mode XPP model and modified Leonov model is comparable for the given LDPE polymer and processing conditions even if, surprisingly, single-mode version of the Leonov model was used. The consequent parametric study revealed that firstly, if planar to uniaxial extensional viscosity ratio decreases or uniaxial extensional strain hardening increases, intensity of normalized neck-in as well as its sensitivity to draw ratio decreases and secondly, an increase in the second to first normal stress difference ratio at the die exit, $-N_2/N_1$, and Deborah number increases both, the normalized neck-in as well as its sensitivity to planar to uniaxial extensional viscosity ratio. It has also been found that normalized neck-in can be correlated to all the above mentioned variables via a simple dimensionless analytical equation. This correlation can provide detailed view into the complicated relationship between polymer melt rheology, die design, process conditions and undesirable neck-in phenomenon. Obtained results have been validated against literature experimental data for different polyethylene melts and processing conditions.
- It was revealed that there exists critical Deborah number (equal to about 0.1), above which, the neck-in phenomenon starts to be strongly dependent on the die exit stress state, $-N_2/N_1$.

- It was found that numerically predicted crystallization onset border in A vs. DR dependence for given HTC and T_{DIE} can be successfully approximated by the simple analytical equation.
- It was possible to determine processing conditions for linear isotactic PP (expressed numerically or via simple analytical approximation), for which isothermal simulations are too simplistic and therefore the neck-in phenomenon cannot be predicted realistically.
- It was found that normalized neck-in can be reduced if A or DR decreases or if HTC or T_{DIE} increases.
- It has been found that for the processing conditions, in which the cooling rate is very high, utilization of the flow induced crystallization significantly improves predictions for the film temperature and crystallinity whereas its effect on the neck-in phenomenon and axial velocity profile is predicted to be small. Consequent parametric study has revealed that inclusion of flow induced crystallization in the model allows to predict realistic plateau in the temperature profile as well as monotonic increase in the film crystallinity for the increased HTC .
- It was shown that there is some threshold HTC value, above which the melting temperature is changed considerably, abruptly and more closely to the extrusion die due to flow induced crystallization.

REFERENCES

- [1] KANAI, Toshitaka and CAMPBELL, Gregory A. *Film Processing*. Munich : Hanser Publishers, 1999. Progress in polymer processing. ISBN 9781569902523.
- [2] KANAI, Toshitaka and CAMPBELL, Gregory A. *Film Processing Advances*. Second Edi. Munich : Hanser Publishers, 2014. ISBN 978-1-56990-529-6.
- [3] TADMOR, Zehev and GOGOS, Costas G. *Principles of Polymer Processing, 2nd Edition*. Hoboken, New Jersey : John Wiley & Sons, 2006. SPE technical volume. ISBN 978-0-471-38770-1.
- [4] PEARSON, J.R.A. *Mechanics of Polymer Processing*. London : Elsevier Applied Science Publishers, 1985. ISBN 0-85334-308-X.
- [5] SMITH, W.S. *Nonisothermal film casting of a viscous fluid*. McMaster University, 1997.
- [6] COTTO, D., DUFFO, P. and HAUDIN, J.M. Cast film extrusion of polypropylene films. *Int. Polym. Process.* 1989. Vol. 4, no. 2, p. 103–113.
- [7] SHIROMOTO, Seiji, MASUTANI, Yasushi, TSUTSUBUCHI, Masaaki, TOGAWA, Yoshiaki and KAJIWARA, Toshihisa. The effect of viscoelasticity on the extrusion drawing in film-casting process. *Rheologica Acta*. 2010. Vol. 49, no. 7, p. 757–767.
- [8] SHIROMOTO, Seiji. The Mechanism of Neck-in Phenomenon in Film Casting Process. *International Polymer Processing*. 2014. Vol. 29, no. 2, p. 197–206.
- [9] KOMETANI, H., MATSUMURA, T., SUGA, T. and KANAI, T. Experimental and theoretical analyses of film casting process. *Journal of Polymer Engineering*. 2007. Vol. 27, no. 1, p. 1–28.
- [10] DOBROTH, T. and ERWIN, Lewis. Causes of edge beads in cast films. *Polymer Engineering and Science*. 1986. Vol. 26, no. 7, p. 462–467.
- [11] BARQ, P., HAUDIN, J.M., AGASSANT, Jean François, ROTH, H. and BOURGIN, P. Instability phenomena in film casting process. *Int. Polym. Proc.* 1990. Vol. 5, no. 4, p. 264–271.
- [12] SILAGY, David, DEMAY, Yves and AGASSANT, Jean François. Stationary and stability analysis of the film casting process. *Journal of Non-Newtonian Fluid Mechanics*. 1998. Vol. 79, no. 2–3, p. 563–583.
- [13] ZHENG, Hong, YU, Wei, ZHOU, Chixing and ZHANG, Hongbin. Three-Dimensional Simulation of the Non-Isothermal Cast Film Process of Polymer Melts. *Journal of Polymer Research*. 2006. Vol. 13, no. 6, p. 433–440.

- [14] ZHENG, Hong, YU, Wei, ZHOU, Chixing and ZHANG, Hongbin. Three dimensional simulation of viscoelastic polymer melts flow in a cast film process. *Fibers and Polymers*. 2007. Vol. 8, no. 1, p. 50–59.
- [15] SMITH, Spencer and STOLLE, Dieter. Numerical Simulation of Film Casting Using an Updated Lagrangian Finite Element Algorithm. *Polymer Engineering and Science*. 2003. Vol. 43, no. 5, p. 1105–1122.
- [16] BAIRD, Donald G. and COLLIAS, I. Dimitris. Postdie Processing. In : *Polymer Processing: Principles and Design*. Boston : Butterworth-Heinemann, 1995. p. 346. ISBN 9780750691055.
- [17] PEARSON, J.R.A. *Mechanical Principles of Polymer Melt Processing*. Pergamon Press, 1966. ISBN 978-0080131504.
- [18] BARQ, P., HAUDIN, J.M. and AGASSANT, Jean François. Isothermal and anisothermal models for cast film extrusion. *Int. Polym. Process*. 1992. Vol. 7, no. 4, p. 334–349.
- [19] ACIERNO, D., DI MAIO, L. and AMMIRATI, C. C. Film casting of polyethylene terephthalate: Experiments and model comparisons. *Polymer Engineering and Science*. 2000. Vol. 40, no. 1, p. 108–117.
- [20] DUFFO, P., MONASSE, B. and HAUDIN, J.M. Cast film extrusion of polypropylene. Thermomechanical and physical aspects. *Journal of Polymer Engineering*. 1991. Vol. 10, no. 1–3, p. 151–229.
- [21] LAMBERTI, Gaetano, TITOMANLIO, Giuseppe and BRUCATO, Valerio. Measurement and modelling of the film casting process 1. Width distribution along draw direction. *Chemical Engineering Science*. 2001. Vol. 56, no. 20, p. 5749–5761.
- [22] IYENGAR, Vardarajan R. and CO, Albert. Film casting of a modified Giesekus fluid: a steady-state analysis. *Journal of Non-Newtonian Fluid Mechanics*. 1993. Vol. 48, no. 1–2, p. 1–20.
- [23] POL, H.V., THETE, Sumeet S., DOSHI, Pankaj and LELE, Ashish K. Necking in extrusion film casting: The role of macromolecular architecture. *Journal of Rheology*. 2013. Vol. 57, no. 2, p. 559–583.
- [24] BARQ, P., HAUDIN, J.M., AGASSANT, Jean François and BOURGIN, P. Stationary and dynamic analysis of film casting process. *Int. Polym. Process*. 1994. Vol. 9, no. 4, p. 350–358.
- [25] THETE, Sumeet S., DOSHI, P. and POL, H.V. New insights into the use of multi-mode phenomenological constitutive equations to model extrusion film casting process. *Journal of Plastic Film and Sheeting*. 2017. Vol. 33, no. 1, p. 35–71.

- [26] BARBORIK, Tomas, ZATLOUKAL, M. and TZOGANAKIS, C. On the role of extensional rheology and Deborah number on the neck-in phenomenon during flat film casting. *International Journal of Heat and Mass Transfer*. 2017. Vol. 111, p. 1296–1313.
- [27] BARBORIK, Tomas and ZATLOUKAL, Martin. Effect of die exit stress state, Deborah number, uniaxial and planar extensional rheology on the neck-in phenomenon in polymeric flat film production. *Journal of Non-Newtonian Fluid Mechanics*. 2018. Vol. 255, p. 39–56.
- [28] POL, H.V., BANIK, Sourya, AZAD, Lal Busher, THETE, Sumeet S., DOSHI, Pankaj and LELE, Ashish. Nonisothermal analysis of extrusion film casting process using molecular constitutive equations. *Rheologica Acta*. 2014. Vol. 53, no. 1, p. 85–101.
- [29] CHIKHALIKAR, Kalyani, BANIK, Sourya, AZAD, Lal Busher, JADHAV, Kishor, MAHAJAN, Sunil, AHMAD, Zubair, KULKARNI, Surendra, GUPTA, Surendra, DOSHI, Pankaj, POL, H.V. and LELE, Ashish. Extrusion film casting of long chain branched polypropylene. *Polymer Engineering and Science*. 2015. Vol. 55, no. 9, p. 1977–1987.
- [30] POL, H.V. and THETE, S.S. Necking in Extrusion Film Casting: Numerical Predictions of the Maxwell Model and Comparison with Experiments. *Journal of Macromolecular Science, Part B*. 2016. Vol. 55, no. 10, p. 984–1006.
- [31] ALAIE, S.M. and PAPANASTASIOU, T.C. Film casting of viscoelastic liquid. *Polymer Engineering and Science*. 1991. Vol. 31, no. 2, p. 67–75.
- [32] BEAULNE, M. and MITSOULIS, Evan. Numerical Simulation of the Film Casting Process. *International Polymer Processing*. 1999. Vol. 14, no. 3, p. 261–275.
- [33] SHIROMOTO, Seiji, MASUTANI, Yasushi, TSUTSUBUCHI, Masaaki, TOGAWA, Yoshiaki and KAJIWARA, Toshihisa. A neck-in model in extrusion lamination process. *Polymer Engineering and Science*. 2010. Vol. 50, no. 1, p. 22–31.
- [34] D’HALEWYU, S., AGASSANT, Jean François and DEMAY, Y. Numerical simulation of the cast film process. *Polymer Engineering and Science*. 1990. Vol. 30, no. 6, p. 335–340.
- [35] SMITH, Spencer and STOLLE, Dieter. Nonisothermal two-dimensional film casting of a viscous polymer. *Polymer Engineering and Science*. 2000. Vol. 40, no. 8, p. 1870–1877.
- [36] AGASSANT, Jean François, AVENAS, P., SERGENT, J.P. and CARREAU, P.J. *Polymer Processing: Principles and Modeling*. Hanser Gardner Publications, 1991. ISBN 9781569900000.

- [37] DEBBAUT, B., MARCHAL, J.M. and CROCHET, M.J. Viscoelastic effects in film casting. CASEY, James and CROCHET, Marcel J. (eds.), *Zeitschrift für angewandte Mathematik und Physik*. 1995. Vol. 46, no. SPEC. ISSUE, p. 679–698.
- [38] SHIN, Dong Myeong, LEE, Joo Sung, KIM, Ju Min, JUNG, Hyun Wook and HYUN, Jae Chun. Transient and steady-state solutions of 2D viscoelastic nonisothermal simulation model of film casting process via finite element method. *Journal of Rheology*. 2007. Vol. 51, no. 3, p. 393–407.
- [39] RAJAGOPALAN, Dilip. Impact of viscoelasticity on gage variation in film casting. *Journal of Rheology*. 1999. Vol. 43, no. 1, p. 73–83.
- [40] KAJIWARA, Toshihisa, YAMAMURA, Masato and ASAHINA, Tomoko. Relationship between Neck-in Phenomena and Rheological Properties in Film Casting. *Nihon Reoroji Gakkaishi*. 2006. Vol. 34, no. 2, p. 97–103.
- [41] SOLLOGOUB, C., DEMAY, Y. and AGASSANT, Jean François. Non-isothermal viscoelastic numerical model of the cast-film process. *Journal of Non-Newtonian Fluid Mechanics*. 2006. Vol. 138, no. 2–3, p. 76–86.
- [42] SATOH, Naoki, TOMIYAMA, Hideki and KAJIWARA, Toshihisa. Viscoelastic simulation of film casting process for a polymer melt. *Polymer Engineering and Science*. 2001. Vol. 41, no. 9, p. 1564–1579.
- [43] AGASSANT, Jean François, DEMAY, Y., SOLLOGOUB, C. and SILAGY, D. Cast film extrusion: An overview of experimental and theoretical approaches. In : *International Polymer Processing*. 2005. p. 136–148.
- [44] SAKAKI, Kazutaka, KATSUMOTO, Ryuichi, KAJIWARA, Toshihisa and FUNATSU, Kazumori. Three-dimensional flow simulation of a film-casting process. *Polymer Engineering and Science*. 1996. Vol. 36, no. 13, p. 1821–1831.
- [45] GELDER, David. The stability of fiber drawing processes. *Industrial and Engineering Chemistry Fundamentals*. 1971. Vol. 10, no. 3, p. 534–535.
- [46] FISHER, Robert J. and DENN, Morton M. Finite-amplitude stability and draw resonance in isothermal melt spinning. *Chemical Engineering Science*. 1975. Vol. 30, no. 9, p. 1129–1134.
- [47] FISHER, R.J. and DENN, Morton M. A theory of isothermal melt spinning and draw resonance. *AIChE J.* 1976. Vol. 22, no. 2, p. 236–246.
- [48] CHRISTENSEN, R.E. Extrusion coating of polypropylene. *SPE J.* 1962. Vol. 18, p. 751.
- [49] MILLER, J.C. Swelling behavior in extrusion. *SPE Trans.* 1963. Vol. 3, no. 2, p. 134–137.

- [50] YEOW, Y. Leong. On the stability of extending films: a model for the film casting process. *Journal of Fluid Mechanics*. 1974. Vol. 66, no. 3, p. 613–622.
- [51] AIRD, Graham R. and YEOW, Y. Leong. Stability of film casting of power-law liquids. *Industrial and Engineering Chemistry Fundamentals*. 1983. Vol. 22, no. 1, p. 7–10.
- [52] ANTURKAR, Nitin R. and CO, Albert. Draw resonance in film casting of viscoelastic fluids: A linear stability analysis. *Journal of Non-Newtonian Fluid Mechanics*. 1988. Vol. 28, no. 3, p. 287–307.
- [53] IYENGAR, Vardarajan R. and CO, Albert. Film casting of a modified Giesekus fluid: Stability analysis. *Chemical Engineering Science*. 1996. Vol. 51, no. 9, p. 1417–1430.
- [54] SERGENT, J.P. Etude de deux procédés de fabrication de films. Le soufflage de gaine. L'extrusion de film à plat. In : Strasbourg, France, 1977.
- [55] TOFT, N. and RIGDAHL, M. Extrusion coating with metallocene-catalysed polyethylenes. *International Polymer Processing*. 2002. Vol. 17, no. 3, p. 244–253.
- [56] KOUDA, Shingo. Prediction of processability at extrusion coating for low-density polyethylene. *Polymer Engineering and Science*. 2008. Vol. 48, no. 6, p. 1094–1102.
- [57] ITO, Hisahiro, DOI, Masao, ISAKI, Takeharu and TAKEO, Masaaki. A Model of Neck-in Phenomenon in Film Casting Process. *Journal of the Society of Rheology, Japan*. 2003. Vol. 31, no. 3, p. 157–163.
- [58] SILAGY, David, DEMAY, Yves and AGASSANT, Jean François. Study of the stability of the film casting process. *Polymer Engineering and Science*. 1996. Vol. 36, no. 21, p. 2614–2625.
- [59] NARAYANASWAMY, O.S. A one-dimensional model of stretching float glass. *Journal of the American Ceramic Society*. 1977. Vol. 60, no. 1–2, p. 1–5.
- [60] LAMBERTI, Gaetano, TITOMANLIO, Giuseppe and BRUCATO, Valerio. Measurement and modelling of the film casting process 2. Temperature distribution along draw direction. *Chemical Engineering Science*. 2002. Vol. 57, no. 11, p. 1993–1996.
- [61] LAMBERTI, Gaetano, DE SANTIS, F., BRUCATO, V. and TITOMANLIO, G. Modeling the interactions between light and crystallizing polymer during fast cooling. *Applied Physics A*. 2004. Vol. 78, no. 6, p. 895–901.

- [62] LAMBERTI, Gaetano, BRUCATO, Valerio and TITOMANLIO, Giuseppe. Orientation and crystallinity in film casting of polypropylene. *Journal of Applied Polymer Science*. 2002. Vol. 84, no. 11, p. 1981–1992.
- [63] TITOMANLIO, Giuseppe and LAMBERTI, Gaetano. Modeling flow induced crystallization in film casting of polypropylene. *Rheologica Acta*. 2004. Vol. 43, no. 2, p. 146–158.
- [64] LAMBERTI, Gaetano and TITOMANLIO, Giuseppe. Analysis of Film Casting Process: Effect of Cooling during the Path in Air. *Industrial & Engineering Chemistry Research*. 2006. Vol. 45, no. 2, p. 719–723.
- [65] LAMBERTI, Gaetano and TITOMANLIO, Giuseppe. Analysis of film casting process: The heat transfer phenomena. *Chemical Engineering and Processing: Process Intensification*. 2005. Vol. 44, no. 10, p. 1117–1122.
- [66] LAMBERTI, Gaetano. Flow-induced crystallization during isotactic polypropylene film casting. *Polymer Engineering and Science*. 2011. Vol. 51, no. 5, p. 851–861.
- [67] ITO, Hisahiro, DOI, Masao, ISAKI, Takeharu, TAKEO, Masaaki and YAGI, Kazuo. 2D Flow Analysis of Film Casting Process. *Journal of the Society of Rheology, Japan*. 2003. Vol. 31, no. 3, p. 149–155.
- [68] MCGRADY, C.D., SEAY, C.W. and BAIRD, D.G. Effect of sparse long-chain branching on the film-casting behavior for a series of well-defined HDPEs. *Int. Polym. Process*. 2009. Vol. 24, no. 5, p. 428–438.
- [69] SEAY, C.W. and BAIRD, D.G. Sparse Long-chain Branching's Effect on the Film-casting Behavior of PE. *International Polymer Processing*. 2009. Vol. 24, no. 1, p. 41–49.
- [70] PIS-LOPEZ, Maria Elena and CO, Albert. Multilayer film casting of modified Giesekus fluids Part 1. Steady-state analysis. *Journal of Non-Newtonian Fluid Mechanics*. 1996. Vol. 66, no. 1, p. 71–93.
- [71] PIS-LOPEZ, Maria Elena and CO, Albert. Multilayer film casting of modified Giesekus fluids Part 2. Linear stability analysis. *Journal of Non-Newtonian Fluid Mechanics*. 1996. Vol. 66, no. 1, p. 95–114.
- [72] CHRISTODOULOU, Kostas, HATZIKIRIAKOS, Savvas G. and VLASSOPOULOS, Dimitris. Stability analysis of film casting for PET resins using a multimode Phan-Thien-Tanner constitutive equation. *Journal of Plastic Film and Sheeting*. 2000. Vol. 16, no. 4, p. 312–332.
- [73] DENN, Morton M., PETRIE, Christopher J.S. and AVENAS, Pierre. Mechanics of Steady Spinning of a Viscoelastic Liquid. *AIChE Journal*. 1975. Vol. 21, no. 4, p. 791–799.
- [74] DEMAY, Y. *Instabilité d'étirage et bifurcation de Hopf*. Université de Nice, 1983.

- [75] IYENGAR, Vardarajan R. *Film casting of polymer melts*. Orono, ME : University of Maine, 1993.
- [76] SMITH, W.S. *Simulating the cast film process using an updated Lagrangian finite element algorithm*. McMaster University, 2001.
- [77] DENN, Morton M. *Fibre Spinning*. 1st. Applied Science Publishers Ltd., 1983. ISBN 9789400966345.
- [78] BERIS, Antony N. and LIU, Baichen. Time-dependent fiber spinning equations. 1. Analysis of the mathematical behavior. *Journal of Non-Newtonian Fluid Mechanics*. 1988. Vol. 26, no. 3, p. 341–361.
- [79] LIU, Baichen and BERIS, Antony N. Time-dependent fiber spinning equations. 2. Analysis of the stability of numerical approximations. *Journal of Non-Newtonian Fluid Mechanics*. 1988. Vol. 26, no. 3, p. 363–394.
- [80] DEVEREUX, Brian M. and DENN, Morton M. Frequency response analysis of polymer melt spinning. *Industrial and Engineering Chemistry Research*. 1994. Vol. 33, no. 10, p. 2384–2390.
- [81] GAGON, Del Kenneth and DENN, Morton M. Computer simulation of steady polymer melt spinning. *Polymer Engineering and Science*. 1981. Vol. 21, no. 13, p. 844–853.
- [82] MINOSHIMA, Wataru and WHITE, James L. Stability of continuous film extrusion processes. *Journal of Polymer Engineering*. 1983. Vol. 2, no. 3, p. 211–226.
- [83] LEONOV, A.I. Nonequilibrium thermodynamics and rheology of viscoelastic polymer media. *Rheologica Acta*. 1976. Vol. 15, no. 2, p. 85–98.
- [84] LEONOV, A.I., LIPKINA, E.H., PASKHIN, E.D. and PROKUNIN, A.N. Theoretical and experimental investigation of shearing in elastic polymer liquids. *Rheologica Acta*. 1976. Vol. 15, no. 7, p. 411–426.
- [85] LEONOV, A.I. and PROKUNIN, A.N. An improved simple version of a nonlinear theory of elasto-viscous polymer media. *Rheologica Acta*. 1980. Vol. 19, no. 4, p. 393–403.
- [86] LEONOV, A.I. and PROKUNIN, A.N. On nonlinear effects in the extensional flow of polymeric liquids. *Rheologica Acta*. 1983. Vol. 22, no. 2, p. 137–150.
- [87] SIMHAMBHATLA, Murthy and LEONOV, Arkadii I. On the rheological modeling of viscoelastic polymer liquids with stable constitutive equations. *Rheologica Acta*. 1995. Vol. 34, no. 3, p. 259–273.

- [88] LEONOV, A.I. Constitutive equations for viscoelastic liquids: Formulation, analysis and comparison with data. *Rheology Series*. 1999. Vol. 8, no. C, p. 519–575.
- [89] ZATLOUKAL, Martin. Differential viscoelastic constitutive equations for polymer melts in steady shear and elongational flows. *Journal of Non-Newtonian Fluid Mechanics*. 2003. Vol. 113, no. 2–3, p. 209–227.
- [90] RESCH, Katharina, WALLNER, Gernot M, TEICHERT, Christian, MAIER, Günther and GAHLEITNER, Markus. Optical properties of highly transparent polypropylene cast films: Influence of material structure, additives, and processing conditions. *Polymer Engineering & Science*. 2006. Vol. 46, no. 4, p. 520–531.
- [91] COPPOLA, Salvatore, BALZANO, Luigi, GIOFFREDI, Emilia, MAFFETTONE, Pier Luca and GRIZZUTI, Nino. Effects of the degree of undercooling on flow induced crystallization in polymer melts. *Polymer*. 2004. Vol. 45, no. 10, p. 3249–3256.
- [92] CASTEJÓN, Pilar, HABIBI, Kian, SAFFAR, Amir, AJJI, Abdellah, MARTÍNEZ, Antonio B and ARENCÓN, David. Polypropylene-Based Porous Membranes: Influence of Polymer Composition, Extrusion Draw Ratio and Uniaxial Strain. *Polymers*. 2018. Vol. 10, no. 1, p. 33.
- [93] TABATABAEI, Seyed H., CARREAU, Pierre J. and AJJI, Abdellah. Effect of processing on the crystalline orientation, morphology, and mechanical properties of polypropylene cast films and microporous membrane formation. *Polymer*. 2009. Vol. 50, no. 17, p. 4228–4240.
- [94] XU, Meng, ZHANG, Shijun, LIANG, Jieying, QUAN, Hui, LIU, Jianye, SHI, Hongwei, GAO, Dali and LIU, Jie. Influences of processing on the phase transition and crystallization of polypropylene cast films. *Journal of Applied Polymer Science*. 2014. Vol. 131, no. 22, p. 41100.
- [95] ZIABICKI, A. Crystallization of polymers in variable external conditions. 1. General equations. *Colloid and Polymer Science*. 1996. Vol. 274, no. 3, p. 209–217.
- [96] ZIABICKI, A. Crystallization of polymers in variable external conditions. II. Effects of cooling in the absence of stress and orientation. *Colloid and Polymer Science*. 1996. Vol. 274, no. 8, p. 705–716.
- [97] LAMBERTI, Gaetano and TITOMANLIO, Giuseppe. Crystallization kinetics of iPP. Model and experiments. *Polymer Bulletin*. 2001. Vol. 46, no. 2–3, p. 231–238.

- [98] TITOMANLIO, G., SPERANZA, V. and BRUCATO, V. On the simulation of thermoplastic injection moulding process: II Relevance of interaction between flow and crystallization. *International Polymer Processing*. 1997. Vol. 12, no. 1, p. 45–53.
- [99] PANTANI, Roberto, DE SANTIS, Felice, SPERANZA, Vito and TITOMANLIO, Giuseppe. Analysis of flow induced crystallization through molecular stretch. *Polymer*. 2016. Vol. 105, p. 187–194.
- [100] LAMBERTI, Gaetano and TITOMANLIO, Giuseppe. Evidences of flow induced crystallization during characterized film casting experiments. *Macromolecular Symposia*. 2002. Vol. 185, no. 1, p. 167–180.

LIST OF FIGURES

Fig. 1: Schematics of the extrusion film casting kinematics.	11
Fig. 2: Visualization of neck-in phenomenon during extrusion film casting.	13
Fig. 3: Visualization of edge-beading phenomenon during extrusion film casting.	14
Fig. 4: Visualization of draw resonance experienced during extrusion film casting.	15
Fig. 5: Visualization of planar and uniaxial extensional flows during extrusion film casting.	18
Fig. 6: Flow chart of iteration scheme used to solve of non-isothermal viscoelastic film casting model.	43
Fig. 7: Normalized maximum attainable neck-in value, NI^* , as the function of Deborah number for LDPE 170A, PE-A, PE-B, PE-C, and LDPE C polymers for the processing conditions summarized in Table 6 in [27]. Experimental data (taken from [23, 25, 28], [7] and [42]) and proposed analytical model predictions (Eq. 99) are given here by the open and filled symbols, respectively. (7a) $-N_2/N_1$ is given by the modified Leonov model predictions for particular die exit shear rates, which are provided in Table 7 in [27] for each individual case, (7b) $-N_2/N_1$ is considered to be constant, equal to 0.2.	45
Fig. 8: Comparison between experimental data for iPP T30G ($T_{DIE}=200^\circ\text{C}$) and given processing conditions ($De=6 \cdot 10^{-4}$, $DR=34.7$, $X=0.4$ m) taken from [100] and model predictions for dimensionless drawing distance variables considering constant heat transfer coefficient, $HTC=16 \text{ J} \cdot \text{s}^{-1} \cdot \text{K}^{-1} \cdot \text{m}^{-2}$. (8a) Dimensionless Final Half-width, (8a) Film crystallinity.	47
Fig. 9: Effect of draw ratio and heat transfer coefficient (see numbers in $\text{J} \cdot \text{s}^{-1} \cdot \text{K}^{-1} \cdot \text{m}^{-2}$ provided at each data set) on the critical aspect ratio for linear iPP at die exit temperature equal to 200°C . (9a) Crystallization onset borders defining conditions for film production with (area above the border symbols) and without (area below the border symbols) the crystallized phase, (9b) Isothermality boundaries below which the non-isothermal and isothermal calculations gives practically the same neck-in values.	48
Fig. 10: Comparison between film casting model predictions with and without consideration of Flow Induced Crystallization, FIC, and experimental data taken from [66], $HTC=31 \text{ J} \cdot \text{s}^{-1} \cdot \text{K}^{-1} \cdot \text{m}^{-2}$. (10a) Temperature profile, (10b) Crystallinity profile.	50
Fig. 11: Predicted effect of HTC on the film crystallinity (left) and melting temperature (right) for iPP at the reference processing conditions.	50

LIST OF TABLES

Table 1: Overview of steady-state analyses of film casting process (table adapted from [13–15] and updated for new studies).	17
--	----

LIST OF SYMBOLS

Latin Symbols	Meaning	Unit
A	Aspect ratio	1
A_1, A_2	Fitting parameters in analytical model for normalized maximum attainable neck-in	1
A_{ath}	Fitting parameter in crystallization kinetics	1
B_{ath}	Fitting parameter in crystallization kinetics	s
b	Dissipation term	s^{-1}
\bar{b}	Dimensionless dissipation term	1
C_p	Specific heat capacity of polymer	$J \cdot kg^{-1} \cdot K^{-1}$
c_{xx}	Normal component of the recoverable Finger tensor in axial x-direction	1
c_{yy}	Normal component of the recoverable Finger tensor in transverse y-direction	1
c_{zz}	Normal component of the recoverable Finger tensor in thickness z-direction	1
$\underset{=}{\overset{\circ}{c}}$	Jaumann (corotational) time derivative of the recoverable Finger strain tensor	s^{-1}
$\underline{\underline{c}}, \underline{\underline{c}}_{ii}$	Recoverable Finger tensor	1
$\underline{\underline{c}}^{-1}, \underline{\underline{c}}_{ii}^{-1}$	Inverse recoverable Finger tensor	1
De	Deborah number	1
DR	Draw ratio	1
$\underline{\underline{D}}$	Deformation rate tensor	s^{-1}
E	Dimensionless take-up/drawing force	1
E_a	Flow activation energy	$J \cdot mol^{-1}$

E_c	Fitting parameter in crystallization kinetics	K
e	Half-thickness of the film at any x location	m
e_0	Die half-gap (half-thickness of the film at the die exit)	m
\bar{e}	Dimensionless half-thickness of the film at any x location	1
$\underline{\underline{e}}_p$	Irreversible rate of strain tensor	s^{-1}
F	Take-up force (drawing force)	N
f	Parameter in function describing the effect of crystallinity on elastic modulus	1
$f(x)$	Rate of deformation in transverse y -direction	s^{-1}
\bar{f}	Dimensionless rate of deformation in transverse y -direction	1
G	Linear Hookean elastic modulus (Relaxation modulus)	Pa
G_0	Linear Hookean elastic modulus at the die exit	Pa
$g(x)$	Rate of deformation in thickness z -direction	s^{-1}
\bar{g}	Dimensionless rate of deformation in thickness z -direction	1
HTC	Heat transfer coefficient	$J \cdot s^{-1} \cdot K^{-1} \cdot m^{-2}$
h	Parameter in function describing the effect of crystallinity on elastic modulus	1
$I_{1,c}$	First invariant of recoverable Finger tensor	1
$I_{2,c}$	Second invariant of recoverable Finger tensor	1
i	Index i , noting the spatial direction	1

j	Relaxation mode identification number	1
$K(t)$	Crystallization kinetics function	s^{-1}
K_{th}	Isothermal function of crystallization kinetics	s^{-1}
k_{iso}	Slope function for determination of isothermal boundary	1
k_{Xc}	Slope function for crystallization on-set	1
L	Half-width of the film at any x location	m
L_0	Half-width of the die (half-width of the film at the die exit)	m
\bar{L}	Dimensionless half-width of the film at any x location	1
MFR, \dot{m}	Mass flow rate	$kg \cdot h^{-1}$
m	Parameter in function describing the effect of crystallinity on elastic modulus	1
M_n	Number average molar mass	$g \cdot mol^{-1}$
M_w	Mass average molar mass	$g \cdot mol^{-1}$
NI	Maximum attainable neck-in	m
NI*	Normalized maximum neck-in value	1
N_1	First normal stress difference	Pa
N_2	Second normal stress difference	Pa
$-N_2/N_1$	Stress state at the die exit	1
n	Non-linear Leonov model parameter	1
n_c	Type of crystallization growth	1
\underline{n}	The normal vector to the free surface	1

$P(t)$	Function of non-linear crystallinity evolution	1
p	Isotropic pressure	Pa
Q	Volumetric flow rate	$m^3 \cdot s^{-1}$
q_{iso}	Intercept function for determination of isothermal boundary	1
q_{Xc}	Intercept function for crystallization on-set	1
R	Gas constant	$J \cdot K^{-1} \cdot mol^{-1}$
\dot{T}	Rate of cooling	$^{\circ}C \cdot s^{-1}$
T_{DIE}	Melt temperature at the die	$^{\circ}C$
T_m	Melting temperature of polymer	$^{\circ}C$
T_{mq}^0	Flow induced equilibrium melting temperature	$^{\circ}C$
T	Melt temperature	$^{\circ}C$
T_r	Reference temperature in the Arrhenius Law	$^{\circ}C$
t	Time coordinate	s
u	Axial velocity component of the film at any x location	$m \cdot s^{-1}$
u_0	Axial velocity component at the die exit (velocity in the machine direction)	$m \cdot s^{-1}$
$u(X)$	Chill roll speed	$m \cdot s^{-1}$
\bar{u}	Dimensionless axial velocity component of the film at any x location	1
\underline{u}	The tangential velocity at film-air interface	$m \cdot s^{-1}$
v	Velocity component of the film in transverse y -direction at any x location	$m \cdot s^{-1}$

w	Velocity component of the film in thickness z-direction at any x location	$\text{m}\cdot\text{s}^{-1}$
W	Elastic potential	Pa
X	Take-up length (drawing distance, air gap)	m
X_c	Crystallinity content in the polymer volume	1
X_{eq}	Equilibrium level of crystallinity in the polymer volume	1
x, y, z	Spatial coordinates in axial, transverse and thickness direction, respectively	1
x	Position in axial x-direction	m
\bar{x}	Dimensionless position in axial x-direction	1
Z	Non-isothermal function of crystallization kinetics	1
Z_x, Z_y, Z_z, X_p	Substitution variables	1
$\frac{dc_{xx}}{d\bar{x}}, \frac{dc_{yy}}{d\bar{x}}, \frac{dc_{zz}}{d\bar{x}}$	Derivative of Finger tensor components with respect to dimensionless \bar{x} position	1
$\frac{d\bar{u}}{d\bar{x}}, \frac{d\bar{L}}{d\bar{x}}, \frac{d\bar{e}}{d\bar{x}}$	Derivative of dimensionless axial velocity, width and thickness with respect to dimensionless \bar{x} position	1
$\frac{dX_c}{d\bar{x}}$	Derivative of crystallinity with respect to dimensionless \bar{x} position	1
$\frac{dT}{d\bar{x}}$	Derivative of temperature with respect to dimensionless \bar{x} position	$^{\circ}\text{C}$
Greek Symbols	Meaning	Unit
α_1, α_2	Fitting parameters in analytical model for normalized maximum attainable neck-in	1
α_T	Arrhenius law parameter	1

$\alpha_{\text{iso}}, \beta_{\text{iso}}, \gamma_{\text{iso}}, \delta_{\text{iso}}$	Fitting parameters in isothermal boundary function	1
$\alpha_{\text{k}}, \beta_{\text{k}}, \gamma_{\text{k}}, \delta_{\text{k}},$ $\alpha_{\text{q}}, \beta_{\text{q}}, \gamma_{\text{q}}, \delta_{\text{q}}$	Fitting parameters in crystallization on-set function	1
β	Non-linear Leonov model parameter	1
δ	Shift function in analytical model for normalized maximum attainable neck-in	1
$\underline{\underline{\delta}}$	Unit tensor (Kronecker delta)	1
$\eta_{\text{E,P}}$	Steady planar extensional viscosity	Pa·s
$\eta_{\text{E,P,max}}$	Maximal steady planar extensional viscosity	Pa·s
$\eta_{\text{E,U}}$	Steady uniaxial extensional viscosity	Pa·s
$\eta_{\text{E,U,max}}$	Maximal steady uniaxial extensional viscosity	Pa·s
$\frac{\eta_{\text{E,P,max}}}{4\eta_0}$	Planar extensional strain hardening	1
$\frac{\eta_{\text{E,U,max}}}{3\eta_0}$	Uniaxial extensional strain hardening	1
η_0	Newtonian viscosity	Pa·s
θ	Fitting parameter in analytical model for normalized maximum attainable neck-in	1
κ_1	Fitting parameter in crystallization kinetics	s ⁻¹
κ_2	Fitting parameter in crystallization kinetics	1
λ	Melt relaxation time	s
λ_0	Melt relaxation time at the die exit	s

μ_{X_c}	Effect of crystallinity on elastic modulus function	1
ν	Non-linear Leonov model parameter	1
ξ	Non-linear Leonov model parameter	1
ρ_P	Polymer density	$\text{kg}\cdot\text{m}^{-3}$
σ_{xx}	Total normal stress in the axial direction (machine direction)	Pa
σ_{yy}	Total normal stress in transverse y-direction	Pa
σ_{zz}	Total normal stress in thickness z-direction	Pa
$\underline{\underline{\sigma}}$	Total stress tensor	Pa
τ_{xx}	Normal stress in axial x-direction	Pa
τ_{yy}	Normal stress in transverse y-direction	Pa
τ_{zz}	Normal stress in thickness z-direction	Pa
$\bar{\tau}_{xx}$	Dimensionless normal stress in x-direction	1
$\bar{\tau}_{yy}$	Dimensionless normal stress in y-direction	1
$\bar{\tau}_{zz}$	Dimensionless normal stress in z-direction	1
$\underline{\underline{\tau}}$	Extra stress tensor	Pa
ϕ_1, ϕ_2	Fitting parameters in analytical model for normalized maximum attainable neck-in	1
χ_c	Volume fraction of crystallized phase	1
$\Psi_1, \Psi_2, \Psi_3, \Psi_4$	Fitting parameters in analytical model for normalized maximum attainable neck-in	1

PAPER I



On the role of extensional rheology and Deborah number on the neck-in phenomenon during flat film casting



Tomas Barborik^a, Martin Zatloukal^{a,*}, Costas Tzoganakis^b

^a Polymer Centre, Faculty of Technology, Tomas Bata University in Zlin, Vavreckova 275, 760 01 Zlin, Czech Republic

^b Department of Chemical Engineering, University of Waterloo, 200 University Avenue West, Waterloo, Ontario, Canada

ARTICLE INFO

Article history:

Received 6 March 2017

Accepted 18 April 2017

Available online 28 April 2017

Keywords:

Flat film production

Polymer melt

Rheology

Neck-in phenomenon

Uniaxial extensional viscosity

Planar extensional viscosity

ABSTRACT

In this work, viscoelastic, isothermal extrusion film casting simulations have been performed utilizing a 1D membrane model and the viscoelastic modified Leonov model as the constitutive equation in order to elucidate the role of planar to uniaxial extensional viscosity ratio, extensional strain hardening and Deborah number on the neck-in phenomenon. Based on the performed theoretical parametric study, it has been found that neck-in can be correlated to all the above mentioned variables via a simple dimensionless analytical equation. This correlation can provide detailed view into the complicated relationship between polymer melt rheology, die design, process conditions and undesirable neck-in phenomenon. Obtained results have been validated against literature experimental data for different polyethylene melts and processing conditions.

© 2017 Elsevier Ltd. All rights reserved.

1. Introduction

Extrusion film casting (EFC) is a continuous, high-speed manufacturing process during which a thin, highly oriented polymer film is produced [1,2]. In this widely used and dominant process, a molten polymer is extruded through a slit die with a narrow gap to form a thick sheet of polymer that is subsequently intensively stretched in the machine direction by means of a rotating take-up drum, whose linear velocity is higher than the extrusion one, providing the macromolecular orientation and reduction in the sheet thickness and finally the dimensions of the created thin film are fixed by cooling down on a chill roll. The intensity of film drawing is usually measured by means of draw ratio defined as a linear velocity at the take-up drum divided by polymer exit velocity at the extrusion die.

In the section where the formation of the thin film takes place, i.e. within the drawing length, the cross-sectional dimensions of the sheet decreases monotonically as it travels towards the cooling stage (except in the swell region near the die exit). Under certain processing conditions, several phenomena may be encountered in this region, which hamper the required production in film quality and quantity. One of them is called neck-in causing an undesirable reduction in film width (see Fig. 1) and interrelated phenomenon of edge-beads (also called dog-bone defect) making

the edge portions of the film substantially thicker than its central part. Both of these steady state disruptions result in necessary post-production film trimming since only the central part of the film is uniform in thickness. From a practical viewpoint, it is of great importance, therefore, to understand the underlying mechanism of neck-in formation in order to minimize these unwanted effects. In addition, outside of the steady state processing window at high drawing rates, the transient disruption, called draw resonance, causing periodical variations in dimensions of the produced film as well as film brakeage itself may occur [3,4].

Polymer sheet or filament drawing has been studied extensively over the past four decades both experimentally and theoretically due to its great importance in the polymer processing industry. Initial efforts were made on a fiber spinning process for which the flow kinematics are similar from a mathematical point of view if considered as the one-dimensional flow case, for Newtonian and Maxwell fluids by Gelder [5] and Fisher [6,7], respectively. Those studies were aimed on investigating the draw resonance phenomenon which was encountered for the first time by Christensen [8] and Miller [9], and who postulated that the nature of this phenomenon was not of viscoelastic nature because it could be observed in Newtonian fluids as well. Extending the process kinematics into two or three dimensions, the processes differ and one can observe phenomena in film casting that do not have a counterpart in fiber spinning, i.e. neck-in and edge-beading. The preliminary studies mentioned above provided the background for extended studies on EFC. Initial attempts to simulate EFC

* Corresponding author.

E-mail address: mzatloukal@ft.utb.cz (M. Zatloukal).

List of symbols

$\underline{\underline{\tau}}$	extra stress tensor, Pa	X	take-up length (stretching distance), mm
$\underline{\underline{\sigma}}$	total stress tensor, Pa	DR	draw ratio, 1
$\underline{\underline{W}}$	elastic potential, Pa	A	aspect ratio, 1
G	linear Hookean elastic modulus (Relaxation modulus), Pa	De	Deborah number, 1
$\underline{\underline{c}}, \underline{\underline{c}}_{ii}$	recoverable finger tensor, 1	\bar{x}	dimensionless position in x-direction, 1
$\underline{\underline{c}}^{-1}, \underline{\underline{c}}_{ii}^{-1}$	inverse recoverable finger tensor, 1	\bar{e}	dimensionless half-thickness of the film at any x location, 1
$I_{1,c}$	first invariant of recoverable finger tensor, 1	\bar{L}	dimensionless half-width of the film at any x location, 1
$I_{2,c}$	second invariant of recoverable finger tensor, 1	\bar{u}	dimensionless axial velocity of the film at any x location, 1
β	non-linear Leonov model parameter, 1	$\bar{\tau}_{xx}$	dimensionless normal stress in x-direction, 1
n	non-linear Leonov model parameter, 1	$\bar{\tau}_{yy}$	dimensionless normal stress in y-direction, 1
$\underline{\underline{e}}_p$	irreversible rate of strain tensor, s^{-1}	$\bar{\tau}_{zz}$	dimensionless normal stress in z-direction, 1
$\underline{\underline{b}}$	dissipation term, s^{-1}	\bar{f}	dimensionless rate of deformation in y-direction, 1
$\underline{\underline{\delta}}$	unit tensor (Kronecker delta), 1	\bar{g}	dimensionless rate of deformation in z-direction, 1
$\underline{\underline{D}}$	deformation rate tensor, s^{-1}	$\underline{\underline{b}}$	dimensionless dissipation term, 1
λ	relaxation time, s	Z_x, Z_y, Z_z, X_p	substitution variables, 1
ζ	non-linear Leonov model parameter, 1	$\underline{\underline{u}}$	the tangential velocity at film-air interface, $mm\ s^{-1}$
γ	non-linear Leonov model parameter, 1	$\underline{\underline{n}}$	the normal vector to the free surface, 1
$\dot{\underline{\underline{c}}}$	Jaumann (corotational) time derivative of the recoverable finger strain tensor, s^{-1}	Q	volumetric flow rate, $m^3\ s^{-1}$
N_1	first normal stress difference, Pa	T	melt temperature, $^{\circ}C$
N_2	second normal stress difference, Pa	T_{die}	melt temperature at the die, $^{\circ}C$
σ_{xx}	total normal stress in the axial direction (machine direction), Pa	T_r	reference temperature in the Arrhenius law, $^{\circ}C$
σ_{yy}	total normal stress in y-direction, Pa	E_a	flow activation energy, $J\ mol^{-1}$
σ_{zz}	total normal stress in z-direction, Pa	R	gas constant, $J\ K^{-1}\ mol^{-1}$
τ_{xx}	normal stress in the axial direction (machine direction), Pa	i	index i noting the spatial direction, 1
τ_{yy}	normal stress in y-direction (transverse direction), Pa	j	index j, 1
τ_{zz}	normal stress in z-direction (thickness direction), Pa	a_S	shift parameter for normalized necking prediction, 1
p	isotropic pressure, Pa	x, y, z	spatial coordinates, 1
c_{xx}	component of the recoverable finger tensor in x-direction, 1	t	time coordinate, s
c_{yy}	component of the recoverable finger tensor in y-direction, 1	$\eta_{E,U}$	steady uniaxial extensional viscosity, Pa s
c_{zz}	component of the recoverable finger tensor in z-direction, 1	$\eta_{E,P}$	steady planar extensional viscosity, Pa s
e	half-thickness of the film at any x location, mm	η_0	Newtonian viscosity, Pa s
L	half-width of the film at any x location, mm	$\eta_{E,U,max}$	maximal steady uniaxial extensional viscosity, Pa s
u	axial velocity of the film at any x location, $mm\ s^{-1}$	$\eta_{E,P,max}$	maximal steady planar extensional viscosity, Pa s
$u(X)$	chill roll speed, $mm\ s^{-1}$	NI	maximum neck-in, mm
F	take-up force (stretching force), N	NI^*	normalized maximum neck-in value, 1
E	dimensionless force, 1	α	Arrhenius law parameter, K
x	position in x-direction, m	k	slope of the line, 1
v	velocity of the film in y-direction at any x location, $mm\ s^{-1}$	Q	the NI^* intercept, 1
w	velocity of the film in z-direction at any x location, $mm\ s^{-1}$	k^*	reduced slope of the line, 1
f	rate of deformation in y-direction, s^{-1}	Q^*	reduced NI^* intercept, 1
g	rate of deformation in z-direction, s^{-1}	a_S	shift factor, 1
e_0	die half-gap (half-thickness of the film at the die exit), mm	$A_1, A_2, \alpha_1, \alpha_2, \varphi_1, \varphi_2$	fitting parameters of analytical model, 1
L_0	half-width of the die (half-width of the film at the die exit), mm	n_s	number of samples (points), 1
u_0	axial velocity at the die exit (velocity in the machine direction), $mm\ s^{-1}$	y_i	observed value, 1
		\hat{y}_i	predicted value, 1
		M_w	mass average molar mass, $g\ mol^{-1}$
		M_n	number average molar mass, $g\ mol^{-1}$
		M_z	Z average molar mass, $g\ mol^{-1}$
		MFR	mass flow rate, $kg\ h^{-1}$
		R_h	the hydrodynamic radius of a macromolecule, nm
		PDI	polydispersity index, 1
		MFI	mass flow index, $g/10\ min$
		ρ	polymer density, $g\ cm^{-3}$

operations were dedicated to investigation of process stability and determination of draw resonance onset rather than to quantify the extent of neck-in phenomenon. The very first study on modeling of EFC process in this manner was carried out by Yeow [10] involving a Newtonian fluid with simplified kinematics based on the assumption of infinite film width under isothermal conditions. In

other words, the width of the film was deemed as a constant so that the model did not account for either neck-in or edge-bead defect. Aird and Yeow [11] continued on this equation background of 1D model and extended analysis for power-law fluids, and then Anturkar and Co [12] and Iyengar and Co [13,14] utilizing isothermal modified convected-Maxwell fluid and Giesekus constitutive

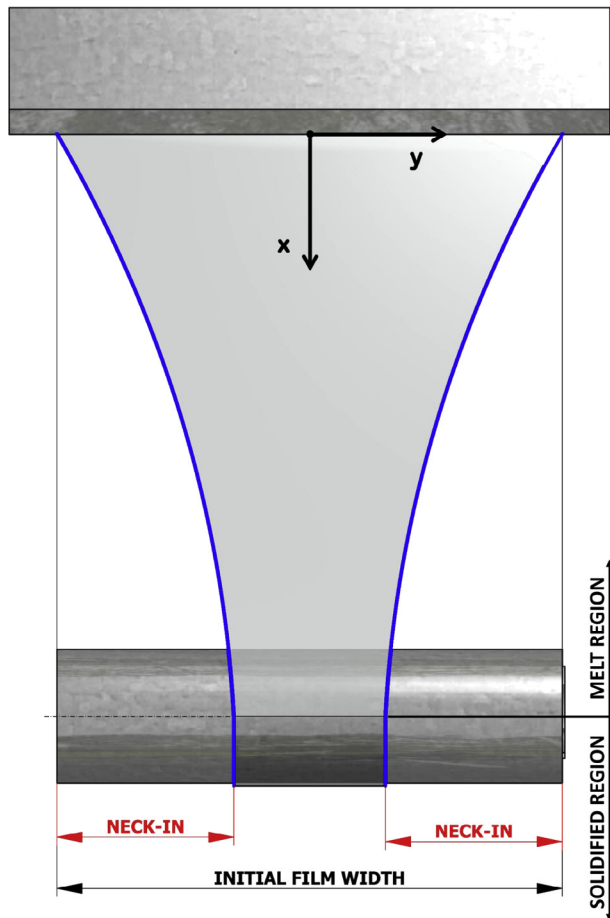


Fig. 1. Neck-in phenomenon during the extrusion film casting process.

equations for linear and non-linear analysis in simulations of viscoelastic fluids. First isothermal trials towards necking phenomena modeling were carried out by Sergent [15] and then by Cotto, Duffo and Barq [16–18] for non-isothermal conditions.

Another milestone work has been set by Dobroth and Erwin [19] who pointed out that the deformation flow in the drawing length comprises of two related regions and the extent of edge-beads and interrelated neck-in phenomenon is determined by the interplay between them through an edge stress effect. While the center of the film undergoes planar elongational deformation, the edge sections are subjected to uniaxial elongational one (see Fig. 2).

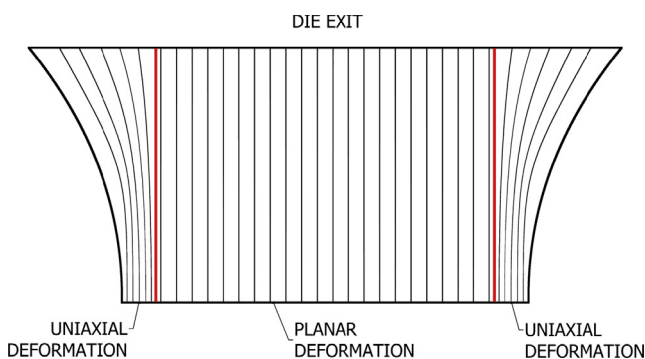


Fig. 2. Visualization of planar and uniaxial extensional flows during the extrusion film casting process.

In the case of fiber spinning, however, one can observe uniaxial elongational flow only. Some authors endeavoured to relate and quantify the gauge of the observed necking in terms of rheological parameters, such as shear, uniaxial and planar viscosity. Many authors reported that the strain hardening in uniaxial elongational viscosity may depress the extent of necking phenomena [20–23]. This idea was continued by Ito [24], who related the neck-in extent to rheological parameters such as the ratio of planar viscosities in axial and transverse directions, and derived an analytical equation for the edge line of a molten film of Newtonian and Maxwell fluid. Along the line of Dobroth and Erwin's article [19], who as the first recognized deformation type in the drawing area, Shiromoto [25–27], recently, presented the idea that the extent of the necking should not have been described by uniaxial elongational viscosity only in addition to take-up length but as the ratio of planar and uniaxial elongational viscosities reflecting the deformation type in the central and edge portion of the film in the drawing section. Aside from performing non-isothermal viscoelastic simulations, they also proposed a theoretical model based on force balance and deformation type of a film in order to predict necking behavior.

More recently, a 2D membrane model was presented by d'Halewy [28] and Debbaud [20] for Newtonian and viscoelastic fluids, respectively. This frequently used model was capable of predicting the dog-bone defect, i.e. development of edge-beads, under the stationary conditions. Silagy et al. [29] proceeded forward and enriched the membrane model by a supplementary kinematic hypothesis that was originally brought by Narayanaswamy [30] in his paper on float glass stretching, and carried out an extended isothermal study on the influence of processing conditions on film geometry, and stability analysis of EFC for Newtonian and Maxwell fluid using the UCM constitutive equation. Because of the assumptions used in flow kinematics, this model was able to cover film width reduction and thus predict the neck-in phenomenon but was still not able to predict edge-beading. This limitation was removed in their succeeding work [31] where the 2D isothermal membrane model combined with PTT constitutive equation was developed and obtained steady and transient stability results compared with its 1D predecessor. In the following years, the 1D version of Sylagy's membrane model was used in many studies and considerable amount of work has been done on EFC under non-isothermal conditions including crystallization effects by Lamberti et al. [32–35], Lamberti and Titomanlio [34,36–38], and Lamberti [39]. A three dimensional model for EFC simulation was further developed by Sakaki et al. [40] and Zheng et al. [41] for isothermal and non-isothermal steady Newtonian fluid, respectively.

The influence of macromolecular architecture on the extent of necking phenomenon has been investigated by Ito et al. [24,42] (effects of draw ratio and take-up length on necking for LDPE, HDPE and mLLDPE) and Baird et al. [43,44] (effects of long chain branching and molecular weight distribution on necking for LDPE, mLLDPE and Ziegler-Natta catalyzed LLDPE). Recently, Pol et al. [45,46] and Chikhalikar et al. [47] have published a series of articles in which they have performed experimental and theoretical investigations of the effects of long chain branching and molecular weight distribution on the necking phenomenon extent. For this purpose, they utilized the 1D membrane model, originally proposed by Silagy [29], the multi-mode eXtended Pom-Pom constitutive equation and the multi-mode Rolie-Poly stretch constitutive equation, respectively, for the long chain branched (LDPE, PP) and the linear (HDPE, PP) polymers. Fixing the DR and TUL, they found that the extent of necking is lesser for HDPE with a broader molecular weight distribution than that for LLDPE with a narrower molecular weight distribution and further that long chain branched LDPE necks-into lower extent than linear HDPE or LLDPE. In their latest work [48], they addressed the effects of the individual viscoelastic relaxation modes of a polymer melt on its behavior

in polymer melt extrusion film casting process using UCM and PTT constitutive equations. They found that experimental data for long-chain branched LDPE was described better by UCM model, whereas PTT model provided better simulation results for the linear LLDPE experimental data.

Even though, the real EFC manufacturing process involves complex kinematics and is considered as a 3D problem whose numerical simulation can be very demanding, it has been proven by many authors that the EFC 1D membrane model originally proposed by Silagy [29], if used in combination with appropriate constitutive equations, is capable of providing results that are in good agreement with experiment data.

In the present work, a theoretical study of the neck-in phenomenon under steady-state isothermal conditions is carried out utilizing the 1D membrane model together with viscoelastic modified Leonov constitutive equations. The influence of uniaxial extensional strain hardening, planar to uniaxial extensional viscosity ratio and Deborah number is systematically studied and the results are compared with corresponding experimental data taken from the open literature.

2. Mathematical modeling

2.1. Modified Leonov model

This constitutive equation is based on heuristic thermodynamic arguments resulting from the theory of rubber elasticity [49–54]. In the model, fading memory of the melts is determined through an irreversible dissipation process driven by the dissipation term, b . Mathematically, it is relating the stress and elastic strain stored in the material as:

$$\underline{\tau} = 2 \left(\underline{\underline{c}} \frac{\partial W}{\partial I_{1,c}} - \underline{\underline{c}}^{-1} \frac{\partial W}{\partial I_{2,c}} \right) \quad (1)$$

where $\underline{\tau}$ is the stress, and W , the elastic potential, which depends on the invariants $I_{1,c}$ and $I_{2,c}$ of the recoverable Finger tensor $\underline{\underline{c}}$,

$$W = \frac{3G}{2(n+1)} \left\{ [1 - \beta] \left[\left(\frac{I_{1,c}}{3} \right)^{n+1} - 1 \right] + \beta \left[\left(\frac{I_{2,c}}{3} \right)^{n+1} - 1 \right] \right\} \quad (2)$$

where G denotes linear Hookean elastic modulus, β and n are numerical parameters. Leonov assumed that the dissipative process acts to produce an irreversible rate of strain \underline{e}_p

$$\underline{e}_p = b \left[\underline{\underline{c}} - \frac{I_{1,c}}{3} \underline{\underline{\delta}} \right] - b \left[\underline{\underline{c}}^{-1} - \frac{I_{2,c}}{3} \underline{\underline{\delta}} \right] \quad (3)$$

which spontaneously reduces the rate of elastic strain accumulation. Here, $\underline{\underline{\delta}}$ is the unit tensor and b stands for dissipation function defined by Eq. (5). This elastic strain $\underline{\underline{c}}$ is related to the deformation rate tensor $\underline{\underline{D}}$ as follows

$$\overset{\circ}{\underline{\underline{c}}} - \underline{\underline{c}} \cdot \underline{\underline{D}} - \underline{\underline{D}} \cdot \underline{\underline{c}} + 2 \underline{\underline{c}} \cdot \underline{e}_p = 0 \quad (4)$$

where $\overset{\circ}{\underline{\underline{c}}}$ is the Jaumann (corotational) time derivative of the recoverable Finger strain tensor. In this work, the Mooney potential (i.e. $n = 0$ in Eq. (2)), and the dissipation function b proposed in [55] (see Eq. (5)) have been employed.

$$b(I_{1,c}) = \frac{1}{4\lambda} \left\{ \exp[-\xi \sqrt{I_{1,c} - 3}] + \frac{\sinh[v(I_{1,c} - 3)]}{v(I_{1,c} - 3) + 1} \right\} \quad (5)$$

Here, ξ and v are adjustable model parameters.

$$I_{1,c} = tr(\underline{\underline{c}}) \quad (6)$$

$$tr(\underline{\underline{c}}) = c_{xx} + c_{yy} + c_{zz} \quad (7)$$

$$I_{2,c} = \frac{1}{2} \{ [tr(\underline{\underline{c}})]^2 - tr(\underline{\underline{c}}^2) \} \quad (8)$$

$$I_{2,c} = c_{xx}^{-1} + c_{yy}^{-1} + c_{zz}^{-1} \quad (9)$$

Differentiating Eq. (2) with respect to the first and second invariant of the recoverable Finger tensor yields

$$\frac{\partial W}{\partial I_{1,c}} = \frac{1}{2} G \left(\frac{I_{1,c}}{3} \right)^n (1 - \beta) \quad (10)$$

$$\frac{\partial W}{\partial I_{2,c}} = \frac{1}{2} G \beta \left(\frac{I_{2,c}}{3} \right)^n \quad (11)$$

Combination of Eq. (1) with Eqs. (10) and (11) leads to the following expression for the extra stress tensor.

$$\underline{\tau} = G \left\{ \underline{\underline{c}} \left[\left(\frac{I_{1,c}}{3} \right)^n (1 - \beta) \right] - \underline{\underline{c}}^{-1} \left[\beta \left(\frac{I_{2,c}}{3} \right)^n \right] \right\} \quad (12)$$

2.2. Extrusion film casting model

In this work, the one-dimensional membrane model developed by Silagy et al. [29] was used to model the isothermal extrusion film casting process (see Fig. 3). The model essentially features two hypotheses to facilitate the description of the stress and velocity field development in the film drawing. Firstly, the total stress in the film thickness direction is assumed to be equal to zero because this dimension is small compared to other dimensions and secondly, velocities in the width and thickness direction are allowed to vary linearly with y and z position, respectively, for the given x location, which represents a supplementary kinematic hypothesis (formerly adopted in the work of Narayanaswamy [30] for the modeling of glass manufacturing by the float process) in order to reduce the dimensionality of the task. As a result, all model variables are x -direction dependent only and the model can be considered as one-dimensional although lateral film width and thickness reduction can be modeled. Furthermore, the inertia, gravity, surface tension and aerodynamic drag are neglected in this model because they are usually much smaller in comparison with the stresses generated in the viscoelastic polymer melt. Finally, the process is treated here as an isothermal one, which can be justifiable for small enough drawing lengths and/or very high draw-down speeds [56]. The detailed description of the utilized model is provided below.

2.2.1. Velocity field

The Cartesian system axes are directed as follows (see Fig. 3): in-film-plane axes x and y , where x points in the streamwise direction and y is perpendicular onto it, and z axis is normal to the film xy plane with origin deployment in the cross-sectional center of gravity at the die exit. The dimensions of the film are denoted as follows: take up length is X , initial film half-width is L_0 , and initial half-thickness is e_0 . The intensity of film drawing is expressed in terms of draw ratio (DR) that relates the final tangential velocity of the film at the chill roll, $u(X)$, to the film velocity at the die exit, u_0 . The quantities without a zero subscript denotes non-initial corresponding dimensions at any given x position. The influence of extrudate swelling on the casting process is assumed to be negligible here. Using the symmetry of the problem and the kinematic hypothesis, the complexity of the velocity field involved in the film drawing is reduced, where each of the components is the function of all spatial and time variables. In the resulting form, the velocity field for steady solution is approximated as follows:

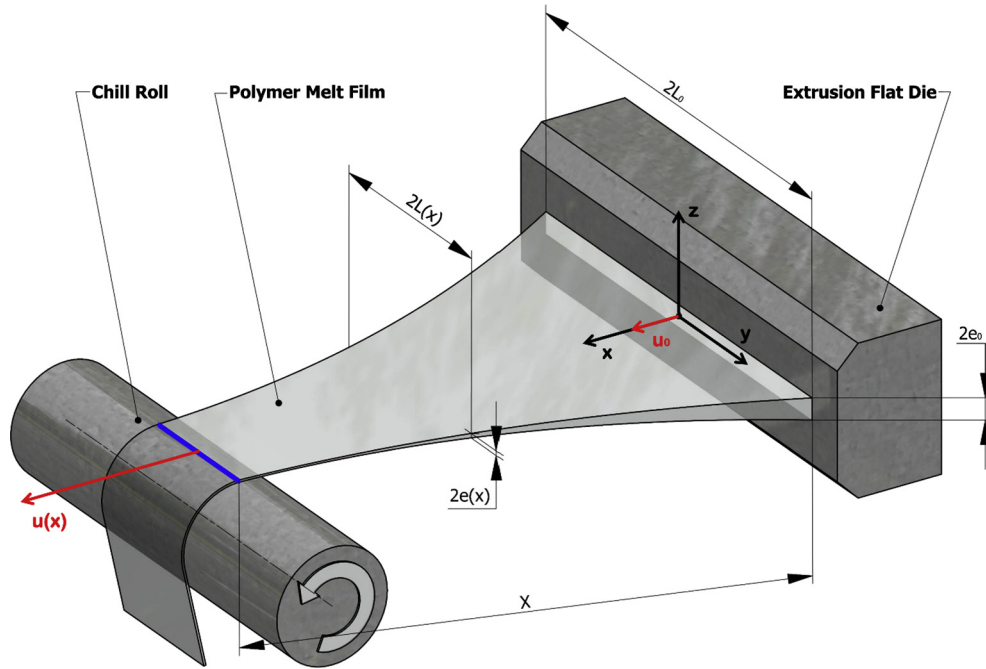


Fig. 3. Schematic of the extrusion film casting process kinematic.

$$\begin{aligned}
 u &= u(x) \\
 v &= v(x, y) = yf(x) \\
 w &= w(x, z) = zg(x)
 \end{aligned}
 \tag{13}$$

where u , v and w are the velocity components in the machine, transverse, and thickness direction, respectively. The deformation rate tensor, which is based on Eq. (13), takes the following form:

$$\underline{\underline{D}} = \begin{bmatrix} \frac{du}{dx} & \frac{1}{2}y\frac{df}{dx} & \frac{1}{2}z\frac{dg}{dx} \\ \frac{1}{2}y\frac{df}{dx} & f(x) & 0 \\ \frac{1}{2}z\frac{dg}{dx} & 0 & g(x) \end{bmatrix}
 \tag{14}$$

Since the polymer flow in EFC is mainly extensional and in an effort to increase simplicity, the shear rate components can be neglected in favour of elongational ones in Eq. (14), which leads to the following final expression for the deformation rate tensor:

$$\underline{\underline{D}} = \begin{bmatrix} \frac{du}{dx} & 0 & 0 \\ 0 & f(x) & 0 \\ 0 & 0 & g(x) \end{bmatrix}
 \tag{15}$$

The film thickness is constant throughout the film width due to the assumed velocity field, where the v and w velocity components are dependent on x variable only and are allowed to vary linearly over the film width and thickness, respectively, due to the applied Narayanaswamy's supplementary kinematic hypothesis as mentioned above.

2.2.2. Continuity equation

The continuity equation requires the conservation of mass at any given streamwise position and with the incompressibility hypothesis takes the following form.

$$\frac{d}{dt}(eL) + \frac{d}{dx}(eLu) = 0
 \tag{16}$$

Since the transient solution of the equation is not an objective of this study, the derivative with respect to time can be neglected. For steady state solution, the derivative with respect to time is

$$\frac{d}{dx}(eL) = 0
 \tag{17}$$

and thus, the volumetric flow rate at the die exit position and at any given streamwise position is given by Eqs. (18) and (19), respectively.

$$e_0L_0u_0 = Q
 \tag{18}$$

$$e(x)L(x)u(x) = Q
 \tag{19}$$

It is important to mention that the volumetric flow rate Q here corresponds to 1/4th of the cross-section only due to the process symmetry as show in [57].

2.2.3. Momentum conservation equation

Considering the membrane approximation for the thin film in the presence of a constant drawing force, the stresses are constant over the cross section of the film, which leads to the force balance having the following form

$$\frac{d}{dx}(\sigma_{xx}Le) = \frac{dF}{dx} = 0
 \tag{20}$$

Neglecting gravity, inertia, aerodynamic friction and surface tension forces, the drawing force becomes x -direction independent, which is fully balanced by the stresses generated in the film.

$$F = const = \sigma_{xx}Le
 \tag{21}$$

In this equation, σ_{xx} stands for the first diagonal component of the total stress tensor, $\underline{\underline{\sigma}}$, which is defined via the extra stress tensor, $\underline{\underline{\tau}}$, as follows

$$\underline{\underline{\sigma}} = -p\underline{\underline{\delta}} + \underline{\underline{\tau}} = \begin{bmatrix} -p + \tau_{xx} & 0 & 0 \\ 0 & -p + \tau_{yy} & 0 \\ 0 & 0 & -p + \tau_{zz} \end{bmatrix}
 \tag{22}$$

where p stands for the isotropic pressure, $\underline{\underline{\delta}}$ is the unity tensor. As it can be seen from Eq. (22), the diagonal components of the total stress tensor are defined as

$$\begin{aligned}
 \sigma_{xx} &= -p + \tau_{xx} \\
 \sigma_{yy} &= -p + \tau_{yy} \\
 \sigma_{zz} &= -p + \tau_{zz}
 \end{aligned}
 \tag{23}$$

The membrane approximation requires zero value of the thickness-wise component of total stress tensor, $\sigma_{zz} = 0$, which leads to

$$0 = -p + \tau_{zz} \tag{24}$$

i.e.

$$\tau_{zz} = p \tag{25}$$

Substituting Eq. (25) back into expression for stress components Eq. (23), the hydrostatic pressure term is eliminated, which leads to the following final expression for the diagonal components of the total stress tensor

$$\begin{aligned} \sigma_{xx} &= \tau_{xx} - \tau_{zz} \\ \sigma_{yy} &= \tau_{yy} - \tau_{zz} \\ \sigma_{zz} &= 0 \end{aligned} \tag{26}$$

After substitution of σ_{xx} , which is given by Eq. (26), into Eq. (21), the final form of the force balance equation is obtained

$$(\tau_{xx} - \tau_{zz})Le = F \tag{27}$$

2.2.4. The stress-free surface boundary condition

Assuming the surface tension and air drag are negligible, the net force per unit surface at the film free surface is equal to zero:

$$\underline{\underline{\sigma}} \cdot \underline{\underline{n}} = 0 \tag{28}$$

where the $\underline{\underline{n}}$ is the unit vector normal to the free film surface. This yields the following expression relating the stress state of the film with the film half-width at given x position:

$$\left(\frac{dL}{dx}\right)^2 = \frac{\sigma_{yy}}{\sigma_{xx}} \tag{29}$$

2.2.5. The kinematic free-surface boundary condition

The fluid is enclosed in the boundaries of the free surface, which can be expressed as

$$\underline{\underline{u}} \cdot \underline{\underline{n}} = 0 \tag{30}$$

where $\underline{\underline{u}}$ is the tangential velocity at the film-air interface. Combination of Eq. (30) with the equation of continuity leads to

$$u(x) \frac{dL}{dx} - f(x)L = 0 \tag{31}$$

$$u(x) \frac{de}{dx} - g(x)e = 0 \tag{32}$$

where $f(x)$ and $g(x)$ are components of the deformation rate tensor (see Eq. (15)) in the width and thickness direction, respectively, which can simply be expressed as

$$f(x) = \frac{u(x)}{L} \frac{dL}{dx} \tag{33}$$

$$g(x) = \frac{u(x)}{e} \frac{de}{dx} \tag{34}$$

2.2.6. Dimensionless transformation

For the sake of simplicity and scaling purposes, the dimensionless transformation has been introduced into the previously derived equations (having similar form as in [29]). Corresponding dimensionless quantities are denoted here with the overline symbol. Dimensionless transformation for the extra stress tensor and total stress tensor is defined here as

$$\bar{\tau}_{ii} = \frac{\tau_{ii}e_0L_0}{F} \tag{35}$$

$$\bar{\sigma}_{ii} = \frac{\sigma_{ii}e_0L_0}{F} \tag{36}$$

whereas the dimensionless spatial dimensions and streamwise velocity component are

$$\bar{x} = \frac{x}{X} \tag{37}$$

$$\bar{e} = \frac{e}{e_0} \tag{38}$$

$$\bar{L} = \frac{L}{L_0} \tag{39}$$

$$\bar{u} = \frac{u}{u_0} \tag{40}$$

Dimensionless numbers such as draw ratio, DR , Deborah number, De , aspect ratio, A and dimensionless force, E , are defined as follows

$$DR = \frac{u(X)}{u_0} \tag{41}$$

$$De = \frac{\lambda u_0}{X} \tag{42}$$

$$A = \frac{X}{L_0} \tag{43}$$

$$\bar{E} = \frac{FX}{G\lambda e_0 L_0 u_0} \tag{44}$$

Introducing the dimensionless transformation into the continuity equation (Eq. (19)) and momentum conservation equation (Eq. (27)) leads to the following dimensionless implicit forms

$$\bar{e}\bar{L}\bar{u} = 1 \tag{45}$$

$$(\bar{\tau}_{xx} - \bar{\tau}_{zz})\bar{L}\bar{e} = 1 \tag{46}$$

Substitution of Eq. (45) into Eq. (46) gives

$$(\bar{\tau}_{xx} - \bar{\tau}_{zz}) - \bar{u} = 0 \tag{47}$$

and differentiating Eqs. (45) and (47) with respect to x variable, one can obtain

$$\frac{1}{\bar{e}} \frac{d\bar{e}}{d\bar{x}} + \frac{1}{\bar{L}} \frac{d\bar{L}}{d\bar{x}} + \frac{1}{\bar{u}} \frac{d\bar{u}}{d\bar{x}} = 0 \tag{48}$$

$$\frac{\bar{\tau}_{xx}}{d\bar{x}} - \frac{\bar{\tau}_{zz}}{d\bar{x}} - \frac{d\bar{u}}{d\bar{x}} = 0 \tag{49}$$

After rearrangement, the derivative of the dimensionless film half-thickness and axial velocity with respect to x are finally defined as

$$\frac{d\bar{e}}{d\bar{x}} = -\left(\frac{1}{\bar{L}} \frac{d\bar{L}}{d\bar{x}} + \frac{1}{\bar{u}} \frac{d\bar{u}}{d\bar{x}}\right)\bar{e} \tag{50}$$

$$\frac{d\bar{u}}{d\bar{x}} = \frac{d\bar{\tau}_{xx}}{d\bar{x}} - \frac{d\bar{\tau}_{zz}}{d\bar{x}} \tag{51}$$

The dimensionless forms for $f(x)$ and $g(x)$ functions, which were derived from the kinematic free-surface boundary condition and appear in the deformation rate tensor, are the following

$$\bar{f} = \frac{L_0}{u_0} f(x) \tag{52}$$

$$\bar{g} = \frac{e_0}{u_0} g(x) \tag{53}$$

Finally, the dimensionless transformation for the x-direction derivative of the film half-width (arising from Eqs. (26) and (29)) yields

$$\frac{d\bar{L}}{d\bar{x}} = -A \sqrt{\frac{\bar{\tau}_{yy} - \bar{\tau}_{zz}}{\bar{\tau}_{xx} - \bar{\tau}_{zz}}} \tag{54}$$

2.3. Extrusion film casting model for the modified Leonov model

In order to combine the modified Leonov constitutive equation and the extrusion film casting model equations, it is necessary to derive the equation for particular stress development along the x axis. The relationship between the dimensionless stress and the recoverable strain, imposed from the modified Leonov model (Eqs. (1) and (12)), can be described by the following formula (for the case of the Mooney potential, i.e. when $n = 0$ and $\beta \neq 0$):

$$\bar{\tau}_{ii} = \frac{E}{De} c_{ii} - \frac{E}{De} c_{ii} \beta - \frac{E}{De} c_{ii}^{-1} \beta \tag{55}$$

Differentiating this equation with respect to x leads to

$$\frac{d\bar{\tau}_{ii}}{d\bar{x}} = \frac{E}{De} \frac{dc_{ii}}{d\bar{x}} - \frac{E}{De} \beta \frac{dc_{ii}}{d\bar{x}} - \frac{E}{De} \beta \left(-\frac{1}{c_{ii}^2} \frac{dc_{ii}}{d\bar{x}} \right) \tag{56}$$

where $\frac{dc_{ii}}{d\bar{x}}$ stands for the x-direction derivative of the recoverable strain tensor. This term is defined by Eq. (4) and for each component of the recoverable strain tensor it takes the following form:

$$\frac{dc_{xx}}{d\bar{x}} = 2c_{xx} \frac{1}{\bar{u}} \frac{d\bar{u}}{d\bar{x}} - \frac{2\bar{b}}{\bar{u}} Z_x \tag{57}$$

$$\frac{dc_{yy}}{d\bar{x}} = 2c_{yy} \frac{1}{\bar{L}} \frac{d\bar{L}}{d\bar{x}} - \frac{2\bar{b}}{\bar{u}} Z_y \tag{58}$$

$$\frac{dc_{zz}}{d\bar{x}} = 2c_{zz} \frac{1}{\bar{e}} \frac{d\bar{e}}{d\bar{x}} - \frac{2\bar{b}}{\bar{u}} Z_z \tag{59}$$

where \bar{b} , Z_i and X_p are defined as

$$\bar{b}(I_{1,c}) = \frac{1}{4De} \left\{ \exp[-\xi \sqrt{I_{1,c} - 3}] + \frac{\sinh[\nu(I_{1,c} - 3)]}{\nu(I_{1,c} - 3) + 1} \right\} \tag{60}$$

$$Z_i = c_{ii}(c_{ii} - c_{ii}^{-1} + X_p) \tag{61}$$

$$X_p = \frac{1}{3}(c_{xx}^{-1} + c_{yy}^{-1} + c_{zz}^{-1} - c_{xx} - c_{yy} - c_{zz}) \tag{62}$$

Combination of Eqs. (51) and (56) leads to the dimensionless streamwise deformation rate, which takes the following form

$$\frac{d\bar{u}}{d\bar{x}} = \frac{\bar{b}[\beta(Z_x - Z_z) - Z_x + Z_z] + \bar{b}\beta\left(\frac{1}{c_{zz}^2}Z_z - \frac{1}{c_{xx}^2}Z_x\right) + \frac{\bar{u}}{L} \frac{d\bar{L}}{d\bar{x}} \left(c_{zz}(1 - \beta) + \frac{\beta}{c_{zz}} \right)}{\beta(c_{xx} + c_{zz}) - c_{xx} - c_{zz} - \frac{\beta}{c_{xx}} \left(\frac{c_{zz} + c_{xx}}{c_{zz}} \right) + \frac{De\bar{u}}{2E}} \tag{63}$$

2.4. Boundary conditions

The complex and essential explicit model equations constituted in the previous section, namely Eqs. (50), (54), (63), and (57)–(59) has to be solved with the appropriate set of the boundary conditions. Detailed description of the utilized boundary conditions is provided below.

2.4.1. Upstream boundary conditions

Taking advantage of the dimensionless transformation, the initial half-width, half-thickness, and streamwise velocity are equal to one.

$$\bar{u}(0) = 1 \tag{64}$$

$$\bar{e}(0) = 1 \tag{65}$$

$$\bar{L}(0) = 1 \tag{66}$$

Since a viscoelastic constitutive equation is involved in this study, it is necessary to define initial boundary conditions for all three diagonal components of the extra stress tensor $\bar{\tau}_{xx}(0)$, $\bar{\tau}_{yy}(0)$ and $\bar{\tau}_{zz}(0)$ by using Eq. (55). To do that, diagonal components of the recoverable strain tensor at the die exit must be determined as the first by solving the following set of equations

$$\frac{E}{De} [(c_{xx} - c_{zz})(1 - \beta) + \beta(c_{zz}^{-1} - c_{xx}^{-1})] - 1 = 0 \tag{67}$$

$$c_{xx}c_{yy}c_{zz} = 1 \tag{68}$$

$$\frac{N_2}{N_1} = \frac{E [c_{zz} - c_{yy} + \beta(c_{yy} + c_{yy}^{-1} - c_{zz} - c_{zz}^{-1})]}{De\bar{u}} \tag{69}$$

Eq. (67) comes from the combination of Eqs. (47), (55) and (64) whereas Eq. (68) represents the incompressibility condition for the given flow situation. Eq. (69) represents normal stress difference ratio at the die exit, which is defined as the ratio of the secondary normal stress difference and primary normal stress difference

$$\frac{N_2}{N_1} = \frac{\bar{\tau}_{zz}(0) - \bar{\tau}_{yy}(0)}{\bar{\tau}_{xx}(0) - \bar{\tau}_{zz}(0)} \tag{70}$$

Note, that in this equation $\bar{\tau}_{xx}(0) - \bar{\tau}_{zz}(0) = 1$ as the result of Eqs. (47) and (64). As it can clearly be seen from Eq. (69), the N_2/N_1 ratio, which characterizes the polymer melt stress state at the die exit region, has to be provided in order to calculate the initial boundary conditions for the extra stress tensor.

2.4.2. Downstream boundary conditions

Downstream boundary condition, draw ratio, is prescribed as the desired value that is satisfied by a priori unknown magnitude of the drawing force.

$$\bar{u}(X) = DR \tag{71}$$

2.5. Numerical scheme

The whole system of the first-order ordinary differential equations (namely Eqs. (50), (54), and (63) for film half-thickness, half-width and velocity as well as Eqs. (57)–(59) for the components of the recoverable elastic strain tensor c_{xx} , c_{yy} and c_{zz}) was numerically solved by the 4th order Runge-Kutta algorithm with adaptive step-size control. For the given take-up force value, it was necessary to determine the components of the recoverable elastic strain tensor in order to satisfy Eqs. (50), (54) and (63) along with the other boundary conditions for the die exit region, that are constant with the force, and thus do not require evaluation in every iteration (Eqs. (64)–(66) and N_2/N_1 ratio). The value of the force was guessed for the first iteration and then increased or decreased throughout foregoing iterations in order to meet the DR boundary condition (convergence) by Newton-Raphson method. It was preferred to develop the solver itself in the C++ programming language, to avoid a black box effect, which could have appeared in the case of using a built-in solver in any other commercial mathematical-modeling software. The equation evaluation was performed on the PC with the following hardware parameters: CPU Intel Core 2 Quad Q9650 (3.00 GHz), RAM 8 GB DDR2, GPU Sapphire Radeon HD 3870, SSD Crucial 256 GB. Typical computational time for one calculation was about 2 min. A schematic representation of the utilized numerical scheme is provided in Fig. 4.

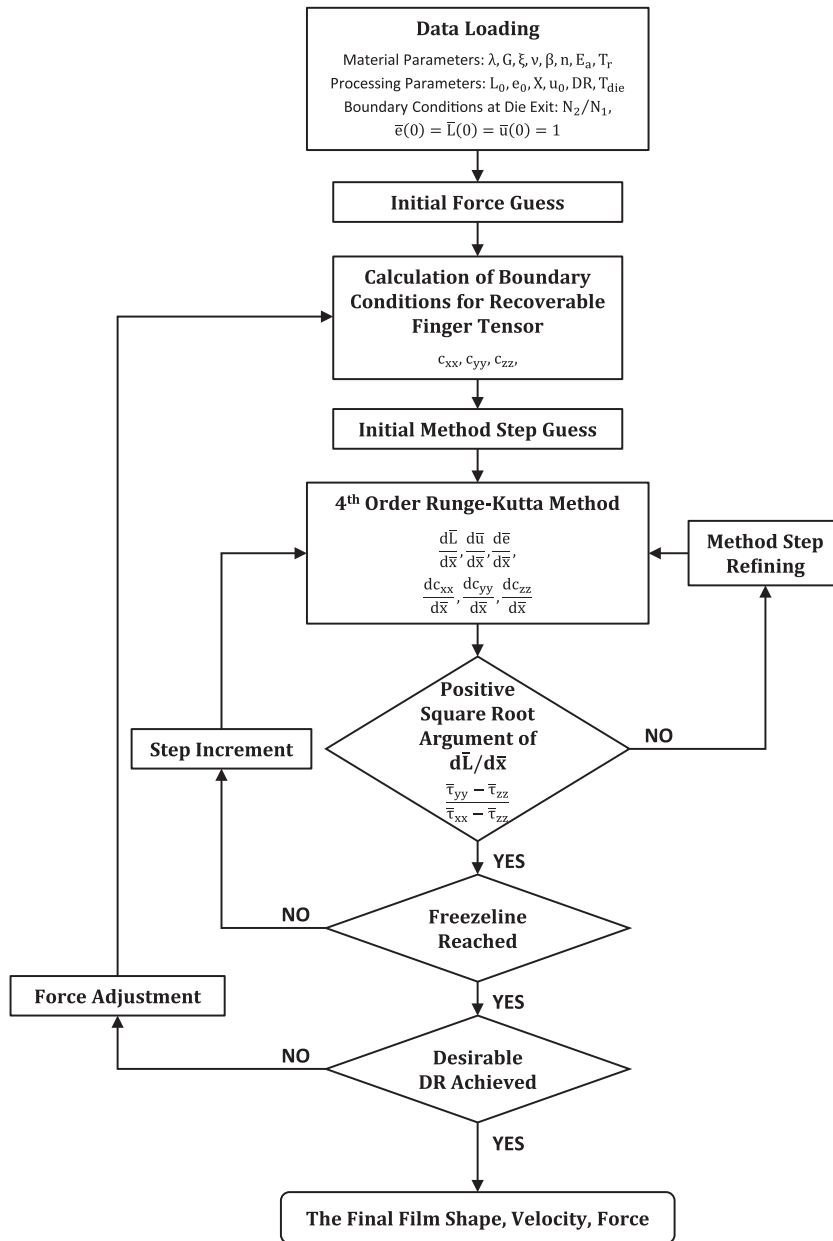


Fig. 4. Iteration scheme for the utilized viscoelastic film casting model.

3. Results and discussion

3.1. Film casting model validation

In order to validate the utilized film casting model, we have used recent experimental and theoretical data provided in [45,46,48] for very well characterized LDPE 170A polymer (produced by The Dow Chemical Company, Freeport, TX, USA) having a flow activation energy 40 kJ/mol and molecular characteristics, which are provided in Table 1.

In this work, the single-mode modified Leonov model was utilized to simplify the calculation. The model parameters were identified by using deformation rate dependent ‘steady state’ uniaxial extensional viscosity experimental data taken from Fig. 2b in [46] (i.e. from the peaks appearing on the transient extensional viscosity curves for corresponding extensional strain rates). Obtained model parameters are provided in Table 2. Interestingly, the measured data can be represented by the single-mode modified Leonov model very well as shown in Fig. 5a).

Modeled processing conditions for the film casting process were the same as described in [45,46], i.e. isothermal, die width = 100 mm, gap size = 0.46 mm, melt exit velocity = 4.3 mm/s, and distance between the die and roll 230 mm. As it has already been mentioned, in the fully viscoelastic calculation based on the modified Leonov model, it is necessary to define the stress state at the end of the extrusion die, namely the ratio of the second normal stress difference, N_2 , and first normal stress difference, N_1 , which is given by the flow history inside the flat extrusion die. However, this rheological characteristic is not available for the given LDPE 170A from [45,46,48] and thus typical $-N_2/N_1 = 0.2$ value was taken from the open literature [58] to define the stress boundary condition at the die exit. Comparison between the film casting model predictions based on the single-mode modified Leonov model (this work), multi-mode XPP model and the corresponding experimental data (both taken from [45,46]) is provided in Fig. 5b–d and Fig. 6. In Fig. 5b–d, the basic dimensionless variables such as film half-width, half-thickness and center-line velocity are provided as the function of dimensionless distance

Table 1Molecular characteristics for Dow LDPE 170A with density 0.924 g/cm³ and MFI 0.7 g/10 min (190 °C, 2.16 kg) [46].

Mn (g/mol)	Mw (g/mol)	Mz (g/mol)	PDI (1)	Newtonian viscosity at 150 °C (Pa s)	Rh (nm)	LCB (per 10,000 C atoms) ^a	Branched ≥ 6 C atoms (per 10,000 C atoms) ^b
30,600	185,900	528,400	6.07	134,992.70	16.40	11	80

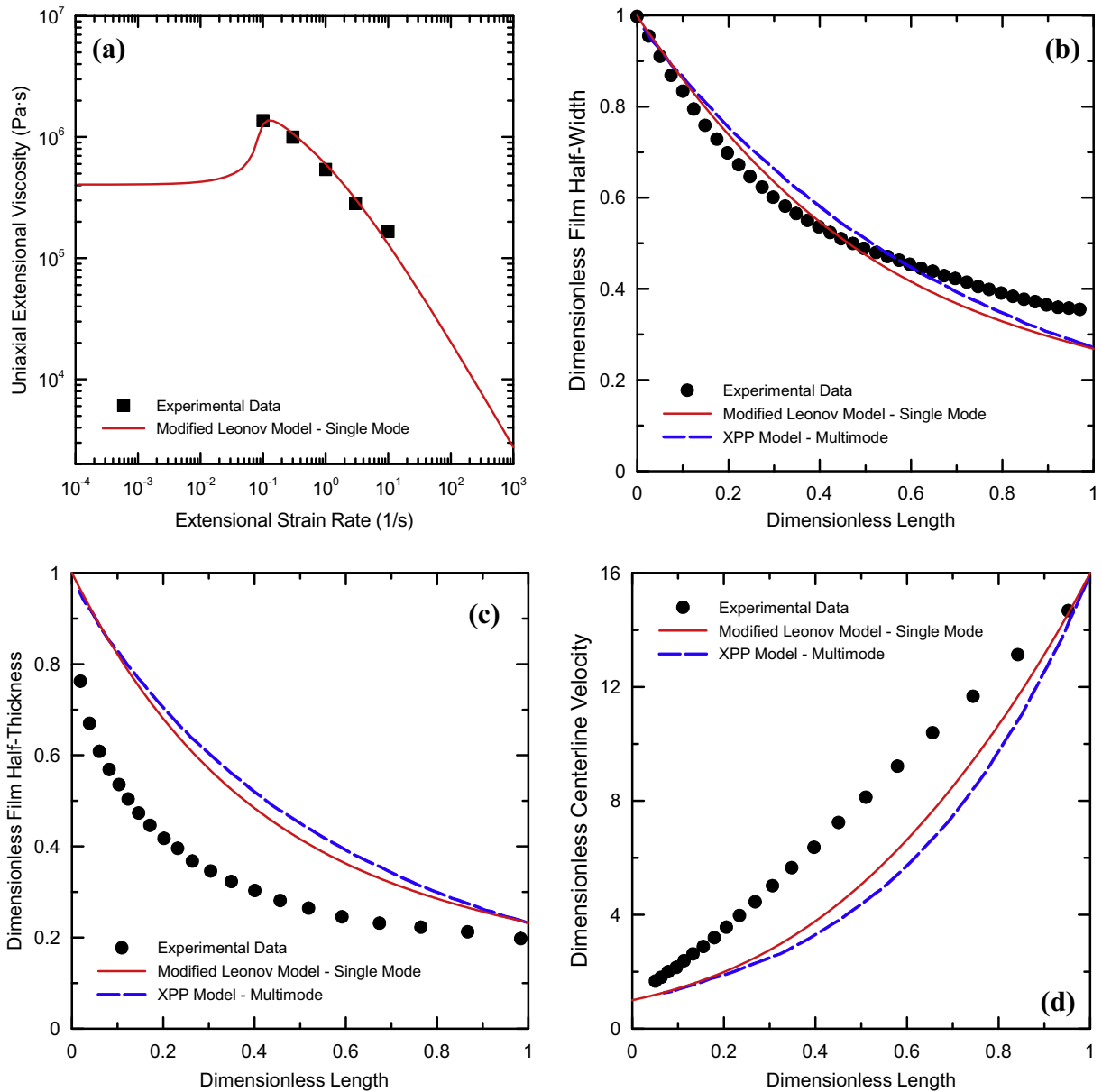
PDI – Polydispersity Index.

LCB – Long Chain Branching.

^a Data acquired from HT-GPC (High-temperature Gel Permeation Chromatography).^b Data acquired from HT-NMR (High-temperature Nuclear Magnetic Resonance).**Table 2**

Modified Leonov model parameters for T = 150 °C; LDPE 170A.

λ (s)	G (Pa)	ξ (1)	ν (1)	β (1)
1.57	85,982.61	1.816	0.174	0.4

**Fig. 5.** Comparison between experimental data for LDPE 170A (T = 150 °C) and given processing conditions (De = 0.011, DR = 16, X = 230 mm) taken from the open literature [46] and corresponding model predictions considering that $-N_2/N_1 = 0.2$. (a) LDPE 170A extensional rheology, (b) film half-width profile between die and roll, (c) film half-thickness profile between die and roll, and (d) velocity profile between die and roll.

between the die ($\bar{x} = 0$) and the chill roll ($\bar{x} = 1$) for high draw ratio (DR = 16) and Deborah number (De = 0.011) whereas Fig. 6 shows the effect of draw ratio on dimensionless final film half-width for low (0.011) and high (0.253) Deborah numbers. As it can be seen, the behavior of both models is comparable and the agreement with the experimental data is good for the given range of draw ratios and Deborah numbers. Such a reasonably good agreement with

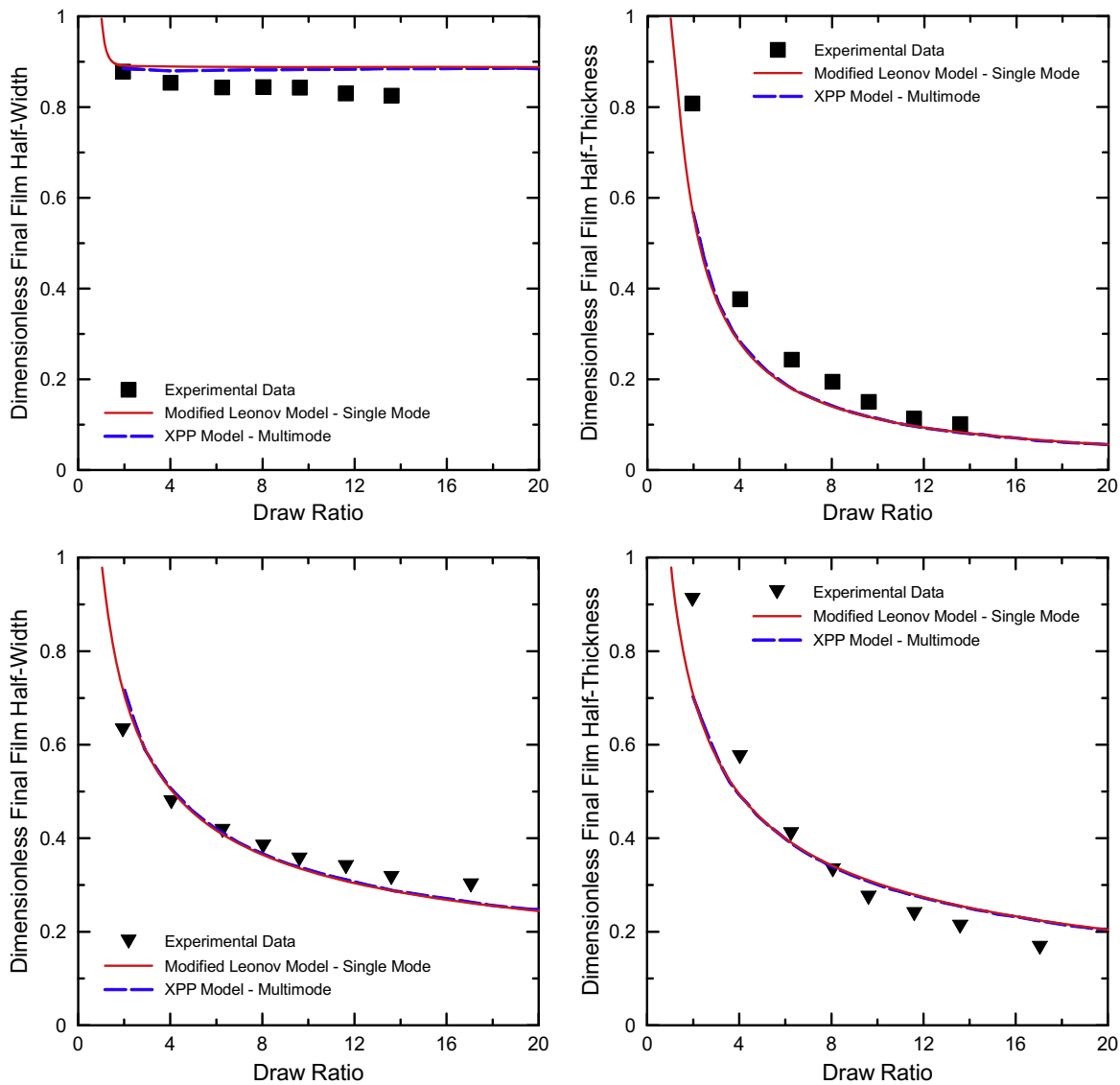


Fig. 6. Comparison between experimental data for LDPE 170A taken from the open literature [45] for different Deborah numbers (top – $De = 0.253$, $X = 10$ mm, bottom – $De = 0.011$, $X = 228$ mm) and corresponding model predictions considering that $-N_2/N_1 = 0.2$. Left – dimensionless final film half-width vs. draw ratio, Right – dimensionless final film half-thickness vs. draw ratio.

the experimental data justifies to use of the given film casting model with all applied assumptions together with even single-mode Leonov model for detailed parametric study of the neck-in phenomenon. In order to understand the undesired neck-in phenomenon in more detail, the role of Deborah number and extensional rheology was systematically investigated via a theoretical parametric study, which is described in the next section.

3.2. Theoretical analysis of neck-in phenomenon

3.2.1. The role of extensional rheology

With the aim to understand the role of extensional behavior of polymer melts on the neck-in phenomenon, 3 groups of virtual materials were generated with high, middle and low level of uniaxial extensional strain hardening defined as

$$\frac{\eta_{E,U,max}}{3\eta_0} \tag{72}$$

Here, $\eta_{E,U,max}$ represents the maximum value in the steady uniaxial extensional viscosity and η_0 is the Newtonian viscosity. In each

group, 5 virtual materials were generated having the same level of uniaxial extensional strain hardening but different level of planar extensional strain hardening defined as

$$\frac{\eta_{E,P,max}}{4\eta_0} \tag{73}$$

where $\eta_{E,P,max}$ represents the maximum value in the steady planar extensional viscosity. Modified Leonov model parameters for the 15 utilized virtual polymer melts (one of them, Melt3_Middle, has identical parameters as the LDPE 170A melt described in Model validation section) are provided in Table 3 whereas their extensional rheology is provided in Fig. 7.

The title of each virtual melt contains information about the level of uniaxial extensional strain hardening (Low, Middle, and High) as well as about the level of planar extensional strain hardening (1 – the lowest, 2, 3, 4, and 5 – the highest). For example, the virtual samples entitled here as Melt1_High and Melt5_High means that both samples have different planar extensional strain hardening (i.e. the lowest in the first case and the highest in the second case) whereas their uniaxial extensional strain hardening

Table 3

Modified Leonov model parameters for the utilized virtual polymer melts at 150 °C.

Virtual material name	λ (s)	G (Pa)	ξ (1)	ν (1)	β (1)	$\frac{\eta_{E,U,max}}{3\eta_0}$	$\frac{\eta_{E,P,max}}{4\eta_0}$
Melt1_High	1.57	85,982.61	4.414	0.276	0.1	7.1	6.2
Melt2_High	1.57	85,982.61	4.042	0.208	0.3	7.1	6.6
Melt3_High	1.57	85,982.61	3.816	0.174	0.4	7.1	6.8
Melt4_High	1.57	85,982.61	3.54	0.14	0.5	7.1	7.1
Melt5_High	1.57	85,982.61	2.806	0.072	0.7	7.1	7.9
Melt1_Middle	1.57	85,982.61	2.014	0.276	0.1	3.4	2.9
Melt2_Middle	1.57	85,982.61	1.882	0.208	0.3	3.4	3.1
Melt3_Middle	1.57	85,982.61	1.816	0.174	0.4	3.4	3.2
Melt4_Middle	1.57	85,982.61	1.75	0.14	0.5	3.4	3.4
Melt5_Middle	1.57	85,982.61	1.53	0.072	0.7	3.4	4.2
Melt1_Low	1.57	85,982.61	0.338	0.276	0.1	1.3	1.10
Melt2_Low	1.57	85,982.61	0.38	0.208	0.3	1.3	1.17
Melt3_Low	1.57	85,982.61	0.4	0.174	0.4	1.3	1.22
Melt4_Low	1.57	85,982.61	0.418	0.14	0.5	1.3	1.29
Melt5_Low	1.57	85,982.61	0.426	0.072	0.7	1.3	1.53

is identical (high). Similarly, the virtual samples entitled as Melt1_High and Melt1_Low means that both samples have identical (the lowest) planar extensional strain hardening but different uniaxial extensional strain hardening (i.e. high and low in the first and second case, respectively). Each group of virtual materials (having the given level of uniaxial extensional strain hardening) can be then characterized by steady-state planar to uniaxial extensional viscosity ratio, $\frac{\eta_{E,P}}{\eta_{E,U}}$, plotted as the function of extensional strain rate, as visualized on the left side of Fig. 8.

In the next step, the dimensionless final film half-width as the function of draw ratio was calculated for all 15 virtual polymer melts by using the film casting model keeping the Deborah number and $-N_2/N_1$ ratio the same, equal to 0.07 and 0.2, respectively. Results are depicted on the right side of Fig. 8. As it can be seen, if $\frac{\eta_{E,P}}{\eta_{E,U}}$ increases or $\frac{\eta_{E,U,max}}{3\eta_0}$ decreases, the intensity of neck-in phenomenon as well as its sensitivity to draw ratio increases. It is also visible that for the given conditions and virtual materials used, there is always a critical draw ratio above which the dimensionless final film width (i.e. also the neck-in) becomes constant and draw ratio independent. Under such flow conditions, the applied extensional strains are high enough to reach steady state values in uniaxial and planar extensional viscosities. It is important to mention that such high draw down ratios ($DR > 20$) are typically achieved in industrial high speed productions [1,2]. In order to follow industrial practice, our attention will focus on flow conditions at which the maximum draw ratio independent neck-in occurs.

3.2.2. The role of Deborah number

In order to understand the role of Deborah number on the maximum attainable neck-in, its value was varied from 0.01 to 0.1 in the film casting model for all 15 virtual polymer melts keeping the $-N_2/N_1$ ratio the same, equal to 0.2. For each simulation case, the draw ratio was adjusted high enough (typically equal to 40) in order to reach maximum and draw ratio independent neck-in value, NI . The maximum neck-in value was consequently normalized by the take-up length (stretching distance) X as follows

$$NI^* = \frac{NI}{X} \quad (74)$$

Calculated maximum neck-in value NI^* as a function of the square root of planar to uniaxial extensional viscosity ratio, $\sqrt{\eta_{E,P}/\eta_{E,U}}$, is provided in Fig. 9a–c for different Deborah numbers and uniaxial extensional strain hardening values. It is clear that an increase in the Deborah number increases both, the neck-in as well as its sensitivity to $\sqrt{\eta_{E,P}/\eta_{E,U}}$.

3.2.3. Simple approximate and analytical solution for NI^*

Closer analysis of numerical solutions depicted in Figs. 9a–c reveals that NI^* varies with $\sqrt{\eta_{E,P}/\eta_{E,U}}$ almost linearly for all considered uniaxial extensional strain hardening levels. In order to quantify all calculated data, let us consider the following linear relationship between these two variables, i.e.:

$$NI^* = k \left(\sqrt{\frac{\eta_{E,P}}{\eta_{E,U}}} - 1 \right) + Q \quad (75)$$

where k (the slope of the line) and Q (the NI^* intercept) are constants for given De and $\frac{\eta_{E,U,max}}{3\eta_0}$. In order to capture the effect of De and $\frac{\eta_{E,U,max}}{3\eta_0}$ on both constants, let us assume the following relationships for k and Q parameters (motivated by the well-known Avrami equation):

$$k^* = ka_5 = A_1 [1 - \exp(-\alpha_1 De^{\varphi_1})] \quad (76)$$

$$Q^* = Qa_5 = A_2 [1 - \exp(-\alpha_2 De^{\varphi_2})] \quad (77)$$

where $A_1, A_2, \alpha_1, \alpha_2, \varphi_1, \varphi_2$ represent constants whereas k^* and Q^* are the reduced slope and reduced NI^* intercept, respectively, and a_5 is the shift factor defined as

$$a_5 = \sqrt[10]{\frac{\eta_{E,U,max}}{3\eta_0}} \quad (78)$$

Eq. (75) was used to fit all numerical data provided in Fig. 9a–c in order to identify k and Q parameters for given Deborah numbers and $\frac{\eta_{E,U,max}}{3\eta_0}$ ratios. Both parameters were reduced by a_5 factor, plotted as the function of the Deborah number and finally fitted by Eqs. (76) and (77) to identify all model parameters, which are summarized in Table 4. Note that the fitting error was evaluated for both equations via the Root Mean Squared Error (RMSE) defined as

$$RMSE = \sqrt{\frac{1}{n_s} \sum_{j=1}^{n_s} [y_j - \hat{y}_j]^2} \quad (79)$$

where n_s is the number of points whereas y_j and \hat{y}_j represent given and predicted points, respectively. Comparison between Deborah number dependent k^* and Q^* and model fits is provided in Fig. 9d and e. As it is shown, the suggested Eqs. (76) and (77) have the capability to describe k^* and Q^* parameters reasonably well.

If Eqs. (75)–(78) are combined together, the following expression for the normalized maximum neck-in is obtained

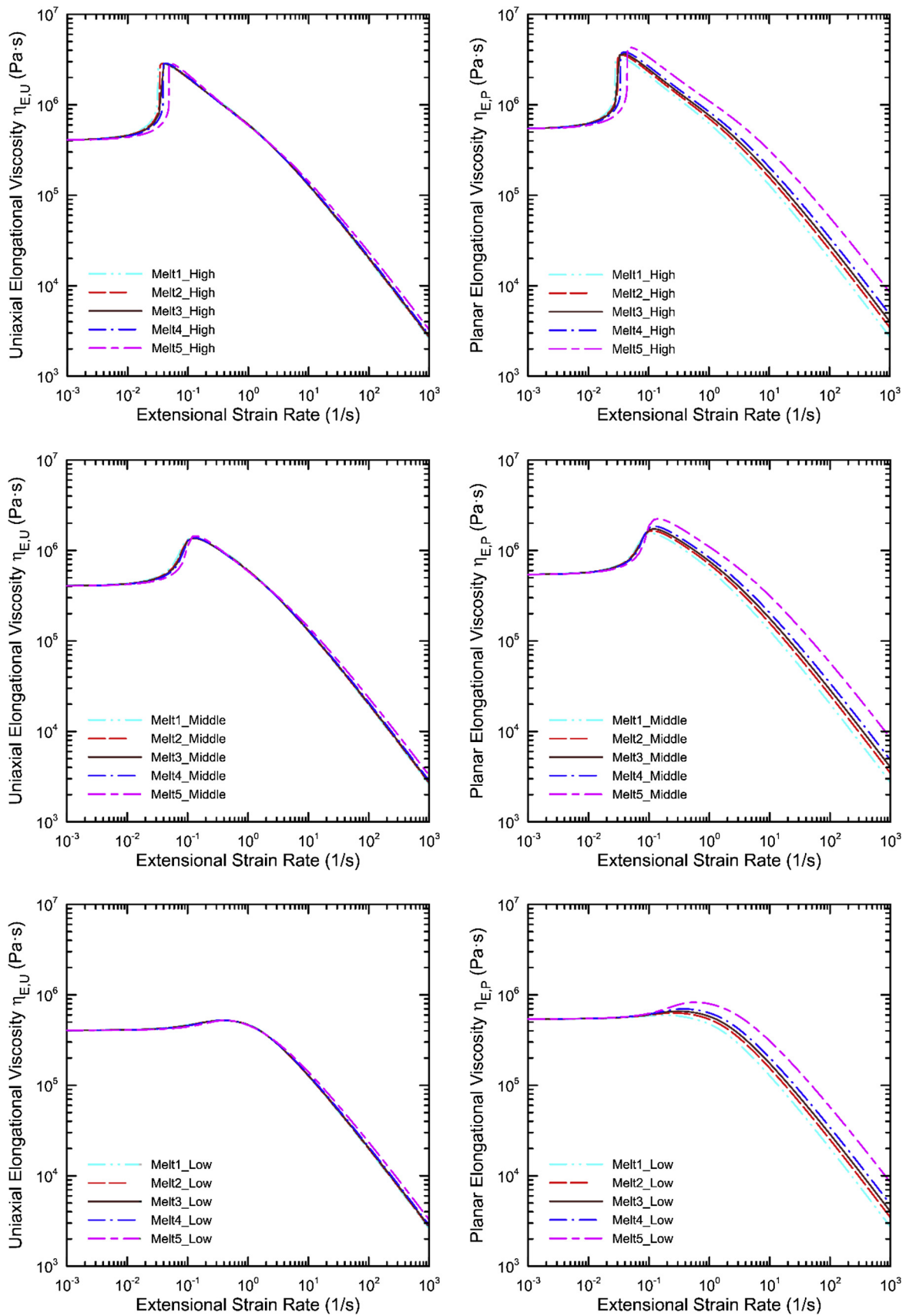


Fig. 7. Uniaxial and planar extensional viscosities of different virtual polymer melts utilized in this work having high (top), medium (middle) and low (bottom) level of extensional strain hardening at $T = 150^\circ\text{C}$.

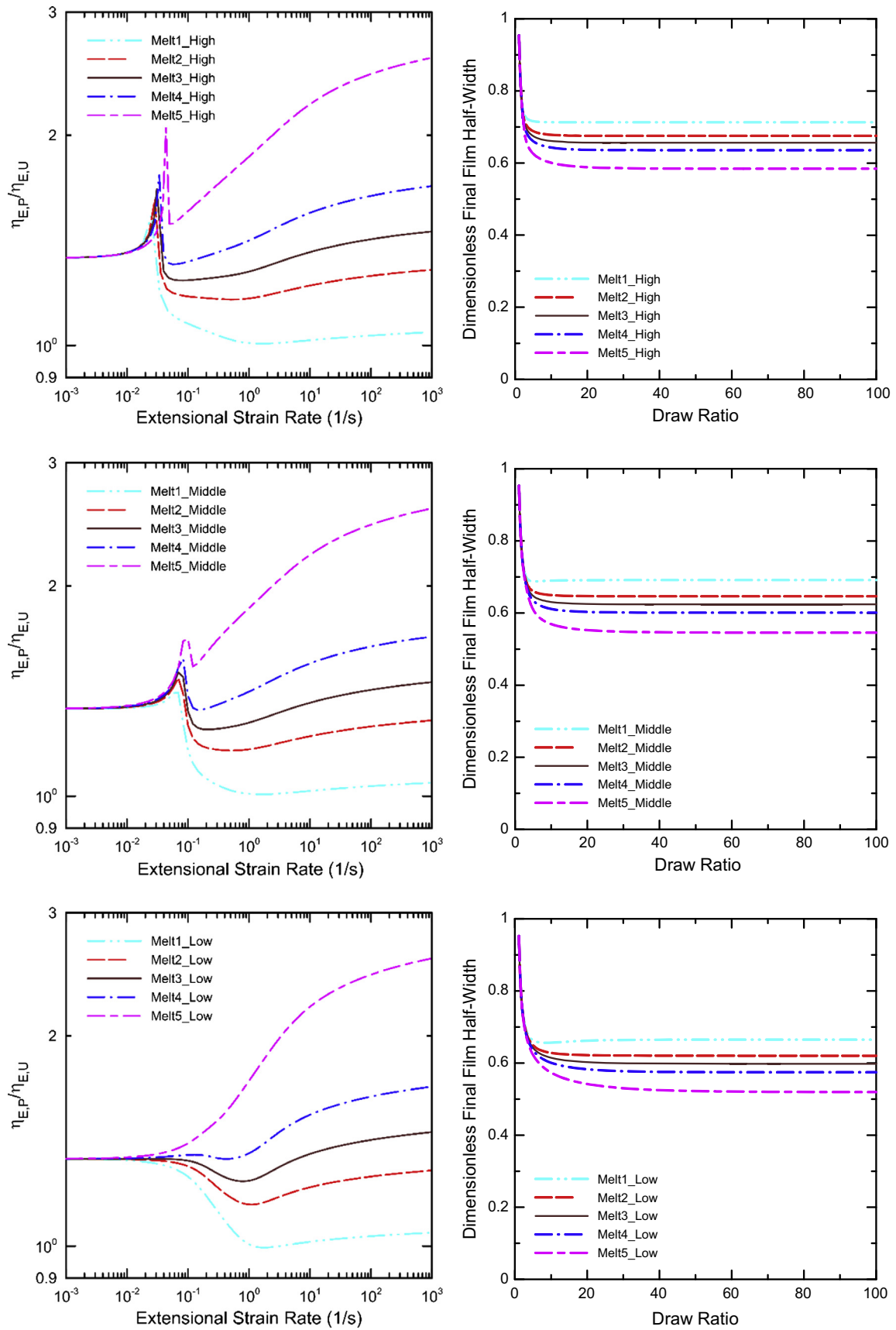


Fig. 8. Effect of planar to uniaxial extensional viscosity ratio, $\eta_{E,P}/\eta_{E,U}$, on draw ratio dependent dimensionless final film half-width for high (top), medium (middle) and low (bottom) level of extensional strain hardening polymer melts considering that $-N_2/N_1 = 0.2$.

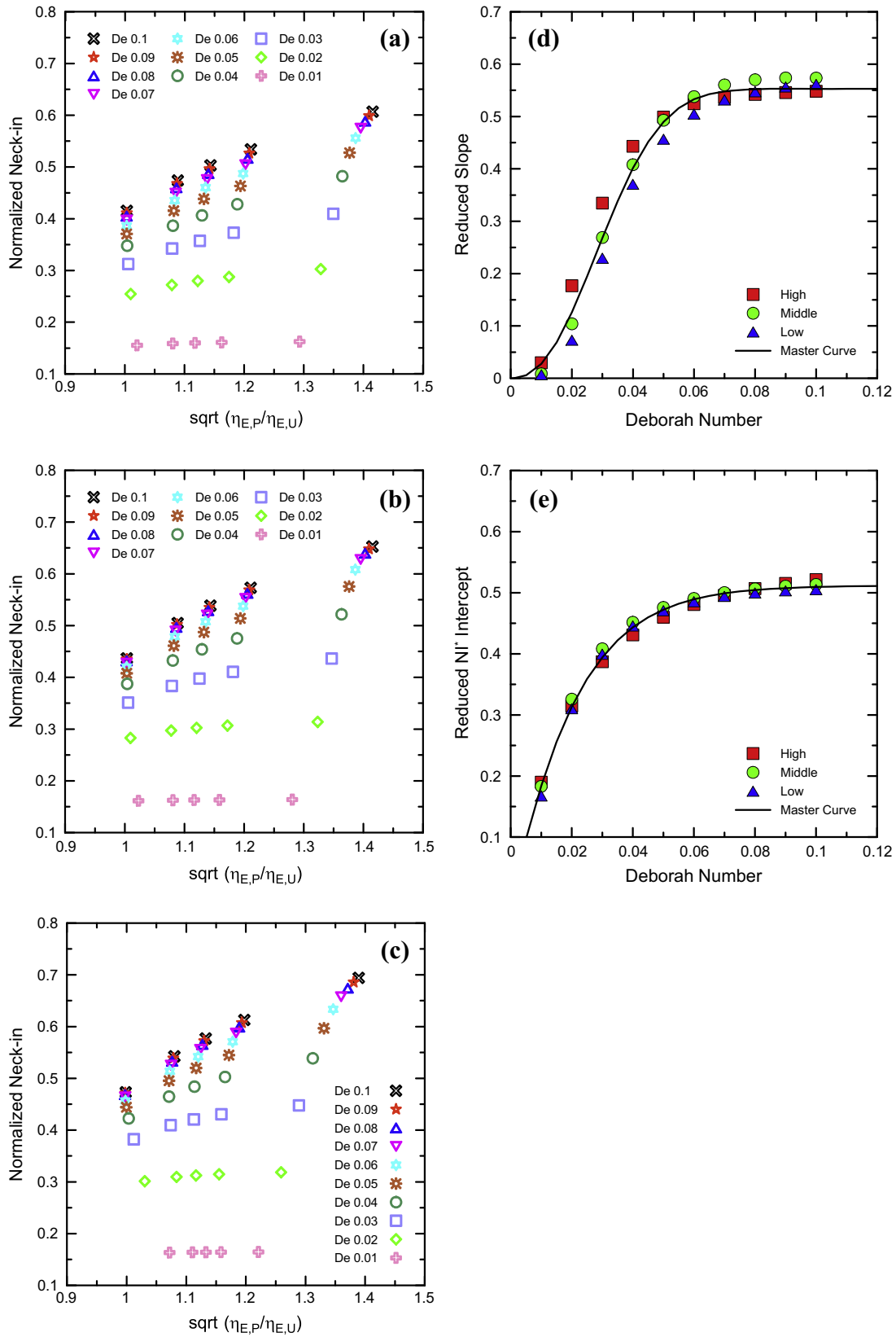


Fig. 9. The effect of Deborah number and square root of planar to uniaxial extensional viscosity ratio, $\sqrt{\eta_{E,P}/\eta_{E,U}}$, on the normalized neck-in for high (a) medium (b) and low (c) level of extensional strain hardening polymer melts considering that $-N_2/N_1 = 0.2$. Fig. 9d and 9e shows Deborah number dependent reduced slope k^* and the reduced NI^* intercept Q^* (both calculated from k and Q in Eq. (75)), respectively, in comparison with the model fitting lines, which are given by Eqs. (76) and (77).

Table 4
Parameters for Eqs. (76) and (77) defining k and Q values.

f(De)	j	A _j	α _j	φ _j	RMSE
Reduced slope	1	0.553	2,287.854	2.323	0.0255
Reduced NI* intercept	2	0.512	66.712	1.087	0.00726

$$NI^* = \frac{1}{\sqrt[10]{\frac{\eta_{E,U,max}}{3\eta_0}}} \left\{ A_1 [1 - \exp(-\alpha_1 De^{\phi_1})] \left(\sqrt{\frac{\eta_{E,P}}{\eta_{E,U}}} - 1 \right) + A_2 [1 - \exp(-\alpha_2 De^{\phi_2})] \right\} \quad (80)$$

This equation represents the final form of the simple analytical expression for the normalized and draw ratio independent neck-in value, which approximates the true numerical film casting model solution for the chosen range of Deborah numbers, $\frac{\eta_{E,U,max}}{3\eta_0}$ and $\frac{\eta_{E,P}}{\eta_{E,U}}$ ratios. Comparison between the true numerical film casting model predictions and approximate solution (given by Eq. (80)) for NI^* as a function of $\sqrt{(\eta_{E,P}/\eta_{E,U})}$, De and $\frac{\eta_{E,U,max}}{3\eta_0}$ is provided in Fig. 10. Based on this figure, it can be stated that the simple approximate solution model (Eq. (80)) is capable of representing NI^* predictions of the utilized 1D viscoelastic membrane model predictions very well.

3.2.4. Behaviour of simple approximate solution for NI^* at high Deborah numbers

If the Deborah number in Eq. (80) becomes high enough, the expression for NI^* is simplified to

$$\lim_{De \rightarrow \infty} NI^* = \frac{1}{\sqrt[10]{\frac{\eta_{E,U,max}}{3\eta_0}}} \left[A_1 \left(\sqrt{\frac{\eta_{E,P}}{\eta_{E,U}}} - 1 \right) + A_2 \right] \quad (81)$$

As indicated from Table 4, A_1 and A_2 constants are very similar. This suggests that both constants could be considered to be the same. This can be justified by the very small increase in RMSE (from 0.00726 to 0.01506) when this assumption is applied to identify corresponding α_2 and ϕ_2 parameters via Eq. (77). Thus, considering that $A_2 = A_1 = 0.553$, Eq. (81) simplifies to

$$\lim_{De \rightarrow \infty} NI^* = \frac{0.553}{\sqrt[10]{\frac{\eta_{E,U,max}}{3\eta_0}}} \sqrt{\frac{\eta_{E,P}}{\eta_{E,U}}} \quad (82)$$

Based on Eq. (82), it can be concluded that the maximum attainable NI^* , which is given by the approximate solution at very high Deborah numbers, is a linear function of $\sqrt{\frac{\eta_{E,P}}{\eta_{E,U}}}$ with a slope of $\frac{0.553}{\sqrt[10]{\frac{\eta_{E,U,max}}{3\eta_0}}}$.

3.3. Simple approximate solution for NI^* vs. experimental data

In this part, the validity of the simple approximate solution for NI^* , which is given by Eq. (80) and parameters provided in Table 4, is tested for the Dow LDPE 170A sample (see Table 1) as well as for three additional PE samples taken from [26], whose basic characteristics are provided in Table 5. Normalized maximum neck-in, NI^* , together with the corresponding extrusion film casting processing parameters for each polymer sample are taken from [26,45] and they are summarized in Table 6.

In the first step, deformation rate dependent uniaxial extensional viscosity data were successfully fitted for each polymer melt

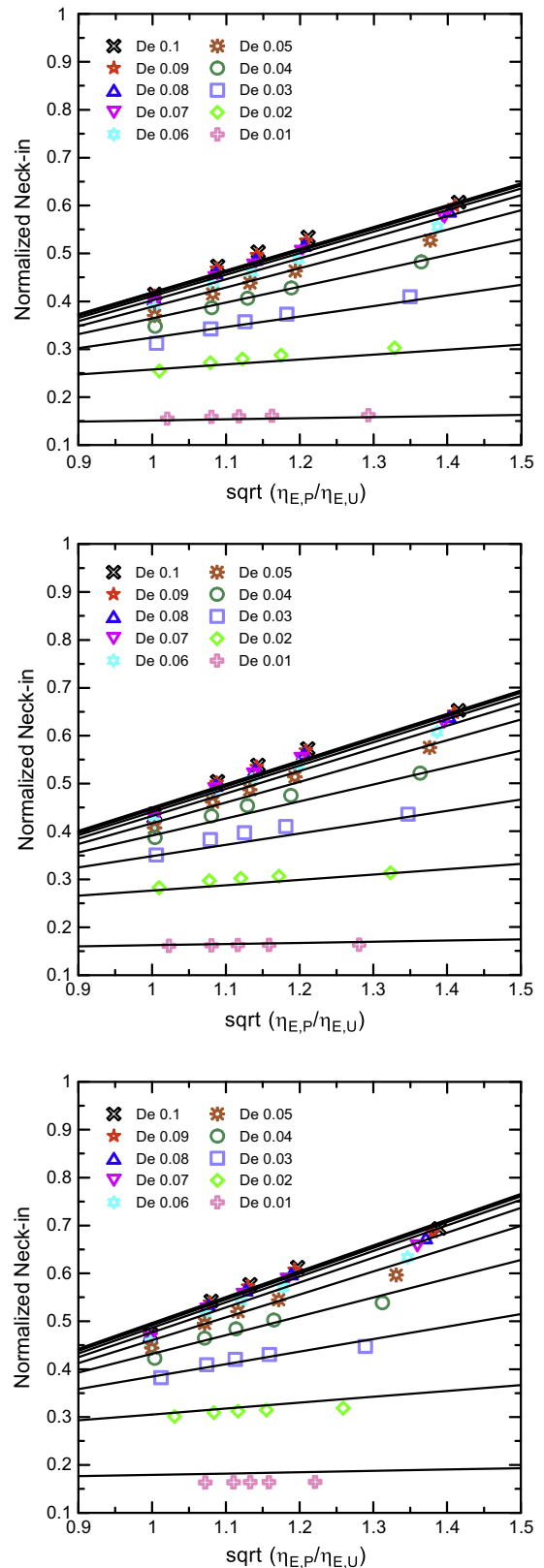


Fig. 10. The effect of Deborah number on the normalized neck-in vs. planar to uniaxial extensional viscosity ratio for virtual polymer melts having high (top), medium (middle) and low (bottom) level of extensional strain hardening. Here, symbols and lines represent utilized viscoelastic 1D membrane model and simple approximate solution model (Eq. (80)) predictions, respectively.

Table 5
Basic characteristics for PE-A, PE-B and PE-C samples [26].

Polymer sample	MFI (g/10 min)	Melt tension (cN)	M_w (kg/mol)	M_w/M_n (1)	Newtonian viscosity at 130 °C (Pa s)	Polymerization process
PE-A	6.7	2.1	163	9.1	16,220	Autoclave
PE-B	4.1	3.3	102	6.6	37,720	Tubular
PE-C	4.3	1.9	85	6.0	36,033	Tubular

Flow activation energy, E_a , for all three samples is 49.887 kJ/mol. Note, that E_a was calculated here as $E_a = \alpha R$, where α is Arrhenius law parameter equal to 6,000 K provided in [26] and R is the universal gas constant equal to 8.3144598 J/K/mol.

Table 6
Extrusion film casting processing parameters for all considered polymer samples taken from the open literature.

Polymer sample	Die width (mm)	Die gap (mm)	Air gap (mm)	Temperature (°C)	Die exit velocity (mm/s)	Draw ratio (1)	NI^* (1)	Ref.
LDPE 170A	100	0.46	228	190	4.3	17.1	0.1537	[45]
PE-A	600	0.80	160	320	46.6 ^a	42.91 ^b	0.2466	[26]
PE-B	600	0.80	190	320	46.6 ^a	42.91 ^b	0.3275	[26]
PE-C	600	0.80	220	320	46.6 ^a	42.91 ^b	0.5159	[26]

^a Die exit velocity was determined based on the die width (L_0), die gap (e_0), melt density (ρ) and mass flow rate (MFR) as $u_0 = MFR/(\rho L_0 e_0)$, where $MFR = 60$ kg/h and melt density $\rho = 745$ kg/m³ [26].

^b Draw ratio was determined from die exit velocity and take-up velocity as $DR = u/u_0$. Take-up velocity is provided in [26] as $u = 120$ m/min.

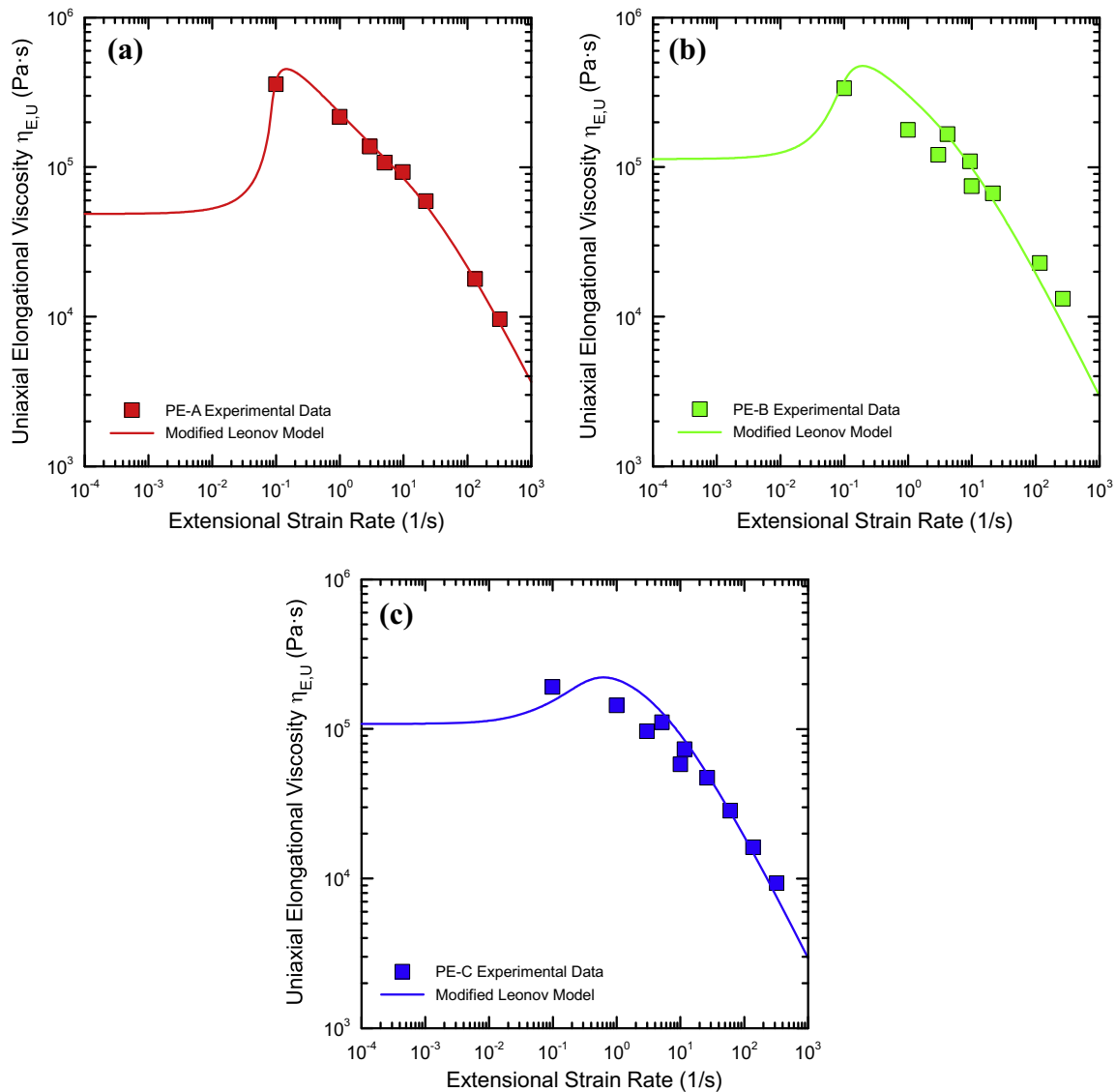


Fig. 11. Comparison between experimentally determined deformation rate dependent uniaxial extensional viscosity data for different polymer samples at 130 °C taken from [26] and single mode modified Leonov model predictions. (a) PE-A, (b) PE-B, and (c) PE-C.

Table 7

Modified Leonov model parameters for PE-A, PE-B and PE-C polymer samples at 130 °C.

Polymer sample	λ (s)	G (Pa)	ξ (1)	ν (1)	β (1)
PE-A	9.5	1,707.37	0.41	0.0015	0.4
PE-B	15	2,514.67	0.29	0.0034	0.4
PE-C	30	1,201.10	0.09	0.0013	0.5

Table 8

Analytical model parameters for all considered polymer materials for the given processing parameters.

Polymer sample	λ (s)	De (1)	Mean du/dx (1/s)	$\frac{\eta_{EP}}{\eta_{EU}}$	$\frac{\eta_{EU,max}}{3\eta_0}$
LDPE 170A	0.588	0.011	0.300	1.280	3.393
PE-A	0.079	0.019	10.281	0.833	9.299
PE-B	0.125	0.026	8.879	1.102	4.198
PE-C	0.250	0.061	10.281	1.293	2.047

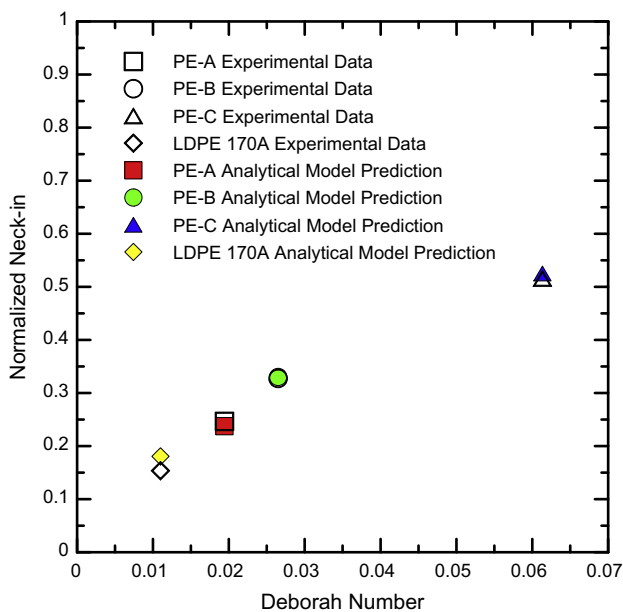


Fig. 12. Normalized maximum and draw ratio independent neck-in value, NI^* , as the function of Deborah number for LDPE 170A, PE-A, PE-B and PE-C polymer samples for the processing conditions summarized in Table 8. Experimental data (taken from [45,26]) are represented here by the open symbols whereas the predictions of the proposed analytical model, Eq. (80), are given by the filled symbols.

at given temperature by the single mode modified Leonov model, as it can be seen in Fig. 11. Model parameters for PE-A, PE-B and PE-C samples are provided in Table 7 for 130 °C. Note, that the Leonov model parameters for the Dow LDPE 170A sample have already been identified in the ‘Film Casting Model Validation’ section (see Fig. 5a) and they are provided in Table 2.

In the second step, Leonov model relaxation times, which are provided in Tables 2 and 7 for given polymer samples, were shifted to the particular processing temperature by using the Arrhenius shift factor and the flow activation energy, i.e. from 150 °C to 190 °C for LDPE 170A and from 130 °C to 320 °C for PE-A, PE-B and PE-C samples. This allows calculation of Deborah number according to Eq. (42) via shifted Leonov model relaxation time and process parameters u_0 (die exit velocity) and X (air gap) provided in Table 6. In order to evaluate the average value of planar to uniaxial extensional viscosity ratio, $\frac{\eta_{EP}}{\eta_{EU}}$, by using modified Leonov model, one needs to determine the mean value of deformation rate in the machine direction, du/dx . This variable was estimated

here as the ratio of velocity difference between the die and roll ($u-u_0$) and stretching distance X , which can be justifiable for linear velocity profiles typically occurring for LDPE polymer melts [45,46,48]. Uniaxial extensional strain hardening, $\frac{\eta_{EU,max}}{3\eta_0}$, is simply given by the modified Leonov model for given material and processing temperature. All estimated parameters, which are needed to calculate the maximum normalized neck-in value, NI^* , via the approximate model (Eq. (80)), are summarized in Table 8 for the given materials and processing conditions.

Comparison between the measured NI^* and approximate model predictions, utilizing parameters summarized in Table 8, is provided in Fig. 12. As it can be seen, the simple approximate model can predict neck-in value NI^* for the considered LDPE polymer melts and Deborah numbers very well. Eq. (80) can thus be considered as a useful tool for optimization of process conditions and polymer melt rheology to minimize neck-in phenomena during thin flat film production under industrial processing conditions.

It is important to mention that utilization of Eq. (80) requires experimental determination of the planar-to-uniaxial extensional viscosity ratio, which is one of the most challenging rheological tasks because generation and control of the extensional flow is difficult. Just recently, it has been shown that planar and uniaxial extensional viscosity can be measured in a wide temperature and deformation rate range by using a standard twin bore capillary rheometer, with novel rectangular and circular orifice (zero-length) dies and the Cogswell model [59].

4. Conclusions

In this work, viscoelastic, isothermal extrusion film casting modeling utilizing a 1D membrane model and a single-mode modified Leonov model was performed in order to understand the role of uniaxial extensional strain hardening, planar-to-uniaxial extensional viscosity ratio and Deborah number on the neck-in phenomenon. For model validation purposes, basic dimensionless variables measured in [45,46,48] for LDPE polymer melt such as film half-width, half-thickness and center-line velocity as the function of stretching distance, DR and Deborah numbers were used. It was found that the film casting modeling by using multi-mode XPP model and modified Leonov model is comparable for the given LDPE polymer and processing conditions even though, surprisingly, a single-mode version of the Leonov model was used. The consequent parametric study revealed that firstly, if planar to uniaxial extensional viscosity ratio, $\frac{\eta_{EP}}{\eta_{EU}}$, decreases or uniaxial extensional strain hardening increases, $\frac{\eta_{EU,max}}{3\eta_0}$, intensity of neck-in phenomenon as well as its sensitivity to draw ratio decreases and secondly, an increase in the Deborah number increases both, the neck-in as well

as its sensitivity to $\frac{\eta_{E,P}}{\eta_{E,U}}$. Obtained numerical solutions were successfully approximated by a simple dimensionless analytical equation relating maximum attainable neck-in value with $\frac{\eta_{E,U,max}}{3\eta_0}$, $\frac{\eta_{E,P}}{\eta_{E,U}}$ and Deborah number. The validity of the suggested equation was tested by using experimental data taken from the open literature [26,45,46] for four different polyethylene melts, for which $0.011 \leq De \leq 0.061$, $0.833 \leq \frac{\eta_{E,P}}{\eta_{E,U}} \leq 1.293$ and $2.047 \leq \frac{\eta_{E,U,max}}{3\eta_0} \leq 9.299$. It was found that the proposed equation can describe for the given polymer melts and processing conditions the experimental data very well. Thus, it is believed that this simple model can be used for material, die design and process conditions optimization in order to minimize unwanted neck-in phenomenon in cast film production.

Acknowledgments

The authors wish to acknowledge the financial support from the Grant Agency of the Czech Republic (Grant registration No. 16-05886S).

References

- [1] T. Kanai, G.A. Campbell, Film Processing, Hanser Publishers, 1999.
- [2] T. Kanai, G.A. Campbell, Film Processing Advances, second ed., Carl Hanser Verlag GmbH & Co. KG, München, 2014.
- [3] A. Co, Chapter 10 draw resonance in film casting, in: S.G. Hatzikiriakos, K.B. Migler (Eds.), Polymer Processing Instabilities: Control and Understanding, CRC Press, 2005, p. 488.
- [4] H.W. Jung, J.C. Hyun, Chapter 11 fiber spinning and film blowing instabilities, in: S.G. Hatzikiriakos, K.B. Migler (Eds.), Polymer Processing Instabilities: Control and Understanding, CRC Press, 2005, p. 488.
- [5] D. Gelder, The stability of fiber drawing processes, Ind. Eng. Chem. Fundam. 10 (1971) 534–535.
- [6] R.J. Fisher, M.M. Denn, Finite-amplitude stability and draw resonance in isothermal melt spinning, Chem. Eng. Sci. 30 (1975) 1129–1134.
- [7] R.J. Fisher, M.M. Denn, A theory of isothermal melt spinning and draw resonance, AIChE J. 22 (1976) 236–246.
- [8] R.E. Christensen, Extrusion coating of polypropylene, SPE J. 18 (1962) 751.
- [9] J.C. Miller, Swelling behavior in extrusion, SPE Trans. 3 (1963) 134–137.
- [10] Y.L. Yeow, On the stability of extending films: a model for the film casting process, J. Fluid Mech. 66 (1974) 613–622.
- [11] G.R. Aird, Y.L. Yeow, Stability of film casting of power-law liquids, Ind. Eng. Chem. Fundam. 22 (1983) 7–10.
- [12] N.R. Anturkar, A. Co, Draw resonance in film casting of viscoelastic fluids: a linear stability analysis, J. Nonnewton. Fluid Mech. 28 (1988) 287–307.
- [13] V.R. Iyengar, A. Co, Film casting of a modified Giesekus fluid: a steady-state analysis, J. Nonnewton. Fluid Mech. 48 (1993) 1–20.
- [14] V.R. Iyengar, A. Co, Film casting of a modified Giesekus fluid: stability analysis, Chem. Eng. Sci. 51 (1996) 1417–1430.
- [15] J.-P. Sergent, Etude De Deux Proce'de's De Fabrication De Films. Le soufflage de gaine. L'extrusion de film a plat, Universite Louis Pasteur, Strasbourg, France, 1977.
- [16] D. Cotto, P. Duffo, J.M. Haudin, Cast film extrusion of polypropylene films, Int. Polym. Process. 4 (1989) 103–113.
- [17] P. Duffo, B. Monasse, J.M. Haudin, Cast film extrusion of polypropylene. thermomechanical and physical aspects, J. Polym. Eng. 10 (1991) 151–229.
- [18] P. Barq, J.M. Haudin, J.F. Agassant, Isothermal and anisothermal models for cast film extrusion, Int. Polym. Process. 7 (1992) 334–349.
- [19] T. Dobroth, L. Erwin, Causes of edge beads in cast films, Polym. Eng. Sci. 26 (1986) 462–467.
- [20] B. Debbaut, J.M. Marchal, M.J. Crochet, Viscoelastic effects in film casting, in: J. Casey, M.J. Crochet (Eds.), Theoretical, Experimental and Numerical Contributions to the Mechanics of Fluids Solids, Birkhauser Verlag, Basel, Switzerland; Boston, Berlin, 1995, pp. 679–698.
- [21] N. Toft, M. Rigdahl, Extrusion coating with metallocene-catalysed polyethylenes, Int. Polym. Process. 17 (2002) 244–253.
- [22] S. Kouada, Prediction of processability at extrusion coating for low-density polyethylene, Polym. Eng. Sci. 48 (2008) 1094–1102.
- [23] N. Satoh, H. Tomiyama, T. Kajiwara, Viscoelastic simulation of film casting process for a polymer melt, Polym. Eng. Sci. 41 (2001) 1564–1579.
- [24] H. Ito, M. Doi, T. Isaki, M. Takeo, A model of neck-in phenomenon in film casting process, J. Soc. Rheol. Japan. 31 (2003) 157–163.
- [25] S. Shiromoto, Y. Masutani, M. Tsutsubuchi, Y. Togawa, T. Kajiwara, A neck-in model in extrusion lamination process, Polym. Eng. Sci. 50 (2010) 22–31.
- [26] S. Shiromoto, Y. Masutani, M. Tsutsubuchi, Y. Togawa, T. Kajiwara, The effect of viscoelasticity on the extrusion drawing in film-casting process, Rheol. Acta 49 (2010) 757–767.
- [27] S. Shiromoto, The mechanism of neck-in phenomenon in film casting process, Int. Polym. Process. 29 (2014) 197–206.
- [28] S. D'Halewyu, J.F. Agassant, Y. Demay, Numerical simulation of the cast film process, Polym. Eng. Sci. 30 (1990) 335–340.
- [29] D. Silagy, Y. Demay, J.F. Agassant, Study of the stability of the film casting process, Polym. Eng. Sci. 36 (1996) 2614–2625.
- [30] O.S. Narayanaswamy, A one-dimensional model of stretching float glass, J. Am. Ceram. Soc. 60 (1977) 1–5.
- [31] D. Silagy, Y. Demay, J.F. Agassant, Stationary and stability analysis of the film casting process, J. Nonnewton. Fluid Mech. 79 (1998) 563–583.
- [32] G. Lamberti, G. Titomanlio, V. Brucato, Measurement and modelling of the film casting process 1. Width distribution along draw direction, Chem. Eng. Sci. 56 (2001) 5749–5761.
- [33] G. Lamberti, G. Titomanlio, V. Brucato, Measurement and modelling of the film casting process 2. Temperature distribution along draw direction, Chem. Eng. Sci. 57 (2002) 1993–1996.
- [34] G. Lamberti, V. Brucato, G. Titomanlio, Orientation and crystallinity in film casting of polypropylene, J. Appl. Polym. Sci. 84 (2002) 1981–1992.
- [35] G. Lamberti, F. De Santis, V. Brucato, G. Titomanlio, Modeling the interactions between light and crystallizing polymer during fast cooling, Appl. Phys. A 78 (2004) 895–901.
- [36] G. Titomanlio, G. Lamberti, Modeling flow induced crystallization in film casting of polypropylene, Rheol. Acta 43 (2004) 146–158.
- [37] G. Lamberti, G. Titomanlio, Analysis of film casting process: the heat transfer phenomena, Chem. Eng. Process. Process Intensif. 44 (2005) 1117–1122.
- [38] G. Lamberti, G. Titomanlio, Analysis of film casting process: effect of cooling during the path in air, Ind. Eng. Chem. Res. 45 (2006) 719–723.
- [39] G. Lamberti, Flow-induced crystallization during isotactic polypropylene film casting, Polym. Eng. Sci. 51 (2011) 851–861.
- [40] K. Sakaki, R. Katsumoto, T. Kajiwara, K. Funatsu, Three-dimensional flow simulation of a film-casting process, Polym. Eng. Sci. 36 (1996) 1821–1831.
- [41] H. Zheng, W. Yu, C. Zhou, H. Zhang, Three-dimensional simulation of the non-isothermal cast film process of polymer melts, J. Polym. Res. 13 (2006) 433–440.
- [42] H. Ito, M. Doi, T. Isaki, M. Takeo, K. Yagi, 2D flow analysis of film casting process, J. Soc. Rheol. Japan. 31 (2003) 149–155.
- [43] C.W. Seay, D.G. Baird, Sparse long-chain branching's effect on the film-casting behavior of PE, Int. Polym. Process. 24 (2009) 41–49.
- [44] C.D. McGrady, C.W. Seay, D.G. Baird, Effect of sparse long-chain branching on the film-casting behavior for a series of well-defined HDPEs, Int. Polym. Process. 24 (2009) 428–438.
- [45] H.V. Pol, S.S. Thete, P. Doshi, A.K. Lele, Necking in extrusion film casting: the role of macromolecular architecture, J. Rheol. 57 (2013) 559–583.
- [46] H. Pol, S. Banik, L.B. Azad, S.S. Thete, P. Doshi, A. Lele, Nonisothermal analysis of extrusion film casting process using molecular constitutive equations, Rheol. Acta 53 (2014) 85–101.
- [47] K. Chikhalikar, S. Banik, L.B. Azad, K. Jadhav, S. Mahajan, Z. Ahmad, S. Kulkarni, S. Gupta, P. Doshi, H. Pol, A. Lele, Extrusion film casting of long chain branched polypropylene, Polym. Eng. Sci. 55 (2015) 1977–1987.
- [48] S.S. Thete, P. Doshi, H.V. Pol, New insights into the use of multi-mode phenomenological constitutive equations to model extrusion film casting process, J. Plast. Film Sheet. 33 (2017) 35–71.
- [49] A.I. Leonov, Nonequilibrium thermodynamics and rheology of viscoelastic polymer media, Rheol. Acta 15 (1976) 85–98.
- [50] A.I. Leonov, E.H. Lipkina, E.D. Paskhin, A.N. Prokunin, Theoretical and experimental investigation of shearing in elastic polymer liquids, Rheol. Acta 15 (1976) 411–426.
- [51] A.I. Leonov, A.N. Prokunin, An improved simple version of a nonlinear theory of elasto-viscous polymer media, Rheol. Acta 19 (1980) 393–403.
- [52] A.I. Leonov, A.N. Prokunin, On nonlinear effects in the extensional flow of polymeric liquids, Rheol. Acta 22 (1983) 137–150.
- [53] M. Simhambhatla, A.I. Leonov, On the rheological modeling of viscoelastic polymer liquids with stable constitutive equations, Rheol. Acta 34 (1995) 259–273.
- [54] A.I. Leonov, Constitutive equations for viscoelastic liquids: formulation, analysis and comparison with data, Rheol. Ser. 8 (1999) 519–575.
- [55] M. Zatloukal, Differential viscoelastic constitutive equations for polymer melts in steady shear and elongational flows, J. Nonnewton. Fluid Mech. 113 (2003) 209–227.
- [56] D. Acerno, L. Di Maio, C.C. Ammirati, Film casting of polyethylene terephthalate: experiments and model comparisons, Polym. Eng. Sci. 40 (2000) 108–117.
- [57] M. Beaulne, E. Mitsoulis, Numerical simulation of the film casting process, Int. Polym. Process. 14 (1999) 261–275.
- [58] E.A. Jensen, J. deC. Christiansen, Measurements of first and second normal stress differences in a polymer melt, J. Nonnewton. Fluid Mech. 148 (2008) 41–46.
- [59] M. Zatloukal, Measurements and modeling of temperature-strain rate dependent uniaxial and planar extensional viscosities for branched LDPE polymer melt, Polymer 104 (2016) 258–267.

PAPER II



Effect of die exit stress state, Deborah number, uniaxial and planar extensional rheology on the neck-in phenomenon in polymeric flat film production

Tomas Barborik, Martin Zatloukal*

Polymer Centre, Faculty of Technology, Tomas Bata University in Zlin, Vavreckova 275, 760 01 Zlin, Czech Republic

ARTICLE INFO

Keywords:

Flat film production
Polymer melt
Rheology
Neck-in phenomenon
Deborah number
Second to first normal stress difference ratio
Uniaxial extensional viscosity
Planar extensional viscosity

ABSTRACT

In this work, effect of the second to first normal stress difference ratio at the die exit, $-N_2/N_1$, uniaxial extensional strain hardening, $\frac{\eta_{E,U,max}}{3\eta_0}$, planar-to-uniaxial extensional viscosity ratio, $\frac{\eta_{E,P}}{\eta_{E,U}}$, and Deborah number, De , has been investigated via viscoelastic isothermal modeling utilizing 1D membrane model and a single-mode modified Leonov model as the constitutive equation. Based on the performed parametric study, it was found that there exists a threshold value for De and $\frac{\eta_{E,U,max}}{3\eta_0}$, above which, the neck-in starts to be strongly dependent on $-N_2/N_1$. It was found that such critical De decreases if $-N_2/N_1$, $\frac{\eta_{E,U,max}}{3\eta_0}$ increases and/or $\frac{\eta_{E,P}}{\eta_{E,U}}$ decreases. Numerical solutions of the utilized model were successfully approximated by a dimensionless analytical equation relating the normalized maximum attainable neck-in with $\frac{\eta_{E,U,max}}{3\eta_0}$, $\frac{\eta_{E,P}}{\eta_{E,U}}$, $-N_2/N_1$ and De . Suggested equation was tested by using literature experimental data considering that $-N_2/N_1$ depends on die exit shear rate, temperature and utilized constitutive model parameters for given polymer melt. It was found that approximate model predictions are in a very good agreement with the corresponding experimental data for low as well as very high Deborah numbers, at which neck-in strongly depends on $-N_2/N_1$. It is believed that the obtained knowledge together with the suggested simple model can be used for optimization of the extrusion die design (influencing flow history and thus die exit stress state), molecular architecture of polymer melts and processing conditions to suppress neck-in phenomenon in production of very thin polymeric flat films.

1. Introduction

The extrusion film casting technology is an industrially important process that has a firm position on the market due to its capability to produce high quality thin polymeric films at high production rates. Those films can be used in different applications such as wrapping materials, barriers reducing permeability for air and vapor, or as a separator membrane for rechargeable batteries in mobile devices and electric vehicles.

In this technology, the polymer melt is extruded through a slit die to form a thick sheet that is subsequently intensively stretched in the axial direction, hauled off and quenched by a rotating drum stabilizing the film dimensions. [1,2] (Fig. 1). Except of an initial swelling, the thickness of the film decreases monotonically due to high Draw ratio (the haul off speed divided by the die exit velocity). In such a case, film width is gradually reduced toward the stretching/cooling roll, which is called neck-in phenomenon.

Aside from that, the interrelated defect of edge-beads promotes the lateral portion of the film to being substantially thicker than its central part (Fig. 2). While the first phenomenon affects a production rate, the second calls for a post-production trimming since solely central portion of the film is uniform in thickness. Understanding the relationship between material parameters and processing conditions including the flow in the die might be the way to effectively control the extent of neck-in and edge-beading as even a small reduction of these defects may bring increased efficiency considering high production rates in this manufacturing process.

Scientific investigation of the extrusion film casting process has been addressed in many works dealing with both a steady and transient approaches to the problem. Initial studies were dedicated to an investigation of the hydrodynamic instability observed during the production of fibers called draw resonance [3–5] and then expanded for films in [6] where the numerical modeling for film casting using the one-dimensional isothermal model of Newtonian fluid was utilized for

* Corresponding author.

E-mail address: mzatloukal@utb.cz (M. Zatloukal).

<https://doi.org/10.1016/j.jnnfm.2018.03.002>

Received 6 November 2017; Received in revised form 1 March 2018; Accepted 3 March 2018

Available online 06 March 2018

0377-0257/ © 2018 Elsevier B.V. All rights reserved.

List of symbols

A	aspect ratio (1)	$u(X)$	(mm·s ⁻¹)
A_1, A_2	fitting parameters of analytical model (1)	u_0	chill roll speed (mm·s ⁻¹)
b	dissipation term (s ⁻¹)	\bar{u}	axial velocity component at the die exit (mm·s ⁻¹)
\bar{b}	dimensionless dissipation term (1)	v	dimensionless axial velocity component of the film at any x location (1)
$\underline{\underline{c}}$	recoverable Finger tensor (1)	v	transverse velocity component of the film at any x location (mm·s ⁻¹)
$\underline{\underline{c}}_0^{-1}$	inverse recoverable Finger tensor (1)	W	elastic potential (Pa)
$\underline{\underline{c}}$	jaumann (corotational) time derivative of the recoverable Finger strain tensor (s ⁻¹)	w	thickness velocity component of the film at any x location (mm·s ⁻¹)
c_{xx}	normal component of the recoverable Finger tensor in axial x -direction (1)	X	take-up length (stretching distance, air gap) (mm)
c_{yy}	normal component of the recoverable Finger tensor in transverse y -direction (1)	x	position in axial x -direction (mm)
c_{zz}	normal component of the recoverable Finger tensor in thickness z -direction (1)	\bar{x}	dimensionless position in axial x -direction (1)
$\underline{\underline{D}}$	deformation rate tensor (s ⁻¹)	y_i	observed value (1)
De	Deborah number (1)	\hat{y}_i	predicted value (1)
DR	draw ratio (1)	x, y, z	spatial coordinates in axial, transverse and thickness direction, respectively (1)
$\underline{\underline{g}}_p$	irreversible rate of strain tensor (s ⁻¹)	Z_x, Z_y, Z_z	substitution variables (1)
E	dimensionless take-up force (1)	$\left(\frac{du}{dx}\right)_M$	mean value of extensional strain rate in the air gap (s ⁻¹)
E_a	flow activation energy (J·mol ⁻¹)	$\frac{dc_{xx}}{d\bar{x}}, \frac{dc_{yy}}{d\bar{x}}, \frac{dc_{zz}}{d\bar{x}}$	derivative of Finger tensor components with respect to dimensionless \bar{x} position (1)
e	half-thickness of the film at any x location (mm)	$\frac{d\bar{u}}{d\bar{x}}, \frac{d\bar{v}}{d\bar{x}}, \frac{d\bar{w}}{d\bar{x}}$	derivative of dimensionless axial, transverse and thickness velocity component with respect to dimensionless \bar{x} position (1)
e_0	die half-gap (half-thickness of the film at the die exit) (mm)		
\bar{e}	dimensionless half-thickness of the film at any x location (1)		
F	take-up force (stretching force) (N)		
f	rate of deformation in transverse y -direction (s ⁻¹)	Greek symbols	
G	linear Hookean elastic modulus (Pa)	α	Arrhenius law parameter (K)
g	rate of deformation in thickness z -direction (s ⁻¹)	α_1, α_2	fitting parameters of analytical model (1)
i	index i , noting the spatial direction (1)	β	non-linear Leonov model parameter (1)
$I_{1, c}$	first invariant of recoverable Finger tensor (1)	γ_{COR}	corrected shear rate by Rabinowitsch correction for the rectangle channel (s ⁻¹)
$I_{2, c}$	second invariant of recoverable Finger tensor (1)	$\underline{\underline{\delta}}$	unit tensor (Kronecker delta) (1)
j	index j (1)	δ	δ shift function (1)
L	half-width of the film at any x location (mm)	η_0	Newtonian viscosity (Pa·s)
L_0	half-width of the die (half-width of the film at the die exit) (mm)	$\eta_{E, P}$	steady planar extensional viscosity (Pa·s)
\bar{L}	dimensionless half-width of the film at any x location (1)	$\eta_{E, P, \max}$	maximal steady planar extensional viscosity (Pa·s)
MFI	melt flow index (g/10 min)	$\eta_{E, U}$	steady uniaxial extensional viscosity (Pa·s)
MFR	mass flow rate (kg·h ⁻¹)	$\eta_{E, U, \max}$	maximal steady uniaxial extensional viscosity (Pa·s)
M_n	number average molar mass (g·mol ⁻¹)	θ	fitting parameters of analytical model (1)
M_w	mass average molar mass (g·mol ⁻¹)	λ	relaxation time (s)
NI	maximum attainable neck-in (mm)	ν	non-linear Leonov model parameter (1)
NI^*	normalized maximum attainable neck-in (1)	ξ	non-linear Leonov model parameter (1)
N_1	first normal stress difference (Pa)	ρ	polymer density (g·cm ⁻³)
N_2	second normal stress difference (Pa)	$\underline{\underline{\tau}}$	extra stress tensor (Pa)
n	non-linear Leonov model parameter (1)	τ_{xx}	normal stress in axial x -direction (Pa)
n_0	non-Newtonian index (1)	τ_{yy}	normal stress in transverse y -direction (Pa)
n_s	number of sample points (1)	τ_{zz}	normal stress in thickness z -direction (Pa)
Q	volumetric flow rate (m ³ ·s ⁻¹)	$\bar{\tau}_{xx}$	dimensionless normal stress in axial x -direction (1)
R	gas constant (J·K ⁻¹ ·mol ⁻¹)	$\bar{\tau}_{yy}$	dimensionless normal stress in transverse y -direction (1)
T	melt temperature at the die (°C)	$\bar{\tau}_{zz}$	dimensionless normal stress in thickness z -direction (1)
T_0	reference temperature in the Arrhenius law (°C)	Φ_1, Φ_2	fitting parameters of analytical model (1)
u	axial velocity component of the film at any x location	$\psi_1, \psi_2, \psi_3, \psi_4$	fitting parameters of analytical model (1)

the first time. Other authors followed and employed different constitutive equations for power-law [7], and viscoelastic fluids using modified convected-Maxwell [8] and modified Giesekus model [9,10]. Due to the assumed kinematics for the free surface flow at the drawing zone, the model could not capture edge-bead defect and contraction in film width.

First efforts to overcome this limitation and to accommodate ability to predict neck-in were made for a Newtonian fluid at isothermal [11]

and non-isothermal conditions [12–14]. Lately, improved isothermal two-dimensional membrane model having the capability to capture the development of edge-beads under the stationary conditions was released; isothermal Newtonian [15] and viscoelastic Maxwell and Giesekus fluid [16], and models that take thermal effects into account for Newtonian [17] and viscoelastic Larson fluid [18]. In the meantime, simplified one-dimensional membrane approach based on a supplementary kinematic hypothesis, that originally brought for a float glass

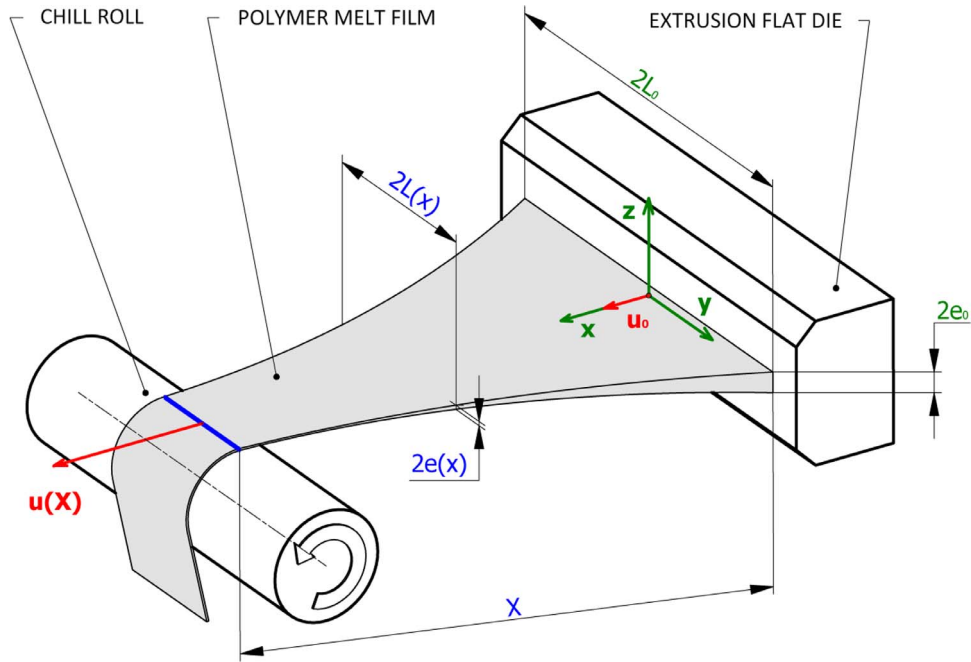


Fig. 1. Schematic visualization of the extrusion film casting process.

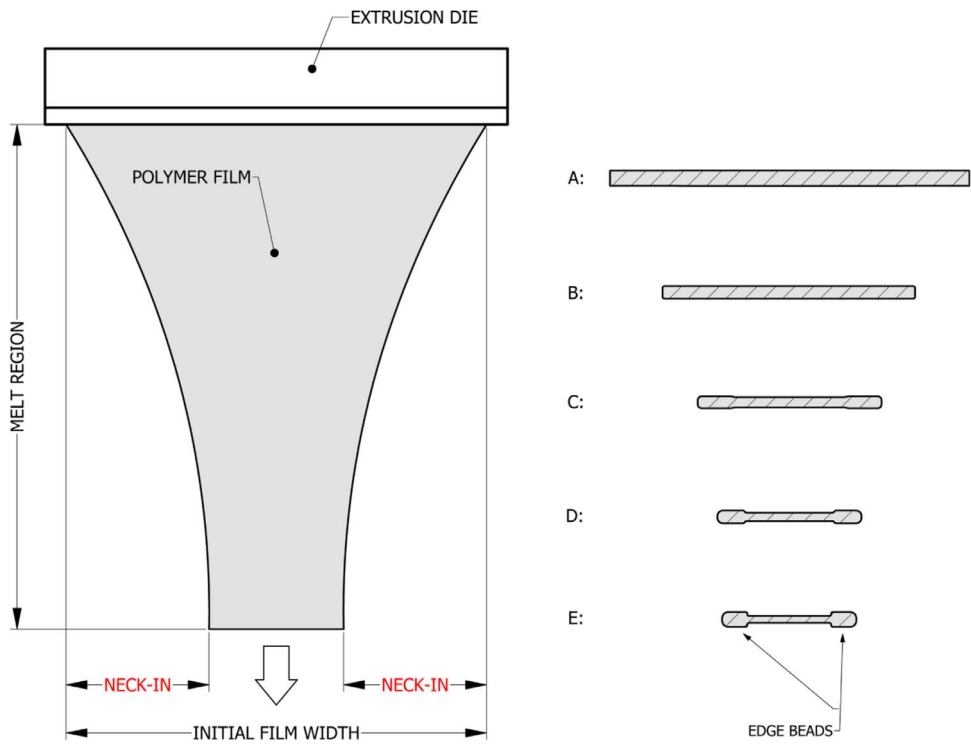


Fig. 2. Neck-in and edge-beading phenomena during the extrusion film casting process.

stretching [19], was proposed [20] and an extended isothermal study on the influence of processing conditions on the film geometry for casting of Newtonian and Maxwell fluids was carried out. Owing to the assumed flow kinematics, this model could cover a film width reduction but was not able to predict edge-beading. This restriction was removed in the succeeding work [21]. A cutting-edge three-dimensional model for extrusion film casting simulation was further established for a steady Newtonian isothermal [22] and non-isothermal [23] fluid.

A specific attention was given at certain aspects of the process. The effect of thermal conditions including crystallization [24–31] as well as

influence of macromolecular architecture on the extent of neck-in [32–36] was put under research abundantly. More recently, a sequence of articles based on the one-dimensional membrane model [20] have been published dealing with both experimental and theoretical investigation of the effects of long chain branching and molecular weight distribution on the neck-in [37–39] (XPP and RP-s), and discussing the role of individual viscoelastic relaxation modes of a polymer melt [40] (UCM and PTT). In the latest works of this series [41,42], the evaluation of a draw resonance onset with model based on PTT constitutive equation and neck-in degree simulation using two-dimensional model

with UCM constitutive equation [33] was addressed, respectively.

The key findings with respect to formation of edge-beads and neck-in were postulated in [43], where the authors pointed out that the deformation flow in the drawing zone comprises of two related regions and the extent of these phenomena is determined by the interplay between them through an edge stress effect, as illustrated in Fig. 3. Planar extensional deformation is experienced in a central region of the film and uniaxial extensional one in lateral parts. This led to that some authors have chosen an approach relating the level of the observed necking in terms of rheological parameters and reported that a degree of neck-in phenomenon may be depressed by a strain hardening in uniaxial extensional viscosity [16,18,44,45]. This conception was slightly more developed in the succeeding studies where the neck-in extent was connected with the ratio of planar viscosities in axial and transverse directions [33], and recently, with the ratio of planar to uniaxial extensional viscosity [46–48] reflecting the flow kinematics in a drawing zone according to [43].

In order to resolve the system of model equations proposed in above mentioned studies, it is necessary to have fully satisfied boundary conditions. This is problematic for the cases, in which viscoelastic constitutive equations are used because an additional boundary stress condition at the die exit must be specified. Its value should be determined by both, a polymer flow in the upstream and downstream region (i.e. depending on an in-die complex flow) and a extensional flow in the drawing zone [49]. Among the various authors, one can find following strategies on how to deal with this problem. First, all stress components are set to zero considering entire stress relaxation due to the die swell phenomenon [16,17,50,51]. Second, at least one stress component is given by a Newtonian solution for downstream side independently on the utilized type of constitutive equation [18,20,21,39,41,52,53]. Third, two extra stress components are adjusted manually without more reasoning [37,38,40]. Fourth, the die exit stress state is given by axial upstream extra stress component [8], thickness to axial extra stress component ratio for upstream/downstream side [9,54] or by second to first normal stress difference ratio, $-N_2/N_1$, calculated from upstream side [55] by using viscoelastic constitutive equation. It has been found that if Deborah number is low (0.00161 [49]; 0.07 [20,21]; 0.1 [9,56]), the choice of the initial stress conditions at the die have only a little influence on the steady-state calculations. However, at high Deborah numbers ($De = 0.124$ [8]) it seems that the die exit stress state, which can be influenced for example by extrusion die design [57] starts to have a significant impact on the neck-in phenomenon.

In this article, as a part of circumstantial set of our studies on the free-surface flow instabilities [58–60], the effect of die exit stress state, extensional rheology and Deborah number on the neck-in phenomenon is systematically investigated via viscoelastic isothermal modeling (utilizing 1D membrane model coupled with a single-mode modified Leonov model) and obtained results are compared with suitable literature experimental data.

2. Mathematical modeling

2.1. Modified Leonov model

The utilized modified Leonov model is based on heuristic thermodynamic arguments resulting from the theory of rubber elasticity [61–66]. In this constitutive equation, a fading memory of the melt is determined through an irreversible dissipation process driven by the dissipation term, b . From mathematical viewpoint, it is relating the stress and elastic strain stored in the material as:

$$\underline{\tau} = 2 \left(\underline{c} \frac{\partial W}{\partial I_{1,c}} - \underline{c}^{-1} \frac{\partial W}{\partial I_{2,c}} \right) \quad (1)$$

where $\underline{\tau}$ is the stress, and W , the elastic potential, which depends on the invariants $I_{1,c}$ and $I_{2,c}$ of the recoverable Finger tensor \underline{c} ,

$$W = \frac{3G}{2(n+1)} \left\{ [1 - \beta] \left[\left(\frac{I_{1,c}}{3} \right)^{n+1} - 1 \right] + \beta \left[\left(\frac{I_{2,c}}{3} \right)^{n+1} - 1 \right] \right\} \quad (2)$$

where G denotes linear Hookean elastic modulus, β and n are numerical parameters. Leonov assumed that the dissipative process acts to produce an irreversible rate of strain \underline{e}_p

$$\underline{e}_p = b \left[\underline{c} - \frac{I_{1,c}}{3} \underline{\delta} \right] - b \left[\underline{c}^{-1} - \frac{I_{2,c}}{3} \underline{\delta} \right] \quad (3)$$

which spontaneously reduces the rate of elastic strain accumulation. Here, $\underline{\delta}$ is the unit tensor and b stands for dissipation function defined by Eq. (5). This elastic strain \underline{c} is related to the deformation rate tensor \underline{D} as follows

$$\dot{\underline{c}} - \underline{c} \cdot \underline{D} - \underline{D} \cdot \underline{c} + 2\underline{c} \cdot \underline{e}_p = 0 \quad (4)$$

where $\dot{\underline{c}}$ is the Jaumann (corotational) time derivative of the recoverable Finger strain tensor. In this work, the Mooney potential (i.e. $n = 0$ in Eq. (2)), and the dissipation function b proposed in [67] (see Eq. (5)) have been employed.

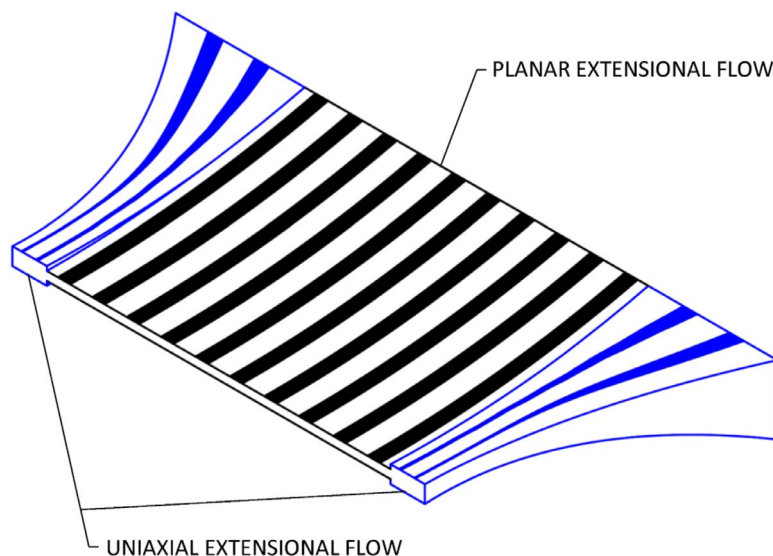


Fig. 3. Visualization of the flow type distribution in the post-die area during the extrusion film casting process.

$$b(I_{1,c}) = \frac{1}{4\lambda} \left\{ \exp[-\xi\sqrt{I_{1,c}-3}] + \frac{\sinh[\nu(I_{1,c}-3)]}{\nu(I_{1,c}-3)+1} \right\} \quad (5)$$

Here, ξ and ν are adjustable model parameters.

2.2. Extrusion film casting model

In this study, one-dimensional membrane model [20] was used to simulate the drawing process of a molten film in the post extrusion die area. The model is capable to predict film width shrinkage despite its dimensionality due to the applied flow kinematics assumptions [19] allowing principal velocity variation along the axial direction (Fig. 1) as follows

$$\begin{aligned} u &= u(x) \\ v &= v(x, y) = yf(x) \\ w &= w(x, z) = zg(x) \end{aligned} \quad (6)$$

Here u , v and w stands for the velocities in axial, transversal and thickness direction, respectively. The membrane model comprises of equations for continuity and momentum conservation that are simultaneously solved with viscoelastic single-mode modified Leonov model as the constitutive equation. The main model equations are summarized below in dimensionless form utilizing dimensionless quantities provided in Table 1 (having a similar form as in [20] to keep consistency with the open literature).

In this table, τ_{ii} is the ii component of the extra stress tensor; F and E , drawing and dimensionless drawing force exerted onto film; DR , draw ratio; De , Deborah number; λ , relaxation time; G , elastic modulus; A , aspect ratio; X and x , drawing distance and actual axial position and L , e , u , are half-width, half-thickness and axial velocity of the film. The zero subscript and overbar sign denotes initial and dimensionless corresponding quantity, respectively.

Mass conservation equation is given by the following equation

$$\bar{e}\bar{L}\bar{u} = 1 \quad (7)$$

Considering the membrane approximation for a thin film in the presence of a constant drawing force, the momentum conservation equation yields

$$(\bar{\tau}_{xx} - \bar{\tau}_{zz}) - \bar{u} = 0 \quad (8)$$

The kinematic free-surface and stress-free surface boundary condition allows determination of unknown functions appearing in Eq. (6). (i.e. $f(x)$ and $g(x)$) and the film width-stress relationship at given dimensionless axial position, \bar{x} , Eq. (9), respectively.

$$\frac{d\bar{L}}{d\bar{x}} = -A \sqrt{\frac{\bar{\tau}_{yy} - \bar{\tau}_{zz}}{\bar{\tau}_{xx} - \bar{\tau}_{zz}}} \quad (9)$$

Differentiating Eqs. (7) and (8) with respect to \bar{x} variable and after algebraic rearrangement, the derivative of the dimensionless film half-thickness with respect to \bar{x} leads to

$$\frac{d\bar{e}}{d\bar{x}} = -\left(\frac{1}{\bar{L}} \frac{d\bar{L}}{d\bar{x}} + \frac{1}{\bar{u}} \frac{d\bar{u}}{d\bar{x}} \right) \bar{e} \quad (10)$$

Utilization of Mooney potential in the modified Leonov model constitutive equation (i.e. when $n = 0$ and $\beta \neq 0$ in Eq. (2)), the relationship between the dimensionless stress and recoverable strain takes the following form

$$\bar{\tau}_{ii} = \frac{E}{De} c_{ii} - \frac{E}{De} c_{ii} \beta - \frac{E}{De} c_{ii}^{-1} \beta \quad (11)$$

In combination of the membrane model and constitutive equation, the derivative of diagonal components of the recoverable strain tensor, c_{ii} , with respect to \bar{x} are given in form

$$\frac{dc_{xx}}{d\bar{x}} = 2c_{xx} \frac{1}{\bar{u}} \frac{d\bar{u}}{d\bar{x}} - \frac{2\bar{b}}{\bar{u}} Z_x \quad (12)$$

$$\frac{dc_{yy}}{d\bar{x}} = 2c_{yy} \frac{1}{\bar{L}} \frac{d\bar{L}}{d\bar{x}} - \frac{2\bar{b}}{\bar{u}} Z_y \quad (13)$$

$$\frac{dc_{zz}}{d\bar{x}} = 2c_{zz} \frac{1}{\bar{e}} \frac{d\bar{e}}{d\bar{x}} - \frac{2\bar{b}}{\bar{u}} Z_z \quad (14)$$

where the dimensionless dissipation function, \bar{b} , and Z_i are defined as

$$\bar{b}(I_{1,c}) = \frac{1}{4De} \left\{ \exp[-\xi\sqrt{I_{1,c}-3}] + \frac{\sinh[\nu(I_{1,c}-3)]}{\nu(I_{1,c}-3)+1} \right\} \quad (15)$$

$$Z_i = c_{ii} \left[c_{ii} - c_{ii}^{-1} + \frac{1}{3}(c_{xx}^{-1} + c_{yy}^{-1} + c_{zz}^{-1} - c_{xx} - c_{yy} - c_{zz}) \right] \quad (16)$$

Combination of Eqs. (7), (8) and (11) leads to the dimensionless streamwise deformation rate, which takes the following form

$$\begin{aligned} &\bar{b} [\beta(Z_x - Z_z) - Z_x + Z_z] + \bar{b}\beta \left(\frac{1}{c_{zz}^2} Z_z - \frac{1}{c_{xx}^2} Z_x \right) \\ &+ \frac{\bar{u}}{\bar{L}} \frac{d\bar{L}}{d\bar{x}} \left(c_{zz}(1-\beta) + \frac{\beta}{c_{zz}} \right) \\ \frac{d\bar{u}}{d\bar{x}} &= \frac{\beta(c_{xx} + c_{zz}) - c_{xx} - c_{zz} - \frac{\beta}{c_{xx}} \left(\frac{c_{zz} + c_{xx}}{c_{zz}} \right) + \frac{De\bar{u}}{2E}}{\beta(c_{xx} + c_{zz}) - c_{xx} - c_{zz} - \frac{\beta}{c_{xx}} \left(\frac{c_{zz} + c_{xx}}{c_{zz}} \right) + \frac{De\bar{u}}{2E}} \end{aligned} \quad (17)$$

Eqs. (9), (10), (12)–(14) and (17) represent the final set of equations for isothermal viscoelastic 1D membrane model utilized in this work. More detailed derivation of the model is provided in our previous work [55]. Note that due to a geometrical symmetry of the film, only 1/4th of the film cross-section can be used in the calculation as showed in [68].

2.3. Boundary conditions

In order to solve the model equations, boundary conditions for downstream, Eq. (18), and upstream region, Eq. (19), have to be provided.

$$\bar{u}(X) = DR \quad (18)$$

$$\begin{aligned} \bar{u}(0) &= 1 & \bar{e}(0) &= 1 & \bar{L}(0) &= 1 \\ \bar{\tau}_{xx}(0) & & \bar{\tau}_{yy}(0) & & \bar{\tau}_{zz}(0) & \end{aligned} \quad (19)$$

At the downstream region, draw ratio is prescribed as the desired value that is satisfied by a priori unknown magnitude of the drawing force. Upstream area (i.e. extrusion die exit region) is defined by the known average melt speed and die dimensions (gap size and width) whereas diagonal components of the extra stress tensor $\bar{\tau}_{xx}$, $\bar{\tau}_{yy}$ and $\bar{\tau}_{zz}$ have to be calculated via Eq. (11) utilizing c_{xx} , c_{yy} and c_{zz} components of the recoverable strain tensor satisfying the following set of equations:

$$\frac{E}{De} [(c_{xx} - c_{zz})(1-\beta) + \beta(c_{zz}^{-1} - c_{xx}^{-1})] - 1 = 0 \quad (20)$$

$$c_{xx} c_{yy} c_{zz} = 1 \quad (21)$$

$$-\frac{N_2}{N_1} = \frac{E [c_{zz} - c_{yy} + \beta(c_{yy} + c_{yy}^{-1} - c_{zz} - c_{zz}^{-1})]}{De\bar{u}} \quad (22)$$

Eq. (20) arises from the momentum conservation equation (Eq. (8)), Eq. (21) from the melt incompressibility assumption and Eq. (23) characterizes the polymer melt stress state at the die exit region as the

Table 1
Summarization of utilized dimensionless quantities.

Dimensionless component of stress tensor	
$\bar{\tau}_{ii}$	$\frac{\tau_{ii} e_0 L_0}{F}$
Dimensionless spatial dimensions and streamwise velocity	
\bar{x}	$\frac{x}{X}$
\bar{e}	$\frac{e}{e_0}$
\bar{L}	$\frac{L}{L_0}$
\bar{u}	$\frac{u}{u_0}$
Dimensionless numbers	
DR	$\frac{u(X)}{u_0}$
De	$\frac{\lambda u_0}{X}$
A	$\frac{X}{L_0}$
$\frac{1}{E}$	$\frac{FX}{G\lambda e_0 L_0 u_0}$

ratio of the secondary to primary normal stress difference, $-N_2/N_1$. This ratio is calculated from the fully-developed slit flow at the extrusion die exit as follows

$$-\frac{N_2}{N_1} = -\frac{\bar{\tau}_{zz}(0) - \bar{\tau}_{yy}(0)}{\bar{\tau}_{xx}(0) - \bar{\tau}_{zz}(0)} \quad (23)$$

2.4. Numerical scheme

The entire set of the first-order ordinary differential equations, which comprises from equations for film half-width (Eq. (9)), half-thickness (Eq. (10)), velocity (Eq. (17)), components of the recoverable elastic strain tensor (Eqs. (12)–(14)) and boundary conditions (Eqs. (20)–(23)), was solved by 4th order Runge–Kutta method implementing adaptive step-size control. At the beginning, take-up force was guessed and consequently increased or decreased for every following iteration until the given draw ratio was achieved. Solver was developed in the C++ programming language and coupled with GNU PLOT plotting software for automatic graph generation. Typical computational time for one calculation of prescribed DR was about 2 min on the PC with the following hardware parameters: CPU: Intel Core 2 Quad Q9650 (3.00 GHz), RAM: 8 GB DDR2, GPU: Sapphire Radeon HD 3870, SSD: Crucial 256 GB.

3. Results and discussion

3.1. Theoretical analysis of neck-in phenomenon

3.1.1. The role of extensional rheology, Deborah number and $-N_2/N_1$ ratio at the die exit

In order to understand the role of extensional rheology, Deborah number and die exit stress state on the maximum attainable neck-in, 3 groups of virtual materials having three different levels of uniaxial strain hardening defined by Eq. (24) were used.

$$\frac{\eta_{E,U,max}}{3\eta_0} \quad (24)$$

Here, $\eta_{E,P,max}$ is the maximum steady uniaxial extensional viscosity and η_0 stands for the Newtonian viscosity. In each group, 5 virtual materials were generated having the same level of uniaxial extensional strain hardening (1.3, 3.4 and 7.1) but different level of planar extensional strain hardening (1.10–1.53, 2.9–4.2 and 6.2–7.9) and the zero-shear rate second to first normal stress difference ratio (0.3–0.6) defined by Eq. (25) and Eq. (26), respectively.

$$\frac{\eta_{E,P,max}}{4\eta_0} \quad (25)$$

Table 2 Modified Leonov model parameters for the utilized virtual polymer melts having $\lambda = 1.57$ s and $G = 85,982.61$ Pa at 150°C.

Virtual material name	ξ (1)	ν (1)	β (1)	$\frac{\eta_{E,U,max}}{3\eta_0}$ (1)	$\frac{\eta_{E,P,max}}{4\eta_0}$ (1)	$\lim_{\dot{\gamma} \rightarrow 0} \left(-\frac{N_2}{N_1} \right)$ (1)
Melt1_High	4.414	0.276	0.1	7.1	6.2	0.3
Melt2_High	4.042	0.208	0.3	7.1	6.6	0.4
Melt3_High	3.816	0.174	0.4	7.1	6.8	0.45
Melt4_High	3.54	0.14	0.5	7.1	7.1	0.5
Melt5_High	2.806	0.072	0.7	7.1	7.9	0.6
Melt1_Middle	2.014	0.276	0.1	3.4	2.9	0.3
Melt2_Middle	1.882	0.208	0.3	3.4	3.1	0.4
Melt3_Middle	1.816	0.174	0.4	3.4	3.2	0.45
Melt4_Middle	1.75	0.14	0.5	3.4	3.4	0.5
Melt5_Middle	1.53	0.072	0.7	3.4	4.2	0.6
Melt1_Low	0.338	0.276	0.1	1.3	1.10	0.3
Melt2_Low	0.38	0.208	0.3	1.3	1.17	0.4
Melt3_Low	0.4	0.174	0.4	1.3	1.22	0.45
Melt4_Low	0.418	0.14	0.5	1.3	1.29	0.5
Melt5_Low	0.426	0.072	0.7	1.3	1.53	0.6

$$\lim_{\dot{\gamma} \rightarrow 0} \left(-\frac{N_2}{N_1} \right) \quad (26)$$

Here, $\eta_{E,P,max}$ is the maximum steady planar extensional viscosity, $\dot{\gamma}$ is the shear rate, N_1 and N_2 is the first and second normal stress difference at the die exit defined (for the post-die coordinate system depicted in Fig. 1) as follows

$$N_1 = \tau_{xx} - \tau_{zz} \quad (27)$$

$$N_2 = \tau_{zz} - \tau_{yy} \quad (28)$$

Modified Leonov model parameters together with corresponding $\frac{\eta_{E,U,max}}{3\eta_0}$, $\frac{\eta_{E,P,max}}{4\eta_0}$ and $\lim_{\dot{\gamma} \rightarrow 0} \left(-\frac{N_2}{N_1} \right)$ values are provided in Table 2 for the 15 utilized virtual polymer melts.

Deborah number was varied from 0.01 to 0.3 in the film casting model for all 15 virtual polymer melts changing the $-N_2/N_1$ ratio from 0.001 to 2. For each simulation case, the draw ratio was adjusted high enough (typically equal to 40) in order to reach a maximum and draw ratio independent neck-in value, NI. Note that the neck-in is defined as $L_0 - L(X)$, see Figs. 1 and 2. The maximum neck-in value was consequently normalized by the take-up length, X, as follows.

$$NI^* = \frac{NI}{X} \quad (29)$$

In order to visualize obtained trend, calculated maximum neck-in value NI^* as a function of the square root of planar to uniaxial extensional viscosity ratio, $\sqrt{\frac{\eta_{E,P}}{\eta_{E,U}}}$, is provided in Fig. 4 for three selected Deborah numbers (0.01, 0.05 and 0.3), two uniaxial extensional strain hardening values (1.3 and 7.1) and two $-N_2/N_1$ ratios (0.001 and 1). It is visible that firstly, an increase in the Deborah number and $-N_2/N_1$ ratio increases both, the normalized neck-in as well as its sensitivity to $\sqrt{\frac{\eta_{E,P}}{\eta_{E,U}}}$ and secondly, there exists threshold value for Deborah number and uniaxial extensional strain hardening, above which, the neck-in phenomenon starts to be dependent on the die exit stress state. Critical Deborah number was calculated for given $-N_2/N_1$ ratio, above which, a considerable deviation (more than 5 %) in the neck-in value starts to occur. Here, the neck-in at $-N_2/N_1 = 0.001$ was taken as the reference. The effect of $-N_2/N_1$ ratio and uniaxial extensional strain hardening, $\frac{\eta_{E,U,max}}{3\eta_0}$, (keeping the ratio of planar to uniaxial extensional strain hardening value, $\frac{\eta_{E,P,max}}{4\eta_0} / \frac{\eta_{E,U,max}}{3\eta_0}$, the same, equal to one) on the critical Deborah number is provided in Fig. 5(a) utilizing three virtual melts (namely Melt4_Low, Melt4_Middle, Melt4_High, see Table 2). In this image, area below the lines represents conditions, at which the $-N_2/N_1$ ratio has practically no effect (namely lower than 5 %) on the normalized maximum attainable neck-in, whereas above these lines, the

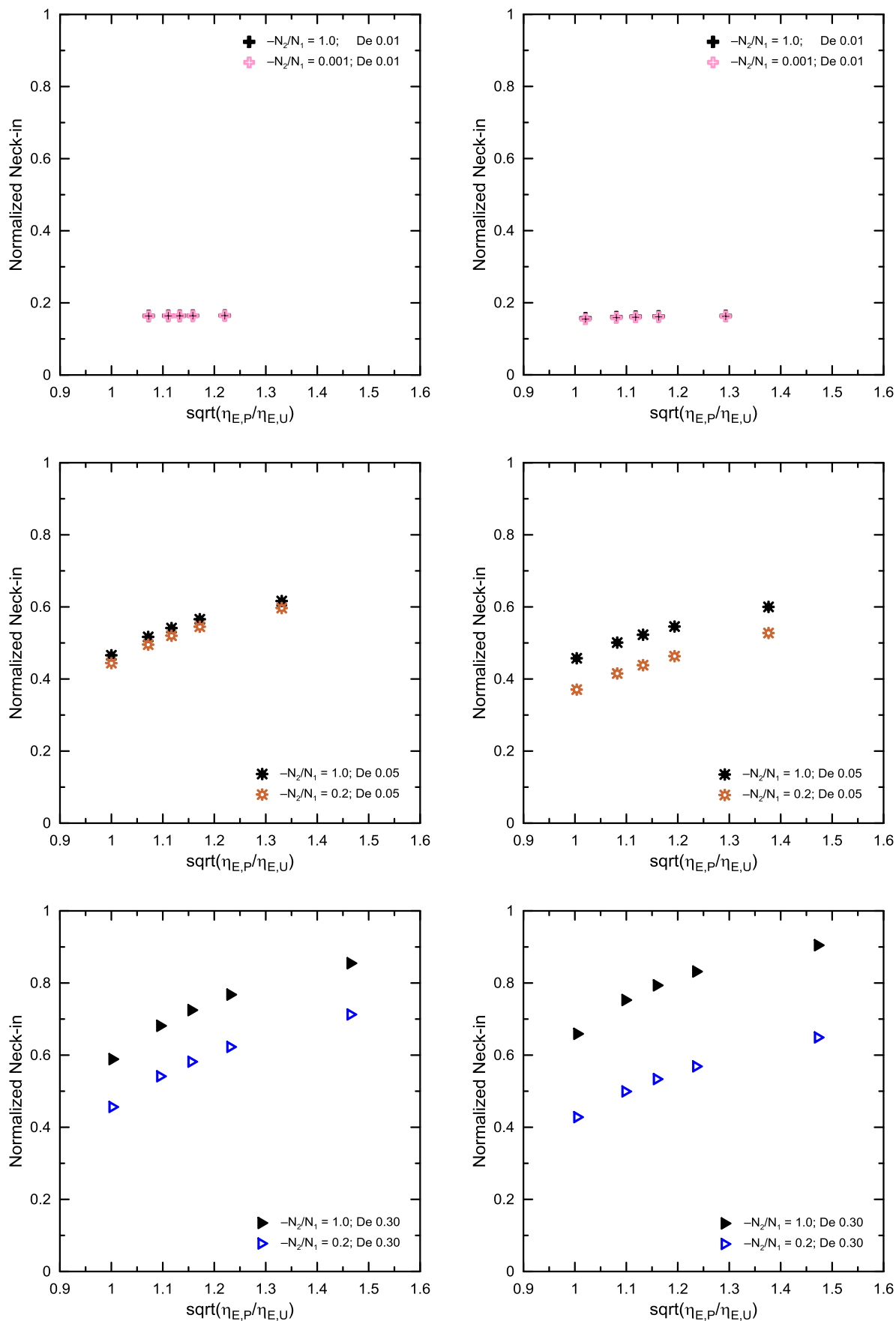


Fig. 4. The effect of die exit stress state ($-N_2/N_1$) on the normalized maximum attainable neck-in vs. $\sqrt{\eta_{E,P}/\eta_{E,U}}$ dependence for three different Deborah numbers ($De = 0.01$ – top, $De = 0.05$ – middle, $De = 0.30$ – bottom) and two virtual polymer melts having low (left) and high (right) uniaxial extensional strain hardening, $\frac{\eta_{E,U,max}}{3\eta_0}$, equal to 1.3 and 7.1, respectively.

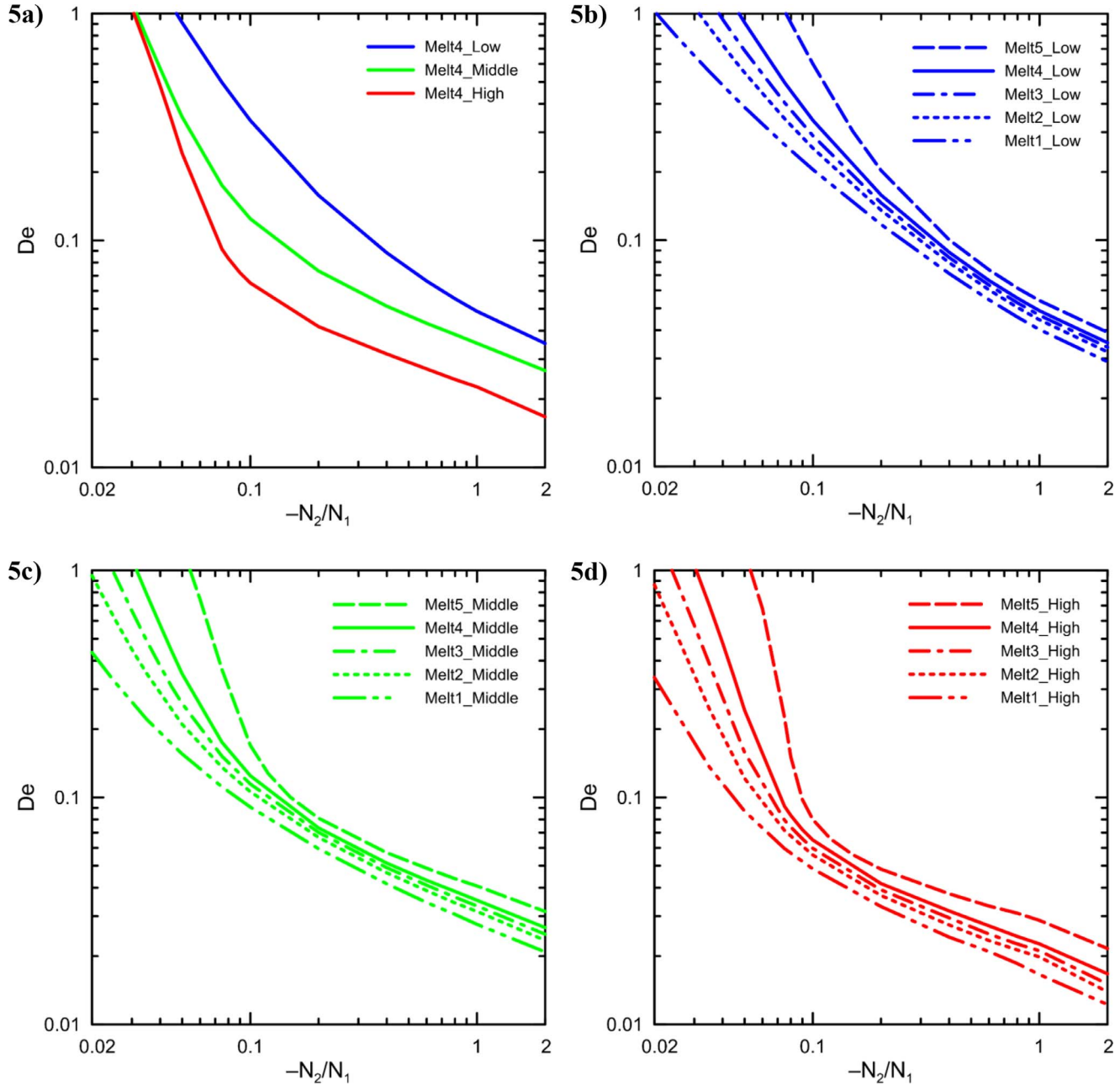


Fig. 5. The effect of die exit stress state ($-N_2/N_1$) on the critical Deborah number, above which, 5% deviation in normalized maximum attainable neck-in starts to occur. (a) Role of uniaxial extensional strain hardening, $\frac{\eta_{E,U,max}}{3\eta_0}$, (keeping ratio of planar to uniaxial extensional strain hardening value, $\frac{\eta_{E,P,max}}{4\eta_0} / \frac{\eta_{E,U,max}}{3\eta_0}$, the same, equal to one). (b)–(d) Role of $\frac{\eta_{E,P,max}}{4\eta_0} / \frac{\eta_{E,U,max}}{3\eta_0}$ (changing from 0.85 to 1.24) at fixed $\frac{\eta_{E,U,max}}{3\eta_0}$, equal to 1.3 (top, right), 3.4 (bottom, left) and 7.1 (bottom, right).

$-N_2/N_1$ starts to have a considerable effect (more than 5 %) on the neck-in phenomenon. As it can be seen, firstly, the critical Deborah number decreases with increased $-N_2/N_1$ and secondly, an increase in $\frac{\eta_{E,U,max}}{3\eta_0}$ decreases the critical Deborah number for given value of $-N_2/N_1$. For example, adjusting $-N_2/N_1 = 0.2$ and changing $\frac{\eta_{E,U,max}}{3\eta_0}$ to 1.3, 3.4 and 7.1 yields critical Deborah number equal to 0.158, 0.073 and 0.042, respectively.

The effect of $\frac{\eta_{E,P,max}}{4\eta_0} / \frac{\eta_{E,U,max}}{3\eta_0}$ (changing from 0.85 to 1.24) and $\frac{\eta_{E,U,max}}{3\eta_0}$ (changing from 1.3 to 7.1) is visualized in Fig. 5(b)–(d). Here, it is visible that increase in $\frac{\eta_{E,P,max}}{4\eta_0} / \frac{\eta_{E,U,max}}{3\eta_0}$ increases the critical Deborah number for given $\frac{\eta_{E,U,max}}{3\eta_0}$ and $-N_2/N_1$ values. The effect was found to be more dominant for lower $-N_2/N_1$ and higher $\frac{\eta_{E,U,max}}{3\eta_0}$.

From these results, it can be concluded that die exit stress state, characterized via $-N_2/N_1$ ratio, has to be defined properly in order to predict the normalized maximum attainable neck-in correctly, especially at high Deborah numbers for polymer melts with high $\frac{\eta_{E,U,max}}{3\eta_0}$ and low $\frac{\eta_{E,P,max}}{4\eta_0} / \frac{\eta_{E,U,max}}{3\eta_0}$.

Note that $-N_2/N_1$ can be viewed as the variable, which is inversely proportional to the melt planar pre-stretching at the die exit. Thus the basic trend depicted in Fig. 5 can be physically interpreted as follows. If the level of planar pre-stretching decreases, its effect on the maximum attainable neck-in starts to occur at lower Deborah numbers.

3.1.2. Analytical approximation for NI^*

All numerical predictions of the utilized viscoelastic film casting model for normalized neck-in value NI^* vs. square root of planar to

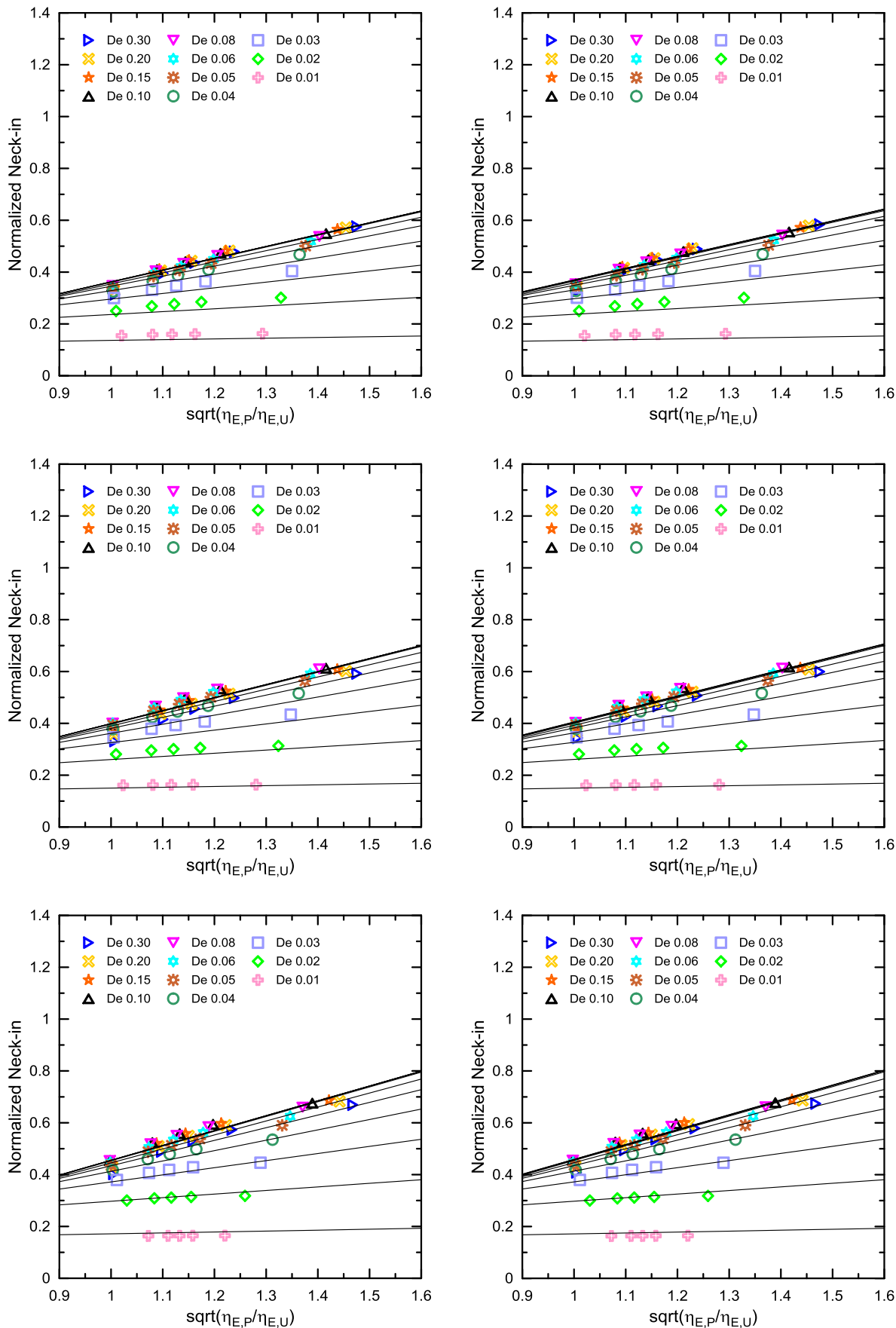


Fig. 6. The effect of Deborah number on the normalized maximum attainable neck-in vs. planar to uniaxial extensional viscosity ratio for virtual polymer melts having high (top), medium (middle) and low (bottom) level of uniaxial extensional strain hardening considering that die exit stress state, $-N_2/N_1$, is equal to 0.001 (left) and 0.02 (right). Here, symbols and lines represent utilized viscoelastic 1D membrane model and simple approximate solution model (Eq. (31)) predictions, respectively.

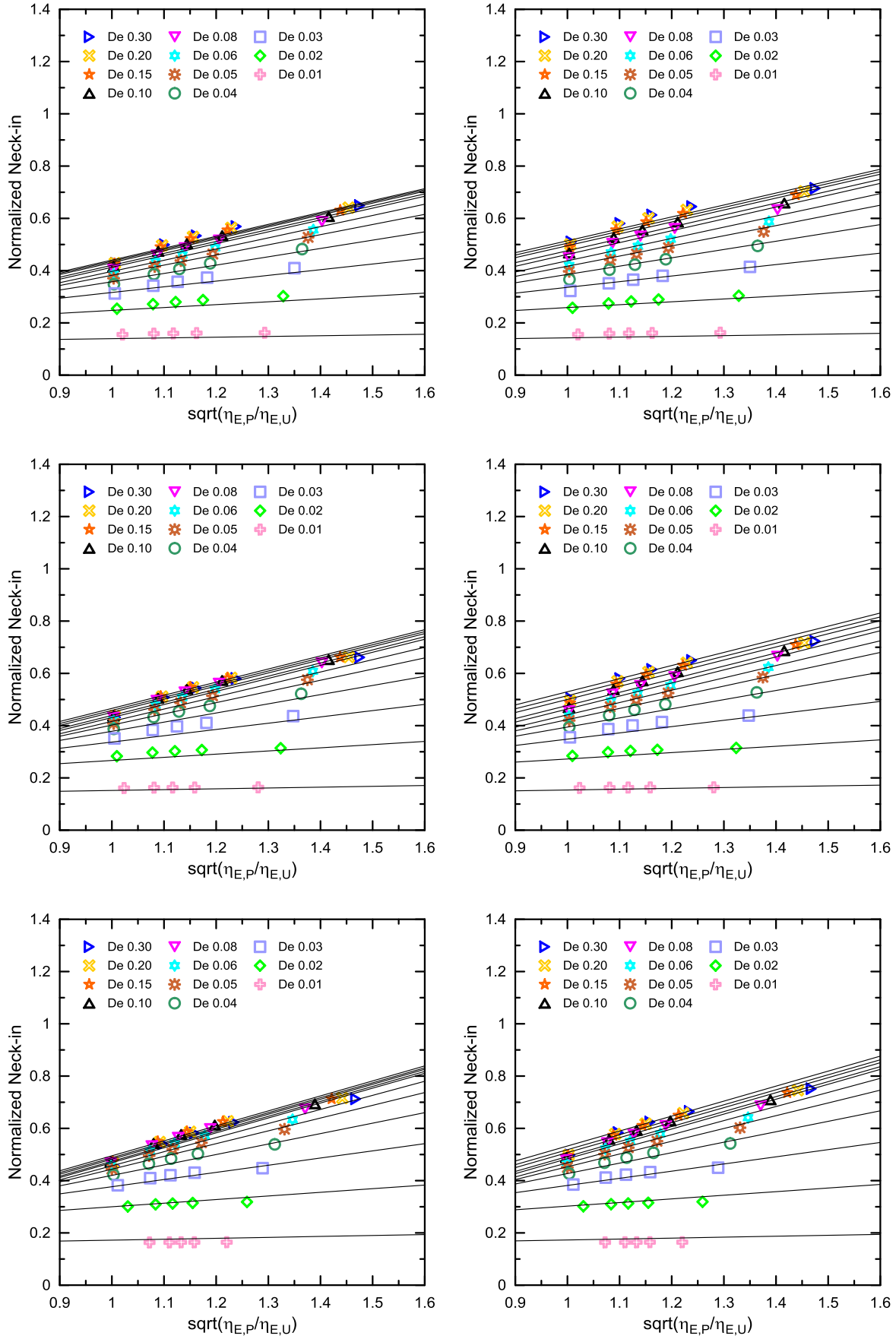


Fig. 7. The effect of Deborah number on the normalized maximum attainable neck-in vs. planar to uniaxial extensional viscosity ratio for virtual polymer melts having high (top), medium (middle) and low (bottom) level of uniaxial extensional strain hardening considering that die exit stress state, $-N_2/N_1$, is equal to 0.2 (left) and 0.4 (right). Here, symbols and lines represent utilized viscoelastic 1D membrane model and simple approximate solution model (Eq. (31)) predictions, respectively.

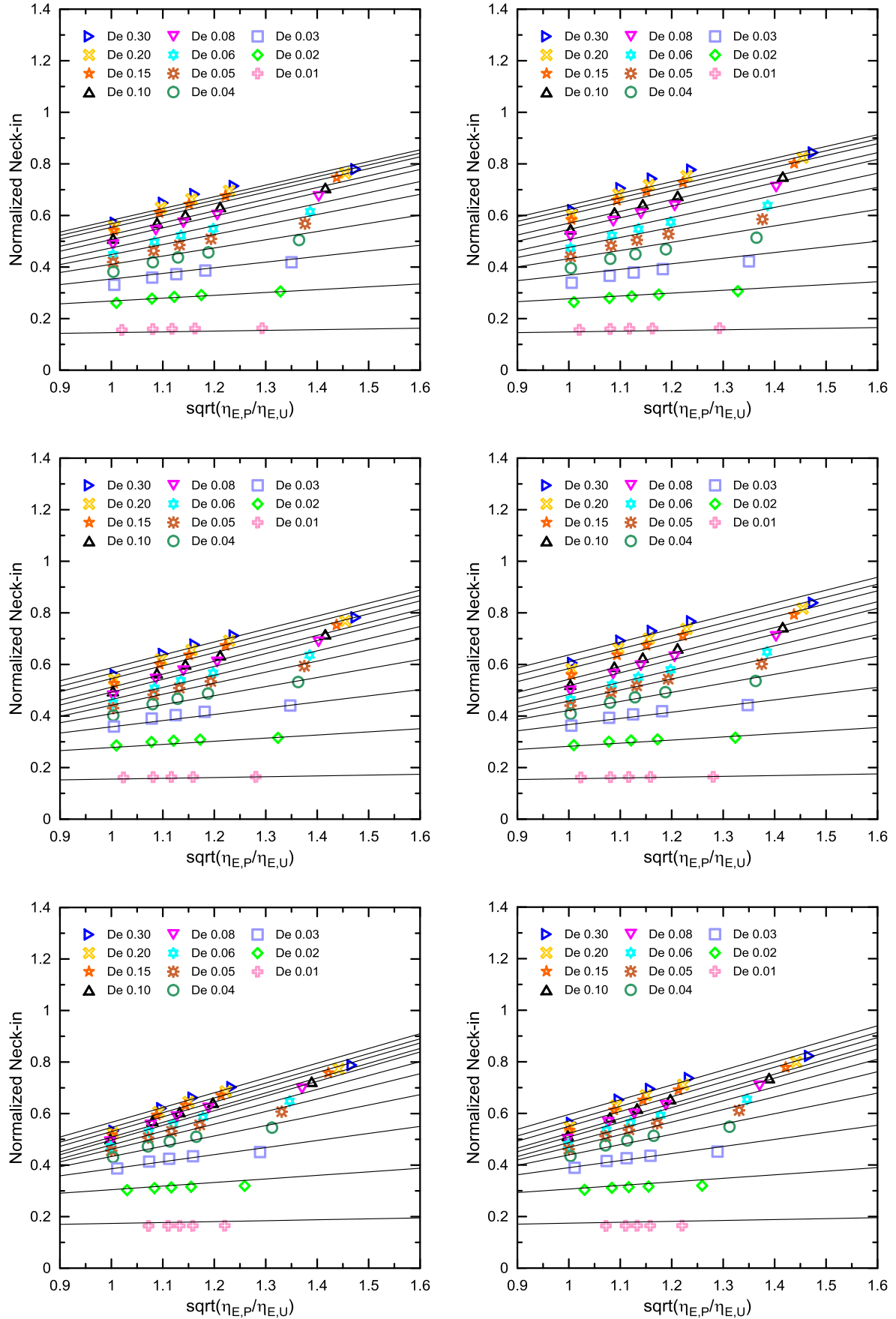


Fig. 8. The effect of Deborah number on the normalized maximum attainable neck-in vs. planar to uniaxial extensional viscosity ratio for virtual polymer melts having high (top), medium (middle) and low (bottom) level of uniaxial extensional strain hardening considering that die exit stress state, $-N_2/N_1$, is equal to 0.6 (left) and 0.8 (right). Here, symbols and lines represent utilized viscoelastic 1D membrane model and simple approximate solution model (Eq. (31)) predictions, respectively.

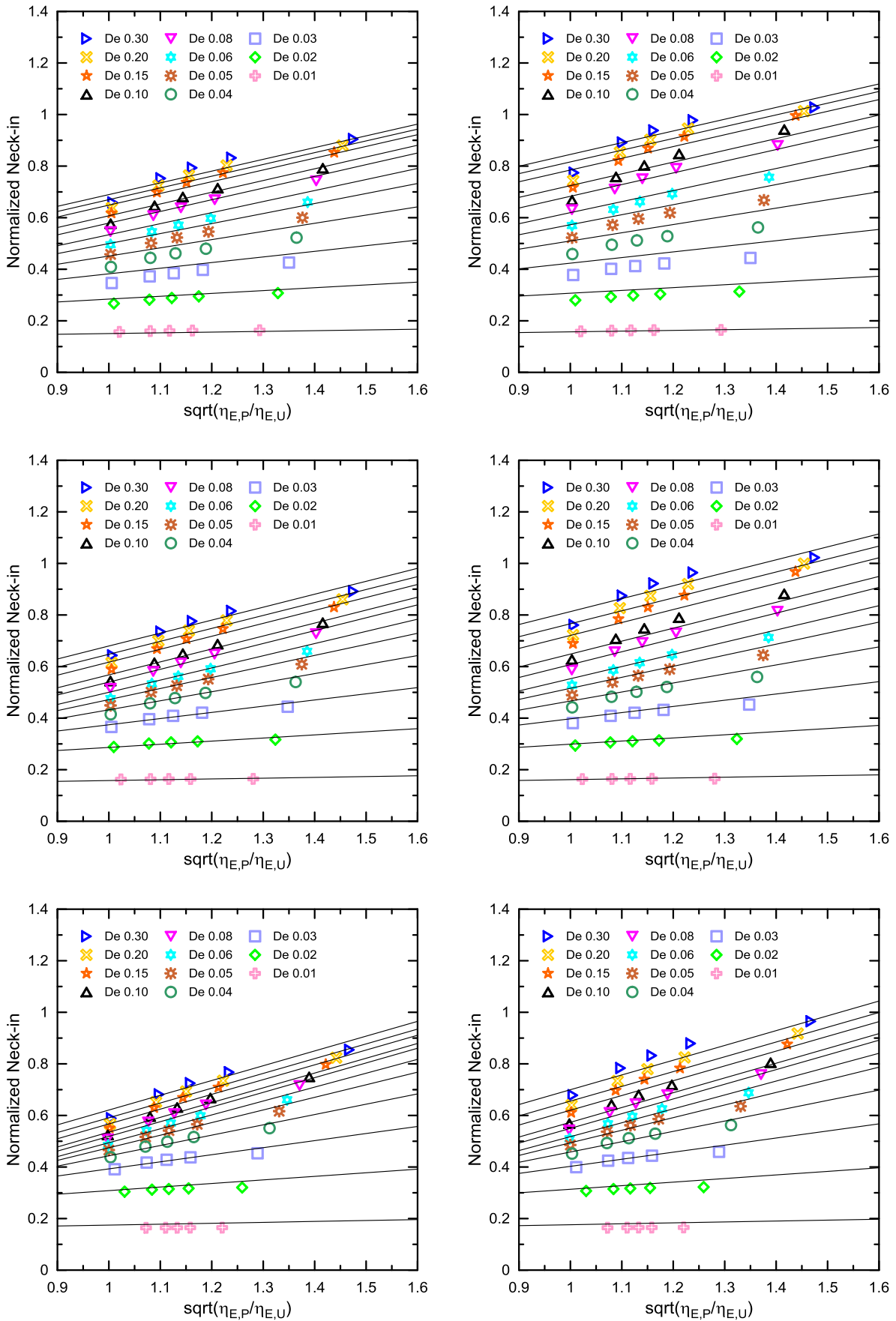


Fig. 9. The effect of Deborah number on the normalized maximum attainable neck-in vs. planar to uniaxial extensional viscosity ratio for virtual polymer melts having high (top), medium (middle) and low (bottom) level of uniaxial extensional strain hardening considering that die exit stress state, $-N_2/N_1$, is equal to 1 (left) and 2 (right). Here, symbols and lines represent utilized viscoelastic 1D membrane model and simple approximate solution model (Eq. (31)) predictions, respectively.

Table 3

Summarization of all constants appearing in Eq. (31) for normalized maximum attainable neck-in, NI^* , which was used to fit all numerical neck-in predictions. The root mean square error, $RMSE$, was equal to 0.020888.

θ	A_1	A_2	α_1	α_2	φ_1	φ_2	Ψ_1	Ψ_2	Ψ_3	Ψ_4
7.43	0.593	0.471	1,073.742	99.757	2.113	1.162	1.027	-0.849	0.514	3.953

Table 4

Basic characteristics for tested polymeric samples.

Polymer sample	MFI (g/10 min)	M_w (kg/mol)	M_w/M_n (1)	Newtonian viscosity, η_0 (Pa s)	Temperature, T_0 (°C)	Flow activation energy, E_a (kJ/mol)	Ref.
LDPE 170A	0.7	185.9	6.07	134,992	150	40	[38,40]
PE-A	6.7	163	9.1	16,220	130	49.887 ^a	[47]
PE-B	4.1	102	6.6	37,720	130	49.887 ^a	[47]
PE-C	4.3	85	6.0	36,033	130	49.887 ^a	[47]
LDPE C	8.07	554	26	21,970	125	52.020 ^b	[18]

^a Note, that E_a was calculated here as $E_a = \alpha R$, where α is the Arrhenius law parameter equal to 6,000 K provided in [47] and R is the universal gas constant equal to 8.3144598 J/K/mol.

^b Converted from Kcal/mol.

uniaxial extensional viscosity ratio $\sqrt{\frac{\eta_{E,P}}{\eta_{E,U}}}$ and considering different Deborah numbers (0.01–0.30), uniaxial extensional strain hardening (1.3–7.1) and $-N_2/N_1$ ratios (0.001–2) is provided in Figs. 6–9 as the symbols. In our previous work [55], it has been found that numerical solution for NI^* can be approximated by Eq. (30), if the role of $-N_2/N_1$ on the neck-in phenomenon is neglected.

$$NI^* = \frac{1}{\sqrt[10]{\frac{\eta_{E,U,max}}{3\eta_0}}} \left\{ A_1 [1 - \exp(-\alpha_1 De^{\varphi_1})] \left(\sqrt{\frac{\eta_{E,P}}{\eta_{E,U}}} - 1 \right) + A_2 [1 - \exp(-\alpha_2 De^{\varphi_2})] \right\} \quad (30)$$

where $A_1, \alpha_1, \varphi_1, A_2, \alpha_2, \varphi_2$ are model constants. In order to include the effect of $-N_2/N_1$ ratio on NI^* , we have modified Eq. (30) for NI^* introducing $-N_2/N_1$ ratio via specific type of δ function and utilizing five additional constants $\theta, \psi_1, \psi_2, \psi_3$ and ψ_4 . Suggested modified equation for the NI^* is given by Eq. (31).

$$NI^* = \frac{1}{\sqrt[10]{\frac{\eta_{E,U,max}}{3\eta_0}}} \left\{ A_1 [1 - \exp(-\alpha_1 De^{\varphi_1})] \left(\sqrt{\frac{\eta_{E,P}}{\eta_{E,U}}} - 1 \right) + \delta A_2 [1 - \exp(-\alpha_2 De^{\varphi_2})] \right\} \quad (31)$$

where

$$\delta = 1 + \psi_1 \arctan\left(\psi_2 \frac{N_2}{N_1}\right) \arctan\left(\psi_3 \frac{\eta_{E,U,max}}{3\eta_0} \tanh(\psi_4 De)\right) \quad (32)$$

and Deborah number, De , is given by $De = \frac{\lambda u_0}{X}$.

Eq. (31) was used to fit all numerical neck-in predictions for all considered planar to uniaxial extensional viscosity ratios, Deborah numbers, uniaxial extensional strain hardenings and $-N_2/N_1$ ratios, which are depicted in Figs. 6–9. All identified constants of Eq. (31) together with Root Mean Square Error, $RMSE$, which characterizes the overall fitting error (see definition below), are provided in Table 3.

$$RMSE = \sqrt{\frac{1}{n_s} \sum_{j=1}^{n_s} [y_j - \hat{y}_j]^2} \quad (33)$$

where n_s is the number of points whereas y_j and \hat{y}_j represent given and predicted points, respectively. As it can be seen, the simple approximate solution model (Eq. (31)) has very high capability to represent NI^* predictions of the utilized 1D viscoelastic membrane model very well.

3.1.3. Behavior of analytical approximation for NI^* at high Deborah numbers

For very high Deborah numbers, Eq. (31) for NI^* simplifies to

$$\lim_{De \rightarrow \infty} NI^* = \frac{1}{\sqrt[10]{\frac{\eta_{E,U,max}}{3\eta_0}}} \left\{ A_1 \left(\sqrt{\frac{\eta_{E,P}}{\eta_{E,U}}} - 1 \right) + A_2 \left[1 + \psi_1 \arctan\left(\psi_2 \frac{N_2}{N_1}\right) \arctan\left(\psi_3 \frac{\eta_{E,U,max}}{3\eta_0}\right) \right] \right\} \quad (34)$$

Considering that A_1 and A_2 are identical during a fitting procedure utilizing Eq. (31), the change in $RMSE$ is very small (from 0.020888 to 0.023903), which justifies to use this assumption to further simplify Eq. (34) as follows

$$\lim_{De \rightarrow \infty} NI^* = \frac{A_1}{\sqrt[10]{\frac{\eta_{E,U,max}}{3\eta_0}}} \left[\sqrt{\frac{\eta_{E,P}}{\eta_{E,U}}} + \psi_1 \arctan\left(\psi_2 \frac{N_2}{N_1}\right) \arctan\left(\psi_3 \frac{\eta_{E,U,max}}{3\eta_0}\right) \right] \quad (35)$$

where $A_1 = 0.493, \theta = 7.65, \psi_1 = 0.985, \psi_2 = -0.812, \psi_3 = 0.524$.

As it can be deduced from Eq. (35), a limiting value of NI^* is a linear function of $\sqrt{\frac{\eta_{E,P}}{\eta_{E,U}}}$ with a slope of $\frac{0.493}{7.65 \sqrt[10]{\frac{\eta_{E,U,max}}{3\eta_0}}}$ and non-zero limiting NI^* intercept value depending on $-N_2/N_1$ as well as $\frac{\eta_{E,U,max}}{3\eta_0}$.

3.2. Analytical approximation for NI^* vs. experimental data

The approximate solution given by Eq. (31), utilizing constants provided in Table 3, was validated for 5 different polyethylenes with basic characteristics summarized in Table 4.

In the first step, deformation rate dependent ‘steady state’ uniaxial extensional viscosity data (taken from the transient viscosity data peaks for given deformation rates, [60,69]) were fitted by the modified Leonov model (Eqs. (1)–(5)) to identify its parameters, which are summarized in Table 5. It is important to note that in the case of LDPE 170A sample, even if it was possible to fit experimental points by 5 different sets of Leonov model parameters with a practically identical error (because number of experimental points was very low, see Fig. 10(a)), corresponding model predictions for $\frac{\eta_{E,P}}{\eta_{E,U}}$ and $-N_2/N_1$ were different (see Fig. 10(b)–(c)). This has a strong impact on the viscoelastic 1D membrane model predictions for dimensionless final film half-width vs. draw ratio, especially, for high Deborah numbers, at which $-N_2/N_1$ (calculated at the die exit for the given shear rate and considering fully developed slit flow) plays an important role (see Fig. 10(d)). This suggests that the Leonov model parameters should be

Table 5
Modified Leonov model parameters for polymeric materials with basic characteristics provided in Table 4.

Polymer sample	λ (s)	G (Pa)	ξ (1)	ν (1)	β (1)	T_0 (°C)
LDPE 170A	1.57	85,982.61	1.53	0.072	0.7	150
PE-A ^a	9.5	1,707.37	0.41	0.0015	0.4	130
PE-B ^a	15	2,514.67	0.29	0.0034	0.4	130
PE-C ^a	30	1,201.10	0.09	0.0013	0.5	130
LDPE C	28.57	768.95	0.51	0.004	0	125

^a Parameters are taken from [55].

determined by using a uniaxial extensional viscosity data measured at very wide extensional strain rates and utilizing other properties such as planar extensional viscosity, N_1 and N_2 , if they are available. A comparison between the uniaxial extensional viscosity data for all five polyethylene samples (taken from [18,37,38,40,47]) and corresponding modified Leonov model predictions for uniaxial as well as planar

extensional viscosities is provided in Fig. 11. As it can be seen, single-mode modified Leonov model has a capability to describe uniaxial extensional viscosity for all samples.

In the second step, material relaxation time, λ , mean extensional strain rate in the air gap, $\left(\frac{du}{dx}\right)_M$, and shear rate at the die exit (corrected for the non-Newtonian behavior) [70,71] $\dot{\gamma}_{COR}$, were determined for processing conditions and summarized for all samples in Table 6 as follows:

$$\lambda = \lambda(T_0) \exp\left[\frac{E_a}{R}\left(\frac{1}{T} - \frac{1}{T_0}\right)\right] \quad (36)$$

$$\left(\frac{du}{dx}\right)_M = \frac{u - u_0}{X} \quad (37)$$

$$\dot{\gamma}_{COR} = \frac{6Q}{8L_0e_0^2} \left(\frac{2n_0 + 1}{3n_0}\right) \quad (38)$$

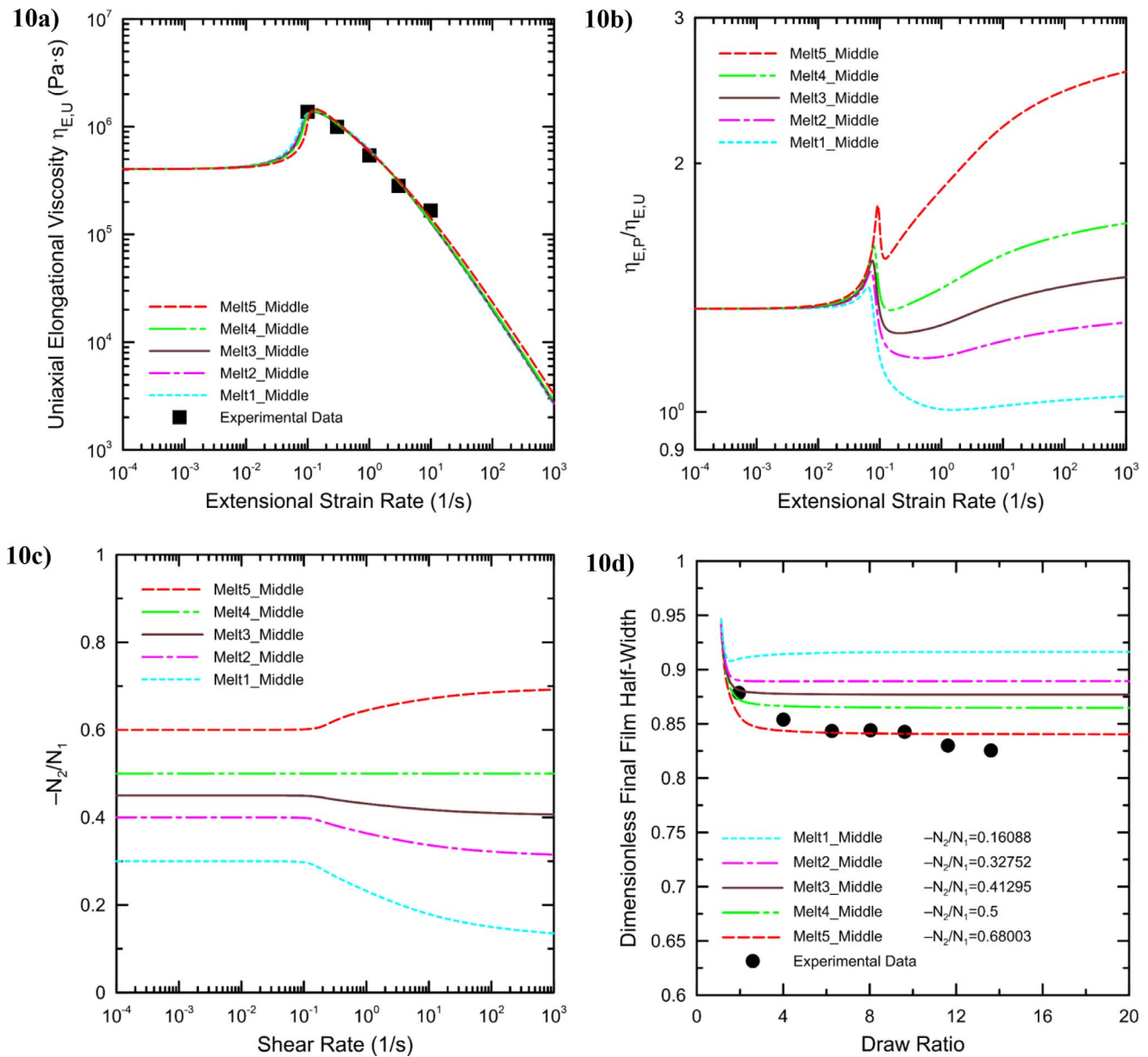


Fig. 10. Comparison between experimental data for LDPE 170A ($T = 150^\circ\text{C}$), given processing data ($De = 0.253$, $X = 10$ mm, see Table 6) taken from [37,38,40] and corresponding model predictions for five virtual materials with modified Leonov model parameters summarized in Table 2. (a) LDPE 170A uniaxial extensional viscosity, (b) planar to uniaxial extensional viscosity ratio, (c) second to first normal stress difference ratio, (d) dimensionless final film half-width as the function of draw ratio.

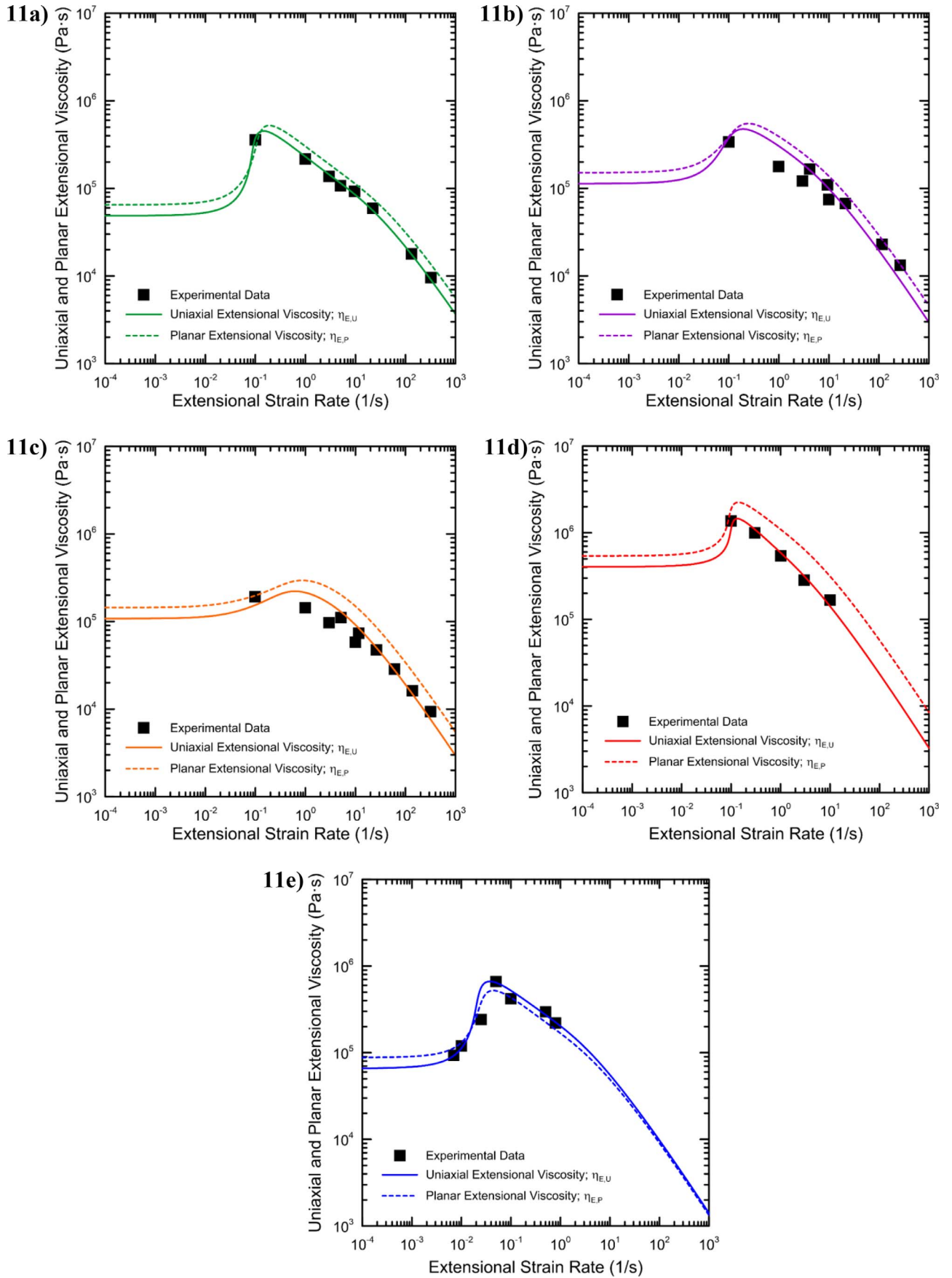


Fig. 11. Comparison between experimental data for deformation rate dependent uniaxial extensional viscosity taken from [18,37,38,40,47], and corresponding single-mode modified Leonov model predictions for uniaxial as well as planar extensional viscosities. (a) PE-A, $T = 130^\circ\text{C}$, (b) PE-B, $T = 130^\circ\text{C}$, (c) PE-C, $T = 130^\circ\text{C}$, (d) LDPE 170A, $T = 150^\circ\text{C}$, (e) LDPE C, $T = 125^\circ\text{C}$.

Table 6
Summarization of extrusion film casting processing parameters for all considered polymer samples taken from the open literature [18,37,47].

Polymer sample	Die Width, $2L_0$ (mm)	Die Gap, $2e_0$ (mm)	Air Gap, X (mm)	Temperature, T (°C)	Die Exit Velocity, u_0 (mm/s)	Draw Ratio, DR (1)	NI^* (1)	Ref.
LDPE 170A	100	0.46	228	190	4.3	17.1	0.1537	[37]
PE-A	600	0.80	160	320	46.6 ^a	42.9 ^b	0.2466	[47]
PE-B	600	0.80	190	320	46.6 ^a	42.9 ^b	0.3275	[47]
PE-C	600	0.80	220	320	46.6 ^a	42.9 ^b	0.5159	[47]
LDPE C	250	0.95	90	190	5.1	65.2 ^c	0.2973	[18]
LDPE 170A	100	0.46	10	190	4.3	9.6	0.7867	[37]

^a Die exit velocity was determined based on the die width ($2L_0$), die gap ($2e_0$), melt density (ρ) and mass flow rate (MFR) as $u_0 = MFR / (\rho 2L_0 2e_0)$, where $MFR = 60$ kg/h and melt density $\rho = 745$ kg/m³ [47].

^b Draw ratio was determined from die exit velocity and take-up velocity as $DR = u/u_0$. Take-up velocity is provided in [47] as $u = 120$ m/min.

^c Calculated based on a take-up velocity at the drawing drum.

Table 7
Summarization of all parameters appearing in Eq. (31) for the normalized maximum attainable normalized neck-in (i.e. De , $\frac{\eta_{E,U,max}}{3\eta_0}$, $\frac{\eta_{E,P}}{\eta_{E,U}}$ and $-N_2/N_1$) calculated by using modified Leonov model utilizing material relaxation time, λ , mean extensional strain rate in the air gap, $(\frac{du}{dx})_M$, and shear rate at the die exit (corrected for the non-Newtonian behavior), $\dot{\gamma}_{COR}$, determined for processing conditions summarized for all samples in Table 6.

Polymer sample	λ (s)	$(\frac{du}{dx})_M$ (1/s)	$\dot{\gamma}_{COR}$ (1/s)	De (1)	$-N_2/N_1$ (1)	$\frac{\eta_{E,P}}{\eta_{E,U}}$ (1)	$\frac{\eta_{E,U,max}}{3\eta_0}$ (1)
LDPE 170A	0.588	0.300	91.363	0.011	0.680	1.547	3.393
PE-A	0.079	10.281	569.402	0.019	0.405	0.833	9.299
PE-B	0.125	8.879	569.402	0.026	0.406	1.102	4.198
PE-C	0.250	10.281	569.402	0.061	0.500	1.293	2.047
LDPE C	3.149	3.638	52.469	0.178	0.017	0.825	10.096
LDPE 170A	0.588	3.707	91.363	0.253	0.680	1.910	3.393

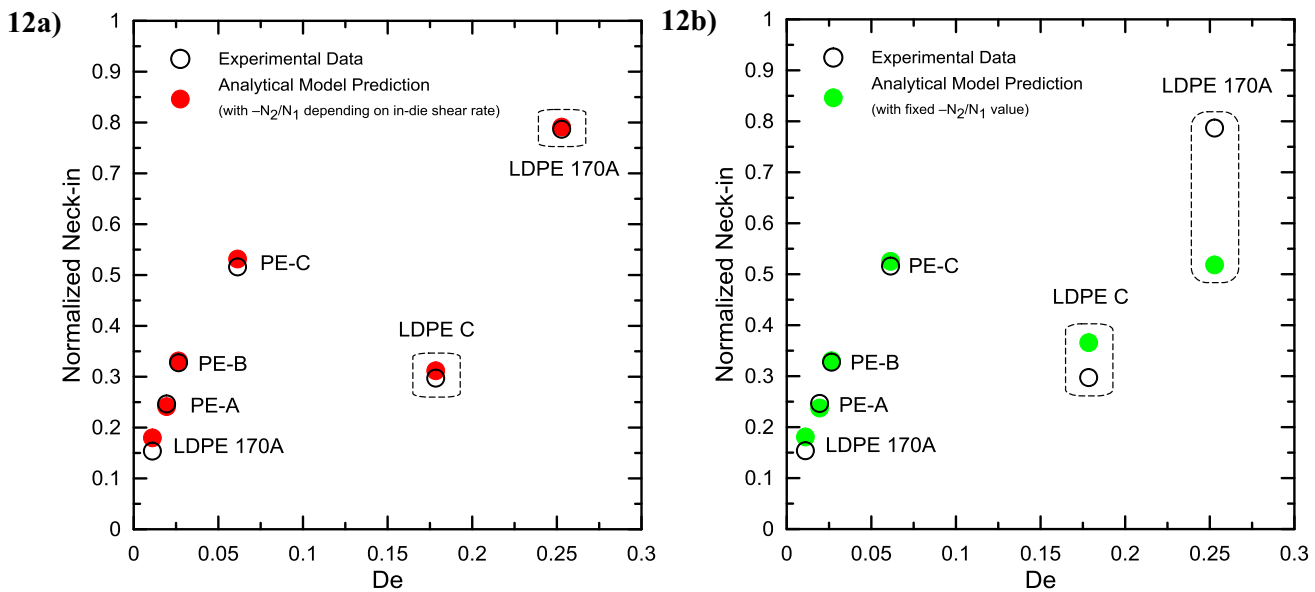


Fig. 12. Normalized maximum attainable neck-in value, NI^* , as the function of Deborah number for LDPE 170A, PE-A, PE-B, PE-C, and LDPE C polymers for the processing conditions summarized in Table 6. Experimental data (taken from [37,38,40,47,18]) and proposed analytical model predictions (Eq. (31)) are given here by the open and filled symbols, respectively. (a) $-N_2/N_1$ is given by the modified Leonov model predictions for particular die exit shear rates, which are provided in Table 7 for each individual case, (b) $-N_2/N_1$ is considered to be constant, equal to 0.2.

Here $\lambda(T_0)$ represents relaxation time at the reference temperature, T_0 , (Table 5), E_a is the flow activation energy (Table 4), R is the universal gas constant equal to 8.3144598 J/K/mol, u is the take-up velocity, u_0 is the die exit velocity, X is the air gap, Q is the overall volumetric flow rate, L_0 is the die half-width, e_0 is the die half-gap and n_0 is the index of non-Newtonian behavior (equal to 0.3464 as the typical value for LDPEs [72]). The exponential term in Eq. (36) represents Arrhenius shift factor [73,74] whereas the second term in Eq. (38) represents Rabinowitsch correction for a rectangle channel [75]. All parameters appearing in Eq. (31) for the normalized maximum attainable normalized neck-in, NI^* , (i.e. De , $\frac{\eta_{E,U,max}}{3\eta_0}$, $\frac{\eta_{E,P}}{\eta_{E,U}}$ and $-N_2/N_1$ for

given processing parameters and materials used) were calculated by using modified Leonov model utilizing λ , $(\frac{du}{dx})_M$ and $\dot{\gamma}_{COR}$ parameters determined via Eqs. (36)–(38) (see their summarization in Table 7).

In the final step, measured values for NI^* , provided in Table 6, were compared with corresponding predictions of approximate model (Eq. (31)) utilizing constants and parameters provided in Tables 3 and 7, respectively (see Fig. 12(a)). As it can be seen, there is a very good agreement between the measured data and approximate model predictions within the whole range of Deborah numbers. If the $-N_2/N_1$ at the die exit region is considered to be unrealistically constant for all tested LDPEs (for example equal to 0.2 as the ‘typical value’ [76]), the

model failed to predict NI^* for Deborah numbers larger than 0.1 (see Fig. 12(b)), which confirms existence of the critical Deborah number, above which, the neck-in phenomenon starts to be strongly dependent on the die exit stress state.

Based on the performed analysis, it can be concluded that the approximate model, which relates the normalized maximum attainable normalized neck-in with De , $\frac{\eta_{E,U,max}}{3\eta_0}$, $\frac{\eta_{E,P}}{\eta_{E,U}}$ and $-N_2/N_1$ according to Eq. (31), can be considered as a useful tool for material, processing and die design optimization in order to suppress unwanted neck-in phenomenon occurring during a production of thin flat films.

4. Conclusions

In this work, the effect of second to first normal stress difference ratio at the die exit, $-N_2/N_1$, uniaxial extensional strain hardening, $\frac{\eta_{E,U,max}}{3\eta_0}$, planar-to-uniaxial extensional viscosity ratio, $\frac{\eta_{E,P}}{\eta_{E,U}}$, and Deborah number, De , has been investigated via viscoelastic isothermal modeling utilizing 1D membrane model and a single-mode modified Leonov model as the constitutive equation. Based on the performed parametric study, it was found that an increase in $-N_2/N_1$ ratio and De increases both, the neck-in as well as its sensitivity to $\sqrt{\frac{\eta_{E,P}}{\eta_{E,U}}}$. There exists a threshold value for Deborah number and $\frac{\eta_{E,U,max}}{3\eta_0}$, above which, the neck-in starts to be strongly dependent on the die exit stress state, $-N_2/N_1$. It was found that such critical De decreases if $-N_2/N_1$, $\frac{\eta_{E,U,max}}{3\eta_0}$ increases and/or $\frac{\eta_{E,P,max}/\eta_{E,U,max}}{4\eta_0}$ decreases. Numerical solutions of the 1D membrane viscoelastic model, utilizing modified single-mode Leonov model as the constitutive equation, were successfully approximated by a dimensionless analytical equation expressing the normalized maximum attainable neck-in with $\frac{\eta_{E,U,max}}{3\eta_0}$, $\frac{\eta_{E,P}}{\eta_{E,U}}$, $-N_2/N_1$ and De . Suggested equation was tested by using the experimental data taken from [18,37,38,40,47] for five different polyethylenes where $0.011 \leq De \leq 0.253$, $0.825 \leq \frac{\eta_{E,U,max}}{3\eta_0} \leq 1.910$, $2.047 \leq \frac{\eta_{E,U,max}}{3\eta_0} \leq 10.096$ and $0.017 \leq \frac{-N_2}{N_1} \leq 0.680$. It was found that approximate model predictions are in a very good agreement with the corresponding experimental data within the whole range of investigated Deborah numbers. Interestingly, the neck-in predictions for Deborah numbers larger than 0.1 became unrealistic, if the $-N_2/N_1$ at the die exit region is not taken into account, which confirms the existence of critical Deborah number, above which, the neck-in phenomenon starts to be strongly dependent on the die exit stress state. It is believed that the obtained knowledge together with the suggested simple analytical model can be used for optimization of the extrusion die design (influencing flow history and thus die exit stress state), molecular architecture of polymer melts and processing conditions to suppress neck-in phenomenon in a production of very thin flat films.

Acknowledgments

The authors wish to acknowledge the financial support from the Grant Agency of the Czech Republic (Grant registration No. 16-05886S).

References

- [1] T. Kanai, G.A. Campbell, *Film Processing Advances*, Second Ed., Hanser Publishers, Munich, 2014.
- [2] T. Kanai, G.A. Campbell, *Film Processing*, Hanser Publishers, Munich, 1999.
- [3] R.J. Fisher, M.M. Denn, Finite-amplitude stability and draw resonance in isothermal melt spinning, *Chemical Engineering Science* 30 (1975) 1129–1134.
- [4] R.J. Fisher, M.M. Denn, A theory of isothermal melt spinning and draw resonance, *AIChE Journal* 22 (1976) 236–246.
- [5] D. Gelder, The stability of fiber drawing processes, *Industrial & Engineering Chemistry Fundamentals* 10 (1971) 534–535.
- [6] Y.L. Yeow, On the stability of extending films: a model for the film casting process, *Journal of Fluid Mechanics* 66 (1974) 613–622.
- [7] G.R. Aird, Y.L. Yeow, Stability of film casting of power-law liquids, *Industrial & Engineering Chemistry Fundamentals* 22 (1983) 7–10.
- [8] N.R. Anturkar, A. Co, Draw resonance in film casting of viscoelastic fluids: a linear stability analysis, *Journal of Non-Newtonian Fluid Mechanics* 28 (1988) 287–307.
- [9] V.R. Iyengar, A. Co, Film casting of a modified Giesekus fluid: a steady-state analysis, *Journal of Non-Newtonian Fluid Mechanics* 48 (1993) 1–20.
- [10] V.R. Iyengar, A. Co, Film casting of a modified Giesekus fluid: stability analysis, *Chemical Engineering Science* 51 (1996) 1417–1430.
- [11] J.P. Sergent, *Etude de deux procédés de fabrication de films. Le soufflage de gaine. L'extrusion de film à plat*, in: Strasbourg, France, 1977.
- [12] D. Cotto, P. Duffo, J.M. Haudin, Cast film extrusion of polypropylene films, *International Polymer Processing* 4 (1989) 103–113.
- [13] P. Duffo, B. Monasse, J.M. Haudin, Cast film extrusion of polypropylene. Thermomechanical and physical aspects, *Journal of Polymer Engineering* 10 (1991) 151–229.
- [14] P. Barq, J.M. Haudin, J.F. Agassant, Isothermal and anisothermal models for cast film extrusion, *International Polymer Processing* 7 (1992) 334–349.
- [15] S. D'Halewyu, J.F. Agassant, Y. Demay, Numerical simulation of the cast film process, *Polymer Engineering & Science* 30 (1990) 335–340.
- [16] B. Debaut, J.M. Marchal, M.J. Crochet, Viscoelastic effects in film casting, *Zeitschrift für angewandte Mathematik und Physik* 46 (1995) 679–698.
- [17] W.S. Smith, *Simulating the Cast Film Process Using an Updated Lagrangian Finite Element Algorithm*, McMaster University, 2001.
- [18] N. Satoh, H. Tomiyama, T. Kajiwara, Viscoelastic simulation of film casting process for a polymer melt, *Polymer Engineering & Science* 41 (2001) 1564–1579.
- [19] O.S. Narayanaswamy, A one-dimensional model of stretching float glass, *Journal of the American Ceramic Society* 60 (1977) 1–5.
- [20] D. Silagy, Y. Demay, J.F. Agassant, Study of the stability of the film casting process, *Polymer Engineering & Science* 36 (1996) 2614–2625.
- [21] D. Silagy, Y. Demay, J.F. Agassant, Stationary and stability analysis of the film casting process, *Journal of Non-Newtonian Fluid Mechanics* 79 (1998) 563–583.
- [22] K. Sakaki, R. Katsumoto, T. Kajiwara, K. Funatsu, Three-dimensional flow simulation of a film-casting process, *Polymer Engineering & Science* 36 (1996) 1821–1831.
- [23] H. Zheng, W. Yu, C. Zhou, H. Zhang, Three-dimensional simulation of the non-isothermal cast film process of polymer melts, *Journal of Polymer Research* 13 (2006) 433–440.
- [24] G. Lamberti, G. Titomanlio, V. Brucato, Measurement and modelling of the film casting process 1. Width distribution along draw direction, *Chemical Engineering Science* 56 (2001) 5749–5761.
- [25] G. Lamberti, G. Titomanlio, V. Brucato, Measurement and modelling of the film casting process 2. Temperature distribution along draw direction, *Chemical Engineering Science* 57 (2002) 1993–1996.
- [26] G. Lamberti, V. Brucato, G. Titomanlio, Orientation and crystallinity in film casting of polypropylene, *Journal of Applied Polymer Science* 84 (2002) 1981–1992.
- [27] G. Lamberti, F. De Santis, V. Brucato, G. Titomanlio, Modeling the interactions between light and crystallizing polymer during fast cooling, *Applied Physics A* 78 (2004) 895–901.
- [28] G. Lamberti, Flow-induced crystallization during isotactic polypropylene film casting, *Polymer Engineering & Science* 51 (2011) 851–861.
- [29] G. Titomanlio, G. Lamberti, Modeling flow induced crystallization in film casting of polypropylene, *Rheologica Acta* 43 (2004) 146–158.
- [30] G. Lamberti, G. Titomanlio, Analysis of film casting process: the heat transfer phenomena, *Chemical Engineering and Processing Process Intensification* 44 (2005) 1117–1122.
- [31] G. Lamberti, G. Titomanlio, Analysis of film casting process: effect of cooling during the path in air, *Industrial & Engineering Chemistry Research* 45 (2006) 719–723.
- [32] H. Ito, M. Doi, T. Isaki, M. Takeo, K. Yagi, 2D flow analysis of film casting process, *Journal of Society of Rheology Japan* 31 (2003) 149–155.
- [33] H. Ito, M. Doi, T. Isaki, M. Takeo, A model of neck-in phenomenon in film casting process, *Journal of Society of Rheology Japan* 31 (2003) 157–163.
- [34] C.W. Seay, D.G. Baird, Sparse long-chain branching's effect on the film-casting behavior of PE, *International Polymer Processing* 24 (2009) 41–49.
- [35] C.D. McGrady, C.W. Seay, D.G. Baird, Effect of sparse long-chain branching on the film-casting behavior for a series of well-defined HDPEs, *International Polymer Processing* 24 (2009) 428–438.
- [36] H. Kometani, T. Matsumura, T. Suga, T. Kanai, Experimental and theoretical analyses of film casting process, *Journal of Polymer Engineering* 27 (2007) 1–28.
- [37] H.V. Pol, S.S. Thete, P. Doshi, A.K. Lele, Necking in extrusion film casting: the role of macromolecular architecture, *Journal of Rheology* 57 (2013) 559–583.
- [38] H.V. Pol, S. Banik, L.B. Azad, S.S. Thete, P. Doshi, A. Lele, Nonisothermal analysis of extrusion film casting process using molecular constitutive equations, *Rheologica Acta* 53 (2014) 85–101.
- [39] K. Chikhalikar, S. Banik, L.B. Azad, K. Jadhav, S. Mahajan, Z. Ahmad, S. Kulkarni, S. Gupta, P. Doshi, H.V. Pol, A. Lele, Extrusion film casting of long chain branched polypropylene, *Polymer Engineering & Science* 55 (2015) 1977–1987.
- [40] S.S. Thete, P. Doshi, H.V. Pol, New insights into the use of multi-mode phenomenological constitutive equations to model extrusion film casting process, *Journal of Plastic Film and Sheeting* 33 (2017) 35–71.
- [41] R. Dhadwal, S. Banik, P. Doshi, H.V. Pol, Effect of viscoelastic relaxation modes on stability of extrusion film casting process modeled using multi-mode Phan-Thien-Tanner constitutive equation, *Applied Mathematical Modelling* 47 (2017) 487–500.
- [42] H.V. Pol, S.S. Thete, Necking in extrusion film casting: numerical predictions of the Maxwell model and comparison with experiments, *Journal of Macromolecular Science Part B* 55 (2016) 984–1006.

- [43] T. Dobroth, L. Erwin, Causes of edge beads in cast films, *Polymer Engineering & Science* 26 (1986) 462–467.
- [44] N. Toft, M. Rigdahl, Extrusion coating with metallocene-catalysed polyethylenes, *International Polymer Processing* 17 (2002) 244–253.
- [45] S. Kouda, Prediction of processability at extrusion coating for low-density polyethylene, *Polymer Engineering & Science* 48 (2008) 1094–1102.
- [46] S. Shiromoto, Y. Masutani, M. Tsutsubuchi, Y. Togawa, T. Kajiwara, A neck-in model in extrusion lamination process, *Polymer Engineering & Science* 50 (2010) 22–31.
- [47] S. Shiromoto, Y. Masutani, M. Tsutsubuchi, Y. Togawa, T. Kajiwara, The effect of viscoelasticity on the extrusion drawing in film-casting process, *Rheologica Acta* 49 (2010) 757–767.
- [48] S. Shiromoto, The mechanism of neck-in phenomenon in film casting process, *International Polymer Processing* 29 (2014) 197–206.
- [49] K. Christodoulou, S.G. Hatzikiriakos, D. Vlassopoulos, Stability analysis of film casting for PET resins using a multimode Phan–Thien–Tanner constitutive equation, *Journal of Plastic Film and Sheeting* 16 (2000) 312–332.
- [50] S. Smith, D. Stolle, Numerical simulation of film casting using an updated Lagrangian finite element algorithm, *Polymer Engineering & Science* 43 (2003) 1105–1122.
- [51] S. Bourrigaud, G. Marin, V. Dabas, C. Dupuy, D. Silagy, The draw ratio-Deborah number diagram: a useful tool for coating applications, *Polymer Engineering & Science* 46 (2006) 372–380.
- [52] J.M. Kim, J.S. Lee, D.M. Shin, H.W. Jung, J.C. Hyun, Transient solutions of the dynamics of film casting process using a 2-D viscoelastic model, *Journal of Non-Newtonian Fluid Mechanics* 132 (2005) 53–60.
- [53] T. Kajiwara, M. Yamamura, T. Asahina, Relationship between Neck-in phenomena and rheological properties in film casting, *Nihon Reoroji Gakkaishi* 34 (2006) 97–103.
- [54] M.E. Pis-Lopez, A. Co, Multilayer film casting of modified Giesekus fluids Part 1. Steady-state analysis, *Journal of Non-Newtonian Fluid Mechanics* 66 (1996) 71–93.
- [55] T. Barborik, M. Zatloukal, C. Tzoganakis, On the role of extensional rheology and Deborah number on the neck-in phenomenon during flat film casting, *International Journal of Heat and Mass Transfer* 111 (2017) 1296–1313.
- [56] V.R. Iyengar, *Film Casting of Polymer Melts*, University of Maine, 1993.
- [57] G. Oliver, Internally deckled coating dies, *Proceedings of the TAPPI European PLACE Conference, Athens; Greece, 2007*, pp. 311–339.
- [58] M. Zatloukal, R. Kolarik, Investigation of convective heat transfer in 9-layer film blowing process by using variational principles, *International Journal of Heat and Mass Transfer* 86 (2015) 258–267.
- [59] J. Musil, M. Zatloukal, Effect of die exit geometry on internal die drool phenomenon during linear HDPE melt extrusion, *International Journal of Heat and Mass Transfer* 56 (2013) 667–673.
- [60] R. Kolarik, M. Zatloukal, M. Martyn, The effect of polyolefin extensional rheology on non-isothermal film blowing process stability, *International Journal of Heat and Mass Transfer* 56 (2013) 694–708.
- [61] A.I. Leonov, Nonequilibrium thermodynamics and rheology of viscoelastic polymer media, *Rheologica Acta* 15 (1976) 85–98.
- [62] A.I. Leonov, E.H. Lipkina, E.D. Paskhin, A.N. Prokunin, Theoretical and experimental investigation of shearing in elastic polymer liquids, *Rheologica Acta* 15 (1976) 411–426.
- [63] A.I. Leonov, A.N. Prokunin, An improved simple version of a nonlinear theory of elasto-viscous polymer media, *Rheologica Acta* 19 (1980) 393–403.
- [64] A.I. Leonov, A.N. Prokunin, On nonlinear effects in the extensional flow of polymeric liquids, *Rheologica Acta* 22 (1983) 137–150.
- [65] M. Simhambhatla, A.I. Leonov, On the rheological modeling of viscoelastic polymer liquids with stable constitutive equations, *Rheologica Acta* 34 (1995) 259–273.
- [66] A.I. Leonov, Constitutive equations for viscoelastic liquids: formulation, analysis and comparison with data, *Rheology Series* 8 (1999) 519–575.
- [67] M. Zatloukal, Differential viscoelastic constitutive equations for polymer melts in steady shear and elongational flows, *Journal of Non-Newtonian Fluid Mechanics* 113 (2003) 209–227.
- [68] M. Beaulne, E. Mitsoulis, Numerical simulation of the film casting process, *International Polymer Processing* 14 (1999) 261–275.
- [69] J. Drabek, M. Zatloukal, Evaluation of Thermally induced degradation of branched polypropylene by using rheology and different constitutive equations, *Polymers (Basel)* 8 (2016) 317.
- [70] C.W. Macosko, *Rheology: Principles, Measurements, and Applications*, VCH, 1994.
- [71] J. Vlachopoulos, J.R. Wagner, *The SPE Guide on Extrusion Technology and Troubleshooting*, The Society of Plastics Engineers, Brookfield, 2001.
- [72] M. Zatloukal, Measurements and modeling of temperature-strain rate dependent uniaxial and planar extensional viscosities for branched LDPE polymer melt, *Polymer (Guildf)* 104 (2016) 258–267.
- [73] J.D. Ferry, *Viscoelastic Properties of Polymers*, Third Ed., John Wiley & Sons, New York, 1980.
- [74] J.M. Dealy, R.G. Larson, *Structure and Rheology of Molten Polymers – From Structure to Flow Behavior and Back Again*, Hanser Publishers, Munich, 2006.
- [75] C.W. Macosko, *Rheology: Principles, Measurements, and Applications*, Wiley, New York, NY, 1994.
- [76] E.A. Jensen, J.deC. Christiansen, Measurements of first and second normal stress differences in a polymer melt, *Journal of Non-Newtonian Fluid Mechanics* 148 (2008) 41–46.

PAPER III

**EFFECT OF HEAT TRANSFER COEFFICIENT, DRAW RATIO AND
DIE EXIT TEMPERATURE ON THE PRODUCTION OF FLAT
iPP MEMBRANES**

Tomas Barborik, Martin Zatloukal*

Polymer Centre, Faculty of Technology, Tomas Bata University in Zlin,

Vavreckova 275, 760 01 Zlin, Czech Republic

Keywords: Flat film production, polymer melt, rheology, neck-in phenomenon, heat transfer, crystallization, linear isotactic polypropylene.

*Corresponding author: mzatloukal@utb.cz

ABSTRACT

In this work, stable numerical scheme has been developed for 1.5D film casting model of Silagy et al. (Polym Eng Sci 36:2614-2625, 1996) utilizing viscoelastic modified Leonov model as the constitutive equation and energy equation coupled with crystallization kinetics of semicrystalline polymers taking into account actual temperature as well as cooling rate. Model has been successfully validated on the experimental data for linear isotactic polypropylene taken from the open literature. Drawing distance, draw ratio, heat transfer coefficient and die exit melt temperature were systematically varied in the utilized model in order to understand the role of process conditions on the neck-in phenomenon (unwanted film width shrinkage during stretching in the post die area) and crystalline phase development during flat film production. It is believed that the utilized numerical model together with suggested stable numerical scheme as well as obtained research results can help to understand processing window for production of flat porous membranes from linear iPP considerably.

1 INTRODUCTION

For the production of transparent packaging materials via cast film process, high demands are required on the optical properties of the manufactured thin films, which can be achieved by the use of wide extrusion dies, very high processing temperatures and short stretching distances minimizing the neck-in phenomenon and related dog-bone defect. The film cooling is not sufficient and the temperature field is rather uniform in this spatial configuration. It was shown in early studies devoted to the heat transfer in film casting, [1–3] and [4] (measured temperature drop by IR camera was less than 15°C), that such flows can be viewed as the isothermal. On the other hand, if the stretching distance increases too much, film temperature decreases, melt viscosity increases and temperature and/or stress induced crystallization may start to occur, which can influence the process considerably. Effect of the temperature in film casting [5] have been experimentally investigated for PET polymer using infrared thermography apparatus with the capability to measure the temperature variation in film width and axial direction (machine direction). It was concluded that the temperature variations should be accounted for geometries with large die width and take-up length greater than 1/10 of die width.

There are two contradictory practices of setting up the processing conditions depending on whether final film is to be used for packaging or membrane applications. Thin films for wrapping/packaging should possess transparency with low haze and high clarity whereas precursor films for microporous membrane should contain crystalline phase. The crystallization evolution of semi-crystalline polymers is strongly influenced by applied processing conditions, when under quiescent isothermal conditions of crystallization, the kinetics is a function of temperature whilst in quiescent non-isothermal case, additionally, rate of cooling comes into play [6]. Especially, during high cooling rates often encountered in a fabrication of porous membranes. A great amount of research effort on the crystallization and flow induced crystallization in the film casting process has been done by group of Titomanlio and

Lamberti [7–17]. Very early crystallization models [18–20] were developed for metal materials under the constant temperature, that is, crystallization rate and thermal history is not linked together. Next step in the model development was introduction of Kolmogoroff-Avrami-Evans equation describing the evolution of crystallization through the time [19, 21–23]. Further works [24, 25] and [26] used isokinetic hypothesis which accounts for proportionality between crystal nucleation and its growth rate. Advantage in this case is quite simple determination of model parameters that does not require any special apparatus, just differential scanning calorimetry (DSC) is needed. More recently, Ziabicki has introduced model, which includes transient and non-isothermal effects [27, 28].

Experimental investigation of crystallization in fast-cooling experiments were carried out [29, 30] usually by DSC or by using fast scanning chip calorimetry, FSC, allowing to reach cooling rates in order of thousands of K/s [31]. For polypropylene, it has been shown that high chain orientation in the melt state can lead to production row nucleated lamellar structure [32].

Isotactic polypropylene is significant commercial thermoplastic polymer with variety industrial applications and can be considered as a good candidate for gas separation, filtration, medical application, air-permeable membranes in advanced apparel.

In the last decades, polypropylene microporous membranes are broadly applied in industry for Lithium ion batteries in the form of separators to keep electrodes away from each other (avoidance of electrical short circuit) as well as to simultaneously allow the transportation of ionic charge carriers [33–35]. PP has certain superior properties that favors it over polyethylene for such use as excellent dimensional stability at high temperatures, high melting temperature, higher chemical resistance and good mechanical properties. Isotactic Polypropylene and its inherited polymorphism enables crystallization into different crystal modifications during solidification depending on the cooling conditions [36–38].

Polypropylene membranes are usually fabricated by thermal-induced phase separation, non-solvent-induced phase separation (using e.g. mineral fillers) and dry process based on melt-stretching mechanism. In particular, the latter method, so-called MEAUS (melt extrusion-annealing-uniaxial stretching) technology, possesses advantage of low environmental pollution footprint since use of solvents may be avoided and lower expenses.

The fabrication process of membranes based on melt-stretching approach is applicable for semi-crystalline polymers and can be distinguished into three major consecutive stages: first, precursor film with lamellar crystalline structure is produced; second, the film is annealed to thicken lamellae and obliterate the defects of crystalline phase (improved uniformity and lamellae orientation through melting and recrystallization [39]); third, stretching is applied upon the film at low and high temperature to create voids due to lamellae separation and enlarge them into the microporous structure, respectively. To keep good dimensional stability over time and lower the shrinkage of the produced microporous membranes, additional treatment step of heat setting [40] is usually included. During the first stage, polymer characteristics and extrusion processing conditions are important in generation of row-nucleated lamellar structure [41]. Polymer architecture, molecular weight and molecular weight distribution seem to be the key material characteristics responsible for the formation of appropriate crystalline microstructure [39, 42–45] as necessary presumption for creation of stretching-generated pores with even spatial distribution and suitable size. For cast film processing conditions, it has been reported [46] that increasing in the draw ratio and severe cooling conditions at the area of die exit has a significant effect on the crystal orientation. Further research was conducted for a much lower chill roll temperatures and different die temperatures [47].

Investigation of crystallization development/flow-induced crystallization by means of simultaneous modelling with process kinematic equations has already been conducted in the field of fiber spinning process [48–56]; however, to our best knowledge, only a sparse

attention has been paid for the film casting process. Thus, it is not surprising that processing window for the production of porous membranes, flow stability and the role of process parameters are not fully understood yet. In order to fill this knowledge gap, novel viscoelastic film casting model utilizing 1.5D membrane approximation [57], modified Leonov model as the constitutive equation [58, 59] and energy equation coupled with advanced crystallization kinetics [27, 28, 60] was derived, validated and consequently used in the detailed parametric study.

2 MATHEMATICAL MODELLING

2.1 Film casting model

To determine basic process variables in deformation flow with free surface in the post die area, the one-dimensional membrane model [57] for extrusion film casting was employed and numerically solved. Even though the dimensionality of the model is unity, it possess the capability to predict both, the reduction in film thickness as well as film width shrinkage owing to assumed flow kinematics [61]. From this point of view, the model might be considered as a pseudo 2D or 1.5D and principal velocities (see Figure 1) are allowed to varied along the axial direction as follows

$$\begin{aligned}u &= u(x) \\v &= v(x, y) = yf(x) \\w &= w(x, z) = zg(x)\end{aligned}\tag{1}$$

Here, velocity in axial, transversal and thickness direction is denoted as u , v and w , respectively. The membrane model comprises of governing equations for continuity and momentum conservation that are simultaneously solved with equation of energy and viscoelastic single-mode modified Leonov model as the constitutive equation.

2.2 Constitutive equations

The utilized modified Leonov model is based on heuristic thermodynamic arguments resulting from the theory of rubber elasticity [58, 62–66]. In this constitutive equation, a fading memory of the melt is determined through an irreversible dissipation process driven by the dissipation term, b .

From mathematical viewpoint, it is relating the stress and elastic strain stored in the material as:

$$\underline{\underline{\tau}} = 2 \left(\underline{\underline{c}} \cdot \frac{\partial W}{\partial \underline{\underline{I}}_{1,c}} - \underline{\underline{c}}^{-1} \cdot \frac{\partial W}{\partial \underline{\underline{I}}_{2,c}} \right) \quad (2)$$

where $\underline{\underline{\tau}}$ is the stress, and W , the elastic potential, which depends on the invariants $\underline{\underline{I}}_{1,c}$ and $\underline{\underline{I}}_{2,c}$ of the recoverable Finger tensor $\underline{\underline{c}}$,

$$W = \frac{3G}{2(n+1)} \left\{ [1-\beta] \cdot \left[\left(\frac{\underline{\underline{I}}_{1,c}}{3} \right)^{n+1} - 1 \right] + \beta \left[\left(\frac{\underline{\underline{I}}_{2,c}}{3} \right)^{n+1} - 1 \right] \right\} \quad (3)$$

where G denotes linear Hookean elastic modulus, β and n are numerical parameters. Leonov assumed that the dissipative process acts to produce an irreversible rate of strain $\underline{\underline{e}}_p$

$$\underline{\underline{e}}_p = b \left[\underline{\underline{c}} - \frac{\underline{\underline{I}}_{1,c}}{3} \underline{\underline{\delta}} \right] - b \left[\underline{\underline{c}}^{-1} - \frac{\underline{\underline{I}}_{2,c}}{3} \underline{\underline{\delta}} \right] \quad (4)$$

which spontaneously reduces the rate of elastic strain accumulation. Here, $\underline{\underline{\delta}}$ is the unit tensor and b stands for dissipation function defined by Eq. 6. This elastic strain $\underline{\underline{c}}$ is related to the deformation rate tensor $\underline{\underline{D}}$ as follows

$$\overset{\circ}{\underline{\underline{c}}} - \underline{\underline{c}} \cdot \underline{\underline{D}} - \underline{\underline{D}} \cdot \underline{\underline{c}} + 2\underline{\underline{c}} \cdot \underline{\underline{e}}_p = 0 \quad (5)$$

where $\overset{\circ}{\underline{\underline{c}}}$ is the Jaumann (corotational) time derivative of the recoverable Finger strain tensor.

In this work, the Mooney potential (i.e. $n=0$ in Eq. 3), and the dissipation function b proposed in [59] (see Eq. 6) have been employed.

$$b(\underline{\underline{I}}_{1,c}) = \frac{1}{4\lambda} \left\{ \exp \left[-\xi \sqrt{\underline{\underline{I}}_{1,c} - 3} \right] + \frac{\sinh \left[\nu (\underline{\underline{I}}_{1,c} - 3) \right]}{\nu (\underline{\underline{I}}_{1,c} - 3) + 1} \right\} \quad (6)$$

Here, ξ and ν are adjustable model parameters.

2.3 Continuity and momentum conservation equations

The essential model equations in this section were transformed to the dimensionless form with the following convention and in accordance with the open literature [57]: the zero subscript and overbar sign denotes initial (at the die values) and dimensionless corresponding quantity, respectively. Then, the dimensionless component ii of the extra stress tensor $\bar{\tau}_{ii}$ writes

$$\bar{\tau}_{ii} = \frac{\tau_{ii} e_0 L_0}{F} \quad (7)$$

where F is drawing force exerted onto film, e_0 and L_0 is half-width and half-thickness of the film at the die, respectively.

Another set of dimensionless numbers is related to the film dimensions and velocities.

$$\bar{x} = \frac{x}{X}; \quad \bar{e} = \frac{e}{e_0}; \quad \bar{L} = \frac{L}{L_0}; \quad \bar{u} = \frac{u}{u_0} \quad (8)$$

Where, x is the actual axial position in air gap, X is the length of air gap and u is axial velocity of the film. Further dimensionless numbers express intensity of film drawing as draw ratio, DR , melt elasticity as Deborah number, De , basic geometry of the process as aspect ratio, A , and dimensionless drawing force as E .

$$DR = \frac{u(X)}{u_0}; \quad De = \frac{\lambda u_0}{X}; \quad A = \frac{X}{L_0}; \quad \frac{1}{E} = \frac{FX}{G\lambda e_0 L_0 u_0} \quad (9)$$

Here, melt relaxation time and elastic modulus, both at the die, is denoted as λ and G , respectively.

Then, the conservation of mass under the assumption of melt incompressibility in any position within the drawing distance must comply following formula

$$\bar{e}\bar{L}\bar{u} = 1 \quad (10)$$

Considering the membrane approximation for a thin film in the presence of a constant drawing force, the momentum conservation equation yields

$$(\bar{\tau}_{xx} - \bar{\tau}_{zz}) - \bar{u} = 0 \quad (11)$$

Making use of the kinematic free-surface and stress-free surface boundary condition, the unknown functions in Eq. 1. (i.e. $f(x)$ and $g(x)$) can be determined and the film width-stress relationship at given dimensionless axial position, \bar{x} , Eq. 12 deduced as

$$\frac{d\bar{L}}{d\bar{x}} = -A \sqrt{\frac{\bar{\tau}_{yy} - \bar{\tau}_{zz}}{\bar{\tau}_{xx} - \bar{\tau}_{zz}}} \quad (12)$$

Differentiating Eqs. 10 and 11 with respect to \bar{x} variable and after algebraic rearrangement, the derivative of the dimensionless film half-thickness with respect to \bar{x} leads to

$$\frac{d\bar{e}}{d\bar{x}} = -\left(\frac{1}{\bar{L}} \frac{d\bar{L}}{d\bar{x}} + \frac{1}{\bar{u}} \frac{d\bar{u}}{d\bar{x}}\right) \bar{e} \quad (13)$$

Utilization of Mooney potential in the modified Leonov model constitutive equation (i.e. when $n=0$ and $\beta \neq 0$ in Eq. 3), the relationship between the dimensionless stress and recoverable strain takes the following form

$$\bar{\tau}_{ii} = \frac{E}{De} c_{ii} - \frac{E}{De} c_{ii} \cdot \beta - \frac{E}{De} c_{ii}^{-1} \cdot \beta \quad (14)$$

To determine the diagonal components of the recoverable strain tensor, c_{ii} , and their derivatives with respect to \bar{x} , the membrane model and constitutive equations were linked together yielding following formulas

$$\frac{dc_{xx}}{d\bar{x}} = 2c_{xx} \frac{1}{\bar{u}} \frac{d\bar{u}}{d\bar{x}} - \frac{2\bar{b}}{\bar{u}} Z_x \quad (15)$$

$$\frac{dc_{yy}}{d\bar{x}} = 2c_{yy} \frac{1}{\bar{L}} \frac{d\bar{L}}{d\bar{x}} - \frac{2\bar{b}}{\bar{u}} Z_y \quad (16)$$

$$\frac{dc_{zz}}{d\bar{x}} = 2c_{zz} \frac{1}{\bar{e}} \frac{d\bar{e}}{d\bar{x}} - \frac{2\bar{b}}{\bar{u}} Z_z \quad (17)$$

where the dimensionless dissipation function, \bar{b} , and Z_i are defined as

$$\bar{b}(I_{1,c}) = \frac{1}{4De} \left\{ \exp \left[-\xi \sqrt{I_{1,c} - 3} \right] + \frac{\sinh \left[v(I_{1,c} - 3) \right]}{v(I_{1,c} - 3) + 1} \right\} \quad (18)$$

$$Z_i = c_{ii} \left[c_{ii} - c_{ii}^{-1} + \frac{1}{3} (c_{xx}^{-1} + c_{yy}^{-1} + c_{zz}^{-1} - c_{xx} - c_{yy} - c_{zz}) \right] \quad (19)$$

To complete the ensemble of equations, the express for dimensionless streamwise deformation rate is constituted by combination of Eqs. 10, 11 and 14 as follows

$$\frac{d\bar{u}}{d\bar{x}} = \frac{\bar{b} \left[\beta (Z_x - Z_z) - Z_x + Z_z \right] + \bar{b} \beta \left(\frac{1}{c_{zz}^2} Z_z - \frac{1}{c_{xx}^2} Z_x \right) + \frac{\bar{u}}{\bar{L}} \frac{d\bar{L}}{d\bar{x}} \left(c_{zz} (1 - \beta) + \frac{\beta}{c_{zz}} \right)}{\beta (c_{xx} + c_{zz}) - c_{xx} - c_{zz} - \frac{\beta}{c_{xx}} \left(\frac{c_{zz} + c_{xx}}{c_{zz}} \right) + \frac{De\bar{u}}{2E}} \quad (20)$$

Listed equations in this section, namely Eqs. 12, 13, 15, 16, 17 and 20, represent the basic isothermal viscoelastic 1.5D membrane model based on the constitutive equation of modified Leonov model and their more detail derivation can be found elsewhere [67]. In order to extend the model into a non-isothermal variant with capability to predict crystallization, the energy equation with an appropriate crystallization kinetics has to be incorporated as described in the following paragraph.

2.4 Energy Equation

The energy balance equation [14] takes the following form and accounts for the temperature change, crystallinity and flow dependency of melt viscosity.

$$\frac{dT}{dx} = \frac{2HTC(T_a - T)L}{C_p \dot{m}} + \frac{\Delta H}{C_p} \frac{dX_c}{dx} \quad (21)$$

where, the $L(x)$ is film half-width, HTC is heat transfer coefficient, C_p is specific heat capacity, \dot{m} is mass flow rate in quarter-cross-section, ΔH is latent heat of crystallization, $T(x)$ and T_a is melt and ambient air temperature, respectively, and finally $X_c(x)$ stands for content of

crystallinity in the polymer volume. Heat transfer coefficient was chosen to be a constant for current study as a simplification representing a total heat exchange with the surrounding environment. The temperature dependence of melt relaxation time, λ , is described by Arrhenius form with a constant activation energy E_a as follows

$$\lambda = \alpha_T \lambda_0 \quad (22)$$

$$\alpha_T = \exp \left[\frac{E_a}{R} \left(\frac{1}{T} - \frac{1}{T_r} \right) \right] \quad (23)$$

where λ_0 denotes melt relaxation time at the die exit, R is universal gas constant and T_r is reference melt temperature.

Crystallization kinetics

The crystallization kinetics model adopted in this study was originally drawn by Ziabicki [27, 28] and later modified by Lamberti [60]. The quiescent conditions are defined as

$$T_m = T_{mq}^0 \quad (24)$$

Since the flow induced crystallization is not included for the current study, the polymer melting temperature and flow induced equilibrium melting temperature are equal.

The volume fraction of crystallized phase, χ_c , and function $P(t)$ expressing the non-linear description of crystallinity evolution, derived according time as

$$\chi_c(t) = \frac{X_c(t)}{X_{eq}} = 1 - \exp \left\{ -[P(t)]^{n_c} \right\} \quad (25)$$

where $K(t)$ is crystallization kinetics constant representing crystallization rate, X_{eq} is the equilibrium volume content of crystallinity (maximum in a crystal phase that melt can possess) and constant n_c is of value 3 and thus nucleation is assumed as heterogeneous according to [28] with three dimensional crystal evolution. After differentiation with respect to time, the time-evolution formula is

$$\frac{dX_c(t)}{dt} = -X_{eq} \exp\left\{-[P(t)]^{n_c}\right\} \left\{-n[P(t)]^{n_c-1}\right\} \frac{dP(t)}{dt} \quad (26)$$

In the simplified form, the model kinetics proposed by Ziabicki [27, 28] and adopted in this work is as follows

$$K(t) = \frac{d}{dt} P(t) \quad (27)$$

$$K = K_{th} (1 + \dot{T}Z)^{1/n_c} \quad (28)$$

Here, K_{th} term is responsible for the low cooling rate crystallization, κ_1 , κ_2 and E_c are material parameters determined from isothermal test, R is universal gas constant and T_{mq}^0 denotes equilibrium crystallization temperature. B_{ath} and A_{ath} are material parameters included into the model by Lamberti considering cooling history and promoting model to be capable to describe a crystallinity evolution at high cooling rates. Fitting parameters, κ_1 , κ_2 , E_c , B_{ath} and A_{ath} , for material used in this work were determined in [60].

$$K_{th} = \kappa_1 \frac{T(T_m - T)}{(T_m)^2} \exp\left[-\frac{E_c}{RT}\right] \exp\left[-\kappa_2 \frac{(T_m)^2}{T(T_m - T)}\right] \quad (29)$$

Effect of cooling rate on crystallization kinetics constant is covered by non-isothermal function, Z , taking form of

$$Z = -B_{ath} |\dot{T}|^{A_{ath}} \frac{(T_m)^5}{T(T_m - T)^5} \exp\left[\frac{E_c}{RT}\right] \quad (30)$$

where, cooling rate is marked as \dot{T} , the derivative of the film temperature with respect to time, t .

The formula for the transition from time to spatial coordinates is following

$$\dot{T} = \frac{dT}{dt} = u \frac{dT}{dx} \quad (31)$$

After its application on Eq. 26 with dimensionless transformation introduced in previous section and some rearrangement, the final form of equation for the crystallinity evolution in dimensionless spatial coordinates demands

$$\frac{dX_c(\bar{x})}{d\bar{x}} = X_{eq} \exp\left\{-[P(\bar{x})]^{n_c}\right\} n_c [P(\bar{x})]^{n_c-1} \frac{dP(\bar{x})}{d\bar{x}} \frac{X}{\bar{u}u_0} \quad (32)$$

and semi-dimensionless form of energy equation, Eq. 21, is then given as

$$\frac{dT}{d\bar{x}} = \frac{2HTC(T_a - T)\bar{L}X}{C_p \dot{m}} + \frac{\Delta H}{C_p} \frac{dX_c}{d\bar{x}} \quad (33)$$

Effect of crystallinity on viscosity

Beside the effect of temperature on the melt relaxation time, the effect of crystallinity on viscosity is included into the model through the function μ_{X_c} that acts directly on the initial elastic modulus G_0 ; this approach was presented by Titomanlio in [68].

$$G = \mu_{X_c}(X_c)G_0 \quad (34)$$

This S-shaped function remains unity as the amount of crystallinity in volume is low and at the certain point starts to deviate and sharply raise simulating the phase transition from melt to the solid state:

$$\mu_{X_c}(X_c) = 1 + f \exp\left(-\frac{h}{X_c^m}\right) \quad (35)$$

It is worth to note that Eq. 11 is no more globally satisfied as in previous works where modulus G was taken as a constant [67, 69] and must be treated as follows

$$\int_0^{\bar{\tau}_{xx}(X)} d\bar{\tau}_{xx} - \int_0^{\bar{\tau}_{zz}(X)} d\bar{\tau}_{zz} - \int_0^{\bar{u}(X)} d\bar{u} = 0 \quad (36)$$

2.5 Boundary Conditions

Proposed model equations can be mathematically solved only if an appropriate boundary conditions for downstream, Eq. 37, and upstream region, Eq. 38, are defined.

$$\bar{u}(X) = DR \quad (37)$$

$$\bar{u}(0) = 1 \quad \bar{e}(0) = 1 \quad \bar{L}(0) = 1$$

$$\bar{\tau}_{xx}(0) \quad \bar{\tau}_{yy}(0) \quad \bar{\tau}_{zz}(0) \quad (38)$$

$$X_c(0) = 0 \quad T(0) = T_{DIE}$$

Regarding the downstream region, only the desired value of draw ratio must be prescribed that is satisfied by a priori unknown magnitude of the drawing force which is an object of search. In upstream area (i.e. extrusion die exit region), the count of required values is broader and includes the definition of axial velocity, die dimensions, that is gap size and width, which are equal to unity due its dimensionless expression, and melt temperature, and crystallinity that is assumed to be zero. Due to the employed viscoelastic constitutive equations, the stress state at the die have to be imposed, therefore the diagonal components of the extra stress tensor $\bar{\tau}_{xx}$, $\bar{\tau}_{yy}$ and $\bar{\tau}_{zz}$ are calculated through Eq. 14 utilizing c_{xx} , c_{yy} and c_{zz} components of the recoverable strain tensor satisfying the following set of equations

$$\frac{E}{De} \left[(c_{xx} - c_{zz})(1 - \beta) + \beta(c_{zz}^{-1} - c_{xx}^{-1}) \right] - 1 = 0 \quad (39)$$

$$c_{xx} c_{yy} c_{zz} = 1 \quad (40)$$

$$-\frac{N_2}{N_1} = \frac{E \left[c_{zz} - c_{yy} + \beta(c_{yy} + c_{yy}^{-1} - c_{zz} - c_{zz}^{-1}) \right]}{De\bar{u}} \quad (41)$$

where Eq. 39 arises from the momentum conservation equation (Eq. 11), Eq. 40 from the melt incompressibility assumption. Eq. 42 characterizes the polymer melt stress state at the die exit

region as the ratio of the secondary to primary normal stress difference, $-N_2/N_1$, and is calculated from the fully-developed slit flow at the extrusion die exit as follows

$$-\frac{N_2}{N_1} = -\frac{\bar{\tau}_{zz}(0) - \bar{\tau}_{yy}(0)}{\bar{\tau}_{xx}(0) - \bar{\tau}_{zz}(0)} \quad (42)$$

2.6 Numerical Scheme

To solve the full set of first-order ordinary differential equations, the numerical scheme based on the 4th order Runge-Kutta method implementing adaptive step-size control was adopted. Process of calculation is commenced by guessing a value of drawing force followed by iterative determination of the stress boundary condition via Eqs. 39–42. Then the main set of eight differential equation is solved in the following order: crystallization kinetics (Eq. 32), energy of equation (Eq. 33), film half-width (Eq. 12), axial velocity (Eq. 20), film half-thickness (Eq. 13) and components of the recoverable elastic strain tensor (Eqs. 15–17). Depending on wheatear the desired draw ratio is achieved, the initially estimated drawing force was iteratively updated (increased/decreased) for every following calculation until convergence (see Figure 2) using bisection method. Oscillations in temperature profile development, that were occasionally present in calculations causing the instability of computation, were fixed by applied stabilizing method of weighting the result of Eq. 33 for actual and previous position x . Due to a geometrical symmetry of the film, only 1/4th of the film cross-section was used in the calculation as showed in [70]. This basic computational scheme for the determination of unknown process variables was looped according demands of currently conducted parametric studies and eventually complemented by module for a grid linear interpolation to create parametric maps. The entire solver was developed in the C++ programming language and coupled with GNUPLOT plotting software for automatic graph generation. Typical computational time for one calculation of prescribed DR was about 1 minute on the PC with the following hardware

specifications: CPU: Intel Core i7-7700 at 3.60 GHz, RAM: 32 GB DDR4, GPU: AMD Radeon Pro WX 4100 with 4 GB of video memory, SSD: HP Z TurboDrive G2 512 GB.

3 RESULTS AND DISCUSSION

3.1 Model validation

Proposed non-isothermal film casting model has been tested for well characterized linear isotactic PP (for the basic characteristics see Table 1) and given processing conditions [8, 15]. All model parameters for given material and processing conditions are summarized in Table 2 and Table 3, respectively. In this work, single-mode modified Leonov model utilizing the lowest relaxation time, $\lambda=0.01$ s, which is typical for polyolefins [71, 72], was used. It was shown by Thete et al. [72] that utilization of lowest relaxation time in the cast film modeling can provide reasonable stress predictions in both, axial and transverse directions. Knowing Newtonian viscosity, $\eta_0=\lambda_0 \cdot G_0$, and relaxation time at $T=220^\circ\text{C}$, temperature independent modulus G was calculated to be 740,199 Pa. The crystallization kinetics parameters in the function given by Eq. 32 were set for given material according to [60], see Table 4. It was shown that the modulus increases significantly with the film crystallinity [14, 16, 73, 74], which can be taken into account during cast film modeling via Eq. 34. In this work, adjustable parameters of Eq. 35 were chosen according to Table 5 in order to predict significant modulus increase even at very low crystallinity levels, which seems to be reasonable [14, 16]. Due to the fact that tested iPP melt is linear, i.e., it shows extensional strain thinning, modified Leonov parameters ξ and ν , appearing in Eq. 6 for dissipation function, were adjusted to be equal to 0 and 0.5, respectively, whereas the parameter β in Eq. 3 was adjusted to be 0.5 (just between 0 and 1 meaning that first as well as second invariant of recoverable Finger tensor contributes equally to the elastic potential). Deborah number at the die exit is equal to $6 \cdot 10^{-4}$ for given material and processing conditions (i.e. much lower than 0.3), which means that there is no role of die exit stress state on the post die calculations as shown in our previous work [69]. Thus, the second to first normal stress ratio at the die exit was kept the same in all

calculations, $-\frac{N_2}{N_1} = 0.2$ according to [75]. The only free parameter in the presented model is heat transfer coefficient, HTC , appearing in energy equation, Eq. 33. This parameter is not a priori known and thus its value was adjusted $16 \text{ J}\cdot\text{s}^{-1}\cdot\text{K}^{-1}\cdot\text{m}^{-2}$ in order to capture experimentally determined temperature profile between die and chill roll. Comparison between proposed model predictions and experimental data for linear iPP and given processing conditions ($T_{DIE}=200^\circ\text{C}$, $De=6\cdot 10^{-4}$, $DR=34.7$, $X=0.4 \text{ m}$, $\dot{m}=1.26\cdot 10^{-4} \text{ kg}\cdot\text{s}^{-1}$) is provided in Figure 3. As it can be seen, model predictions for film half-width, axial velocity, temperature and crystallinity (especially at high draw distances) are in good agreement with the corresponding experimental data. The fact, that non-isothermal model is capable to describe experimental reality for linear iPP at given processing conditions justify to use the model in detailed parametric study.

3.2 Parametric study

3.2.1 *The role of heat transfer coefficient, draw and aspect ratio on the onset of crystalline phase in the produced film*

The key step in production of PP porous membranes is production of a precursor film with a row-nucleated lamellar structure [42], i.e. with shish-kebab crystalline phase created due to extensional flow in the post die area, which consists of an extended chain crystal (a “shish”) and folded chain crystals (“kebabs”) [76]. The processing window is thus rather narrow and detailed role of processing conditions on the development crystalline phase in the resulting film is still rather unclear. In this work, the processing window is defined as the conditions (given by aspect and draw ratios, T_{DIE} and draw ratio), during which produced film contains non-zero crystalline phase. Example is provided in Figure 4 for one fixed heat transfer coefficient value $2.5 \text{ J}\cdot\text{s}^{-1}\cdot\text{K}^{-1}\cdot\text{m}^{-2}$. Here, the area above the symbols (calculated by the numerical model) represents processing conditions leading to non-zero crystallinity whereas space below them

characterizes the region with no crystalline phase in the produced film. In this case, experimental process conditions used in the validation study are considered to be the reference. The predicted trend visualized in Figure 4 (i.e. that low draw ratios, which correspond to longer processing times, give rise to crystalline phase but high draw ratios do not because processing time is too short for crystallization) corresponds well with the experimental data provided in [77]. Note that numerical model predictions given by the symbols used in Figure 4 to determine process conditions for crystalline and no-crystalline phase development are entitled here as the “border symbols”.

In order to understand the role of process conditions on the onset of crystalline phase development in produced film, the following variables were systematically varied in particular ranges: aspect ratio (0.25–4), draw ratio (3–140), heat transfer coefficient ($1.5\text{--}28 \text{ J}\cdot\text{s}^{-1}\cdot\text{K}^{-1}\cdot\text{m}^{-2}$) and die exit melt temperature (200, 225 and 250°C). The chosen ranges correspond to typical values used in the real production of PP porous membranes [42, 47, 78, 79].

Numerical model predictions for “border symbols” at given range of processing conditions are visualized in Figures 5–7. As it can be seen, the processing window for production of film containing crystalline phase is enlarged if T_{DIE} decreases or HTC or A increases. This promotes to reach crystallization temperature in the film between the die and the chill roll. Interestingly, the relationship between A and DR defining “border symbols” for different T_{DIE} and HTC is linear. This suggests that all numerically predicted data visualized in Figure 5–7 as the symbols can be easily approximated by simple analytical equation.

3.2.2 Analytical approximation for critical crystallization border

The following simple analytical equation was chosen to approximate numerical solutions for determination of critical border contour in A vs. DR processing diagrams visualized in Figures 5–7 for different T_{DIE} and HTC .

$$A = \exp[q_{Xc}(HTC, T_{DIE})] DR^{k_{Xc}(HTC, T_{DIE})} \quad (43)$$

where $q_{Xc}(HTC, T_{DIE})$ and $k_{Xc}(HTC, T_{DIE})$ are given as

$$k_{Xc}(HTC, T_{DIE}) = (\gamma_k T_{DIE} + \delta_k) HTC^{(\alpha_k T_{DIE} + \beta_k)} \quad (44)$$

$$q_{Xc}(HTC, T_{DIE}) = (\alpha_q T_{DIE} + \beta_q) \ln(HTC) + (\gamma_q T_{DIE} + \delta_q) \quad (45)$$

These equations utilize 3 independent variables (DR , HTC and T_{DIE}) and 8 adjustable parameters ($\alpha_k, \beta_k, \gamma_k, \delta_k, \alpha_q, \beta_q, \gamma_q, \delta_q$). Analytical equation, Eq. 43, was used to simultaneously fit all numerically determined “border symbols” depicted in Figure 5–7 through last square minimization method and obtained optimum parameters are summarized in Table 6. As it can be seen in Figure 5–7, agreement between fitting lines and numerically obtained “border symbols” is very good. Thus, Eq. 43 together with its parameters can be considered as reliable approximation of true numerical solutions of “border symbols” for linear iPP at given range of processing conditions.

3.2.3 Determination of processing conditions, at which the Neck-in phenomenon starts to be influenced by heat transfer coefficients and crystallization

It was shown that during production of transparent flat films via cast film technology (i.e. at very high temperatures/draw ratios and very small die-roll distances, where no crystalline phase is developed) the neck in phenomenon (unwanted shrinkage of the film in the width direction) can be reliably predicted via isothermal simulations where the heat transfers and crystallization are neglected [67, 69]. It is obvious that there are processing conditions, for which isothermal simulations are too simplistic and therefore the neck-in phenomenon cannot be predicted realistically. Thus, the key question is “what are the processing conditions for linear iPP, at which heat transfer coefficients and crystallization starts to influence the neck-in phenomenon” ? In order to answer this question, DR , A and HTC were systematically varied in the proposed numerical model for the reference processing conditions at the lowest

investigated melt temperature at the die exit, for which the need to utilize non-isothermal calculation is the most probable. For all investigated processing conditions, both, isothermal as well as non-isothermal calculations have been performed. For each simulated case, neck-in value at the chill roll was evaluated. If differences between neck-in values obtained from isothermal and non-isothermal calculations were lower than 5 %, it was considered that neck-in predictions from isothermal calculations were reliable and non-isothermal effects can be viewed as negligible. For the processing conditions, in which differences in neck-in were higher than 5 %, it was considered that non-isothermal effects have to be included in the numerical simulations. Results of the performed parametric study are visualized in Figure 8. Here, the “isothermality boundary symbols” represent processing conditions, at which neck-in differences between isothermal and non-isothermal calculations were 5 % for given HTC value. The area below these symbols represents processing conditions for which isothermal calculations provide good estimate for the neck-in phenomenon whereas above these symbols, non-isothermal effects have to be taken into account to predict neck-in reliably. For the wide range of HTC , it was possible to approximate numerical solutions for “isothermality boundary symbols” via the following simple analytical equation

$$A = \exp[q_{iso}(HTC)]DR^{k_{iso}(HTC)} \quad (46)$$

where $k_{iso}(HTC)$ and $q_{iso}(HTC)$ are defined as

$$k_{iso}(HTC) = \alpha_{iso} \ln(HTC) + \beta_{iso} \quad (47)$$

$$q_{iso}(HTC) = \gamma_{iso} \ln(HTC) + \delta_{iso} \quad (48)$$

These equations utilize 2 independent variables (DR , HTC) and 4 adjustable parameters obtained by numerical data fitting (α_{iso} , β_{iso} , γ_{iso} , δ_{iso}), which are summarized in Table 7. As it

can be seen in Figure 8, Eq. 46 can approximate numerical solutions very well for the following range of variables: $DR \in \langle 3-140 \rangle$, $A \in \langle 0.25-4 \rangle$ and $HTC \in \langle 4-30 \rangle \text{ J}\cdot\text{s}^{-1}\cdot\text{K}^{-1}\cdot\text{m}^{-2}$.

3.2.4 Effect of A , DR , HTC , T_{DIE} on cast film process

In this part, A , DR , HTC , T_{DIE} were systematically varied in the numerical model considering the reference processing conditions ($HTC=16 \text{ J}\cdot\text{s}^{-1}\cdot\text{K}^{-1}\cdot\text{m}^{-2}$, $T_{DIE}=200^\circ\text{C}$, $DR=37.4$, $X=0.4 \text{ m}$) in order to understand their effect on the dimensionless film half-width and axial velocity, temperature and crystallinity; all as the function of dimensionless drawing distance.

In the first step, the aspect ratio, A , was varied from 0.01 up to 10 (via changing drawing distance) keeping another reference processing conditions fixed. Results are provided in Figure 9. From here, it is visible that if A increases, neck-in increases, axial velocity profile is changing from convex to concave shape, film temperature decreases and crystallinity increases.

In the second step, the draw ratio, DR , was changing from 3 to 140 (via step increase in take-up speed). Obtained numerical results are provided in Figure 10. Obviously, increase in DR leads to higher neck-in, axial film velocity, final film temperature and lower crystallinity.

In the third step, the heat transfer coefficient, HTC , was varied from 0 to $100 \text{ J}\cdot\text{s}^{-1}\cdot\text{K}^{-1}\cdot\text{m}^{-2}$. As it can be seen from Figure 11, increase in HTC causes reduction in neck-in, change of axial velocity profile from convex to concave shape as well as decrease in film temperature. There is interesting not fully intuitive relationship between HTC and film crystallinity. In more detail, there is range of $HTCs$ $0-3 \text{ J}\cdot\text{s}^{-1}\cdot\text{K}^{-1}\cdot\text{m}^{-2}$, for which the final film does not contain any crystalline phase. If the HTC increases above some critical value (in this case above $3 \text{ J}\cdot\text{s}^{-1}\cdot\text{K}^{-1}\cdot\text{m}^{-2}$), film crystallinity increases, reaching the maximum and then decreasing. This suggests that there exists optimum HTC for given material and processing conditions, at which the amount of crystalline phase is maximal.

In the final step, melt temperature at the die exit, T_{DIE} , was varied from 150 to 300°C. Obtained model predictions are visualized in Figure 12. Clearly, decrease in T_{DIE} increases neck-in and crystallinity whereas film temperature and axial velocity are reduced.

4 CONCLUSIONS

In this work, stable numerical scheme has been developed for 1.5D film casting model of Silagy et al. [57] utilizing viscoelastic modified Leonov model as the constitutive equation [58, 59] and energy equation coupled with crystallization kinetics of semicrystalline polymers taking into account actual temperature as well as temperature gradient [27, 28, 60]. Model has been successfully validated on the experimental data for linear isotactic polypropylene taken from the open literature [15].

Aspect ratio, A , (0.25–4), draw ratio, DR , (3–140), heat transfer coefficient, HTC , ($1.5–28 \text{ J}\cdot\text{s}^{-1}\cdot\text{K}^{-1}\cdot\text{m}^{-2}$) and die exit melt temperature, T_{DIE} , (200, 225 and 250°C) were systematically varied in the utilized model in order to understand the role of process conditions on the onset of crystalline phase development in production of iPP flat porous membranes via cast film process. It was found that numerically predicted critical crystallization border in A vs. DR dependence for given HTC and T_{DIE} can be successfully approximated by simple analytical equation.

Utilizing isothermal as well as non-isothermal numerical calculations, it was possible to determine processing conditions (in terms of DR , A and HTC at $T_{DIE}=200^\circ\text{C}$) for linear iPP, for which isothermal simulations are too simplistic and therefore the neck-in phenomena cannot be predicted realistically. It was possible to find out suitable analytical approximation for the “isothermality boundary” in A vs. DR dependence for different $HTCs$, which is applicable within the following range of processing variables: $DR \in \langle 3–140 \rangle$, $A \in \langle 0.25–4 \rangle$ and $HTC \in \langle 4–30 \rangle \text{ J}\cdot\text{s}^{-1}\cdot\text{K}^{-1}\cdot\text{m}^{-2}$.

Finally, the effect of A , DR , HTC and T_{DIE} on the dimensionless film half-width and axial velocity, temperature and crystallinity (all as the function of dimensionless drawing distance) was systematically investigated via non-isothermal simulations for linear iPP. It was found that neck-in can be reduced if A or DR decreases or if HTC or T_{DIE} increases. It has also been showed

that produced film crystallinity increases if A increases or if DR or T_{DIE} decreases. The most interestingly, it has been revealed that if the HTC increases above some critical value, film crystallinity increases, reaching the maximum and then decreasing. This suggests that there exists optimum HTC for given material and processing conditions, at which the amount of crystalline phase is maximal. It is believed that the utilized numerical model together with suggested stable numerical scheme as well as obtained research results can help to understand processing window for production of flat porous membranes from linear iPP considerably.

Acknowledgments

The authors wish to acknowledge the financial support from the Grant Agency of the Czech Republic (Grant registration No. 16-05886S).

5 LIST OF SYMBOLS

Latin Symbols	Meaning	Unit
A	Aspect ratio	1
A_{ath}	Fitting parameter in crystallization kinetics	1
B_{ath}	Fitting parameter in crystallization kinetics	s
b	Dissipation term	s^{-1}
\bar{b}	Dimensionless dissipation term	1
$\underline{\underline{c}}$	Recoverable Finger tensor	1
$\underline{\underline{c}}^{-1}$	Inverse recoverable Finger tensor	1
$\overset{0}{\underline{\underline{c}}}$	Jaumann (corotational) time derivative of the recoverable Finger strain tensor	s^{-1}
C_p	Specific heat capacity of polymer	$J \cdot kg^{-1} \cdot K^{-1}$
c_{xx}	Normal component of the recoverable Finger tensor in axial x-direction	1
c_{yy}	Normal component of the recoverable Finger tensor in transverse y-direction	1
c_{zz}	Normal component of the recoverable Finger tensor in thickness z-direction	1
$\underline{\underline{D}}$	Deformation rate tensor	s^{-1}
De	Deborah number	1
DR	Draw ratio	1
$\underline{\underline{e}}_p$	Irreversible rate of strain tensor	s^{-1}
E	Dimensionless take-up force	1
E_a	Flow activation energy	$J \cdot mol^{-1}$
E_c	Fitting parameter in crystallization kinetics	K

e	Half-thickness of the film at any x location	m
e_0	Die half-gap (half-thickness of the film at the die exit)	m
\bar{e}	Dimensionless half-thickness of the film at any x location	1
F	Take-up force (drawing force)	N
f, h, m	Parameters in function describing the effect of crystallinity on elastic modulus	1
$f(x)$	Rate of deformation in transverse y -direction	s^{-1}
G	Linear Hookean elastic modulus	Pa
G_0	Linear Hookean elastic modulus at the die exit	Pa
HTC	Heat transfer coefficient	$J \cdot s^{-1} \cdot K^{-1} \cdot m^{-2}$
$g(x)$	Rate of deformation in thickness z -direction	s^{-1}
i	Index i , noting the spatial direction	1
$I_{1,c}$	First invariant of recoverable Finger tensor	1
$I_{2,c}$	Second invariant of recoverable Finger tensor	1
$K(t)$	Crystallization kinetics function	s^{-1}
K_{th}	Isothermal function of crystallization kinetics	s^{-1}
k_{iso}	Slope function for determination of isothermal boundary	1
k_{xc}	Slope function for crystallization on-set	1
L	Half-width of the film at any x location	m
L_0	Half-width of the die (half-width of the film at the die exit)	m
\bar{L}	Dimensionless half-width of the film at any x location	1
MFR, \dot{m}	Mass flow rate	$kg \cdot h^{-1}$

M_n	Number average molar mass	$\text{g}\cdot\text{mol}^{-1}$
M_w	Mass average molar mass	$\text{g}\cdot\text{mol}^{-1}$
NI	Maximum attainable neck-in	m
N_1	First normal stress difference	Pa
N_2	Second normal stress difference	Pa
n	Non-linear Leonov model parameter	1
n_c	Type of crystallization growth	1
$P(t)$	Function of non-linear crystallinity evolution	1
q_{iso}	Intercept function for determination of isothermal boundary	1
q_{xc}	Intercept function for crystallization on-set	1
R	Gas constant	$\text{J}\cdot\text{K}^{-1}\cdot\text{mol}^{-1}$
\dot{T}	Rate of cooling	$^{\circ}\text{C}\cdot\text{s}^{-1}$
T_{DIE}	Melt temperature at the die	$^{\circ}\text{C}$
T_m	Melting temperature of polymer	$^{\circ}\text{C}$
T_{mq}^0	Flow induced equilibrium melting temperature	$^{\circ}\text{C}$
T	Melt temperature	$^{\circ}\text{C}$
T_r	Reference temperature in the Arrhenius law	$^{\circ}\text{C}$
u	Axial velocity component of the film at any x location	$\text{m}\cdot\text{s}^{-1}$
$u(X)$	Chill roll speed	$\text{m}\cdot\text{s}^{-1}$
u_0	Axial velocity component at the die exit	$\text{m}\cdot\text{s}^{-1}$
\bar{u}	Dimensionless axial velocity component of the film at any x location	1

v	Transverse velocity component of the film at any x location	$\text{m}\cdot\text{s}^{-1}$
W	Elastic potential	Pa
w	Thickness velocity component of the film at any x location	$\text{m}\cdot\text{s}^{-1}$
X	Take-up length (stretching distance, air gap)	m
x	Position in axial x -direction	m
\bar{x}	Dimensionless position in axial x -direction	1
x, y, z	Spatial coordinates in axial, transverse and thickness direction, respectively	1
X_c	Crystallinity content in the polymer volume	1
X_{eq}	Equilibrium level of crystallinity in the polymer volume	1
Z	Non-isothermal function of crystallization kinetics	1
Z_x, Z_y, Z_z	Substitution variables	1
$\frac{dc_{xx}}{d\bar{x}}, \frac{dc_{yy}}{d\bar{x}}, \frac{dc_{zz}}{d\bar{x}}$	Derivative of Finger tensor components with respect to dimensionless \bar{x} position	1
$\frac{d\bar{u}}{d\bar{x}}, \frac{d\bar{L}}{d\bar{x}}, \frac{d\bar{e}}{d\bar{x}}$	Derivative of dimensionless axial velocity, width and thickness with respect to dimensionless \bar{x} position	1
$\frac{dX_c}{d\bar{x}}$	Derivative of crystallinity with respect to dimensionless \bar{x} position	1
$\frac{dT}{d\bar{x}}$	Derivative of temperature with respect to dimensionless \bar{x} position	$^{\circ}\text{C}$
Greek Symbols	Meaning	Unit
$\alpha_{iso}, \beta_{iso}, \gamma_{iso}, \delta_{iso}$	Fitting parameters in isothermal boundary function	1

$\alpha_k, \beta_k, \gamma_k, \delta_k,$ $\alpha_q, \beta_q, \gamma_q, \delta_q$	Fitting parameters in crystallization on-set function	1
α_T	Arrhenius law parameter	1
β	Non-linear Leonov model parameter	1
ΔH	Crystallization latent heat	$\text{kJ}\cdot\text{kg}^{-1}$
$\underline{\underline{\delta}}$	Unit tensor (Kronecker delta)	1
η_0	Newtonian viscosity	$\text{Pa}\cdot\text{s}$
κ_1	Fitting parameter in crystallization kinetics	s^{-1}
κ_2	Fitting parameter in crystallization kinetics	1
λ	Melt relaxation time	s
λ_0	Melt relaxation time at the die exit	s
μ_{x_c}	Effect of crystallinity on elastic modulus function	1
ν	Non-linear Leonov model parameter	1
ξ	Non-linear Leonov model parameter	1
ρ_P	Polymer density	$\text{kg}\cdot\text{m}^{-3}$
$\underline{\underline{\tau}}$	Extra stress tensor	Pa
τ_{xx}	Normal stress in axial x-direction	Pa
τ_{yy}	Normal stress in transverse y-direction	Pa
τ_{zz}	Normal stress in thickness z-direction	Pa
$\bar{\tau}_{xx}$	Dimensionless normal stress in axial x-direction	1
$\bar{\tau}_{yy}$	Dimensionless normal stress in transverse y-direction	1
$\bar{\tau}_{zz}$	Dimensionless normal stress in thickness z-direction	1
χ_c	Volume fraction of crystallized phase	1

6 REFERENCES

- [1] COTTO, D., DUFFO, P. and HAUDIN, J.M. Cast film extrusion of polypropylene films. *Int. Polym. Process.* 1989. Vol. 4, no. 2, p. 103–113.
- [2] DUFFO, P., MONASSE, B. and HAUDIN, J.M. Cast film extrusion of polypropylene. Thermomechanical and physical aspects. *Journal of Polymer Engineering.* 1991. Vol. 10, no. 1–3, p. 151–229.
- [3] BARQ, P., HAUDIN, J.M. and AGASSANT, Jean François. Isothermal and anisothermal models for cast film extrusion. *Int. Polym. Process.* 1992. Vol. 7, no. 4, p. 334–349.
- [4] BOURRIGAUD, S., MARIN, G., DABAS, V., DUPUY, C. and SILAGY, D. The draw ratio–Deborah number diagram: A useful tool for coating applications. *Polymer Engineering & Science.* 2006. Vol. 46, no. 3, p. 372–380.
- [5] ACIERNO, D., DI MAIO, L. and AMMIRATI, C. C. Film casting of polyethylene terephthalate: Experiments and model comparisons. *Polymer Engineering and Science.* 2000. Vol. 40, no. 1, p. 108–117.
- [6] COPPOLA, Salvatore, BALZANO, Luigi, GIOFFREDI, Emilia, MAFFETTONE, Pier Luca and GRIZZUTI, Nino. Effects of the degree of undercooling on flow induced crystallization in polymer melts. *Polymer.* 2004. Vol. 45, no. 10, p. 3249–3256.
- [7] LAMBERTI, Gaetano, TITOMANLIO, Giuseppe and BRUCATO, Valerio. Measurement and modelling of the film casting process 2. Temperature distribution along draw direction. *Chemical Engineering Science.* 2002. Vol. 57, no. 11, p. 1993–1996.
- [8] LAMBERTI, Gaetano, BRUCATO, Valerio and TITOMANLIO, Giuseppe. Orientation and crystallinity in film casting of polypropylene. *Journal of Applied Polymer Science.* 2002. Vol. 84, no. 11, p. 1981–1992.
- [9] LAMBERTI, Gaetano and BRUCATO, Valerio. Real-time orientation and crystallinity measurements during the isotactic polypropylene film-casting process. *Journal of Polymer Science Part B: Polymer Physics.* 2003. Vol. 41, no. 9, p. 998–1008.
- [10] LAMBERTI, Gaetano, LA CARRUBBA, Vincenzo, PICCAROLO, Stefano and BRUCATO, Valerio. Orientation and Crystallinity Measurements in Film Casting Products. *Polymer Bulletin.* 2003. Vol. 50, no. 5–6, p. 413–420.
- [11] TITOMANLIO, Giuseppe and LAMBERTI, Gaetano. Modeling flow induced crystallization in film casting of polypropylene. *Rheologica Acta.* 2004. Vol. 43, no. 2, p. 146–158.
- [12] LAMBERTI, Gaetano and DE SANTIS, Felice. Heat transfer and crystallization kinetics during fast cooling of thin polymer films. *Heat and Mass Transfer.* 2006. Vol. 43, no. 11, p. 1143–1150.
- [13] LAMBERTI, Gaetano and TITOMANLIO, Giuseppe. Analysis of Film Casting Process : Effect of Cooling during the Path in Air. *Industrial & Engineering Chemistry Research.* 2006. Vol. 45, no. 2, p. 719–723.
- [14] LAMBERTI, Gaetano, TITOMANLIO, Giuseppe and BRUCATO, Valerio. Measurement and modelling of the film casting process 1. Width distribution along draw direction. *Chemical Engineering Science.* 2001. Vol. 56, no. 20, p. 5749–5761.

- [15] LAMBERTI, Gaetano and TITOMANLIO, Giuseppe. Evidences of flow induced crystallization during characterized film casting experiments. *Macromolecular Symposia*. 2002. Vol. 185, no. 1, p. 167–180.
- [16] LAMBERTI, Gaetano and TITOMANLIO, Giuseppe. Analysis of film casting process: The heat transfer phenomena. *Chemical Engineering and Processing: Process Intensification*. 2005. Vol. 44, no. 10, p. 1117–1122.
- [17] LAMBERTI, Gaetano. Flow-induced crystallization during isotactic polypropylene film casting. *Polymer Engineering and Science*. 2011. Vol. 51, no. 5, p. 851–861.
- [18] KOLMOGOROFF, A. N. On the statistics of crystallization processes in metals. *Isvest. Akad. Nauk SSSR Ser. Math.* 1937. Vol. 1, p. 335.
- [19] AVRAMI, M. Kinetics of phase change. II Transformation-time relations for random distribution of nuclei. *The Journal of Chemical Physics*. 1940. Vol. 8, no. 2, p. 212–224.
- [20] EVANS, U.R. The laws of expanding circles and spheres in relation to the lateral growth of surface films and the grain-size of metals. *Transactions of the Faraday Society*. 1945. Vol. 41, p. 365–374.
- [21] KOLMOGOROV, A. N. On the Statistical Theory of Crystallization of Metals [in Russian]. *Izv. Akad. Nauk SSSR, Ser. Mat.* 1937. Vol. 3, p. 355–359.
- [22] AVRAMI, Melvin. Kinetics of Phase Change. I General Theory. *The Journal of Chemical Physics*. 1939. Vol. 7, no. 12, p. 1103–1112.
- [23] AVRAMI, Melvin. Granulation, Phase Change, and Microstructure Kinetics of Phase Change. III. *The Journal of Chemical Physics*. 1941. Vol. 9, no. 2, p. 177–184.
- [24] NAKAMURA, K., WATANABE, T., KATAYAMA, K. and AMANO, T. Some aspects of nonisothermal crystallization of polymers. I. Relationship between crystallization temperature, crystallinity, and cooling conditions. *Journal of Applied Polymer Science*. 1972. Vol. 16, no. 5, p. 1077–1091.
- [25] NAKAMURA, K., KATAYAMA, K. and AMANO, T. Some aspects of nonisothermal crystallization of polymers. II. Consideration of the isokinetic condition. *Journal of Applied Polymer Science*. 1973. Vol. 17, no. 4, p. 1031–1041.
- [26] OZAWA, T. Kinetics of non-isothermal crystallization. *Polymer*. 1971. Vol. 12, no. 3, p. 150–158.
- [27] ZIABICKI, A. Crystallization of polymers in variable external conditions. 1. General equations. *Colloid and Polymer Science*. 1996. Vol. 274, no. 3, p. 209–217.
- [28] ZIABICKI, A. Crystallization of polymers in variable external conditions. II. Effects of cooling in the absence of stress and orientation. *Colloid and Polymer Science*. 1996. Vol. 274, no. 8, p. 705–716.
- [29] BRUCATO, V., CRIPPA, G., PICCAROLO, S. and TITOMANLIO, G. Crystallization of polymer melts under fast cooling. I: Nucleated polyamide 6. *Polymer Engineering & Science*. 1991. Vol. 31, no. 19, p. 1411–1416.
- [30] PICCAROLO, S., SAIU, M., BRUCATO, V. and TITOMANLIO, G. Crystallization of polymer melts under fast cooling. II. High-purity iPP. *Journal of Applied Polymer Science*. 1992. Vol. 46, no. 4, p. 625–634.

- [31] MATHOT, Vincent, PYDA, Marek, PIJERS, Thijs, VANDEN POEL, Geert, VAN DE KERKHOFF, Ernst, VAN HERWAARDEN, Sander, VAN HERWAARDEN, Floor and LEENAERS, Archi. The Flash DSC 1, a power compensation twin-type, chip-based fast scanning calorimeter (FSC): First findings on polymers. *Thermochimica Acta*. 2011. Vol. 522, no. 1–2, p. 36–45.
- [32] SADEGHI, F., AJJI, A. and CARREAU, P.J. Study of polypropylene morphology obtained from blown and cast film processes: Initial morphology requirements for making porous membrane by stretching. *Journal of Plastic Film and Sheeting*. 2005. Vol. 21, no. 3, p. 199–216.
- [33] ARORA, Pankaj and ZHANG, Zhengming (John). Battery Separators. *Chemical Reviews*. 2004. Vol. 104, no. 10, p. 4419–4462.
- [34] BAKER, Richard W. *Membrane Technology and Applications*. 2nd ed. West Sussex, UK : John Wiley & Sons, Ltd., 2004. ISBN 9780470854457.
- [35] ZHANG, Sheng Shui. A review on the separators of liquid electrolyte Li-ion batteries. *Journal of Power Sources*. 2007. Vol. 164, no. 1, p. 351–364.
- [36] DE ROSA, Claudio, AURIEMMA, Finizia, VOLLARO, Paolo, RESCONI, Luigi, GUIDOTTI, Simona and CAMURATI, Isabella. Crystallization Behavior of Propylene–Butene Copolymers: The Trigonal Form of Isotactic Polypropylene and Form I of Isotactic Poly(1-butene). *Macromolecules*. 2011. Vol. 44, no. 3, p. 540–549.
- [37] LOTZ, Bernard. A New ϵ Crystal Modification Found in Stereodeficient Isotactic Polypropylene Samples. *Macromolecules*. 2014. Vol. 47, no. 21, p. 7612–7624.
- [38] ANDROSCH, René, DI LORENZO, Maria Laura, SCHICK, Christoph and WUNDERLICH, Bernhard. Mesophases in polyethylene, polypropylene, and poly(1-butene). *Polymer*. 2010. Vol. 51, no. 21, p. 4639–4662.
- [39] SADEGHI, Farhad, AJJI, Abdellah and CARREAU, Pierre J. Analysis of microporous membranes obtained from polypropylene films by stretching. *Journal of Membrane Science*. 2007. Vol. 292, no. 1–2, p. 62–71.
- [40] CAIHONG, Lei, SHUQIU, Wu, QI, Cai, RUIJIE, Xu, BING, Hu and WENQIANG, Shi. Influence of heat-setting temperature on the properties of a stretched polypropylene microporous membrane. *Polymer International*. 2013. Vol. 63, no. 3, p. 584–588.
- [41] SADEGHI, Farhad, AJJI, Abdellah and CARREAU, Pierre J. Analysis of row nucleated lamellar morphology of polypropylene obtained from the cast film process: Effect of melt rheology and process conditions. *Polymer Engineering & Science*. 2007. Vol. 47, no. 7, p. 1170–1178.
- [42] CASTEJÓN, Pilar, HABIBI, Kian, SAFFAR, Amir, AJJI, Abdellah, MARTÍNEZ, Antonio B and ARENCÓN, David. Polypropylene-Based Porous Membranes: Influence of Polymer Composition, Extrusion Draw Ratio and Uniaxial Strain. *Polymers*. 2018. Vol. 10, no. 1, p. 33.
- [43] SADEGHI, Farhad, AJJI, Abdellah and CARREAU, Pierre J. Microporous membranes obtained from polypropylene blends with superior permeability properties. *Journal of Polymer Science Part B: Polymer Physics*. 2008. Vol. 46, no. 2, p. 148–157.
- [44] SOMANI, Rajesh H., YANG, Ling and HSIAO, Benjamin S. Effects of high molecular weight species on shear-induced orientation and crystallization of isotactic polypropylene. *Polymer*. 2006. Vol. 47, no. 15, p. 5657–5668.

- [45] TABATABAEI, Seyed H., CARREAU, Pierre J. and AJJI, Abdellah. Microporous membranes obtained from polypropylene blend films by stretching. *Journal of Membrane Science*. 2008. Vol. 325, no. 2, p. 772–782.
- [46] TABATABAEI, Seyed H., CARREAU, Pierre J. and AJJI, Abdellah. Effect of processing on the crystalline orientation, morphology, and mechanical properties of polypropylene cast films and microporous membrane formation. *Polymer*. 2009. Vol. 50, no. 17, p. 4228–4240.
- [47] XU, Meng, ZHANG, Shijun, LIANG, Jieying, QUAN, Hui, LIU, Jianye, SHI, Hongwei, GAO, Dali and LIU, Jie. Influences of processing on the phase transition and crystallization of polypropylene cast films. *Journal of Applied Polymer Science*. 2014. Vol. 131, no. 22, p. 41100.
- [48] DOUFAS, Antonios K., MCHUGH, Anthony J. and MILLER, Chester. Simulation of melt spinning including flow-induced crystallization Part I. Model development and predictions. *Journal of Non-Newtonian Fluid Mechanics*. 2000. Vol. 92, no. 1, p. 27–66.
- [49] DOUFAS, Antonios K., MCHUGH, Anthony J., MILLER, Chester and IMMANENI, Aravind. Simulation of melt spinning including flow-induced crystallization Part II. Quantitative comparisons with industrial spinline data. *Journal of Non-Newtonian Fluid Mechanics*. 2000. Vol. 92, no. 1, p. 81–103.
- [50] DOUFAS, Antonios K. and MCHUGH, Anthony J. Simulation of melt spinning including flow-induced crystallization. Part III. Quantitative comparisons with PET spinline data. *Journal of Rheology*. 2001. Vol. 45, no. 2, p. 403.
- [51] DOUFAS, Antonios K., MCHUGH, Anthony J. and MILLER, Chester. Simulation of melt spinning including flow-induced crystallization. *Journal of Non-Newtonian Fluid Mechanics*. 2000. Vol. 92, no. 1, p. 27–66.
- [52] DOUFAS, Antonios K. and MCHUGH, Anthony J. Two-dimensional simulation of melt spinning with a microstructural model for flow-induced crystallization. *Journal of Rheology*. 2001. Vol. 45, no. 4, p. 855.
- [53] LEE, Joo Sung, SHIN, Dong Myeong, JUNG, Hyun Wook and HYUN, Jae Chun. Transient solutions of the dynamics in low-speed fiber spinning process accompanied by flow-induced crystallization. *Journal of Non-Newtonian Fluid Mechanics*. 2005. Vol. 130, no. 2–3, p. 110–116.
- [54] SHIN, Dong Myeong, LEE, Joo Sung, JUNG, Hyun Wook and HYUN, Jae Chun. High-speed fiber spinning process with spinline flow-induced crystallization and neck-like deformation. *Rheologica Acta*. 2006. Vol. 45, no. 5, p. 575–582.
- [55] KOHLER, William H. and MCHUGH, Anthony J. Sensitivity analysis of low-speed melt spinning of isotactic polypropylene. *Chemical Engineering Science*. 2007. Vol. 62, no. 10, p. 2690–2697.
- [56] KOHLER, William H. and MCHUGH, Anthony J. Prediction of the influence of flow-enhanced crystallization on the dynamics of fiber spinning. *Polymer Engineering & Science*. 2008. Vol. 48, no. 1, p. 88–96.
- [57] SILAGY, David, DEMAY, Yves and AGASSANT, Jean François. Study of the stability of the film casting process. *Polymer Engineering and Science*. 1996. Vol. 36, no. 21, p. 2614–2625.

- [58] LEONOV, A.I. Nonequilibrium thermodynamics and rheology of viscoelastic polymer media. *Rheologica Acta*. 1976. Vol. 15, no. 2, p. 85–98.
- [59] ZATLOUKAL, Martin. Differential viscoelastic constitutive equations for polymer melts in steady shear and elongational flows. *Journal of Non-Newtonian Fluid Mechanics*. 2003. Vol. 113, no. 2–3, p. 209–227.
- [60] LAMBERTI, Gaetano and TITOMANLIO, Giuseppe. Crystallization kinetics of iPP. Model and experiments. *Polymer Bulletin*. 2001. Vol. 46, no. 2–3, p. 231–238.
- [61] NARAYANASWAMY, O.S. A one-dimensional model of stretching float glass. *Journal of the American Ceramic Society*. 1977. Vol. 60, no. 1–2, p. 1–5.
- [62] LEONOV, A.I., LIPKINA, E.H., PASKHIN, E.D. and PROKUNIN, A.N. Theoretical and experimental investigation of shearing in elastic polymer liquids. *Rheologica Acta*. 1976. Vol. 15, no. 7, p. 411–426.
- [63] LEONOV, A.I. and PROKUNIN, A.N. An improved simple version of a nonlinear theory of elasto-viscous polymer media. *Rheologica Acta*. 1980. Vol. 19, no. 4, p. 393–403.
- [64] LEONOV, A.I. and PROKUNIN, A.N. On nonlinear effects in the extensional flow of polymeric liquids. *Rheologica Acta*. 1983. Vol. 22, no. 2, p. 137–150.
- [65] SIMHAMBHATLA, Murthy and LEONOV, Arkadii I. On the rheological modeling of viscoelastic polymer liquids with stable constitutive equations. *Rheologica Acta*. 1995. Vol. 34, no. 3, p. 259–273.
- [66] LEONOV, A.I. Constitutive equations for viscoelastic liquids: Formulation, analysis and comparison with data. *Rheology Series*. 1999. Vol. 8, no. C, p. 519–575.
- [67] BARBORIK, Tomas, ZATLOUKAL, M. and TZOGANAKIS, C. On the role of extensional rheology and Deborah number on the neck-in phenomenon during flat film casting. *International Journal of Heat and Mass Transfer*. 2017. Vol. 111, p. 1296–1313.
- [68] TITOMANLIO, G., SPERANZA, V. and BRUCATO, V. On the simulation of thermoplastic injection moulding process: II Relevance of interaction between flow and crystallization. *International Polymer Processing*. 1997. Vol. 12, no. 1, p. 45–53.
- [69] BARBORIK, Tomas and ZATLOUKAL, Martin. Effect of die exit stress state, Deborah number, uniaxial and planar extensional rheology on the neck-in phenomenon in polymeric flat film production. *Journal of Non-Newtonian Fluid Mechanics*. 2018. Vol. 255, p. 39–56.
- [70] BEAULNE, M. and MITSOULIS, Evan. Numerical Simulation of the Film Casting Process. *International Polymer Processing*. 1999. Vol. 14, no. 3, p. 261–275.
- [71] PIVOKONSKY, R., ZATLOUKAL, M., FILIP, P. and TZOGANAKIS, C. Rheological characterization and modeling of linear and branched metallocene polypropylenes prepared by reactive processing. *Journal of Non-Newtonian Fluid Mechanics*. 2009. Vol. 156, no. 1–2, p. 1–6.
- [72] THETE, Sumeet S., DOSHI, P. and POL, H.V. New insights into the use of multi-mode phenomenological constitutive equations to model extrusion film casting process. *Journal of Plastic Film and Sheeting*. 2017. Vol. 33, no. 1, p. 35–71.
- [73] PANTANI, R., SPERANZA, V. and TITOMANLIO, G. Simultaneous morphological and rheological measurements on polypropylene: Effect of crystallinity on viscoelastic parameters. *Journal of Rheology*. 2015. Vol. 59, no. 2, p. 377–390.

- [74] PANTANI, R., COCCORULLO, I., SPERANZA, V. and TITOMANLIO, G. Modeling of morphology evolution in the injection molding process of thermoplastic polymers. *Progress in Polymer Science*. 2005. Vol. 30, no. 12, p. 1185–1222.
- [75] JENSEN, E.A. and CHRISTIANSEN, J.deC. Measurements of first and second normal stress differences in a polymer melt. *Journal of Non-Newtonian Fluid Mechanics*. 2008. Vol. 148, no. 1–3, p. 41–46.
- [76] NAGASAWA, Toshio and SHIMOMURA, Yasushi. Mechanism of formation of shish kebab structures. *Journal of Polymer Science: Polymer Physics Edition*. 1974. Vol. 12, no. 11, p. 2291–2308.
- [77] ZHOU, Ying-Guo, WU, Wen-Bin and TURNG, JUN ZOU, Lih-Sheng. Dual-scale modeling and simulation of film casting of isotactic polypropylene. *Journal of Plastic Film and Sheeting*. 2015. Vol. Print.
- [78] WU, Shuqiu, LEI, Caihong, CAI, Qi, XU, Ruijie, HU, Bing, SHI, Wenqiang and PENG, Xinlong. Study of structure and properties of polypropylene microporous membrane by hot stretching. *Polymer Bulletin*. 2014. Vol. 71, no. 9, p. 2205–2217.
- [79] XIANDE, Chen, RUIJIE, Xu, JIAYI, Xie, YUANFEI, Lin, CAIHONG, Lei and LIANGBIN, Li. The study of room-temperature stretching of annealed polypropylene cast film with row-nucleated crystalline structure. *Polymer*. 2016. Vol. 94, p. 31–42.
- [80] POL, H.V., BANIK, Sourya, AZAD, Lal Busher, THETE, Sumeet S., DOSHI, Pankaj and LELE, Ashish. Nonisothermal analysis of extrusion film casting process using molecular constitutive equations. *Rheologica Acta*. 2014. Vol. 53, no. 1, p. 85–101.
- [81] ARROYO, M., LOPEZ-MANCHADO, M.A. and AVALOS, F. Crystallization kinetics of polypropylene: II. Effect of the addition of short glass fibres. *Polymer*. 1997. Vol. 38, no. 22, p. 5587–5593.

7 TABLES

Table 1. Basic characteristics for iPP T30G [8, 16, 17].

M_n ($\text{g}\cdot\text{mol}^{-1}$)	M_w ($\text{g}\cdot\text{mol}^{-1}$)	PDI (1)	$\eta_0^{###}$ at 220°C ($\text{Pa}\cdot\text{s}$)	Tacticity (m \overline{m} m)	E_a ($\text{kJ}\cdot\text{mol}^{-1}$)	$C_p^\#$ ($\text{J}\cdot\text{Kg}^{-1}\cdot\text{K}^{-1}$)	$\rho_r^\#$ ($\text{kg}\cdot\text{m}^{-3}$)	$\Delta H^{##}$ ($\text{kJ}\cdot\text{kg}^{-1}$)
75,000	481,000	6.4	7,402	87.6%	40.092	2,200	920	209

– Value taken from [80] as typical value for polyolefins.

– Value of crystallization latent heat taken from [81] as value for fully crystalline PP.

– Acquired by data digitalization technique from Figure 1 in [8].

Table 2. Modified Leonov model parameters for iPP T30G at $T_r=220^\circ\text{C}$.

λ (s)	G (Pa)	ξ (1)	ν (1)	β (1)
0.01	740,199	0	0.5	0.5

Table 3. Summarization of processing conditions for iPP T30G taken from [15].

Ω (rpm)	MFR ($10^{-4}\text{ kg}\cdot\text{s}^{-1}$)	u_0 ($10^{-3}\text{ m}\cdot\text{s}^{-1}$)	$u(X)$ ($10^{-3}\text{ m}\cdot\text{s}^{-1}$)	X (m)	T_{DIE} (°C)	$2L_0$ (m)	$2e_0$ (10^{-4} m)	DR (1)
20	1.26	1.68	58.3	0.4	200	0.2	5	34.7

Ambient temperature, T_a , was kept at 23°C for all numerical studies.

Table 4. Crystallization kinetics parameters for iPP T30G taken from [60].

X_{eq} (1)	n_c (1)	T_{mq}^0 (K)	E_c/R (K)	κ_1 (10^{69} s^{-1})	κ_2 (1)	A_{ath} (1)	B_{ath} (10^{-57} s)
0.61	3	463.15	45,570	2.778	5.871	1.7721	3.448

Table 5. Parameters used in Eq. 35 describing effect of crystallinity on elastic modulus G .

$f^\#$ (1)	h (1)	$m^\#$ (1)
2,000	10^{-5}	1.2

– Value was taken from [8].

Table 6. Parameters used in Eq. 43.

α_k (1)	β_k (1)	γ_k (1)	δ_k (1)	α_q (1)	β_q (1)	γ_q (1)	δ_q (1)
-0.0056	0.3421	0.0077	-1.2102	0.0001	-1.0453	0.0089	-0.3079

Table 7. Parameters used in Eq. 46.

$\alpha_{\text{iso}} (1)$	$\beta_{\text{iso}} (1)$	$\gamma_{\text{iso}} (1)$	$\delta_{\text{iso}} (1)$
0.067	0.0406	-0.8479	0.9701

8 FIGURES

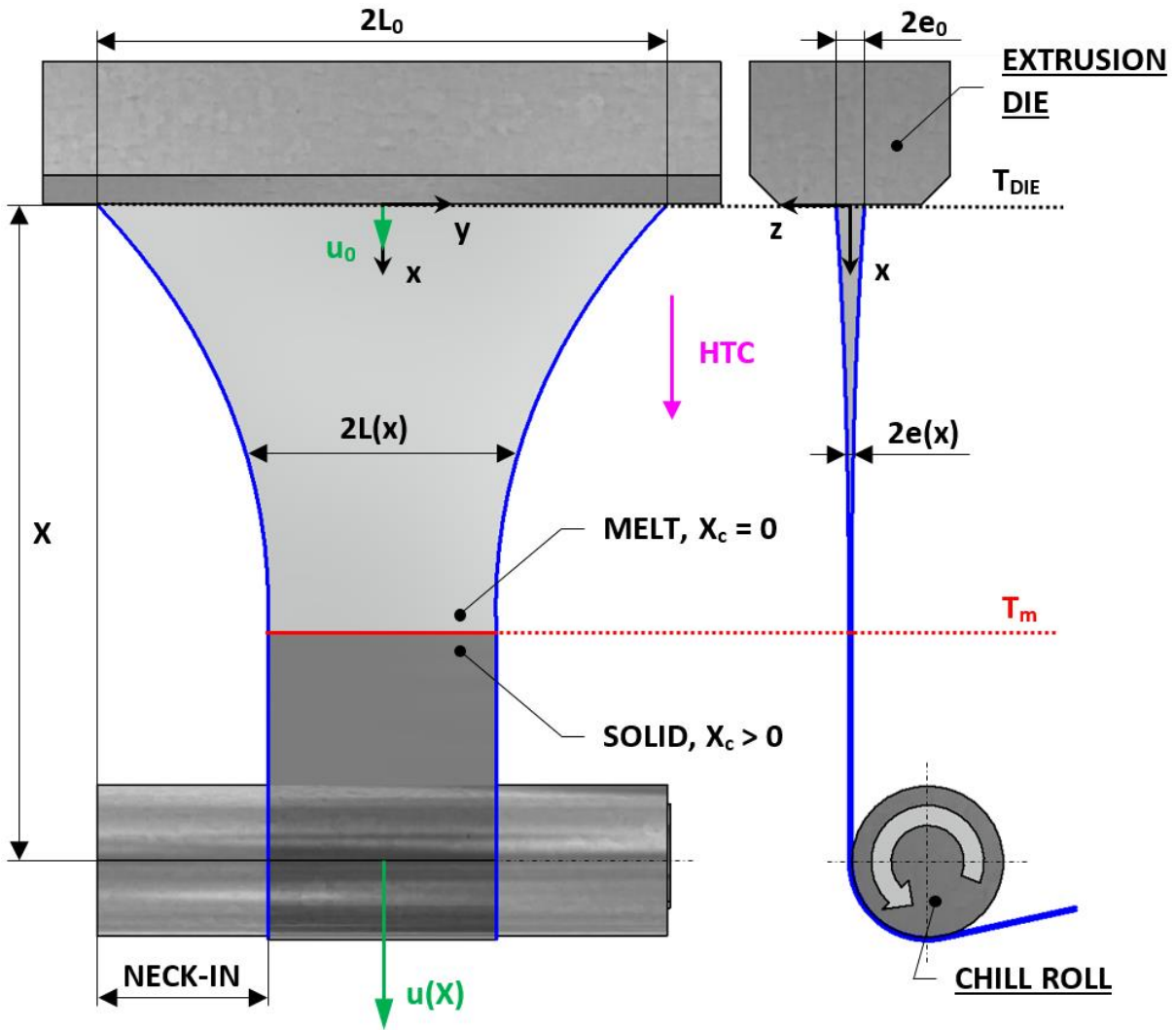


Figure 1. Schematic illustration of extrusion film casting process.

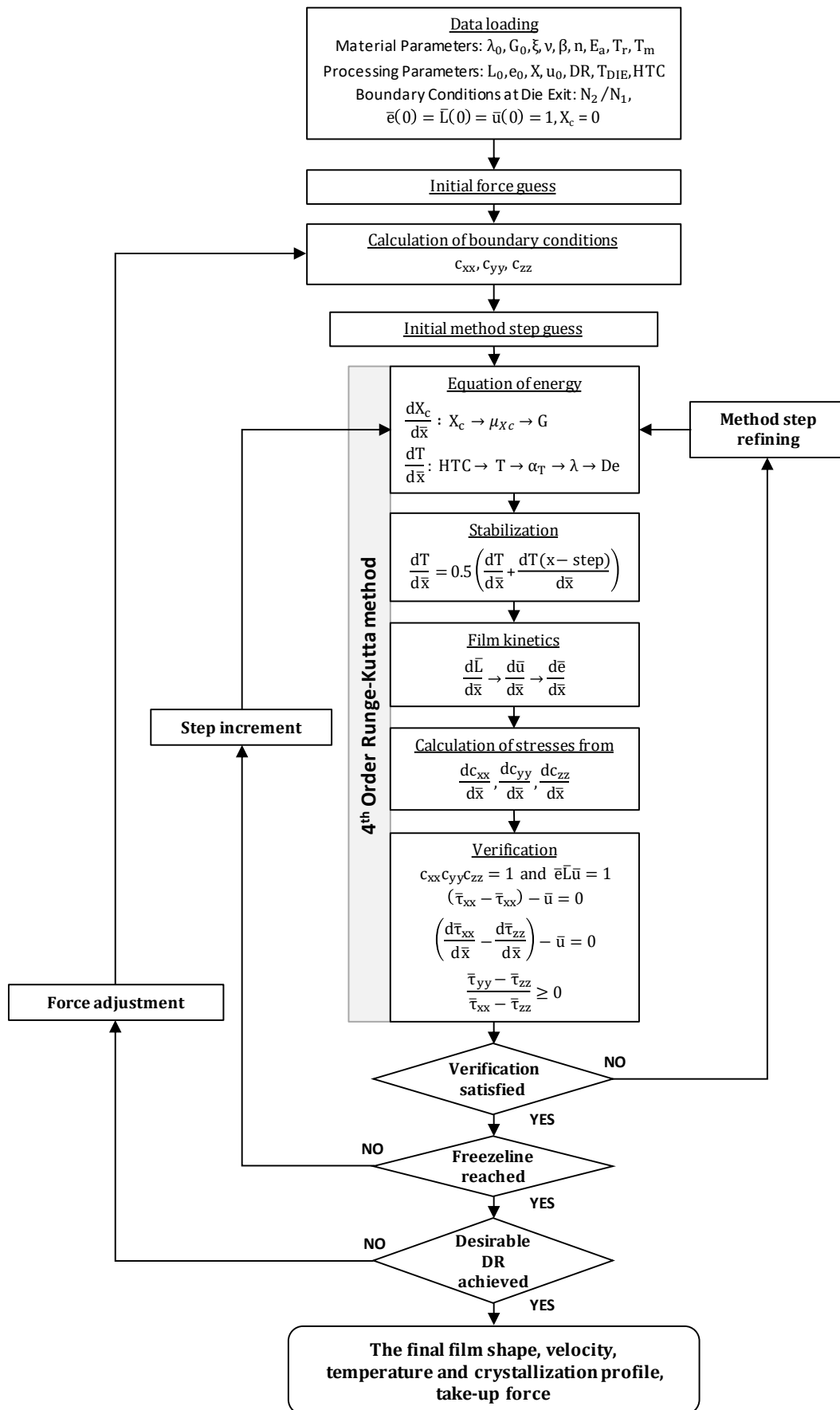


Figure 2. The flow diagram of implemented numerical scheme to solve the proposed film casting model.

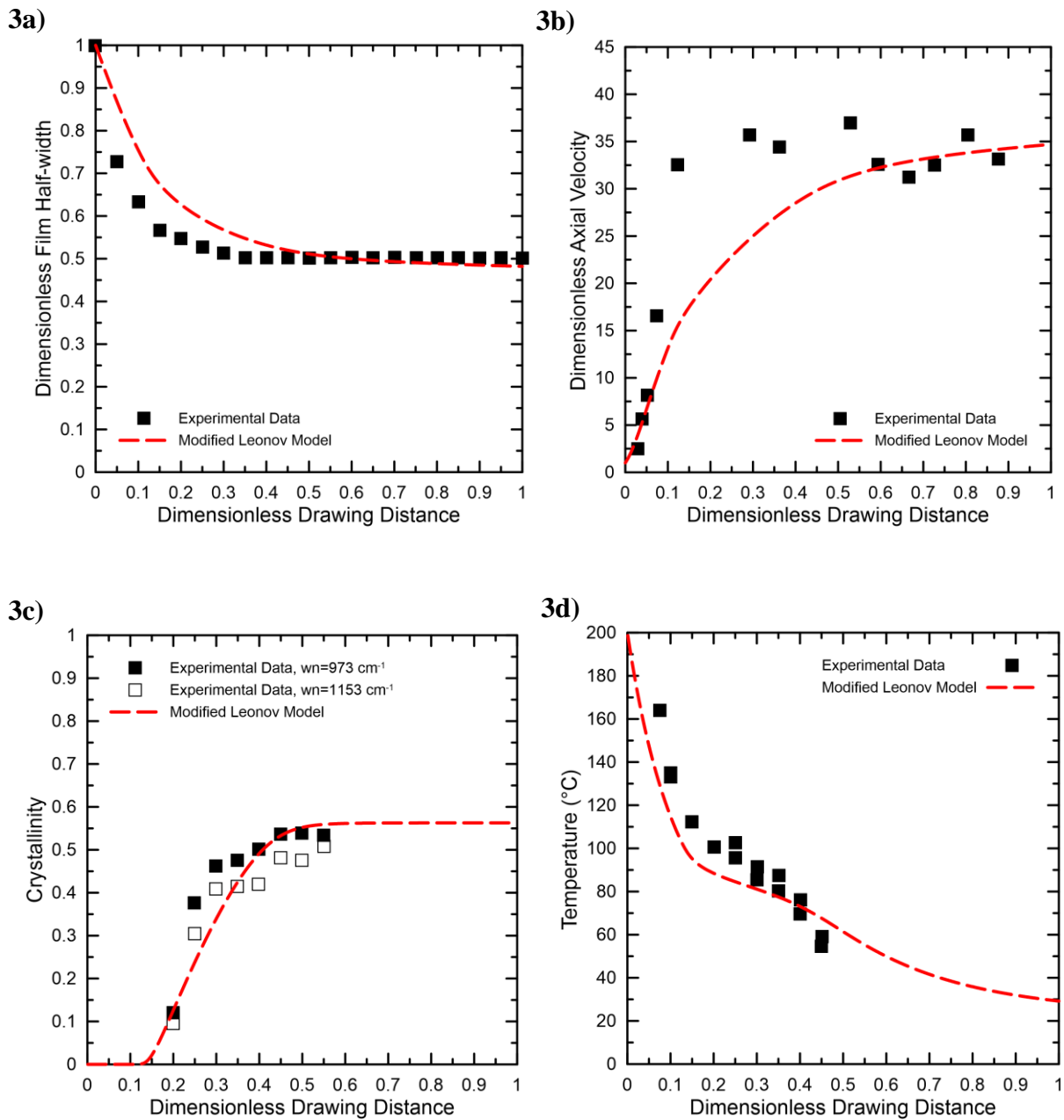


Figure 3. Comparison between experimental data for iPP T30G ($T_{DIE}=200^{\circ}\text{C}$) and given processing conditions ($De=6\cdot 10^{-4}$, $DR=34.7$, $X=0.4\text{ m}$) taken from [15] and model predictions for dimensionless drawing distance variables considering constant heat transfer coefficient, $HTC=16\text{ J}\cdot\text{s}^{-1}\cdot\text{K}^{-1}\cdot\text{m}^{-2}$. (a) Dimensionless Final Half-width, (b) Dimensionless Axial Velocity, (c) Temperature, (d) Crystallinity.

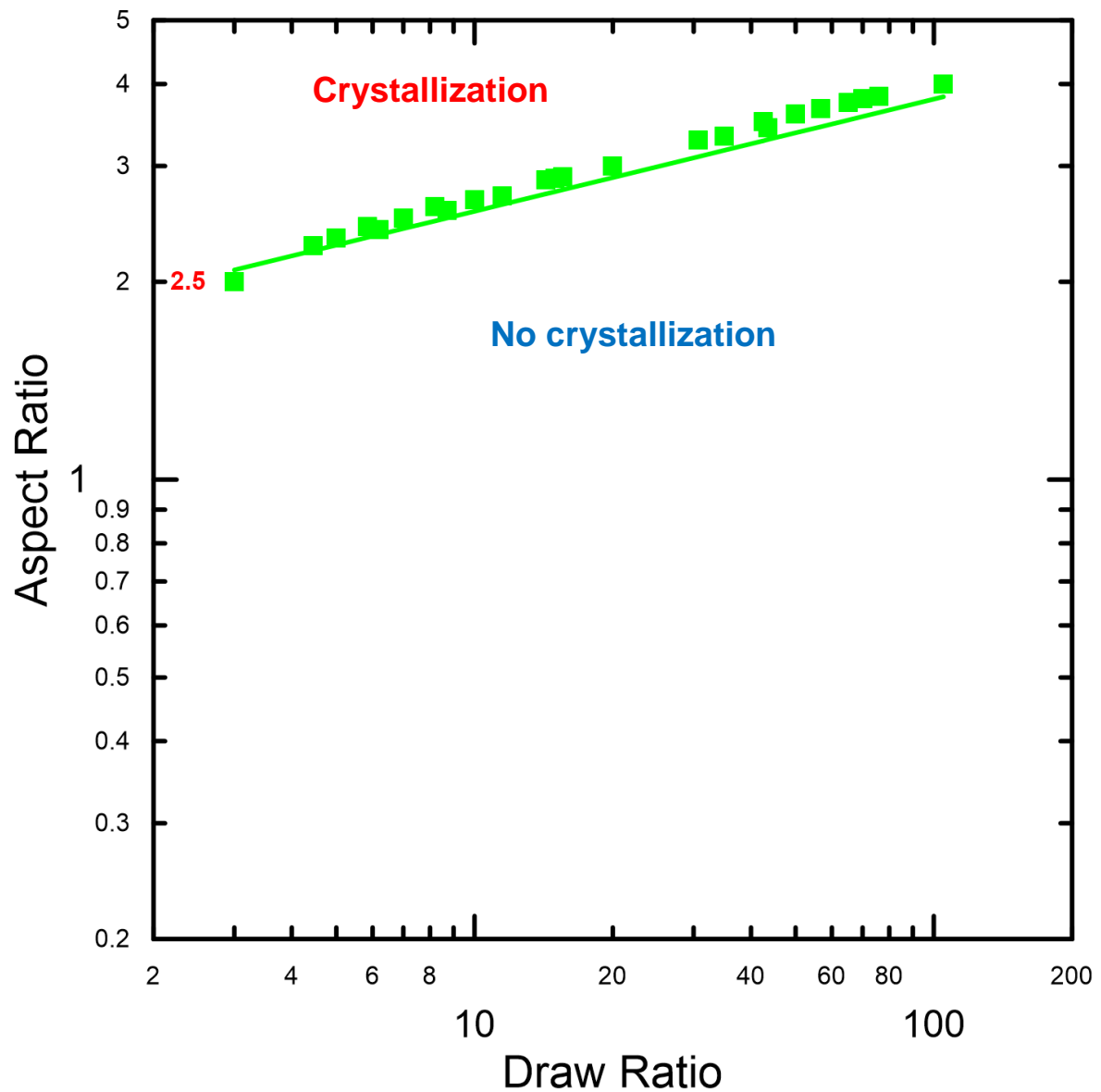


Figure 4. Predicted processing window for production of linear iPP films with (area above the border symbols) and without (area below the border symbols) the crystallized phase for given heat transfer coefficient ($HTC=2.5 \text{ J}\cdot\text{s}^{-1}\cdot\text{K}^{-1}\cdot\text{m}^{-2}$) and melt temperature at the die exit ($T_{DIE}=200^{\circ}\text{C}$).

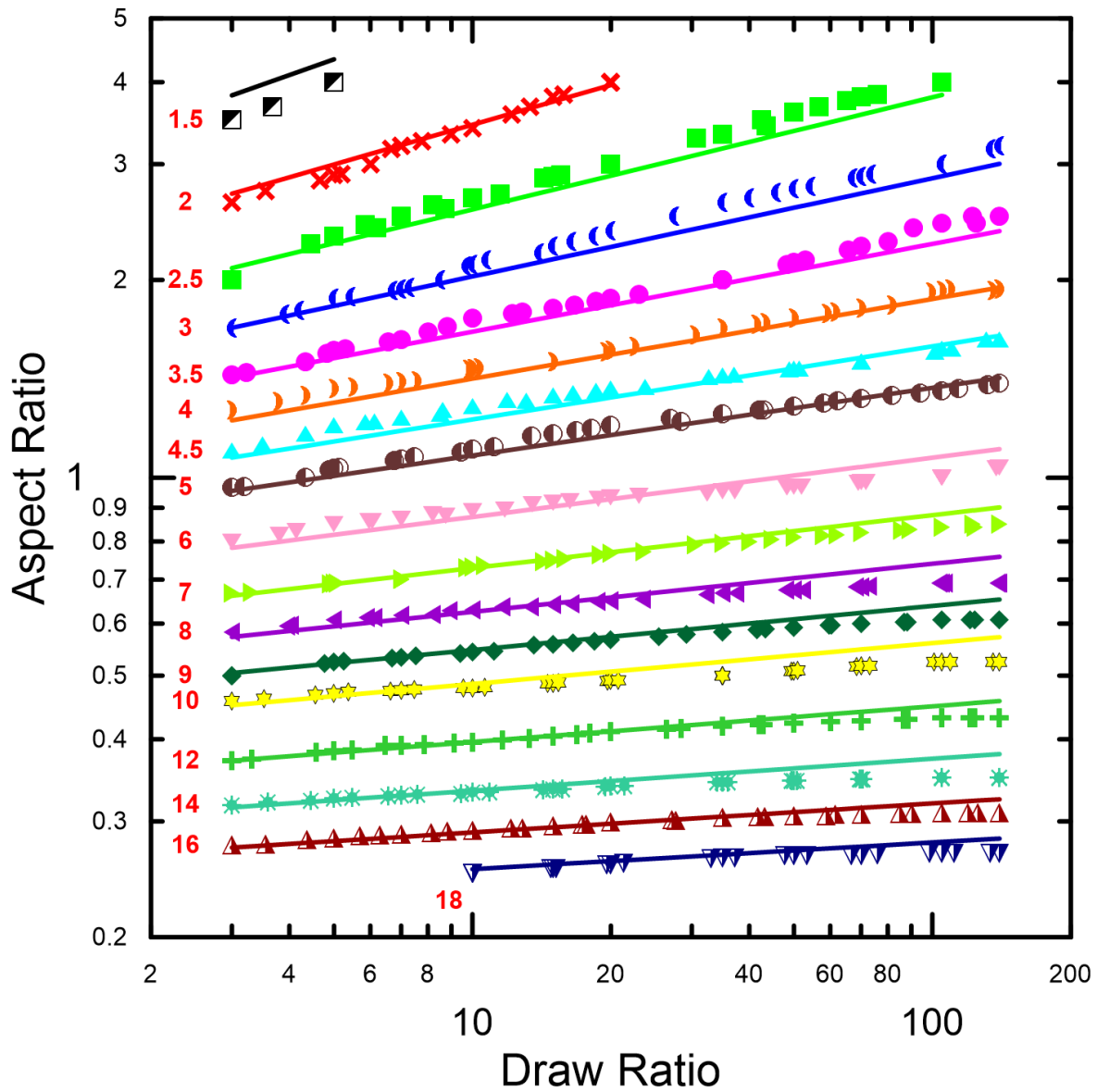


Figure 5. Effect of draw ratio, heat transfer coefficient (see numbers in $\text{J}\cdot\text{s}^{-1}\cdot\text{K}^{-1}\cdot\text{m}^{-2}$ provided at each data set) and melt temperature at the die exit, $T_{\text{DIE}}=200^\circ\text{C}$, on the aspect ratio, at which crystallization in linear iPP film starts to occur (border predicted by numerical model is given by the symbols, lines represents analytical approximation given by Eq. 43).

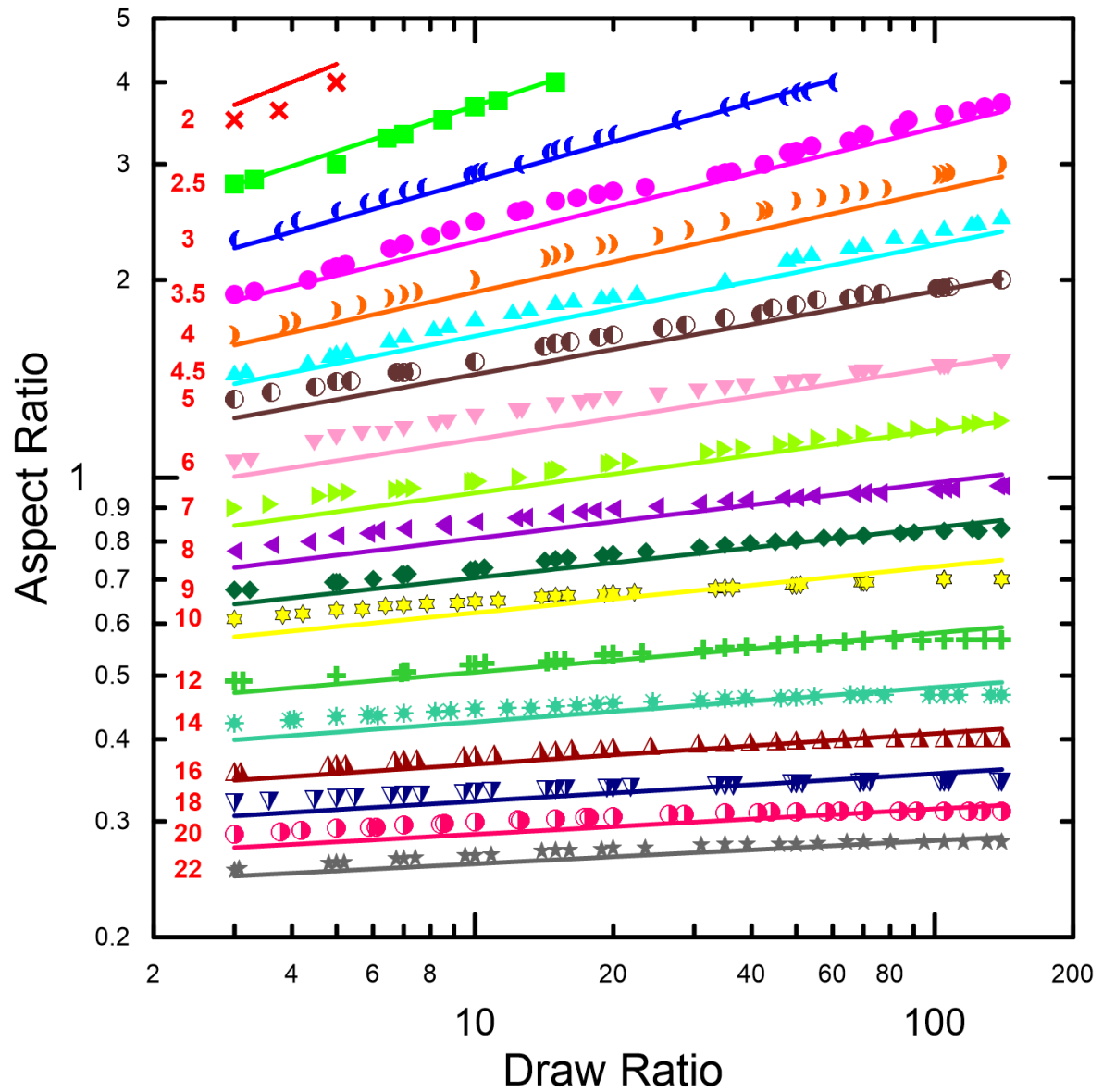


Figure 6. Effect of draw ratio, heat transfer coefficient (see numbers in $\text{J}\cdot\text{s}^{-1}\cdot\text{K}^{-1}\cdot\text{m}^{-2}$ provided at each data set) and melt temperature at the die exit, $T_{\text{DIE}}=225^\circ\text{C}$, on the aspect ratio, at which crystallization in linear iPP film starts to occur (border predicted by numerical model is given by the symbols, lines represents analytical approximation given by Eq. 43).

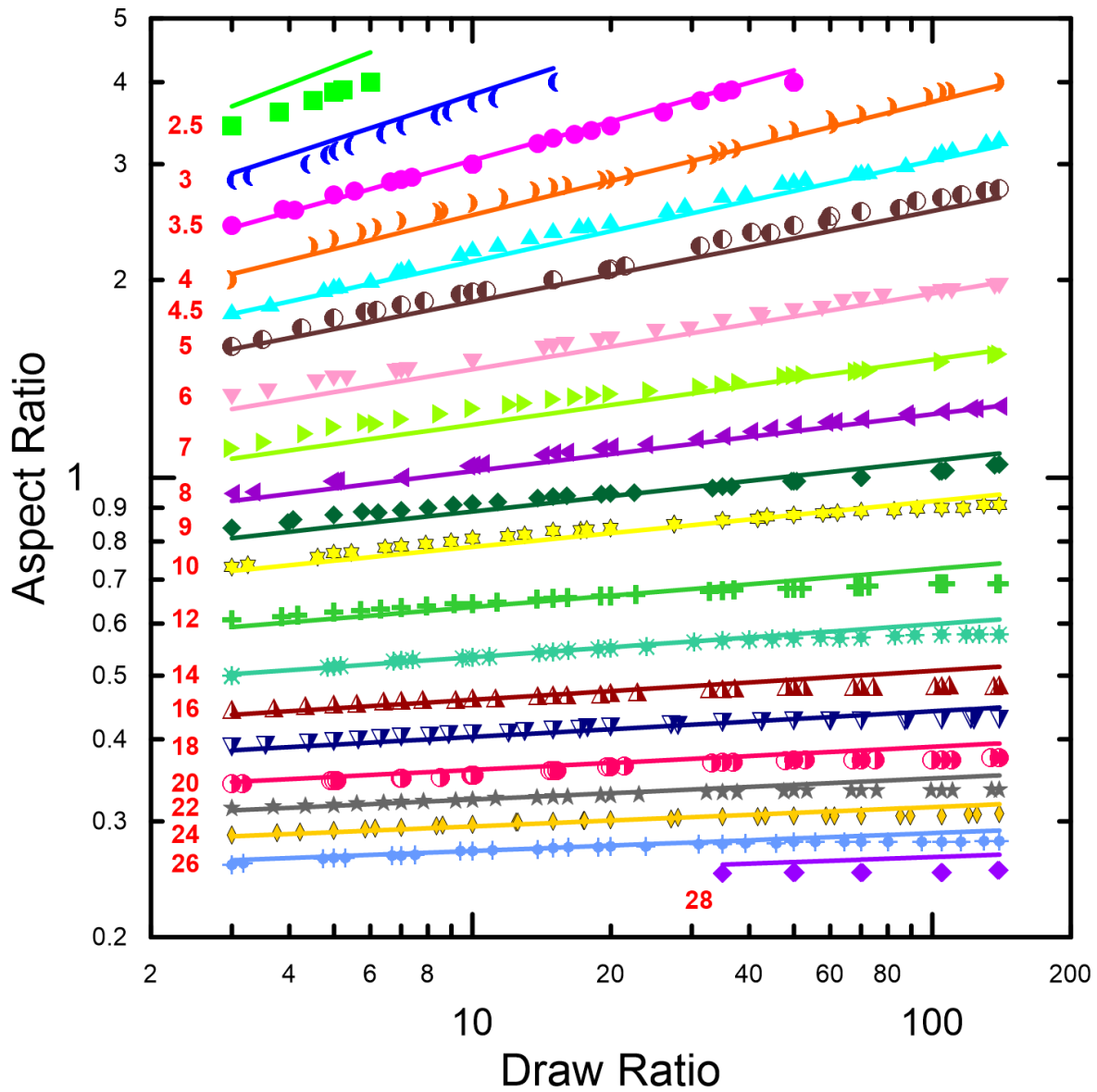


Figure 7. Effect of draw ratio, heat transfer coefficient (see numbers in $\text{J}\cdot\text{s}^{-1}\cdot\text{K}^{-1}\cdot\text{m}^{-2}$ provided at each data set) and melt temperature at the die exit, $T_{\text{DIE}}=250^\circ\text{C}$, on the aspect ratio, at which crystallization in linear iPP film starts to occur (border predicted by numerical model is given by the symbols, lines represents analytical approximation given by Eq. 43).

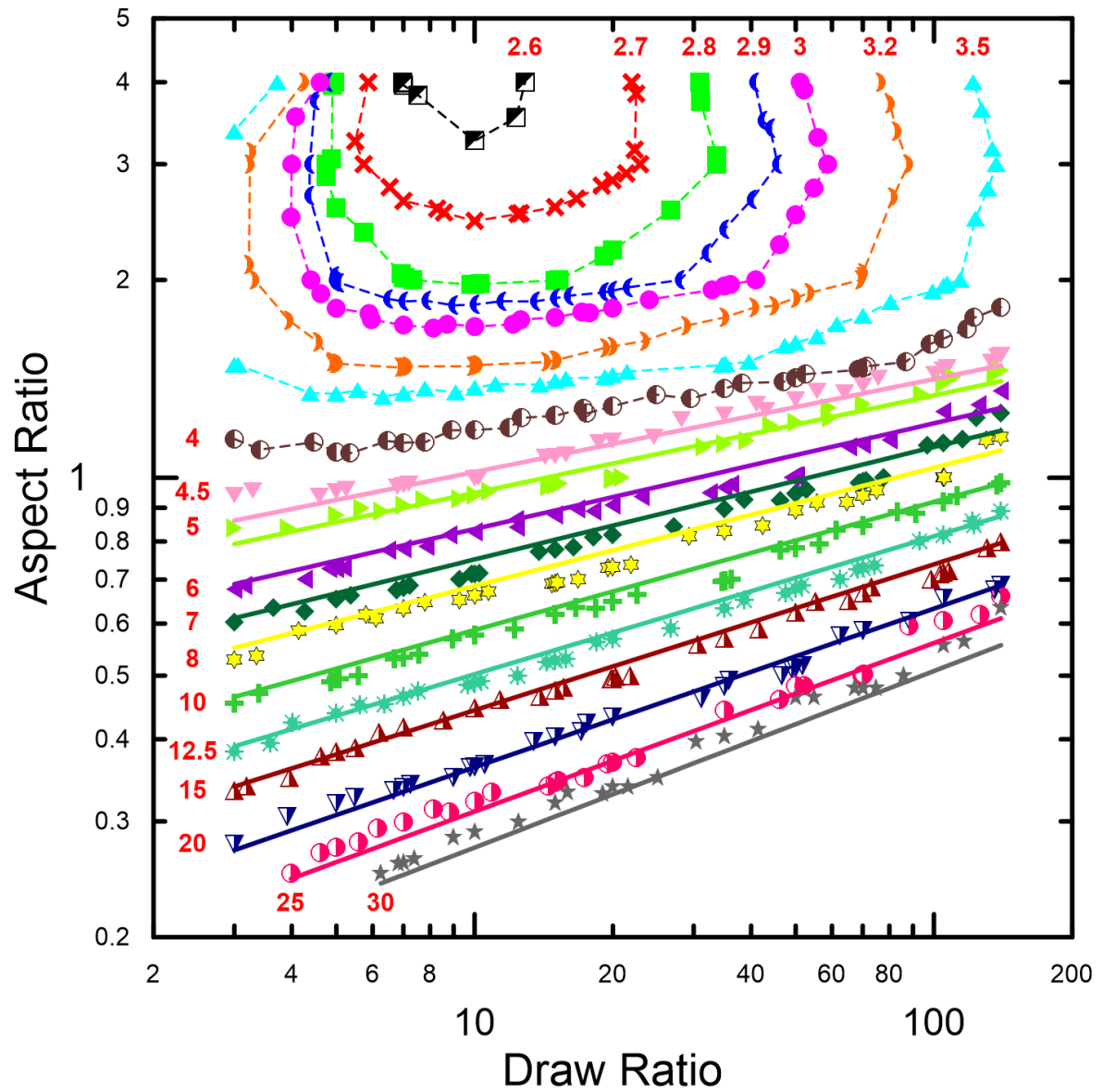


Figure 8. Effect of draw ratio and heat transfer coefficient (see numbers in $J \cdot s^{-1} \cdot K^{-1} \cdot m^{-2}$ provided at each data set) on the critical aspect ratio below which the non-isothermal and isothermal calculations gives for linear iPP practically the same neck-in value (considering melt temperature at the die exit equal to $200^{\circ}C$, border predicted by numerical model is given by the symbols, lines represents analytical approximation given by Eq. 46).

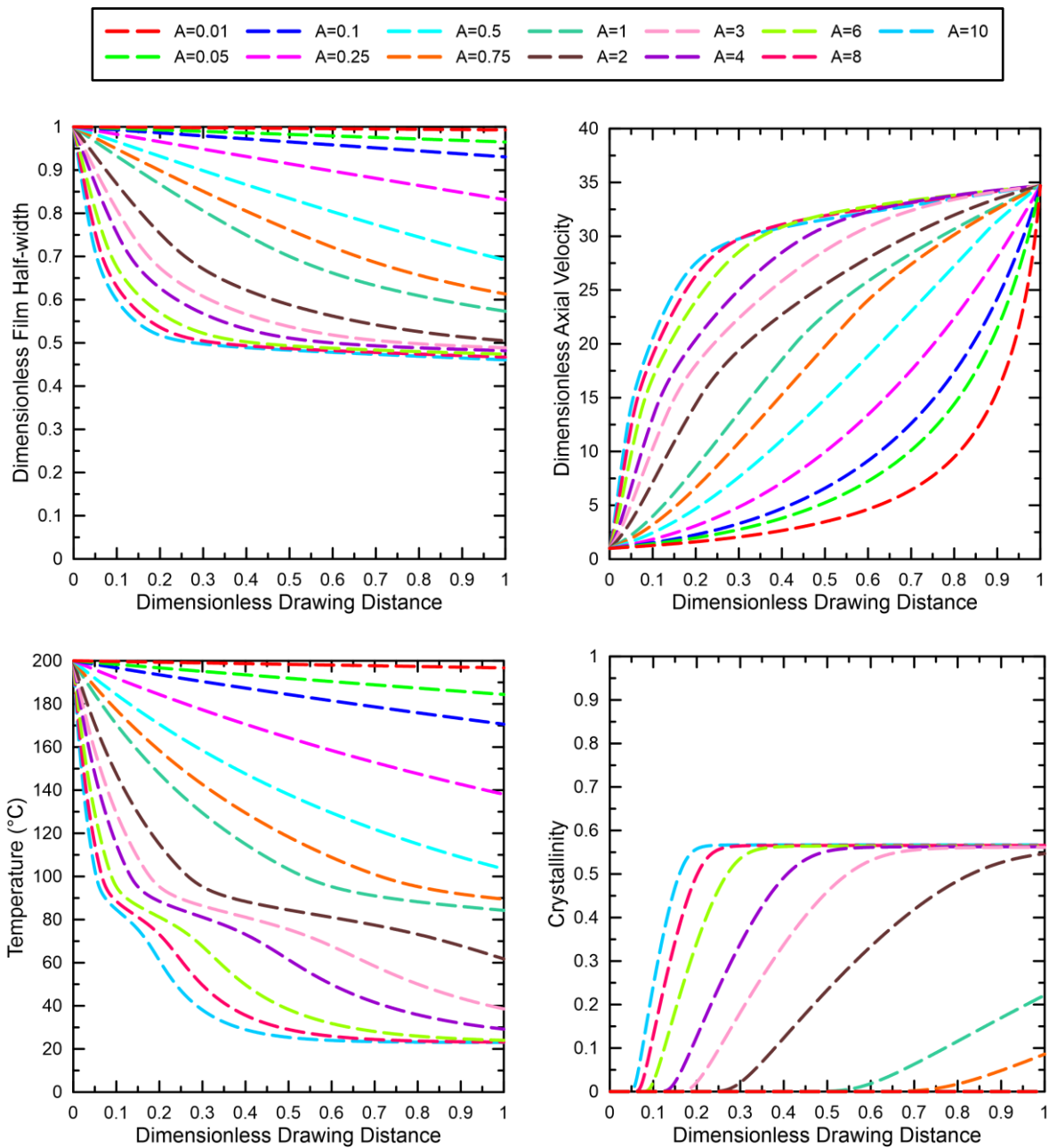


Figure 9. Effect of aspect ratio (changed via drawing distance, X) on dimensionless-drawing-distance dependent dimensionless film half-width (top, left), dimensionless axial velocity (top, right), temperature (bottom, left) and film crystallinity for the linear iPP and the reference flow conditions ($HTC=16 \text{ J}\cdot\text{s}^{-1}\cdot\text{K}^{-1}\cdot\text{m}^{-2}$, $T_{DIE}=200^\circ\text{C}$, $DR=34.7$).

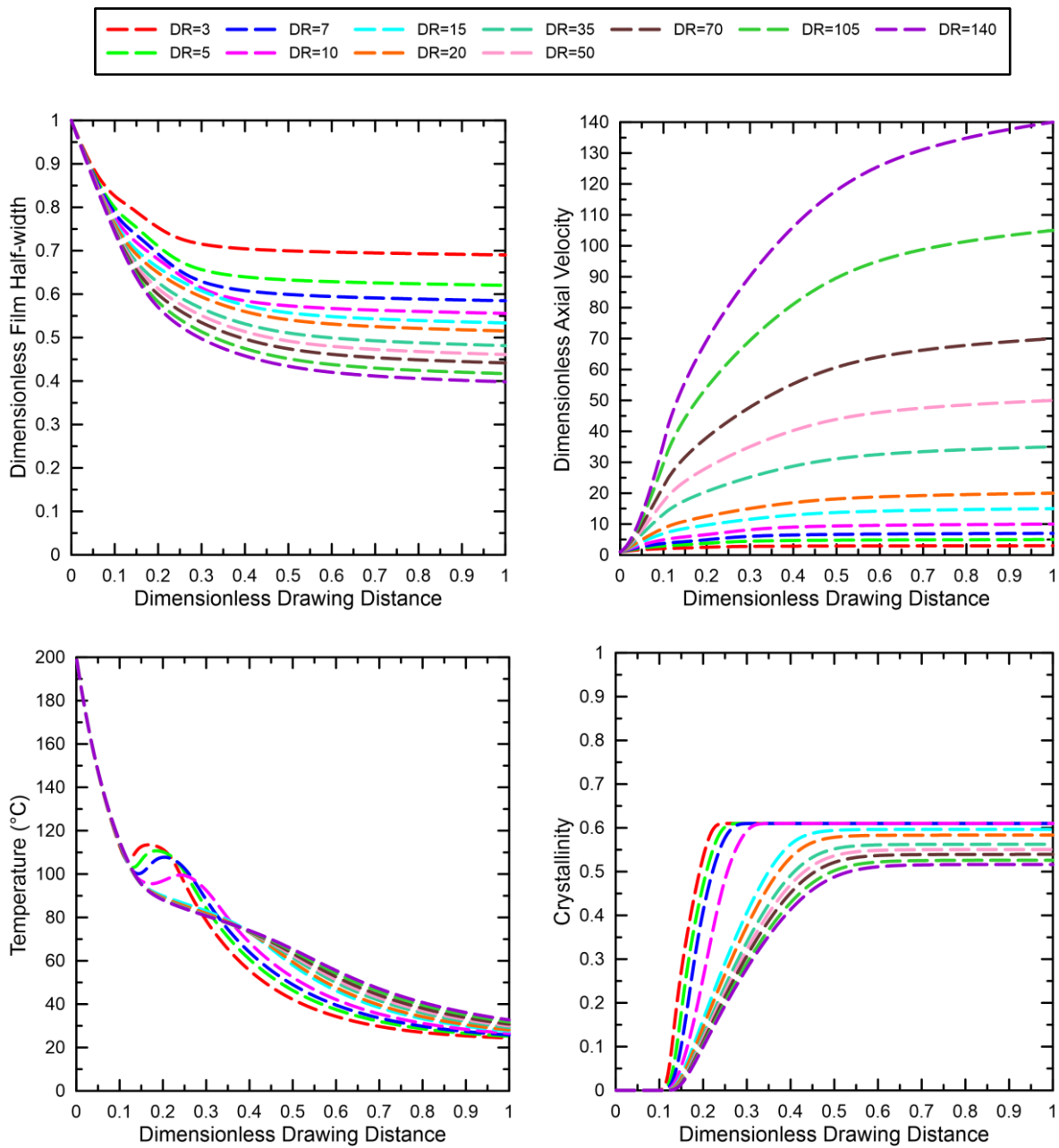


Figure 10. Effect of draw ratio on dimensionless-drawing-distance dependent dimensionless film half-width (top, left), dimensionless axial velocity (top, right), temperature (bottom, left) and film crystallinity for the linear iPP and the reference flow conditions ($A=4$, $HTC=16 \text{ J} \cdot \text{s}^{-1} \cdot \text{K}^{-1} \cdot \text{m}^{-2}$, $T_{\text{DIE}}=200^\circ\text{C}$).

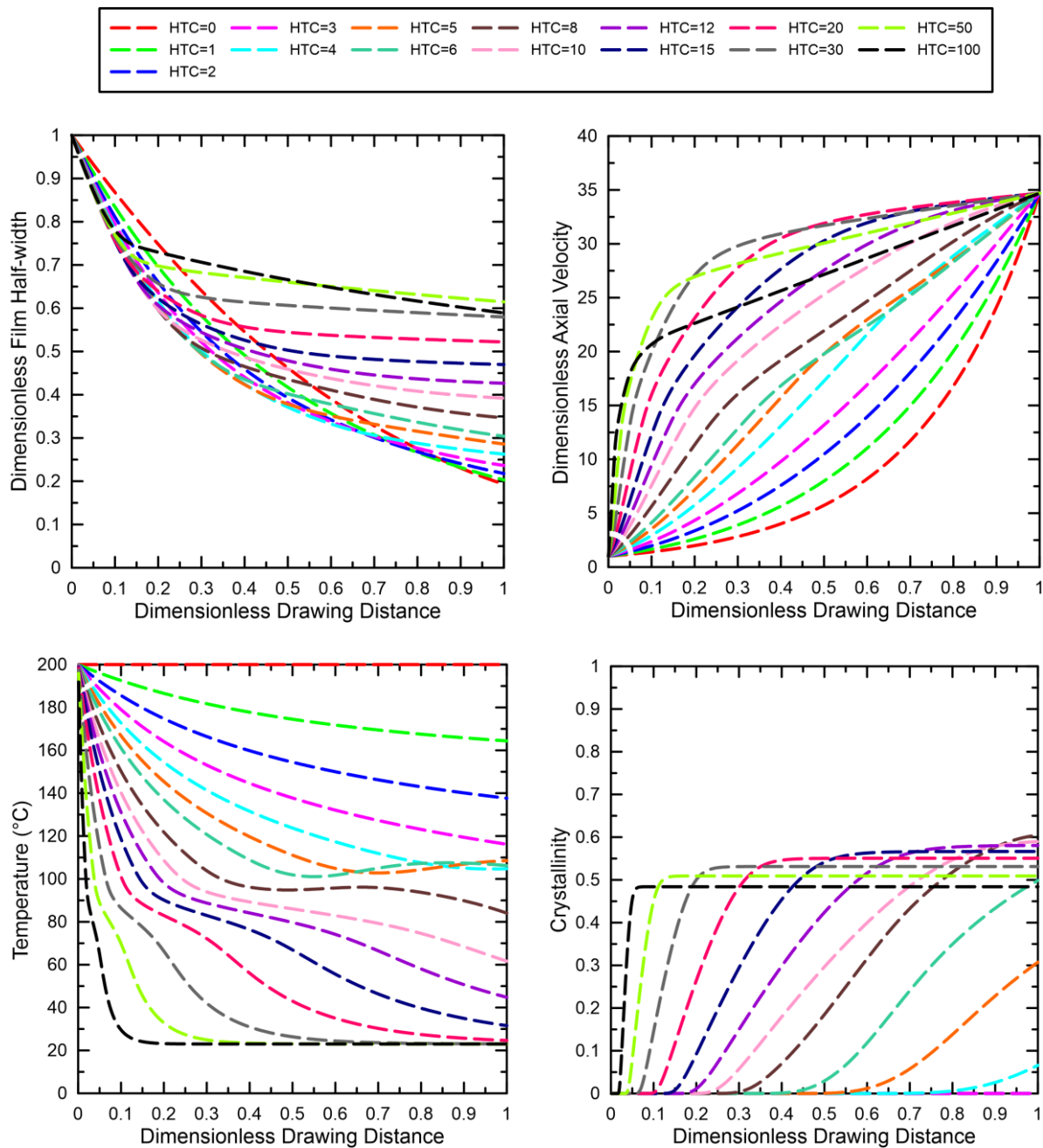


Figure 11. Effect of heat transfer coefficient on dimensionless-drawing-distance dependent dimensionless film half-width (top, left), dimensionless axial velocity (top, right), temperature (bottom, left) and film crystallinity for the linear iPP and the reference flow conditions ($A=4$, $DR=34.7$, $T_{DIE}=200^{\circ}\text{C}$).

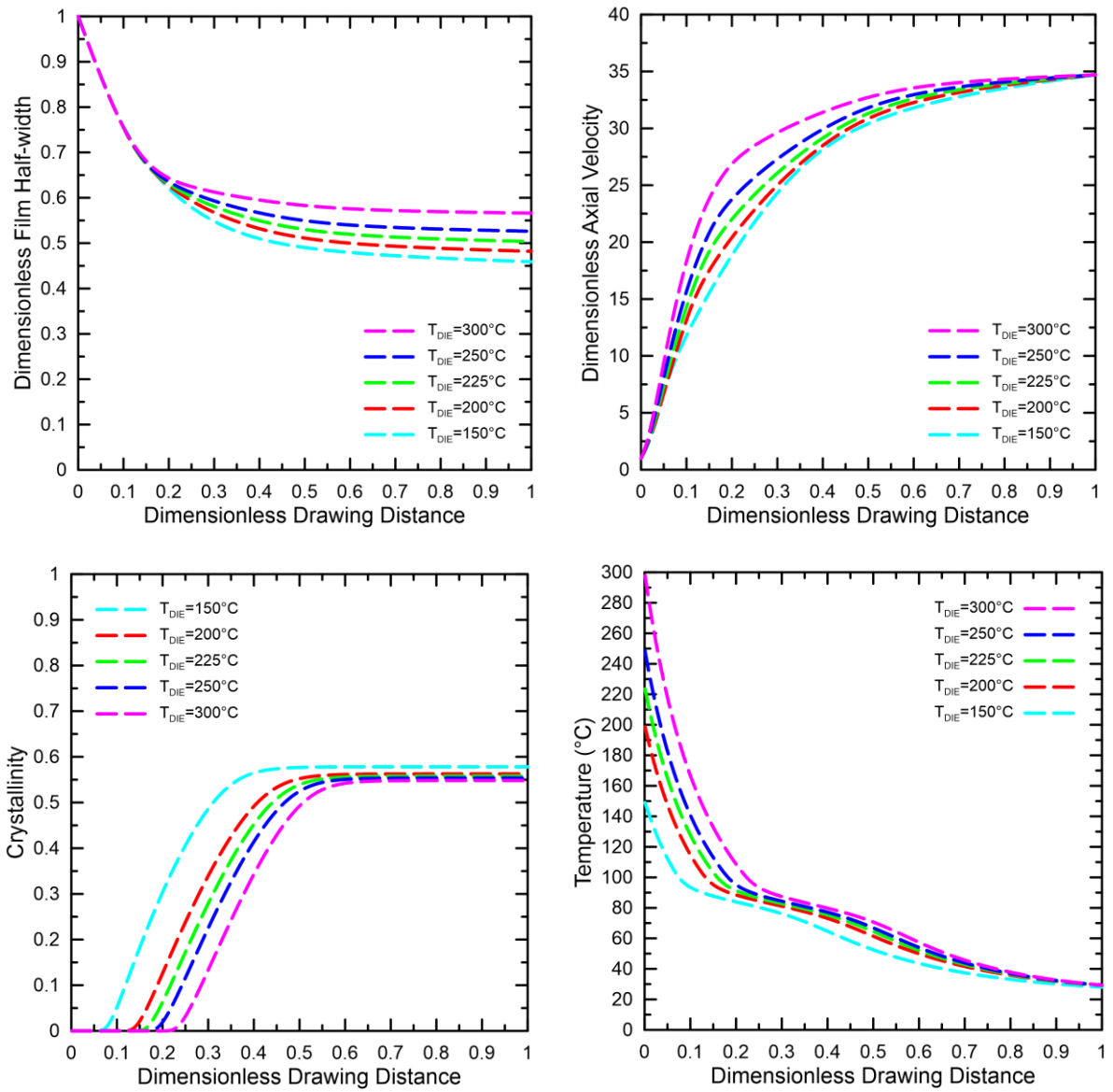


Figure 12. Effect of melt temperature at the die exit on dimensionless-drawing-distance dependent dimensionless film half-width (top, left), dimensionless axial velocity (top, right), temperature (bottom, left) and film crystallinity for the linear iPP and the reference flow conditions ($A=4$, $DR=34.7$, $HTC=16 \text{ J}\cdot\text{s}^{-1}\cdot\text{K}^{-1}\cdot\text{m}^{-2}$).

PAPER IV

**VISCOELASTIC SIMULATION OF EXTRUSION FILM CASTING
FOR LINEAR iPP INCLUDING STRESS INDUCED
CRYSTALLIZATION**

Tomas Barborik, Martin Zatloukal*

Polymer Centre, Faculty of Technology, Tomas Bata University in Zlin,

Vavreckova 275, 760 01 Zlin, Czech Republic

Keywords: Flat film production, polymer melt, rheology, neck-in phenomenon, heat transfer coefficient, flow induced crystallization.

*Corresponding author: mzatloukal@utb.cz

ABSTRACT

In this work, 1.5D film casting membrane model proposed by Silagy et al. (Polym Eng Sci 36:2614-2625, 1996) was generalized considering single-mode modified Leonov model as the viscoelastic constitutive equation and energy equation coupled with crystallization kinetics taking temperature as well as stress induced crystallization into account. The model has been successfully validated for the linear isotactic polypropylene by using experimental data collected under extremely high cooling rate processing conditions ($86^{\circ}\text{C}/\text{s}$), which were taken from the open literature. It has been found that utilization of flow induced crystallization significantly improves model predictions, especially for the film temperature and crystallinity. The model was consequently used to understand the role of heat transfer coefficient on the neck-in phenomenon as well as on the film velocity, temperature and crystallinity profiles.

1 INTRODUCTION

The PP microporous membranes have found many useful applications over time especially in separation processes: from microfiltration to reverse osmosis or as separators in Lithium ion batteries [1–4]. To fulfill high demands laid on those products, in recent decades, there have been introduced the fabrication process of semi-permeable polymeric membranes from semi-crystalline polymers without solvents by the dry method. This fabrication process can be divided to the three significant stages: first of all, primary precursor film is produced with demand on formation of the row-nucleated lamellar crystalline structure; the second: film is annealed to increase a thickness of lamellae and enhance its orientation and uniformity and; the third: film stretching at low temperature is imposed to create voids following by stretching at high temperature to promote voids to larger pores. After those major steps of the secondary processing, the heat setting is usually applied to yield better dimensional stability of produced membranes [5]. Preparation of the primary film with suitable morphology structure seems to be the key requirement for subsequent successful creation of the pores [6] with good spatial and size distribution. For this purpose, the extrusion film casting technology can be used with benefit for the fabrication of the primary film with row-nucleated lamellar crystalline structure if the suitable processing conditions and spatial process configuration are used. According to the past investigations, important parameters are molecular weight and molecular weight distribution together with a polymer architecture [7–10], draw ratio and cooling conditions together with die and roll temperature [11–14]. Polymer melt is subjected to shear and extensional flow in the die and at/behind die lips, respectively, inflicting the enhancement of crystallization kinetics, known as a Flow Induced Crystallization, FIC [13, 15–19] due to the orientation of macromolecules. Consequently, the entropic increase in melting temperature may be encountered [20, 21]. Under such flow conditions, the final polymer morphology can be transformed from spherulites to the lamellar or under severe flows to fibrillary structures. To ensure that the crystallization is commenced in the drawing distance, thus, the primary film

acquire an oriented structure which is a prerequisite for the fabrication of microporous membrane [14, 22, 23], the processing condition should be set in that manner, that is high cooling rate, low temperature at die or long drawing distance. This is on the first sight in direct contrast with conditions for transparent films for packaging applications. Therefore, the processing window for fabrication of suitable precursor films for further conversion into microporous membranes is tight with a difficult optimization.

In order to understand the role of stress induced crystallization in this technology, The novel viscoelastic film casting model utilizing flow induced crystallization was derived for the first time, validated and consequently used for detailed parametric study. Particular attention was paid to the role of heat transfer coefficient on the flow induced crystallization, film kinematics, dimensions and temperature profile.

2 EXTRUSION FILM CASTING MODEL

In this study, the 1.5D membrane model of extrusion film casting [24] was utilized and additionally coupled with the equation of energy and crystallization kinetics to account for non-isothermal effects and crystal phase development, respectively. The first component of the model is based on two essential hypotheses allowing the problem to be treated as a membrane that has one dimension distinctly minor (film thickness) compared to the others, hence the total stress in this direction is assumed to be null. Second supporting hypothesis, stemming from the work of Narayanaswamy [25], is related to process kinematics that allows reducing the dimensionality of the computational task and simultaneously retaining the model predicting capability for both, the development of film width and thickness, although the model variables are dependent on x only.

As the constitutive equation combined with the base model, the modified Leonov model [26, 27] was embraced owing to its good capability of describing extensionally-dominated flows [28]. The stress and strain stored in the polymer melt is expressed in this model as follows

$$\underline{\underline{\tau}} = 2 \left(\underline{\underline{c}} \cdot \frac{\partial W}{\partial \underline{\underline{I}}_{1,c}} - \underline{\underline{c}}^{-1} \cdot \frac{\partial W}{\partial \underline{\underline{I}}_{2,c}} \right) \quad (1)$$

where $\underline{\underline{\tau}}$ is the stress tensor, and W , the elastic potential, which depends on the invariants $I_{1,c}$ and $I_{2,c}$ of the recoverable Finger tensor $\underline{\underline{c}}$,

$$W = \frac{3G}{2(n+1)} \left\{ [1-\beta] \cdot \left[\left(\frac{I_{1,c}}{3} \right)^{n+1} - 1 \right] + \beta \left[\left(\frac{I_{2,c}}{3} \right)^{n+1} - 1 \right] \right\} \quad (2)$$

where G denotes linear Hookean elastic modulus, β and n are numerical parameters. Throughout this work, the Mooney potential (i.e. $n=0$ in Eq. 2) and the following dissipation function b proposed in [27], have been employed.

$$b(I_{1,c}) = \frac{1}{4\lambda} \left\{ \exp \left[-\xi \sqrt{I_{1,c} - 3} \right] + \frac{\sinh \left[\nu (I_{1,c} - 3) \right]}{\nu (I_{1,c} - 3) + 1} \right\} \quad (3)$$

Here, ξ and ν are adjustable model parameters and λ is melt relaxation time.

The non-isothermally of the process is covered by energy balance equation

$$\frac{dT}{d\bar{x}} = \frac{2HTC(T_a - T)\bar{L}X}{C_p \dot{m}} + \frac{\Delta H}{C_p} \frac{dX_c}{d\bar{x}} \quad (4)$$

where, the $L(x)$ is film half-width, HTC is a constant heat transfer coefficient, C_p is specific heat capacity, \dot{m} is mass flow rate in quarter-cross-section, ΔH is latent heat of crystallization, T and T_a is melt and ambient air temperature, respectively, and finally $X_c(x)$ stands for content of crystallinity in the polymer volume. The development of crystallinity $P(t)$ in the film is given by crystallization kinetics [29–31] where the crystallinity content is a function of time, temperature and applied rate of cooling.

$$X_c(t) = X_{eq} - X_{eq} \exp \left\{ -[P(t)]^{n_c} \right\} \quad (5)$$

where X_{eq} is the equilibrium volume content of crystallinity and n_c constant is a constant determining a type of crystal growth. Temperature dependence of melt relaxation time λ is described by Arrhenius form with the constant activation energy E_a and is given as

$$\lambda = \lambda_0 \exp \left[\frac{E_a}{R} \left(\frac{1}{T} - \frac{1}{T_r} \right) \right] \quad (6)$$

here, R is universal gas constant and T_r is reference melt temperature. Apart from that, an increase of the elastic modulus G due to the effect of crystallization is expressed by following formula [32] with parameters f , h and m .

$$G = G_0 \left[1 + f \exp \left(-\frac{h}{X_c^m} \right) \right] \quad (7)$$

Flow-induced crystallization

Effect of flow on crystallization is described via molecular strain that increases both growth and nucleation rates. In the used formulation [33], melting temperature is continuously modified (see Figure 1) according to the current molecular strain as follows

$$T_m(S_F) - T_{mq}^0 = \frac{1}{2} \left[\tanh\left(\frac{S_F - A_1}{A_2}\right) + 1 \right] (A_3 S_F + A_4) \quad (8)$$

where T_{mq}^0 and $T_m(S_F)$ is equilibrium and quiescent melting temperature, and A_{1-4} are experimentally determined parameters, S_F is stretch function expressed here in the following form

$$S_F = I_{1,c} - 3 \quad (9)$$

In this proposed formula, the molecular stretch is measured over the first invariant of recoverable Finger tensor $I_{1,c}$.

Entire set of model equations was numerically solved with appropriate boundary conditions using the 4th order Runge-Kutta method and iteratively searched for the value of drawing force, F , that satisfies the prescribed draw ratio. Computational scheme was implemented in C++ language with GNUPLOT plotting software for external graph generation. Detailed derivation of the model equation can be found in our previous works [34, 35].

3 RESULTS AND DISCUSSION

3.1 Model validation

Utilized model has been validated by using experimental data taken from [21], which were collected during film casting of linear isotactic polypropylene, iPP T30G (for its basic characteristics see Table 1), under extremely high cooling rates of 86°C/s. The processing conditions were the following: $A=0.4$, $DR=25.75$, $T_{DIE}=220^{\circ}\text{C}$, for more details see Table 2. The relaxation spectrum for this material is provided in [36], the Newtonian viscosity, η_0 , at 220°C is equal to 7,402 Pa·s and the flow activation energy, E_a , is 40.092 kJ·mol⁻¹. In order to simplify the simulations, average relaxation time, $\lambda=0.1$ s, instead of full relaxation spectrum, was used in this work. Average modulus G for the polymer melt without any crystalline phase was calculated to satisfy the following basic relation: $\eta_0=G\cdot\lambda$. Modified Leonov model parameters ξ , ν and β were adjusted according to Table 3 in order to impose extensional shear thinning flow behavior, which is typical behavior of linear polymer melts. Deborah number at the die exit was calculated to 10⁻³ for given material and processing conditions, thus according to our previous study [37], the die exit stress state was set to $-N_2/N_1=0.2$ following the results from [38]. Crystallization kinetics parameters for the utilized polymer [20], including the parameters of Eq. 7 describing the effect of crystallinity on the modulus, as well as parameters of Eq. 8 describing evolution of melting temperature with the molecular stretch were taken from [39] and [33] and they are summarized in Tables 4 and 5, respectively. The heat transfer coefficient, the only unknown parameter of the utilized model appearing in Eq. 4, was adjusted be $HTC=31 \text{ J}\cdot\text{s}^{-1}\cdot\text{K}^{-1}\cdot\text{m}^{-2}$, which allows reasonable description of experimentally determined temperature profile for given processing conditions (see Figure 2).

Comparison between experimental data and full model predictions for film temperature and crystallinity (as the function of drawing distance) is provided in Figure 2. Here, two cases are visualized: the first considers Flow Induced Crystallization (FIC) but the second do not

(No FIC). It can be seen that utilization of FIC is necessary to correctly describe these two experimentally determined variables. Interestingly, FIC seems to have only very small effect on the neck-in phenomenon and axial velocity profile (at least for the investigated processing conditions) as it can be seen in Figure 3. On the other hand, if the energy equation (Eq. 4) is fully neglected, i.e. the flow is considered to be isothermal, the model predicts nearly linear decrease in dimensionless film half-width and convex axial velocity profile, which is not realistic [20, 41–43, 45–50].

3.2 Parametric study

It has been reported that the heat transfer coefficient is one of the most important major parameter, which together with flow induced crystallization, has strong impact on the production of porous polypropylene membranes [7, 11, 51–53]. In order to understand its effect on the cast film technology, its value has been varied from 0 to $100 \text{ J}\cdot\text{s}^{-1}\cdot\text{K}^{-1}\cdot\text{m}^{-2}$ in full model for the same processing conditions, which were used in the validation study.

As it can be seen from Figure 4, if *HTC* increases, neck-in decreases (except to the highest *HTC* value, at which neck-in starts to increase), axial velocity profile is changed from the convex to the concave shape, see Figure 5, film temperature decreases, see Figure 6, and crystallinity increases, see Figure 7. Even if these trends are comparable with those reported in our previous work [34], in which FIC was neglected, there are some differences. Firstly, inclusion of FIC in the model allows to predict realistic plateau in the temperature profile, which corresponds with the location of exothermal crystallization (see Figure 2a and compare Figure 6. with Figure 11, bottom-left, from [34]). Secondly, utilization of FIC in the film casting model predicts monotonic increase in the film crystallinity for the increased *HTC*, which seems to be more realistic in comparison with the non-monotonic trend predicted by the cast film model neglecting FIC (compare Figure 7 with Figure 11, bottom-right, in [34]).

The effect of *HTC* on the linear iPP melting temperature plotted as the function of drawing distance is provided in Figure 8 for the given processing conditions. It can be seen that increase in *HTC* increases melt temperature of the given PP melt, especially, if its value becomes higher than about $12 \text{ J}\cdot\text{s}^{-1}\cdot\text{K}^{-1}\cdot\text{m}^{-2}$. Such melt temperature change becomes more abrupt and it occurs closer to the die exit, if the *HTC* increases.

4 CONCLUSION

In this work, 1.5D film casting membrane model proposed by Silagy at [24] was generalized considering single-mode modified Leonov model as the viscoelastic constitutive equation, energy equation, constant heat transfer coefficient, advanced crystallization kinetics taking into account the role of temperature, cooling rate and molecular stretch, crystalline phase dependent modulus and temperature dependent relaxation time. The model has been successfully validated for the linear isotactic polypropylene by using suitable experimental data taken from the open literature.

It has been found that for the given processing conditions, utilization of flow induced crystallization significantly improves predictions for the film temperature and crystallinity whereas its effect on the neck-in phenomenon and axial velocity profile is predicted to be small.

Consequent parametric study has revealed that inclusion of FIC in the model allows to predict realistic plateau in the temperature profile as well as monotonic increase in the film crystallinity for the increased HTC (which seems to be more realistic on this case than non-monotonic trends predicted by the model neglecting FIC). It was also shown that there is some threshold HTC value (about $12 \text{ J}\cdot\text{s}^{-1}\cdot\text{K}^{-1}\cdot\text{m}^{-2}$ for the studied iPP and given processing conditions), above which melting temperature is changed considerably, abruptly and more closely to the extrusion die due to FIC.

Acknowledgments

The authors wish to acknowledge the financial support from the Grant Agency of the Czech Republic (Grant registration No. 16-05886S).

5 LIST OF SYMBOLS

Latin Symbols	Meaning	Unit
A_1, A_2, A_3, A_4	Fitting parameters of FIC model	1
b	Dissipation term	s^{-1}
$\underline{\underline{c}}$	Recoverable Finger tensor	1
$\underline{\underline{c}}^{-1}$	Inverse recoverable Finger tensor	1
$\overset{\circ}{\underline{\underline{c}}}$	Jaumann (corotational) time derivative of the recoverable Finger strain tensor	s^{-1}
C_p	Specific heat capacity of polymer	$J \cdot kg^{-1} \cdot K^{-1}$
De	Deborah number, $De = \lambda_0 u_0 X^{-1}$	1
DR	Draw ratio, $DR = u(X)u_0^{-1}$	1
E_a	Flow activation energy	$J \cdot mol^{-1}$
e_0	Die half-gap (half-thickness of the film at the die exit)	m
F	Take-up force (stretching force)	N
f, h, m	Parameters in function describing the effect of crystallinity on elastic modulus	1
G	Linear Hookean elastic modulus	Pa
G_0	Linear Hookean elastic modulus at the die exit	Pa
HTC	Heat transfer coefficient	$J \cdot s^{-1} \cdot K^{-1} \cdot m^{-2}$
$I_{1,c}$	First invariant of recoverable Finger tensor	1
$I_{2,c}$	Second invariant of recoverable Finger tensor	1
L_0	Half-width of the die (half-width of the film at the die exit)	m

\bar{L}	Dimensionless half-width of the film at any x location	1
MFR , \dot{m}	Mass flow rate	$\text{kg}\cdot\text{h}^{-1}$
M_n	Number average molar mass	$\text{g}\cdot\text{mol}^{-1}$
M_w	Mass average molar mass	$\text{g}\cdot\text{mol}^{-1}$
NI	Neck-in, $\text{NI} = L_0 - L(X)$	mm
N_1	First normal stress difference	Pa
N_2	Second normal stress difference	Pa
n	Non-linear Leonov model parameter	1
n_c	Type of crystallization growth	1
$P(t)$	Function of non-linear crystallinity evolution	1
R	Gas constant	$\text{J}\cdot\text{K}^{-1}\cdot\text{mol}^{-1}$
S_F	Molecular stress function of FIC model	$^{\circ}\text{C}$
T	Melt temperature	$^{\circ}\text{C}$
T_c	Melt temperature at the die	$^{\circ}\text{C}$
T_{DIE}	Melt temperature at the die	$^{\circ}\text{C}$
T_m	Melting temperature of polymer	$^{\circ}\text{C}$
T_{mq}^0	Flow induced equilibrium melting temperature	$^{\circ}\text{C}$
T_r	Reference temperature in the Arrhenius law	$^{\circ}\text{C}$
\dot{T}^*	Rate of cooling	$^{\circ}\text{C}\cdot\text{s}^{-1}$
$u(X)$	Chill roll speed	$\text{m}\cdot\text{s}^{-1}$
u_0	Axial velocity component at the die exit	$\text{m}\cdot\text{s}^{-1}$
W	Elastic potential	Pa
X	Take-up length (stretching distance, air gap)	m

X_c	Crystallinity content in the polymer volume	1
X_{eq}	Equilibrium level of crystallinity in the polymer volume	1
X_{FL}	Experimentally measured film freeze line within air gap	m
x	Position in axial x-direction	m
\bar{x}	Dimensionless position in axial x-direction	1
x, y, z	Spatial coordinates in axial, transverse and thickness direction, respectively	1
$\frac{dX_c}{d\bar{x}}$	Derivative of crystallinity with respect to dimensionless \bar{x} position	1
$\frac{dT}{d\bar{x}}$	Derivative of temperature with respect to dimensionless \bar{x} position	°C

Greek Symbols	Meaning	Unit
β	Non-linear Leonov model parameter	1
ΔH	Crystallization latent heat	$\text{kJ} \cdot \text{kg}^{-1}$
η_0	Newtonian viscosity	$\text{Pa} \cdot \text{s}$
λ	Melt relaxation time	s
λ_0	Melt relaxation time at the die exit	s
μ_{X_c}	Effect of crystallinity on elastic modulus function	1
ν	Non-linear Leonov model parameter	1
ξ	Non-linear Leonov model parameter	1
ρ_P	Polymer density	$\text{kg} \cdot \text{m}^{-3}$
$\underline{\underline{\tau}}$	Extra stress tensor	Pa

6 REFERENCES

- [1] BAKER, Richard W. *Membrane Technology and Applications*. 2nd ed. West Sussex, UK : John Wiley & Sons, Ltd., 2004. ISBN 9780470854457.
- [2] ARORA, Pankaj and ZHANG, Zhengming (John). Battery Separators. *Chemical Reviews*. 2004. Vol. 104, no. 10, p. 4419–4462.
- [3] ZHANG, Sheng Shui. A review on the separators of liquid electrolyte Li-ion batteries. *Journal of Power Sources*. 2007. Vol. 164, no. 1, p. 351–364.
- [4] ULBRICHT, Mathias. Advanced functional polymer membranes. *Polymer*. 2006. Vol. 47, no. 7, p. 2217–2262.
- [5] CAIHONG, Lei, SHUQIU, Wu, QI, Cai, RUIJIE, Xu, BING, Hu and WENQIANG, Shi. Influence of heat-setting temperature on the properties of a stretched polypropylene microporous membrane. *Polymer International*. 2013. Vol. 63, no. 3, p. 584–588.
- [6] LIN, Yuanfei, MENG, Lingpu, WU, Lihui, LI, Xueyu, CHEN, Xiaowei, ZHANG, Qianlei, ZHANG, Rui, ZHANG, Wenhua and LI, Liangbin. A semi-quantitative deformation model for pore formation in isotactic polypropylene microporous membrane. *Polymer*. 2015. Vol. 80, p. 214–227.
- [7] SADEGHI, Farhad, AJJI, Abdellah and CARREAU, Pierre J. Analysis of microporous membranes obtained from polypropylene films by stretching. *Journal of Membrane Science*. 2007. Vol. 292, no. 1–2, p. 62–71.
- [8] SADEGHI, Farhad, AJJI, Abdellah and CARREAU, Pierre J. Microporous membranes obtained from polypropylene blends with superior permeability properties. *Journal of Polymer Science Part B: Polymer Physics*. 2008. Vol. 46, no. 2, p. 148–157.
- [9] SOMANI, Rajesh H., YANG, Ling and HSIAO, Benjamin S. Effects of high molecular weight species on shear-induced orientation and crystallization of isotactic polypropylene. *Polymer*. 2006. Vol. 47, no. 15, p. 5657–5668.
- [10] TABATABAEI, Seyed H., CARREAU, Pierre J. and AJJI, Abdellah. Microporous membranes obtained from polypropylene blend films by stretching. *Journal of Membrane Science*. 2008. Vol. 325, no. 2, p. 772–782.
- [11] TABATABAEI, Seyed H., CARREAU, Pierre J. and AJJI, Abdellah. Effect of processing on the crystalline orientation, morphology, and mechanical properties of polypropylene cast films and microporous membrane formation. *Polymer*. 2009. Vol. 50, no. 17, p. 4228–4240.
- [12] RESCH, Katharina, WALLNER, Gernot M, TEICHERT, Christian, MAIER, Günther and GAHLEITNER, Markus. Optical properties of highly transparent polypropylene cast films: Influence of material structure, additives, and processing conditions. *Polymer Engineering & Science*. 2006. Vol. 46, no. 4, p. 520–531.
- [13] COPPOLA, Salvatore, BALZANO, Luigi, GIOFFREDI, Emilia, MAFFETTONE, Pier Luca and GRIZZUTI, Nino. Effects of the degree of undercooling on flow induced crystallization in polymer melts. *Polymer*. 2004. Vol. 45, no. 10, p. 3249–3256.
- [14] CASTEJÓN, Pilar, HABIBI, Kian, SAFFAR, Amir, AJJI, Abdellah, MARTÍNEZ, Antonio B and ARENCÓN, David. Polypropylene-Based Porous Membranes: Influence of Polymer Composition, Extrusion Draw Ratio and Uniaxial Strain. *Polymers*. 2018. Vol. 10, no. 1, p. 33.

- [15] DOUFAS, A.K., DAIRANIEH, I.S. and MCHUGH, A.J. A continuum model for flow-induced crystallization of polymer melts. *Journal of Rheology*. 1999. Vol. 43, no. 1, p. 85–109.
- [16] DOUFAS, Antonios K., MCHUGH, Anthony J. and MILLER, Chester. Simulation of melt spinning including flow-induced crystallization Part I. Model development and predictions. *Journal of Non-Newtonian Fluid Mechanics*. 2000. Vol. 92, no. 1, p. 27–66.
- [17] DOUFAS, Antonios K., MCHUGH, Anthony J., MILLER, Chester and IMMANENI, Aravind. Simulation of melt spinning including flow-induced crystallization Part II. Quantitative comparisons with industrial spinline data. *Journal of Non-Newtonian Fluid Mechanics*. 2000. Vol. 92, no. 1, p. 81–103.
- [18] DOUFAS, Antonios K. and MCHUGH, Anthony J. Simulation of melt spinning including flow-induced crystallization. Part III. Quantitative comparisons with PET spinline data. *Journal of Rheology*. 2001. Vol. 45, no. 2, p. 403.
- [19] SOMANI, Rajesh H, HSIAO, Benjamin S, NOGALES, Aurora, SRINIVAS, Srivatsan, TSOU, Andy H, SICS, Igors, BALTA-CALLEJA, Francisco J and EZQUERRA, Tiberio A. Structure Development during Shear Flow-Induced Crystallization of i-PP: In-Situ Small-Angle X-ray Scattering Study. *Macromolecules*. 2000. Vol. 33, no. 25, p. 9385–9394.
- [20] LAMBERTI, Gaetano and TITOMANLIO, Giuseppe. Evidences of flow induced crystallization during characterized film casting experiments. *Macromolecular Symposia*. 2002. Vol. 185, no. 1, p. 167–180.
- [21] LAMBERTI, Gaetano. Flow-induced crystallization during isotactic polypropylene film casting. *Polymer Engineering and Science*. 2011. Vol. 51, no. 5, p. 851–861.
- [22] WU, Shuqiu, LEI, Caihong, CAI, Qi, XU, Ruijie, HU, Bing, SHI, Wenqiang and PENG, Xinlong. Study of structure and properties of polypropylene microporous membrane by hot stretching. *Polymer Bulletin*. 2014. Vol. 71, no. 9, p. 2205–2217.
- [23] XIANDE, Chen, RUIJIE, Xu, JIAYI, Xie, YUANFEI, Lin, CAIHONG, Lei and LIANGBIN, Li. The study of room-temperature stretching of annealed polypropylene cast film with row-nucleated crystalline structure. *Polymer*. 2016. Vol. 94, p. 31–42.
- [24] SILAGY, David, DEMAY, Yves and AGASSANT, Jean François. Study of the stability of the film casting process. *Polymer Engineering and Science*. 1996. Vol. 36, no. 21, p. 2614–2625.
- [25] NARAYANASWAMY, O.S. A one-dimensional model of stretching float glass. *Journal of the American Ceramic Society*. 1977. Vol. 60, no. 1–2, p. 1–5.
- [26] LEONOV, A.I. Nonequilibrium thermodynamics and rheology of viscoelastic polymer media. *Rheologica Acta*. 1976. Vol. 15, no. 2, p. 85–98.
- [27] ZATLOUKAL, Martin. Differential viscoelastic constitutive equations for polymer melts in steady shear and elongational flows. *Journal of Non-Newtonian Fluid Mechanics*. 2003. Vol. 113, no. 2–3, p. 209–227.
- [28] ZATLOUKAL, Martin. Measurements and modeling of temperature-strain rate dependent uniaxial and planar extensional viscosities for branched LDPE polymer melt. *Polymer*. 2016. Vol. 104, p. 258–267.
- [29] ZIABICKI, A. Crystallization of polymers in variable external conditions. 1. General equations. *Colloid and Polymer Science*. 1996. Vol. 274, no. 3, p. 209–217.

- [30] ZIABICKI, A. Crystallization of polymers in variable external conditions. II. Effects of cooling in the absence of stress and orientation. *Colloid and Polymer Science*. 1996. Vol. 274, no. 8, p. 705–716.
- [31] LAMBERTI, Gaetano and TITOMANLIO, Giuseppe. Crystallization kinetics of iPP. Model and experiments. *Polymer Bulletin*. 2001. Vol. 46, no. 2–3, p. 231–238.
- [32] TITOMANLIO, G., SPERANZA, V. and BRUCATO, V. On the simulation of thermoplastic injection moulding process: II Relevance of interaction between flow and crystallization. *International Polymer Processing*. 1997. Vol. 12, no. 1, p. 45–53.
- [33] PANTANI, Roberto, DE SANTIS, Felice, SPERANZA, Vito and TITOMANLIO, Giuseppe. Analysis of flow induced crystallization through molecular stretch. *Polymer*. 2016. Vol. 105, p. 187–194.
- [34] BARBORIK, Tomas and ZATLOUKAL, Martin. Effect of heat transfer coefficient, draw ratio and die exit temperature on the production of flat iPP membranes. *Submitted for publication in: International Journal of Heat and Mass Transfer*. 2018. P. x.
- [35] BARBORIK, Tomas, ZATLOUKAL, M. and TZOGANAKIS, C. On the role of extensional rheology and Deborah number on the neck-in phenomenon during flat film casting. *International Journal of Heat and Mass Transfer*. 2017. Vol. 111, p. 1296–1313.
- [36] PANTANI, R, SPERANZA, V and TITOMANLIO, G. Simultaneous morphological and rheological measurements on polypropylene: Effect of crystallinity on viscoelastic parameters. *Journal of Rheology*. 2015. Vol. 59, no. 2, p. 377–390.
- [37] BARBORIK, Tomas and ZATLOUKAL, Martin. Effect of die exit stress state, Deborah number, uniaxial and planar extensional rheology on the neck-in phenomenon in polymeric flat film production. *Journal of Non-Newtonian Fluid Mechanics*. 2018. Vol. 255, p. 39–56.
- [38] JENSEN, E.A. and CHRISTIANSEN, J.deC. Measurements of first and second normal stress differences in a polymer melt. *Journal of Non-Newtonian Fluid Mechanics*. 2008. Vol. 148, no. 1–3, p. 41–46.
- [39] LAMBERTI, Gaetano, BRUCATO, Valerio and TITOMANLIO, Giuseppe. Orientation and crystallinity in film casting of polypropylene. *Journal of Applied Polymer Science*. 2002. Vol. 84, no. 11, p. 1981–1992.
- [40] LAMBERTI, Gaetano and TITOMANLIO, Giuseppe. Analysis of film casting process: The heat transfer phenomena. *Chemical Engineering and Processing: Process Intensification*. 2005. Vol. 44, no. 10, p. 1117–1122.
- [41] POL, H.V., BANIK, Sourya, AZAD, Lal Busher, THETE, Sumeet S., DOSHI, Pankaj and LELE, Ashish. Nonisothermal analysis of extrusion film casting process using molecular constitutive equations. *Rheologica Acta*. 2014. Vol. 53, no. 1, p. 85–101.
- [42] LAMBERTI, Gaetano, TITOMANLIO, Giuseppe and BRUCATO, Valerio. Measurement and modelling of the film casting process 1. Width distribution along draw direction. *Chemical Engineering Science*. 2001. Vol. 56, no. 20, p. 5749–5761.
- [43] ANIUNOH, Kenneth and HARRISON, Graham M. The processing of polypropylene cast films. I. Impact of material properties and processing conditions on film formation. *Polymer Engineering & Science*. 2010. Vol. 50, no. 6, p. 1151–1160.

- [44] ARROYO, M., LOPEZ-MANCHADO, M.A. and AVALOS, F. Crystallization kinetics of polypropylene: II. Effect of the addition of short glass fibres. *Polymer*. 1997. Vol. 38, no. 22, p. 5587–5593.
- [45] SEYFZADEH, Bijan, HARRISON, Graham M. and CARLSON, Charles D. Experimental studies on the development of a cast film. *Polymer Engineering & Science*. 2005. Vol. 45, no. 4, p. 443–450.
- [46] KOMETANI, H., MATSUMURA, T., SUGA, T. and KANAI, T. Experimental and theoretical analyses of film casting process. *Journal of Polymer Engineering*. 2007. Vol. 27, no. 1, p. 1–28.
- [47] ACIERNO, D., DI MAIO, L. and AMMIRATI, C. C. Film casting of polyethylene terephthalate: Experiments and model comparisons. *Polymer Engineering and Science*. 2000. Vol. 40, no. 1, p. 108–117.
- [48] ACIERNO, D., DI MAIO, L.D. and CUCCURULLO, G. Analysis of temperature fields in film casting. *Journal of Polymer Engineering*. 1999. Vol. 19, no. 2, p. 75–94.
- [49] LAMBERTI, Gaetano and TITOMANLIO, Giuseppe. Analysis of Film Casting Process : Effect of Cooling during the Path in Air. *Industrial & Engineering Chemistry Research*. 2006. Vol. 45, no. 2, p. 719–723.
- [50] SEAY, C.W. and BAIRD, D.G. Sparse Long-chain Branching’s Effect on the Film-casting Behavior of PE. *International Polymer Processing*. 2009. Vol. 24, no. 1, p. 41–49.
- [51] SADEGHI, Farhad, AJJI, Abdellah and CARREAU, Pierre J. Analysis of row nucleated lamellar morphology of polypropylene obtained from the cast film process: Effect of melt rheology and process conditions. *Polymer Engineering & Science*. 2007. Vol. 47, no. 7, p. 1170–1178.
- [52] XU, Meng, ZHANG, Shijun, LIANG, Jieying, QUAN, Hui, LIU, Jianye, SHI, Hongwei, GAO, Dali and LIU, Jie. Influences of processing on the phase transition and crystallization of polypropylene cast films. *Journal of Applied Polymer Science*. 2014. Vol. 131, no. 22, p. 41100.
- [53] NOETHER, H.D. and HAY, I.L. Small-angle X-ray diffraction studies and morphology of microporous materials and their “hard” elastic precursors. . 1978.

7 TABLES

Table 1. Basic characteristics for iPP T30G [21, 39, 40].

M_n ($\text{g}\cdot\text{mol}^{-1}$)	M_w ($\text{g}\cdot\text{mol}^{-1}$)	PDI (1)	$\eta_0^{###}$ at 220°C ($\text{Pa}\cdot\text{s}$)	Tacticity (mmmm)	E_a ($\text{kJ}\cdot\text{mol}^{-1}$)	$C_p^\#$ ($\text{J}\cdot\text{Kg}^{-1}\cdot\text{K}^{-1}$)	$\rho_F^\#$ ($\text{kg}\cdot\text{m}^{-3}$)	$\Delta H^{##}$ ($\text{kJ}\cdot\text{kg}^{-1}$)
75,000	481,000	6.4	7,402	87.6%	40.092	2,200	920	209

– Value taken from [41] as typical value for polyolefins.

– Value of crystallization latent heat taken from [44] as value for fully crystalline PP.

– Acquired by data digitalization technique from Figure 1 in [39].

Table 2. Summarization of processing conditions and relevant experimental data for iPP T30G taken from [21].

u_0 ($10^{-3}\text{ m}\cdot\text{s}^{-1}$)	$u(X)$ ($10^{-3}\text{ m}\cdot\text{s}^{-1}$)	X (m)	X_{FL} (m)	T_{DIE} (°C)	T_c (°C)	\dot{T}^* (°C·s ⁻¹)	$2L_0$ (m)	$2e_0$ (10^{-4} m)	DR (1)
4	103	0.4	0.06	220	100	86	0.2	3	25.75

Ambient temperature, T_a , was kept at 23°C for all numerical studies.

Table 3. Modified Leonov model parameters for iPP T30G at $T_r=220^\circ\text{C}$.

λ_0 (s)	G_0 (Pa)	ξ (1)	ν (1)	β (1)
0.1	74,020	0	0.5	0.5

Table 4. Parameters used in Eq. 7 describing effect of crystallinity on elastic modulus G taken from [39].

f (1)	h (1)	m (1)
2,000	0.2	1.2

Table 5. Parameters used in Eq. 8. describing the evolution of T_m^0 were taken from [33].

A_1 (1)	A_2 (1)	A_3 (1)	A_4 (1)	T_{mq}^0 (°C)
1.15	0.26	1	4.92	190

8 FIGURES

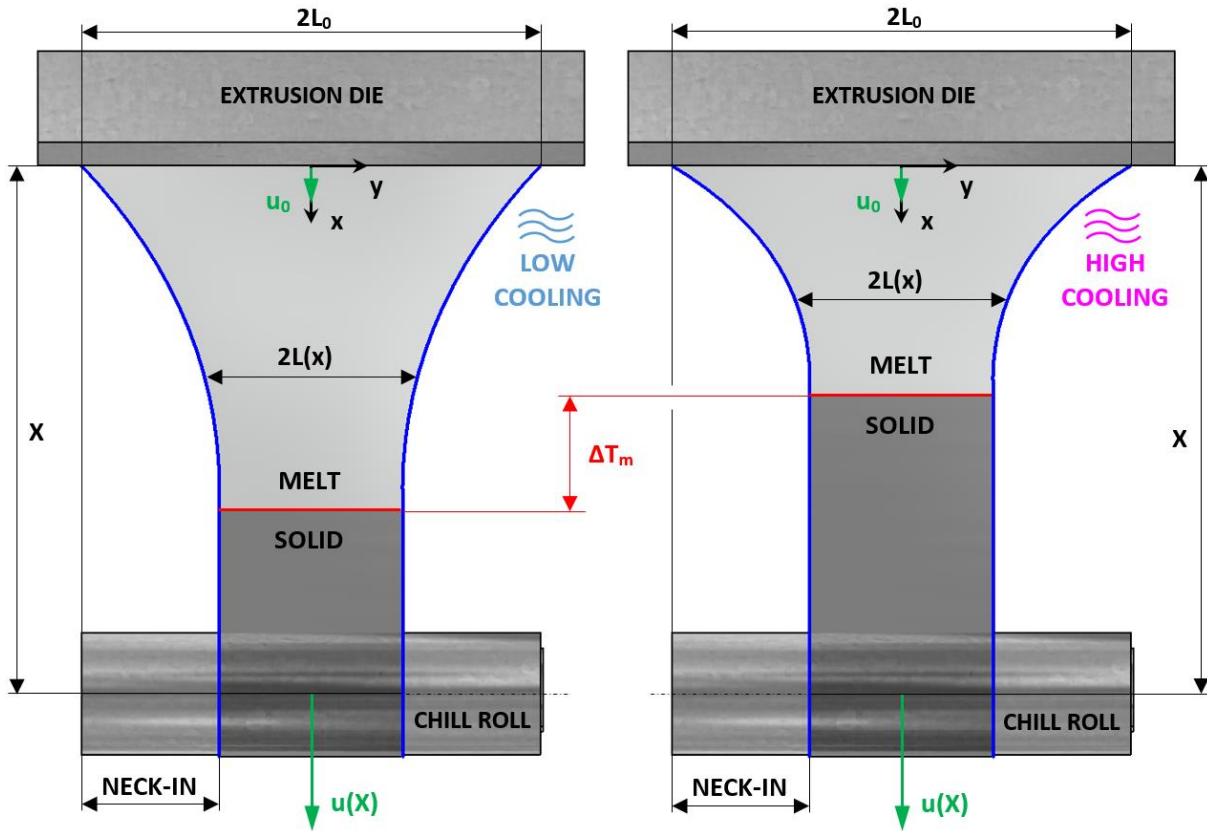


Figure 1. Schematic illustration of extrusion film casting process.

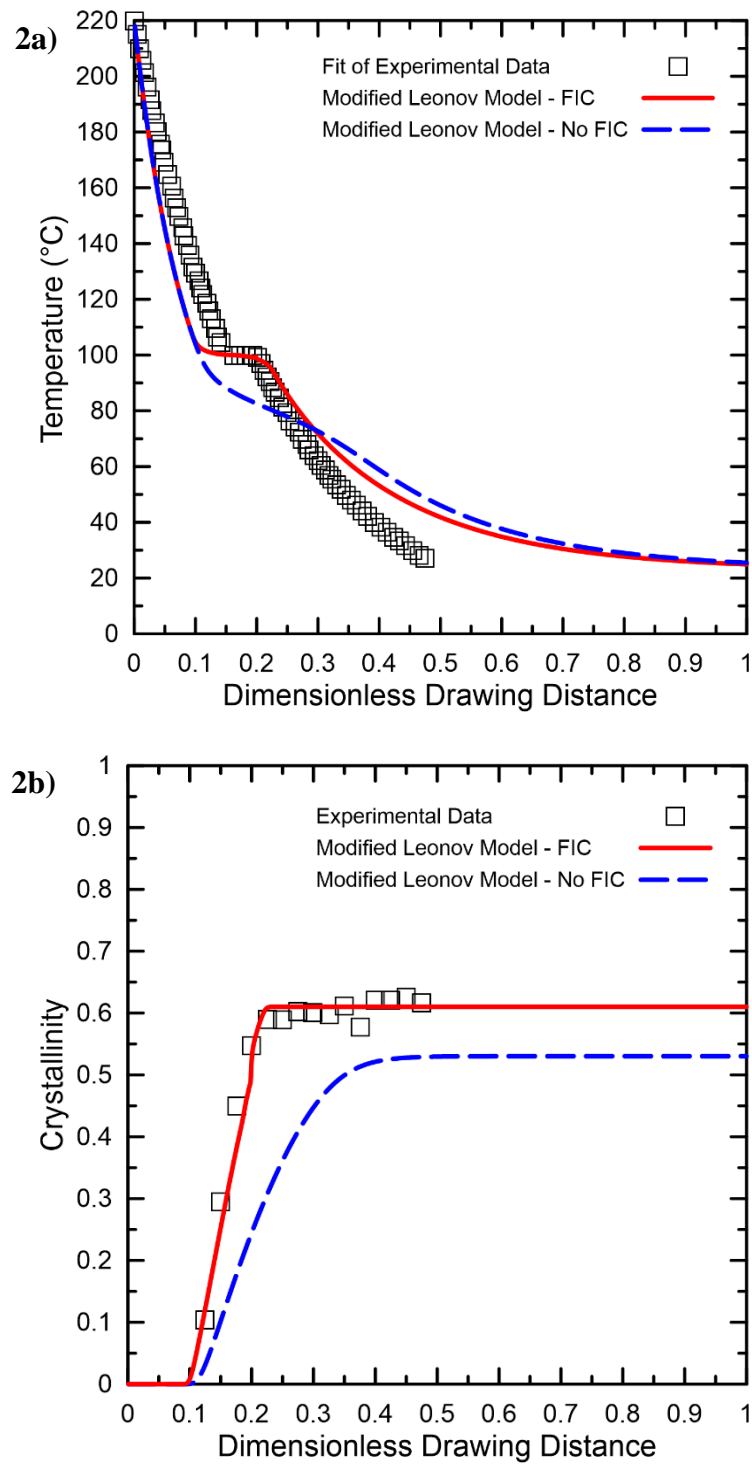


Figure 2. Comparison between non-isothermal film casting model predictions with and without consideration of Flow Induced Crystallization, FIC, and experimental data taken from [21], $HTC=31 \text{ J}\cdot\text{s}^{-1}\cdot\text{K}^{-1}\cdot\text{m}^{-2}$. (a) Temperature profile, (b) Crystallinity profile.

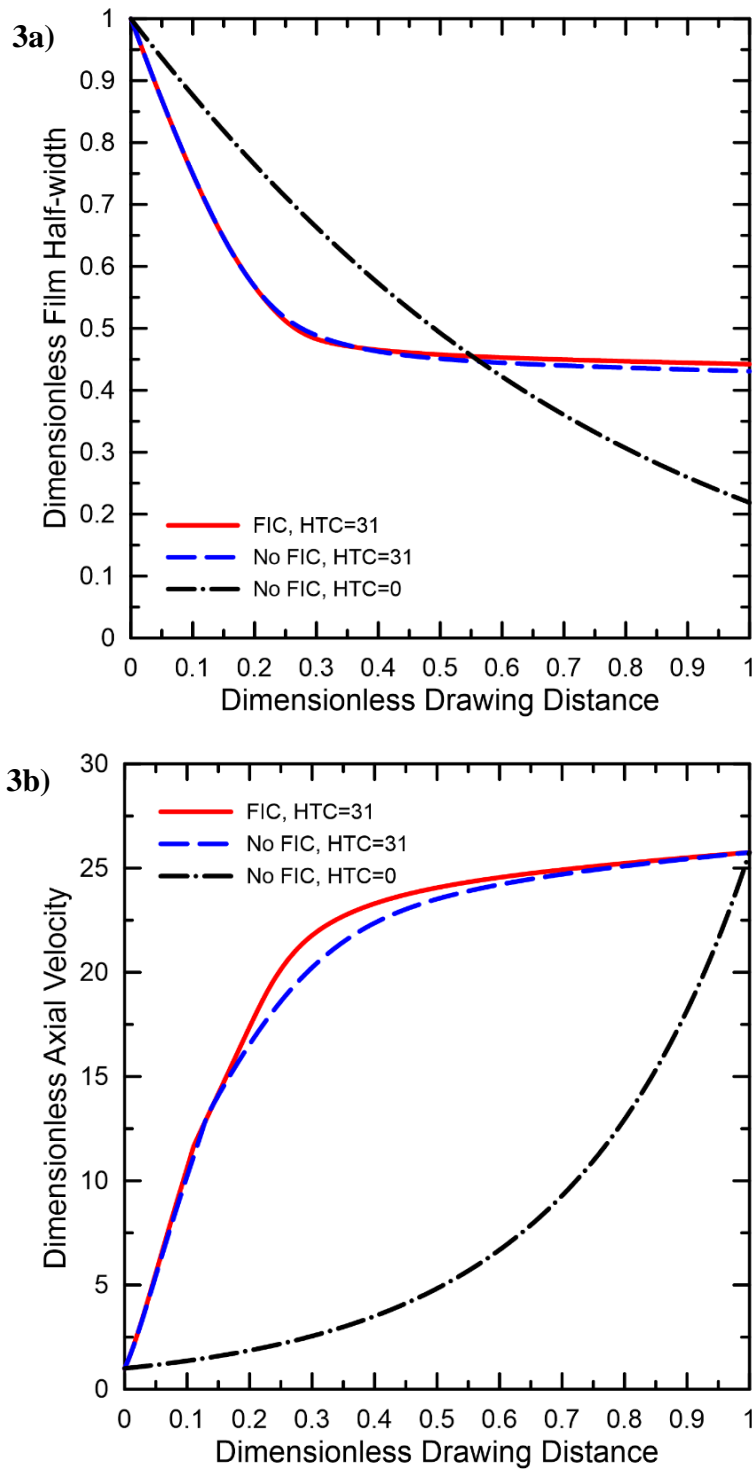


Figure 3. Comparison between isothermal and non-isothermal film casting model predictions with and without consideration of Flow Induced Crystallization, FIC, for the reference processing conditions ($HTC=31 \text{ J}\cdot\text{s}^{-1}\cdot\text{K}^{-1}\cdot\text{m}^{-2}$). (a) Dimensionless film half-width profile, (b) Dimensionless axial velocity profile.

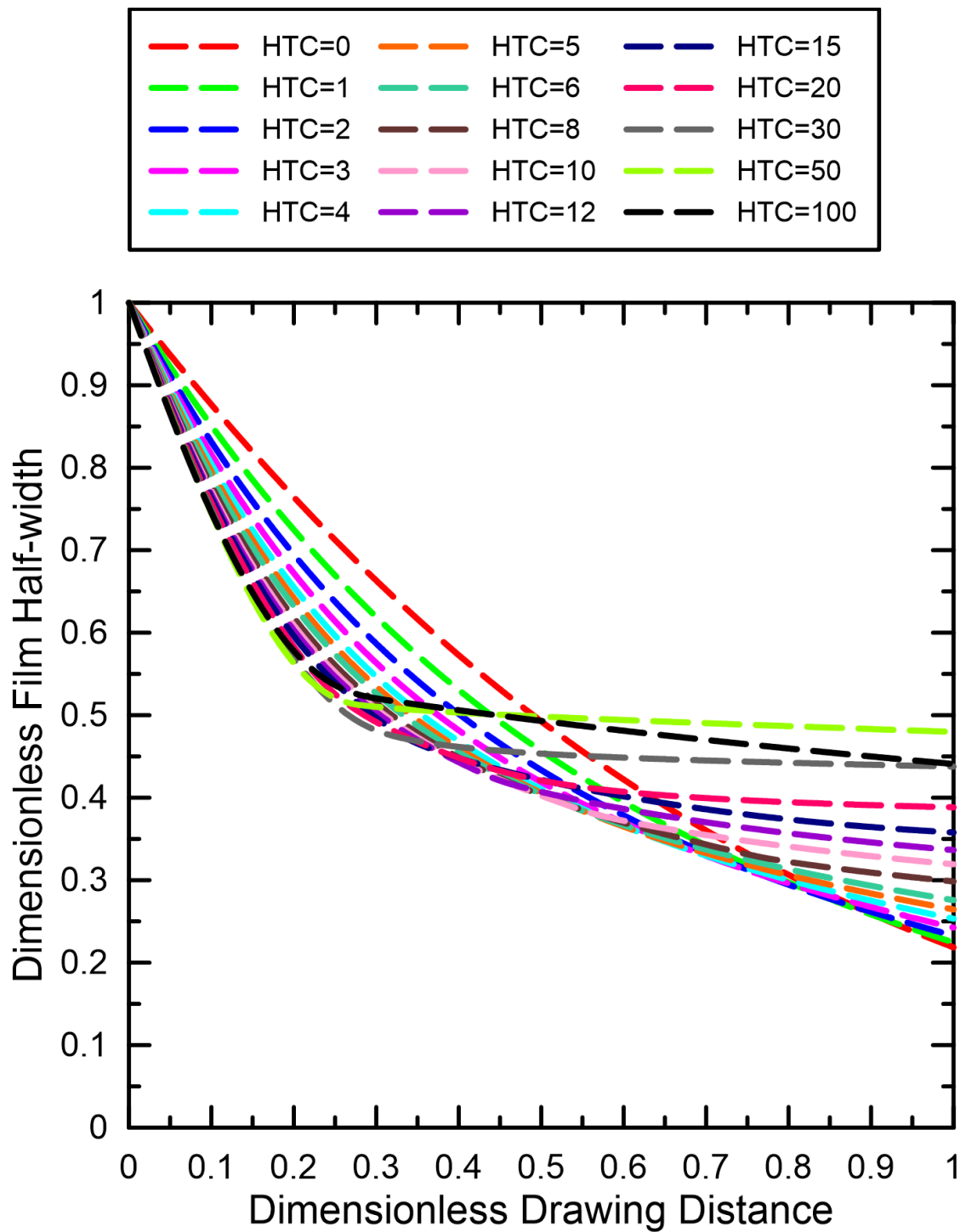


Figure 4. Predicted effect of HTC on the dimensionless film half-width for the reference processing conditions considering the non-isothermal model with flow induced crystallization.

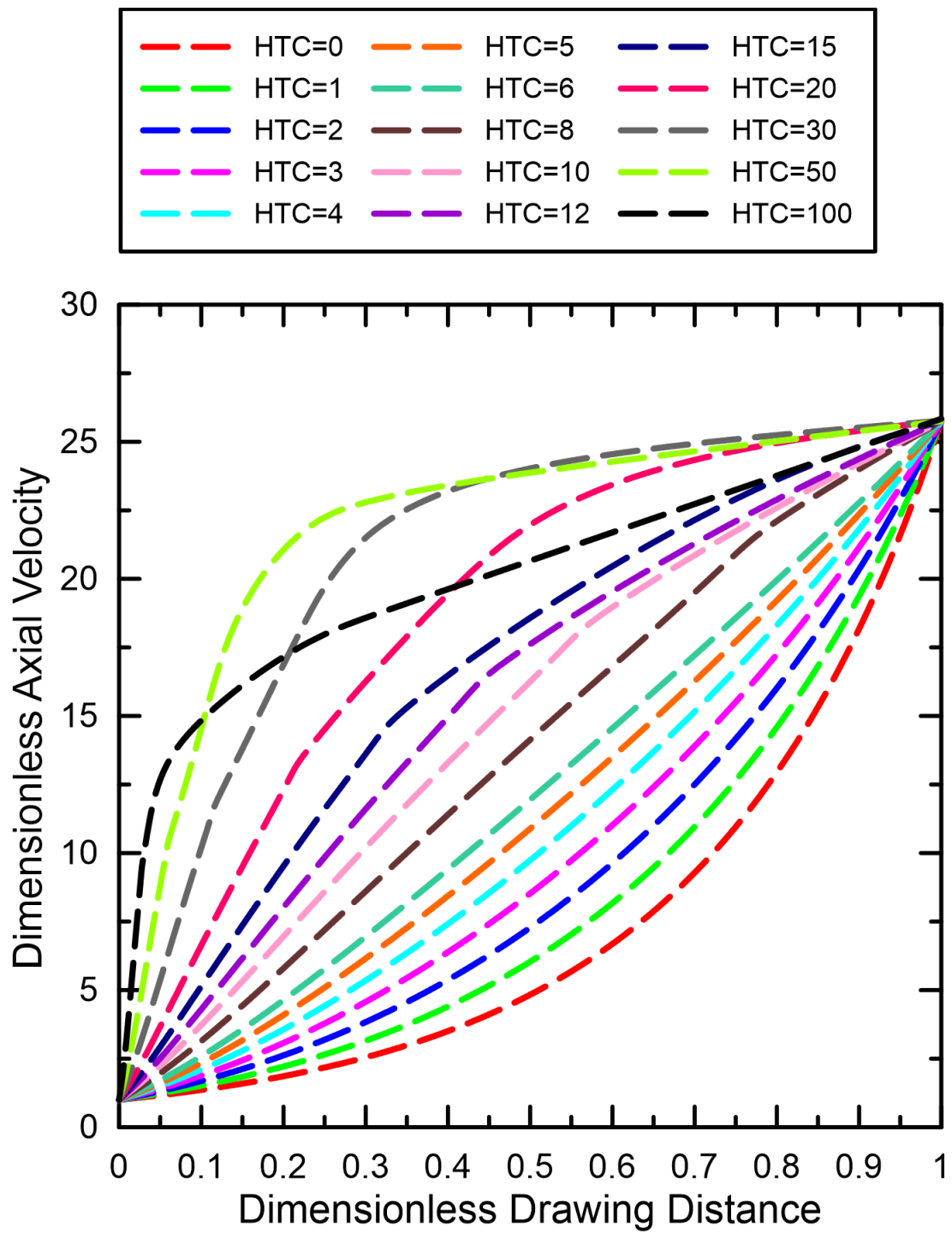


Figure 5. Predicted effect of HTC on the dimensionless axial velocity for the reference processing conditions considering the non-isothermal model with flow induced crystallization.

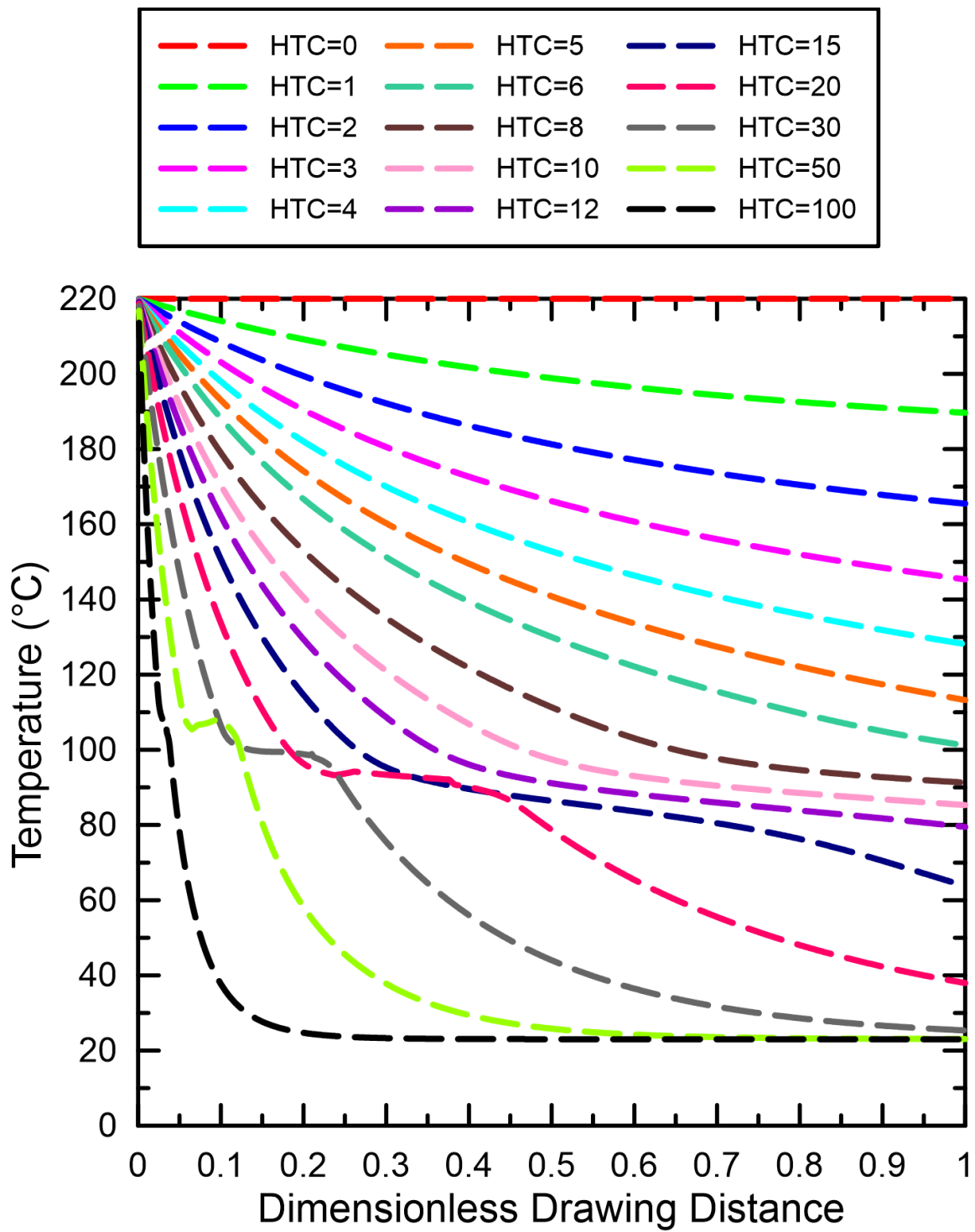


Figure 6. Predicted effect of HTC on the film temperature for the reference processing conditions considering the non-isothermal model with flow induced crystallization.

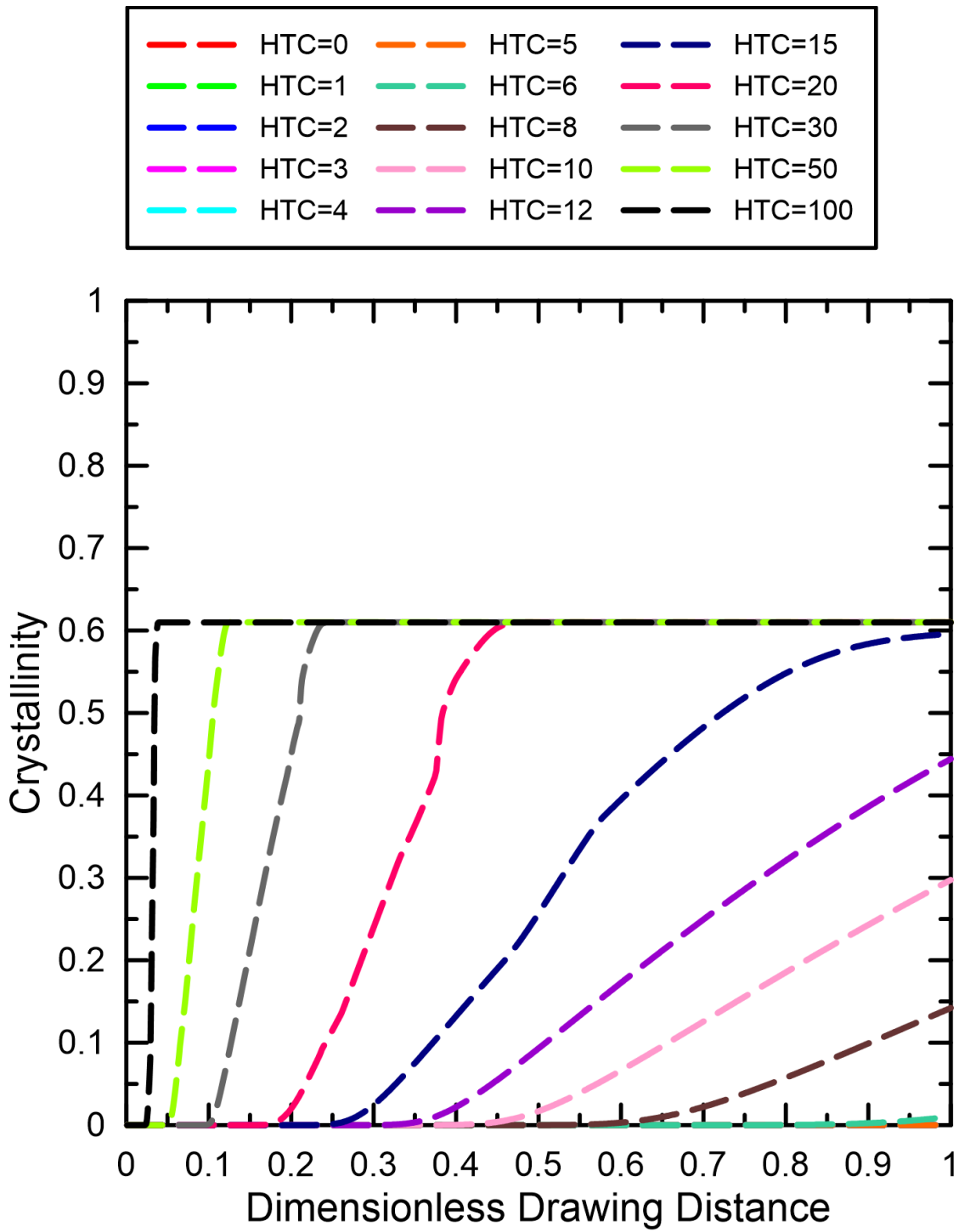


Figure 7. Predicted effect of HTC on the film crystallinity for the reference processing conditions considering the non-isothermal model with flow induced crystallization.

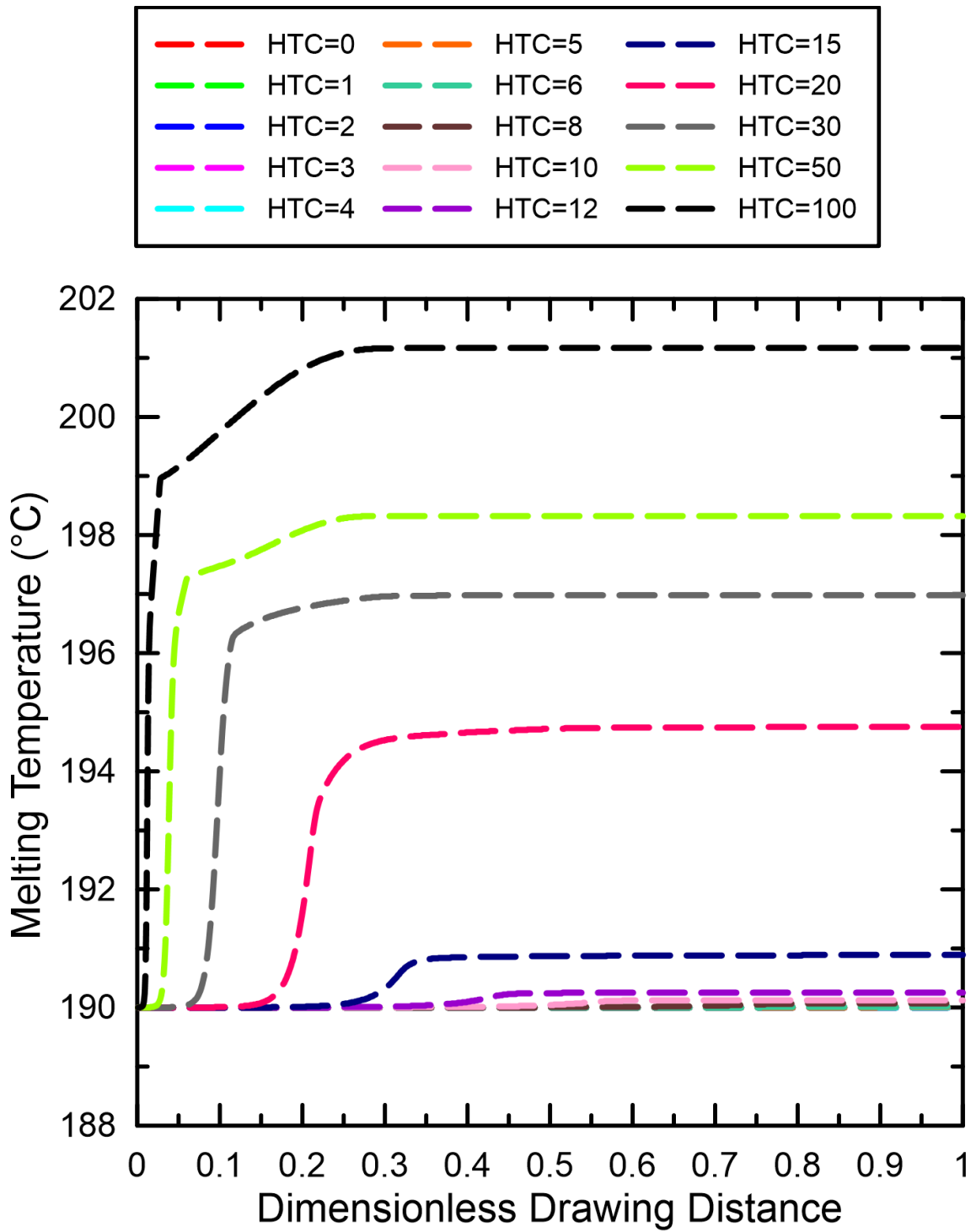


Figure 8. Predicted effect of HTC on the melting temperature of linear iPP for the reference processing conditions considering the non-isothermal model with flow induced crystallization.

LIST OF PUBLICATIONS

Publications in the Journals with AIS abstracted on Web of Science and Scopus Databases

1. BARBORIK, Tomas and ZATLOUKAL, Martin. Effect of die exit stress state, Deborah number, uniaxial and planar extensional rheology on the neck-in phenomenon in polymeric flat film production. *Journal of Non-Newtonian Fluid Mechanics*. 2018. Vol. 255, p. 39–56. AIS=0.769 and IF=2.293 by 2017.
2. BARBORIK, Tomas, ZATLOUKAL, M. and TZOGANAKIS, C. On the role of extensional rheology and Deborah number on the neck-in phenomenon during flat film casting. *International Journal of Heat and Mass Transfer*. 2017. Vol. 111, p. 1296–1313. AIS=0.767 and IF=3.891 by 2017.
3. BARBORIK, Tomas and ZATLOUKAL, Martin. Effect of heat transfer coefficient, draw ratio and die exit temperature on the production of flat iPP membranes. Submitted for publication in: *International Journal of Heat and Mass Transfer*. 2018. AIS=0.767 and IF=3.891 by 2017.
4. BARBORIK, Tomas and ZATLOUKAL, Martin. Viscoelastic simulation of extrusion film casting for linear iPP including stress induced crystallization. Considered for publication in: *Journal of Rheology*. 2018. AIS=1.129 and IF=2.969 by 2017.

Original Full Papers in Conference Proceedings abstracted on Web of Science and/or Scopus Databases

5. BARBORIK, Tomas and ZATLOUKAL, M. Effect of second to first normal stress difference ratio at the die exit on neck-in phenomenon in polymeric flat film production. In: *AIP Conference Proceedings*. Zlin, Czech Republic July 26-27, 2017. 2017. p. 030010. ISBN 978-0-735-41513-3.
6. ZATLOUKAL, Martin, BARBORIK, Tomas and TZOGANAKIS, Costas. On the role of extensional rheology, elasticity and Deborah number on neck-in phenomenon during flat film production. In: *Annual Technical Conference - ANTEC, Conference Proceedings*. Anaheim, California, USA May 8-10, 2017. 2017. p. 1131–1135. ISBN 978-0-692-88309-9.
7. ZATLOUKAL, Martin and BARBORIK, Tomas. Effect of extensional viscosity, elasticity and die exit stress state on neck-in phenomenon during extrusion film casting: Theoretical study. In: *Annual Technical Conference - ANTEC, Conference Proceedings*. Indianapolis, Indiana, USA May 23-25, 2016. 2016. p. 715–719. ISBN 978-0-692-71961-9.
8. BARBORIK, Tomas and ZATLOUKAL, Martin. Effect of viscoelastic stress state at die exit on extrusion film casting process: Theoretical study. In: *AIP Conference Proceedings*. Zlin, Czech Republic July 28-29, 2015. 2015. p. 030013. ISBN 978-0-7354-1306-1.

Conference Contributions not Abstracted in Research Databases

9. ZATLOUKAL, Martin and BARBORIK, Tomas. Effect of Die Exit Stress State, Deborah Number and Extensional Rheology on Neck-in Phenomenon (2018). *Annual Technical Conference - ANTEC*. Orlando, Florida, USA.
10. ZATLOUKAL Martin and Tomas BARBORIK. Effect of die exit stress state, Deborah number, uniaxial and planar extensional rheology on the neck-in phenomenon in polymeric flat film production (2018). *12th Annual European Rheology Conference – AERC 2018*. Sorrento, Italy.

11. ZATLOUKAL Martin and Tomas BARBORIK. Effect of uniaxial and planar extensional viscosities, die exit stress state and Deborah number on neck-in phenomenon during extrusion film casting (2017). *11th Annual European Rheology Conference – AERC 2017*. Copenhagen, Denmark.
12. BARBORIK Tomas and Martin ZATLOUKAL. Effect of Die Exit Stress State, Deborah Number, Extensional Viscosity, Heat Transfer and Crystallization on the Neck-in Phenomenon in Polymeric Flat Film Production (2018). In: *Polymers: Site of Advanced Horizons and Ambits*. Zlin, Czech Republic. ISBN 978-80-7454-729-4.
13. BARBORIK Tomas and Martin ZATLOUKAL. Výzkum jevu Neck-in při výrobě plošných polymerních fólií (2018). In: *Czech Chemical Society Symposium Series 16*. 2018. p. 450. ISSN 2336-7202.

Theses

14. BARBOŘÍK Tomáš. Využití reverzního inženýrství při návrhu vstřikovací formy, *Master Thesis*, Zlin, Tomas Bata University, Faculty of Technology, 2013, p. 116. Supervisor: doc. Ing. Michal Staněk, Ph.D.
15. BARBOŘÍK Tomáš. Konstrukce vstřikovací formy pro plastový díl, *Bachelor Thesis*, Zlin, Tomas Bata University, Faculty of Technology, 2011, p. 69. Supervisor: doc. Ing. Michal Staněk, Ph.D.

CURRICULUM VITAE

Personal Information

First name / Surname	Tomáš Barbořík, Ing.
Address	Tomas Bata University in Zlín Faculty of Technology, Polymer Centre Vavrečkova 275, 760 01 Zlín Czech Republic
Telephone	+420 57 603 1450
E-mail	tbarborik@gmail.com
Nationality	Czech
Date of birth	7. 4. 1988
Birthplace	Zlín, Czech Republic

Education

Period	2013–present
Title of qualification awarded	Ph.D.
Principal branch	Technology of Macromolecular Compounds
Organisation providing education	Tomas Bata University in Zlín, Faculty of Technology Polymer Centre
Period	2011–2013
Title of qualification awarded	Ing. (equivalent to M.Sc.)
Principal branch	Process Engineering, Technological Equipment Construction
Organisation providing education	Tomas Bata University in Zlín, Faculty of Technology, Department of Production Engineering

Education

Period	2008–2011
Title of qualification awarded	Bc. (equivalent to B.Sc.)
Principal branch	Process Engineering, Technological Equipment
Organisation providing education	Tomas Bata University in Zlín, Faculty of Technology, Department of Production Engineering
Period	2004–2008
Principal branch	Engineering; specialization: Computer Graphics
Organisation providing education	Secondary Technical School SPS Zlín, Zlín

Research Abroad Stay

Date	2016 (8 months)
Place	Waterloo, Ontario, Canada
Organisation providing training	University of Waterloo, Faculty of Engineering Department of Chemical Engineering

Work on Projects

2016–2018	Grant GA ČR No. 16-05886S <i>Investigation the effect of polymer melt shear and elongational rheology on production stability of meltblown nanofibers and films</i> Member of research team
2016	Grant UTB IGA/FT/2016/007 <i>Modelling of free surface viscoelastic melt flow</i> Leader of research team

Work on Projects

2015 Grant UTB IGA/FT/2015/013
Investigation of melt flow stability in flat film
Leader of research team

2010–2014 Grant GA ČR No. P108/10/1325
Applied Rheology for Advanced Polymer
Member of research team

Awards

Outstanding Master's Thesis Award by the
Department of Production Engineering

Conferences

2017 Novel Trends in Rheology VII

2015 Novel Trends in Rheology VI

2013 Novel Trends in Rheology V

International conferences held by Tomas Bata
University

Member of organization team

Ing. Tomáš Barbořík

**Viscoelastic Modeling of Extrusion Film Casting
for Polymer Melts: Investigation of Flow Stability**

Viskoelastické modelování extruzního lití polymerních tavenin na válec:
Výzkum stability toku

Doctoral Thesis

Edition: published electronically

Typesetting by: Ing. Tomáš Barbořík

This publication has not undergone any proofreading or editorial review.

Publication year: 2018